

2008

DISSOLUTION OF AEROSOL IRON IN SEA WATER USING FLOW-INJECTION WITH CHEMILUMINESCENCE DETECTION

SEGURET, MARIE JOSIANE MIREILLE

<http://hdl.handle.net/10026.1/1815>

<http://dx.doi.org/10.24382/3516>

University of Plymouth

All content in PEARL is protected by copyright law. Author manuscripts are made available in accordance with publisher policies. Please cite only the published version using the details provided on the item record or document. In the absence of an open licence (e.g. Creative Commons), permissions for further reuse of content should be sought from the publisher or author.

**DISSOLUTION OF AEROSOL IRON IN
SEAWATER USING FLOW-INJECTION WITH
CHEMILUMINESCENCE DETECTION**

by

MARIE JOSIANE MIREILLE SÉGURET

A thesis submitted to the University of Plymouth
in partial fulfilment for the degree of

DOCTOR OF PHILOSOPHY

School of Earth, Ocean and Environmental Sciences
Faculty of Science

December 2008

University of Plymouth
Library

Item No 9008478390

Shelfmark

THESES 551.466 SEG

ABSTRACT

Marie Josiane Mireille Séguret

Iron is an essential micronutrient for the metabolism of marine organisms and impacts on primary productivity and hence indirectly on climate change. The dominant source of iron to the sea surface in open ocean regions is from the atmosphere by aeolian dust transport, but the solubility of iron from dust is poorly constrained. In this thesis, chemical and physical factors impacting on the process of dust dissolution and iron release in seawater were investigated using FI-CL detection.

A manual FI manifold was automated and optimised for the determination of iron, at nanomolar concentrations, released from aerosols in seawater. The limit of detection was 0.04 ± 0.03 nM and the precision (rsd) ranged from 0.2 to 10.8 %. Protocols, maintenance and troubleshooting sections were documented for effective utilisation of the technique. A seawater treatment system to produce low DOC (dissolved organic carbon) and dFe (dissolved iron) seawater was adapted and optimised. This UV photo-oxidation system was poorly efficient in removing DOC (~ 40 %), complexing ligands (~ 60 %) and dFe (apparent removal ~ 90 %).

An autosampler was designed, validated, and integrated with an incubation system for sub-sampling during dissolution experiments of aerosol iron in seawater. Fast release of iron from the aerosol particles occurred within the first 2 h, followed by a decrease over 1 day. Preliminary experiments with UV-irradiated seawater exhibited lower solubilities compared with non UV-irradiated seawater. High dust concentrations gave lower final solubilities compared with low dust concentrations. A 24 h kinetic study was carried out using NIST 1648 under contrasting light and dark regimes. Dissolution of the end-member under dark conditions released 0.36 % of the iron whilst the addition of 20 nM to 200 nM Desferrioxamine B (DFOB) stimulated a release of 0.90 to 1.6 %. In light, the release of iron was 0.50 % with aerosol, whilst the addition of DFOB (20 nM) induced an adsorption (-1.18 %).

Iron release from aerosol samples from three sites around the Eastern Mediterranean: Erdemli, Tel-Shikmona and Heraklion was determined in a NATO funded project. The solubility of contrasting aerosol populations from crustal and anthropogenic sources was investigated. Crustally derived aerosol samples exhibited a variable kinetic profile of iron release with an average of maximum solubility of 0.39 ± 0.52 %. The anthropogenically influenced aerosol samples exhibited consistent kinetic profiles (fast release < 2 h) with an average of maximum solubility of 10.6 ± 8.9 %. From these results, an approximation of the atmospheric dry inputs of soluble iron in seawater to the Levantine Basin was calculated for the first time, ranging from 804 ± 910 t y⁻¹ for the Northern Levantine Basin to $2,670 \pm 3,050$ t y⁻¹ for the Southern Levantine Basin.

RÉSUMÉ

Marie Josiane Mireille Séguret

Le fer est un micronutriment essentiel au métabolisme des organismes marins, qui impacte sur la production primaire et donc indirectement sur le changement climatique. La principale source de fer dans l'océan est issue du transport de poussières atmosphériques mais la solubilité en fer est très peu connue. Dans cette thèse, facteurs chimiques et physiques, impactant sur le processus de dissolution du fer de poussière dans l'eau de mer, furent examinés par FI-CL.

Un system manuel FI-CL fut automatisé et optimisé pour la détermination du fer dans l'eau de mer à faibles concentrations (nano molaire). La limite de détection fut 0.04 ± 0.03 nM et la précision (rsd) varia de 0.2 à 10.8 %. Protocoles et sections d'entretien et dépannage furent documentés pour une utilisation efficace. Un système de production d'eau de mer à faible concentration de carbone organique dissous (COD) et dFe (fer dissous) a été évalué. Le système à radiation ultra violette (UV) fut peu efficace à enlever COD (~ 40 %), complexes moléculaires (~ 60 %) et dFe (enlèvement apparent~ 90 %).

Un système d'échantillonnage automatique a été conçu, validé, et intégré à un système d'incubation pour échantillonner les dissolutions en fer provenant de poussières dans l'eau de mer. La rapide libération en fer des particules se déroula dans les premières 2 h, suivie par une diminution sur 1 jour. Les expériences préliminaires dans l'eau de mer exposée aux UV montrèrent des solubilités plus basses comparées à celles dans l'eau de mer non irradiée. Les fortes concentrations de poussières montrèrent de basses solubilités finales comparées à celles de faibles concentrations. Des études cinétiques furent exécutées sur 24 h utilisant les poussières NIST 1648 à différente condition de lumière. Les dissolutions dans le noir libérèrent 0.36 % de fer alors que les additions de 20 nM à 200 nM Desferrioxamine B (DFOB) stimulèrent des libérations de 0.90 à 1.6 %. A la lumière, le relâchement de fer fut de 0.50 % alors que l'addition de DFOB (20 nM) induisit une adsorption de -1.18 %.

Les dissolutions en fer de poussières provenant de trois sites, Erdemli, Haïfa et Héraklion, autour de la Mer Méditerranée Est, furent déterminées lors d'un projet subventionné par l'OTAN. Les solubilités de poussières de sources contrastées, minérale et anthropogénique, furent examinées. Les poussières minérales ont montré un profil cinétique variable de libération en fer avec une moyenne de solubilité maximum de 0.39 ± 0.52 %. Les poussières anthropogéniques ont montré un profil cohérent et rapide (< 2 h) avec une moyenne de solubilité maximum de 10.6 ± 8.9 %. De ces résultats, une approximation des flux atmosphériques secs de fer soluble dans l'eau de mer du Bassin Levantin a été calculée pour la première fois, variant de 804 ± 910 t y⁻¹ pour le Bassin nord à $2,670 \pm 3,050$ t y⁻¹ pour le Bassin sud.

ACKNOWLEDGEMENTS / REMERCIEMENTS

First of all I would like to say a big thank to Malcolm Nimmo my director of studies, Paul Worsfold and Simon Ussher, my second and third supervisors. You have been really patient during these years, with always an encouraging word. Thanks to Malcolm for making me discovering the dusty world (Turkey was great!), Paul for the analytical part (could be a little bit frustrating...), Simon for the backpressure and micro-column's world. A dusty world is great, love back trajectories and EF, ICPs works much easier than FI-CL and HF digest is a great "adventure" a part on the 8th floor... What a lovely picture of chemiluminescence, I will remember it forever (particularly knowing that everyone was at the pub at the time...). I will remember the 4 replicates instead of 8, thanks Simon, I have been waiting to hear this. Finally, thank you very much for all the demonstrating!

Could say a lot but it will be too long, so I will simply say thanks a million!!!! to my parents for funding me during these years and supporting me with the ups and downs, I appreciate the sacrifices you have made (I will finish the house and take care of you during your old days). Je vous aime et prendrai soin de vous. Merci à ma sœur Émilie et bonne route avec ton adorable petite Margot.

Thanks to the University of Plymouth for the scholarship. Thanks to the colleagues who gave me some demonstrating. Thanks to the organisations which gave me financial supports, particularly the RSC, I could go to Orlando and indirectly a cruise in Bermuda!

Thanks to Maeve Lohan and Peter Statham for accepting to be my internal and external examiners.

Thanks to Simon and Eric Achterberg for the seawaters, Micha Rijkenberg for the CLE-ACSV analysis, Christina Theodosi and Barak Herut for the total digests.

Thanks to Debbie, Annie, Donella, Lee, Jo, Tamsin, Elaine, Marie and Jo.

Thanks to the technicians of the 5th floor, Sally, Andy, Andrew, Ian and Jeremy, for your help for my melting problems, fuses and all the little things from day to day. Thanks also for the chat during the demonstrating, particularly with allo allo.. otherwise I would probably have fell asleep. Thanks Andy for the ICPs. Thanks Rob for the lesson with the wavelengths.

A big thanks to Angie Milne, a lovely girl who helped me a lot with the iron story with Simon. Both of you have been really patient..

A huge thanks to my friend Sophie, a lovely girl and great friend, always here in relax and hard times... It is you who got me here, in Plymouth, I owe you a lot! Thanks a lot of your dynamism during my PhD! I have never tried so much Japanese and Chinese food! Merci ma poulette!!! Une fois payée, je saute dans le premier avion et viens te voir au soleil!!

A big thanks to past and present people from 106, 102 and 509B!! First the ladies: Angie again, Laura, Leyla (with all these really good berries and biscuits!!) Utra the chatty n°1, Cath, Fay the chatty n°3, Marta, Alex and Estela (I know that I have scared you driving...), Inma, Sandra, Kerstin (colleague even in the eye pain, say hello to Alex), Apha, Rachel, Jane chatty n°2 (you managed to be even more chatty than Fay!!), Ying, Kaew, Charlie, Maeve, Cécile and little William, Steph, Rebecca and the gents: Antonio the party animal, Yaswant, Simon, Ed, Omaka, Mohammed, Juanito, and Juan n°2, Frank, Gerald, Bernhard, Enrique, Jinbo, Sebas, Anders, Gary, Joe, Dionysis, Bill, Ian, Richard, Neil, Ramon and David. Thanks to my former flatmates Gabie, Priscilla, Thierry and Manolo.

Thanks to my friends: Maggy, Séverine and Les Amis de la Mer, thanks for the discovery of diving! Big thanks to Fred, Cédric, Karine, Ronan and Yann, and little Yann.

A huge thanks to Nilgun Kubilay, Mustafa Koçak to receive me at the IMS, my stay started on a weird way (thanks for the doctor!) but was great! I really enjoyed it! A huge thanks to Ceren and Ekin (it has been a real pleasure to meet you both! Thanks for all the visits, the lovely milky drink, but particularly for the chats around a nice cup of Turkish coffee!), Cansu, Billur (your dog barks a lot...), Serdar, Fatih, Meltem, and the cats!

A huge thanks to Pete Sedwick for inviting me to the FeAST6 cruise, Bermuda is quite hot and humid though... but the sun is great! It has been a real pleasure to be with you and your lovely family! Thanks to Chris Marsay alias Geordie for the motorbike trip, the tower tour and everything! Thanks to Tom Church for the aerosols and the chats, I have not told you this, but you really look like my lovely grandmother, in masculine of course! Thanks a lot to Ana, Aja, Tim, Jim, Ron, Geordie again, Tom, the crew of the Atlantic Explorer and the Captain, Simon to look after me and to woke me up for the whale shark and of course the famous WII!!

It has been really nice to meet you all, wish you all the best! And if I have forgotten someone, I am sorry!

It has been a pleasure to meet you: Clare, Duncan and their lovely Finlay, Gloria and Ken, Auntie Doris, June, Rob and Craig.

Merci Colin pour ces trois belles années.

Je dédie cette thèse à Maman, Papa, Émilie, Solange, Mamie et Papi de Villefranche, Mamie de Rodez, Sophie, Fifi, Lassie, Kissie, Cédric, Tatie Raymonde et Tonton Roger et Mamie et Papi Bessièrès, et aux familles Palis, Séguret, Ravailhe, Malcayan, Flourens, Brossard, Grousset, Gradels et Leterme.

"Just keep swimming, just keep swimming"

(Finding Nemo)

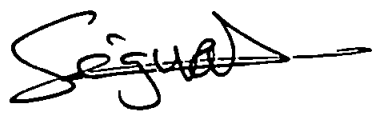
AUTHOR'S DECLARATION

At no time during the registration for the degree of Doctor of Philosophy has the author been registered for any other University award without prior agreement of the Graduate Committee. This study was financed with the aid of a scholarship from the University of Plymouth and by the author's parents.

High volume aerosol samples in Heraklion and Tel-Shikmona were collected by collaborators: Ms Christina Theodosi, Prof Nikos Mihalopoulos and Prof Barak Herut. Aerosol samples were collected in October 2007 by Dr Mustafa Koçak and Prof Nilgün Kubilay. Total digestions of samples from Heraklion and Tel-Shikmona were carried out by collaborators Ms Christina Theodosi and Prof Barak Herut at Tel-Shikmona and sent to the University of Plymouth for ICP-OES and MS analysis.

Relevant scientific seminars and conferences were regularly attended at which work was often presented and external institutions were visited for collaboration.

Word count of main body of thesis: 53,934


5/05/09

PRESENTATIONS AND CONFERENCES ATTENDED

POSTERS

"Design of an integrated dissolution and detection system for evaluating the factors controlling the dissolution of aerosol iron in seawater" presented at: *Postgraduate Research in Marine Earth Science, Southampton, March 2005* and *Analytical Research Forum (RSC), Plymouth, July 2005*.

"Evaluating the factors controlling the dissolution of aerosol iron in seawater" presented at: *Surface Ocean Lower Atmosphere Study Summer School, Cargèse, September 2005*.

"Design of an integrated reaction and detection system (FI-CL) for evaluating the factors controlling the dissolution of aerosol iron in seawater" presented at: *Analytical Research Forum (RSC), Cork, July 2006*.

"An integrated reaction and detection system for evaluating the factors controlling the dissolution of aerosol iron in seawater" presented at: *Challenger Society Meeting, Oban, September 2006*.

"Determination of the factors controlling the dissolution of aerosol iron in seawater by FI-CL detection" presented at: *Challenger Society Meeting Special Interests, Galway, September 2007*.

"Dissolution of aerosol iron in seawater using FI-CL detection" presented at: *14th Ocean Sciences Meeting, March 2008 Orlando, Florida*.

"Physical and chemical factors impacting upon the dissolution of aerosol iron in seawater", accepted at: *ASLO Aquatic Sciences Meeting 2009, Nice, France*.

ORAL PRESENTATIONS

"Evaluating the factors controlling the dissolution of aerosol iron in seawater" presented at: *Biogeochemistry and Environmental Analytical Chemistry Group, December 2004*.

"Evaluating the factors controlling the dissolution of aerosol iron in seawater" presented at: *Surface Ocean Lower Atmosphere Study Summer School, Cargèse, September 2005*.

"Detection of aerosol iron in seawater by Flow Injection Chemiluminescence (FI-CL)" presented at: *Biogeochemistry and Environmental Analytical Chemistry Group, Plymouth, December 2005*.

"Determination of total dFe and iron(II) by Flow Injection Chemiluminescence" presented at: *Biogeochemistry and Environmental Analytical Chemistry Group, Plymouth, March 2006*.

"Mechanisms involved in dust depositions" presented at: *Biogeochemistry and Environmental Analytical Chemistry Group, Plymouth, October 2006.*

"Detection of aerosol iron in seawater by Flow Injection Chemiluminescence detection" presented at: *Biogeochemistry and Environmental Analytical Chemistry Group, Plymouth, March 2007 and Plymouth Marine Laboratory, Plymouth, March 2007.*

"Determination of the factors controlling the dissolution of aerosol iron in seawater with flow injection-chemiluminescence detection" presented at: *Biogeochemistry and Environmental Analytical Chemistry Group, Plymouth, July 2007 and Analytical Research Forum (RSC), Glasgow, July 2007.*

"Dissolution of aerosol iron in seawater using flow injection-chemiluminescence detection" presented at: *Marine Institute Conference, Plymouth, December 2007.*

"Saharan dusts over the Levantine Basin: A NATO project" presented at: *Biogeochemistry and Environmental Analytical Chemistry Group, Plymouth, December 2007.*

"Physical and chemical factors impacting upon the dissolution of aerosol iron in seawater" presented at: *Biogeochemistry and Environmental Analytical Chemistry Group, Plymouth, December 2008.*

PUBLICATIONS

1. Séguret M.J.M., Ussher S.J., Worsfold P.J., Nimmo M. and Wood J.W. (2008) Automatic sampler coupled with Flow Injection-Chemiluminescence detection to monitor particle / natural water interactions. *Instrumentation Science and Technology* 36: 1, 18-31.
2. Ussher S.J., Milne A., Landing W.M., Kakar A.-R., Séguret M.J.M., Holland T., Achterberg E.P., Nabi A. and Worsfold P.J. (2009) Investigation of iron(III) reduction and trace metal interferences in the determination of dissolved iron in seawater using flow injection with luminol chemiluminescence detection. *Analytica Chimica Acta* submitted.

FINANCIAL AWARDS

1. *Royal Society of Chemistry*, travel grant for the Analytical Research Forum, Plymouth, England (July 2005).
2. *SOLAS Summer School financial support*, for the SOLAS Summer School, Cargèse, Corsica (September 2005).
3. *Plymouth Marine Fund Trustees*, student travel award for the SOLAS Summer School, Cargèse, Corsica (September 2005).

-
4. *Royal Society of Chemistry*, travel grant for the Analytical Research Forum, Cork, Ireland (July 2006).
 5. *Plymouth Marine Fund Trustees*, student travel award for the Challenger Society Meeting in Oban, Scotland (September 2006).
 6. *Challenger Society for Marine Science*, student travel award for the Challenger Society Meeting in Oban, Scotland (September 2006).
 7. *Royal Society of Chemistry*, travel grant for the Analytical Research Forum, Glasgow, Scotland (July 2007).
 8. *Challenger Society for Marine Science*, student travel award for the Challenger Special Interest Group Meeting in Galway, Ireland (September 2007).
 9. *Analytical Chemistry Trust Fund of the Royal Society of Chemistry*, overseas conference travel grant for the 14th Ocean Sciences Meeting in Orlando, Florida (March 2008).
 10. *ASLO Aquatic Sciences Meeting 2009*, travel student award for the ASLO Aquatic Sciences Meeting 2009, Nice, France (January 2009).

TRAINING

A NATO funded collaborative project (NATO CLG 982862) enabled the author to gain experience of high volume aerosol sample collection for one month in Erdemli, (Turkey) in collaboration with Dr Mustafa Koçak and Prof Nilgün Kubilay. A total digestion procedure using hydrofluoric acid was followed at the University of Plymouth under the supervision of Margaret Grimbly. Training in back trajectory analysis was taken under the supervision of Dr Mustafa Koçak. Moreover, a cruise in Bermuda, under the supervision of Dr Peter Sedwick and Dr Thomas Church, enabled the collection of low volume aerosol samples in remote marine systems carrying out shipboard dissolution studies and the experience of working at sea. Finally, courses were undertaken to qualify as a demonstrator for laboratory practicals.

TABLE OF CONTENTS

CHAPTER ONE

INTRODUCTION

1.1. MARINE BIOGEOCHEMICAL CYCLE OF IRON	2
1.1.1. Role of iron in marine biogeochemical cycles	2
1.1.2. The iron cycle	5
<i>Atmospheric compartment.....</i>	<i>5</i>
<i>Riverine compartment</i>	<i>11</i>
<i>Hydrothermal compartment</i>	<i>12</i>
<i>Upwelling and vertical mixing.....</i>	<i>13</i>
<i>Biotic compartment.....</i>	<i>14</i>
<i>Aggregation and precipitation.....</i>	<i>15</i>
1.1.3. Iron concentrations in the open ocean.....	15
1.2. SPATIAL AND TEMPORAL VARIABILITY OF IRON IN THE MARINE AEROSOL.....	19
1.3. FACTORS IMPACTING ON SOLUBILITY.....	25
1.3.1. Chemical factors	25
1.3.2. Physical factors	30
1.3.3. Biological factors.....	32
1.4. PRACTICAL APPROACHES ADOPTED TO DETERMINE THE SOLUBILITY OF AEROSOL IRON	32
1.5. FLOW INJECTION WITH CHEMILUMINESCENCE DETECTION	34
1.5.1. Flow Injection (FI).....	34
1.5.2. Chemiluminescence detection (CL)	35
1.5.3. FI-CL.....	36
1.6. AIMS AND OBJECTIVES.....	38

CHAPTER TWO

DETERMINATION OF IRON IN SEAWATER USING FI-CL DETECTION

2.1. INTRODUCTION.....	41
2.2. EXPERIMENTAL	41
2.2.1. Reagents and standards.....	41
2.2.2. Instrumentation	44
<i>Manual FI-CL system without/with 8-hydroxyquinoline column(s).....</i>	<i>44</i>
<i>Automated FI-CL system with three 8-hydroxyquinoline columns</i>	<i>49</i>
2.3. RESULTS AND DISCUSSION	54
2.3.1. Manual FI-CL system without/with 8-hydroxyquinoline columns	54
<i>Optimisation of the system</i>	<i>54</i>
<i>Analytical Figures of merit of the optimised system</i>	<i>57</i>
<i>Troubleshooting</i>	<i>58</i>
2.3.2. Automated FI-CL system	59
<i>Optimisation of the system</i>	<i>59</i>
<i>Interface settings with new design of flow cell</i>	<i>63</i>
<i>Analytical figures of merit using the optimised system</i>	<i>63</i>
<i>Troubleshooting</i>	<i>66</i>

2.3.3. Recommended protocols and maintenance.....	67
<i>Maintenance</i>	67
<i>Recommended protocols</i>	69
2.4. CONCLUSIONS.....	71

CHAPTER THREE

DEVELOPMENT AND ASSESSMENT OF THE EFFICIENCY OF A SEAWATER TREATMENT SYSTEM

3.1. INTRODUCTION.....	73
3.2. EXPERIMENTAL	74
3.2.1. Seawater treatment system	74
3.2.2. UV irradiation system.....	76
3.2.3. Determination of dissolved organic carbon (DOC).....	78
<i>Description of the analytical technique</i>	78
<i>Sample collection and preparation</i>	79
<i>DOC standard preparation</i>	80
3.2.4. Flow injection with chemiluminescence detection	80
3.3. RESULTS AND DISCUSSION	81
3.3.1. Complexing resins.....	81
3.3.2 DOC concentrations	83
<i>Initial set up</i>	83
<i>Optimisation</i>	85
<i>Effect of flow rate</i>	88
3.3.3. Dissolved Fe concentrations	89
<i>Initial set up</i>	89
<i>Optimisation</i>	90
3.3.4. Complexing ligands titration.....	91
3.4. CONCLUSIONS.....	93

CHAPTER FOUR

FACTORS IMPACTING UPON THE DISSOLUTION OF AEROSOL IRON IN SEAWATER

4.1. INTRODUCTION.....	96
4.2. EXPERIMENTAL	98
4.2.1. Autosampler coupled with an incubation vessel.....	98
4.2.2. Interface	99
4.2.3. Experimental dissolution settings: dark and light.....	100
<i>Dark settings</i>	100
<i>Light settings</i>	101
4.2.4. Dissolution procedures and material used	105
<i>Cleaning procedure</i>	105
<i>Dissolution procedure</i>	106
<i>Seawaters</i>	106
<i>End member aerosols</i>	107
<i>Complexing ligand (siderophore)</i>	108
4.3. RESULTS AND DISCUSSION	109
4.3.1. Experimental performances of the autosampler and incubation vessel.....	109

<i>Hardware control</i>	110
<i>Cumulative errors in dFe concentration from the autosampler and FI-CL system</i>	111
<i>Blank controls and dissolutions</i>	112
<i>Adsorption effect</i>	114
<i>Effect of DFOB on FI-CL signal</i>	115
<i>pH changes</i>	116
4.3.2. Development of the aerosol dissolution experimental protocol in seawater.....	117
<i>Mixing: stirred and non-stirred</i>	117
<i>Seawater matrix (i.e. UV and non-UV-irradiated) and dust concentrations</i>	120
4.3.3. Chemical and physical factors impacting upon the dissolution of aerosol iron	123
<i>Dark experiment</i>	124
<i>Light experiments</i>	126
4.4. CONCLUSIONS	130

CHAPTER FIVE

SOLUBILITY OF IRON IN SEAWATER FROM THE EASTERN MEDITERRANEAN MARINE AEROSOL

5.1. INTRODUCTION	134
5.2. THE MEDITERRANEAN SEA AND ATMOSPHERIC INPUTS	135
5.3. EXPERIMENTAL	141
5.3.1. Description of sampling sites.....	141
<i>IMS, Erdemli</i>	141
<i>IOLR, Tel-Shikmona</i>	142
<i>ACD, Heraklion</i>	143
5.3.2. Sampling procedures	142
<i>Choice of filter</i>	143
<i>Filter cleaning procedures</i>	145
<i>Validation of the filter cleaning procedure</i>	146
<i>Collection and storage of filter samples</i>	148
5.3.3. Digestion procedure for major and minor elemental concentrations	150
5.3.4. Analytical techniques and performance characteristics.....	152
<i>Filter and operational blank contributions</i>	153
<i>Operational detection limits</i>	154
<i>Assessment of the experimental and analytical accuracy</i>	155
<i>Determination of the seawater solubility of iron in selected aerosol samples</i>	159
5.3.5. Air mass back trajectories.....	161
5.4. RESULTS AND DISCUSSION	163
5.4.1 The overall chemical characteristics of the Eastern Mediterranean aerosols.....	163
5.4.2. Aerosol elemental sources: application of the enrichment factor (EF_{crust}).....	166
5.4.3. Inter-elemental relationships	168
5.4.4. Temporal variation in elemental aerosol concentrations.....	170
5.4.5. The seawater solubility of iron in the Eastern Mediterranean marine aerosol.....	178
<i>Determination of the contribution of the operational blank filter during dissolution studies</i> ...178	
<i>Repeatability of the determination of the solubility of iron from crustally derived aerosol samples</i>	179
.....	
<i>Solubility of iron in seawater in the eastern Mediterranean marine aerosol</i>	180
<i>Kinetic profiles for the dissolution of iron</i>	188
5.4.6. Dry atmospheric fluxes of seawater soluble iron over the Levantine Basin	191

5.4.7. Residence time of seawater soluble iron in the Cretan Sea	195
5.5. CONCLUSIONS.....	196

CHAPTER SIX

CONCLUSIONS AND FUTURE WORK

6.1 CONCLUSIONS.....	200
6.1.1. Automation of a FI-CL detection system	200
6.1.2. Seawater treatment system	201
6.1.3. Effect of chemical and physical parameters on dust dissolution kinetics	201
6.1.4. Iron solubility in seawater from Eastern Mediterranean marine aerosols	202
6.1.5. Summary of factors impacting upon the aerosol seawater solubility of Fe	203
6.2. FUTURE WORK.....	205

REFERENCES	207
-------------------------	------------

APPENDICES	231
-------------------------	------------

PUBLICATION.....	242
-------------------------	------------

LIST OF FIGURES

Figure 1.1. The marine biogeochemical cycle of iron. Blue arrows: resuspension, purple arrows: sedimentation. Black compartment: dFe. Brown compartment: particulate iron. Units: 10^{12} g yr ⁻¹ . ¹ Goudie (2008), ² Jickells and Spokes (2001), ³ Chester (2000), ⁴ de Baar and de Jong (2001).	6
Figure 1.2. Photochemical cycling of iron in seawater (adapted from Barbeau <i>et al.</i> 2001).	18
Figure 1.3. Chemiluminescence reaction of Fe(II). a) 1 M solution, b) chemical formula of luminol (5-amino-2,3-dihydrophthalazine-1,4-dione).	36
Figure 1.4. Major pathways in the oxidation of luminol (source Rose and Waite 2001).	37
Figure 2.1. Flow injection with chemiluminescence detection manifold for the determination of Fe(II).	44
Figure 2.2. Manual switching valve, showing load and elute positions of the sample.	44
Figure 2.3. a) Picture of the quartz flow cell, b) flow cell and end-window in the housing.	45
Figure 2.4. Reaction scheme for the immobilisation of 8-hydroxyquinoline onto TSK resin.	47
Figure 2.5. Perspex micro-column: a) empty, b) packed with 8-hydroxyquinoline coated resin and mounted onto the injection valve.	48
Figure 2.6. Preconcentration micro-column containing 8-HQ immobilized on TSK, with a space allowing the resin to move when changing from elution to load.	48
Figure 2.7. Final manual FI manifold, with two 8-hydroxyquinoline micro-columns: on the buffer line and the switching valve.	48
Figure 2.8. Automated FI system, with three 8-hydroxyquinoline micro-columns: on the buffer line and UHP water rinse and mounted onto the switching valve.	49
Figure 2.9. Block diagram of the interface, incorporating the 5 units: USB system controller, solenoid and relay controlling switching valves, PMT integrator (2 channels), TTL output and pump.	51
Figure 2.10. LabVIEW front panel (version 14) for the virtual instrument, with current analysis, data history, elapsed time and position of the injection valve.	52
Figure 2.11. Wiring diagram showing the graphical code for instrument control and data acquisition. This code controls the front panel presented in Figure 2.10.	53
Figure 2.12. Effect of changing power supply voltage on standard additions 10 nM of iron(II) to UHP de-ionised water.	55
Figure 2.13. Chelex-100 column for cleaning the luminol reagent: bottom section with the chelating resin and top section preventing the loss of Chelex.	56
Figure 2.14. Chart showing peaks of a calibration of iron(II) from 0 to 30 nM, UHP de-ionised water peaks showed the negative peaks of injection.	58
Figure 2.15. Chart showing a peak calibration of iron(II) from 0 to 4 nM in UHP de-ionised water. ...	58
Figure 2.16. a) PMT opened with flow cell, b) detail of flow cell and mirror.	62
Figure 2.17. a) Detail for the T-piece and its connections, b) Insulation of the PMT from light.	62
Figure 2.18. Chart showing electric interferences a) during analysis, b) during rinse of the system.	66
Figure 2.19. a) increase of the signal when loading column, b and c) oscillations of the baseline and secondary peak, d and e) oscillating peaks and baseline.	68
Figure 2.20. Typical output of standard additions in seawater between 0.8 and 6 nM.	68

Figure 3.1. In-line UV photo-oxidation system coupled with complexing resins. X shows the four strategic sampling points: (1) filtered seawater, (2) after the first series of resins, (3) after the UV mercury lamp and (4) the final product.	75
Figure 3.2. Main components of the mercury vapour lamp and of the UV photo-oxidation system. ...	77
Figure 3.3. Mercury lamp, a) aluminium-housing encapsulating the UV lamp, b) UV lamp with water jacket and photo-reactor coil.	77
Figure 3.4. Spectral irradiance of the Model 3040 mercury lamp.	77
Figure 3.5. Shimadzu TOC 5000A analyser / ASI 5000A auto analyser, from left to right: autosampler, DOC analyser and computer for the acquisition of the data.	79
Figure 3.6. Schematic diagram of the main components of the Shimadzu DOC analyser.	79
Figure 3.7. DOC concentrations (μM) in seawater through the different stages of the UV photo-oxidation system. Error bars= ± 1 s.d.	84
Figure 3.8. Effect on the DOC concentrations (μM) in a new batch coastal water and regeneration of the resins. Error bars= ± 1 s.d.	85
Figure 3.9. Water jacket a) before and b) after cleaning with 50% v/v HCl.....	86
Figure 3.10. The effect of the UV lamp treatment alone on the DOC concentration in two ocean seawaters, (a) open ocean seawater (Atlantic Ocean) (b) coastal ocean (Canary Basin), and (c) 100 μM DOC standard at 1.1 mL min^{-1} . Error bars = ± 1 s.d.	87
Figure 3.11. The effect of flow rate on DOC concentration in 100 μM DOC standard, 1.1 and 0.5 mL min^{-1} . Error bars = ± 1 s.d.....	88
Figure 3.12. Concentrations of Fe (nM) in seawater at different stages of the treatment, error bar= ± 1 s.d.....	90
Figure 3.13. Concentration of dFe in coastal ocean (Canary Basin) and open ocean (Atlantic Ocean) seawaters before and after UV irradiation. Error bar= ± 1 s.d.	91
Figure 3.14. Concentrations of total and free ligands before and after UV irradiation in seawaters collected from (a) the Canary Basin and (b) the Atlantic Ocean.....	92
Figure 4.1. Components of the sampler-incubation vessel for the sampling of dFe released in seawater during model dissolution studies.	98
Figure 4.2. LabVIEW front panel with main elapsed time of the dissolution process, elapsed time of sub-sample collection and indication of the position of the 10-way distribution valve.....	100
Figure 4.3. Wiring diagram showing the graphical code for instrument control.....	100
Figure 4.4. Integration of the incubation vessel with the sample collection box for dissolution in dark.	101
Figure 4.5. Transmission of light (between 250 - 800 nm) of the FEP incubation vessel.	102
Figure 4.6. Incubation vessel with the (a) quartz mounted on the top and (b) detail of the notch.	102
Figure 4.7. Comparison of the spectral intensities of different laboratory light sources with natural light (Roof 1982).	103
Figure 4.8. Equipment set-up for dissolution studies investigating the effects of light.	103
Figure 4.9. Schematic diagram of the incubation vessel with the Xenon lamp.	104
Figure 4.10. Irradiance measured at the positions of the quartz cover and magnetic stirrer in W m^{-2} ...	105
Figure 4.11. Chemical structure of the ligand Desferrioxamine B.	108

Figure 4.12. Percentage solubility of 1.94 mg L ⁻¹ NIST 1648 in seawater (Atlantic Ocean).....	110
Figure 4.13. Blank dissolution profile (± 1 s.d.), along with the mean line (± 1 s.d.) and a typical dissolution profile of NIST 1648, 1.94 mg L ⁻¹	113
Figure 4.14. Effect of the addition of different DFOB concentrations on the FI-CL signal of 2 nM of Fe(III). Error bars represent ± 1 s.d. (n = 4).....	115
Figure 4.15. Effect of stirring and not stirring the seawater on iron a) solubility and b) released concentration (nM, inset: focus on the first 2 h), from NIST 1648 (0.5 mg L ⁻¹ , non UV irradiated Atlantic Ocean seawater) over a 1-day period. Error bars represent ± 1 s.d. (n = 4).	118
Figure 4.16. Effect of UV irradiation on iron a) solubility and b) released concentration (nM) from low and high NIST 1648 loadings (0.25 and 2 mg L ⁻¹). Error bars represent ± 1 s.d. (n = 4).	120
Figure 4.17. Rate of release of iron from the aerosol particles in natural seawater at two different dust loadings, high 2 mg L ⁻¹ and low 0.25 mg L ⁻¹ . Error bars represent ± 1 s.d.	122
Figure 4.18. Effect of complexing ligand concentration DFOB (20 nM, 200 nM) on the kinetic dissolution profiles of 0.5 mg L ⁻¹ NIST 1648 under dark conditions, a) solubility and b) released concentration. Error bars represent ± 1 s.d.	125
Figure 4.19. Effect of light on the kinetic dissolution profile of 0.5 mg L ⁻¹ of NIST 1648. a) solubility and b) released concentrations. Error bars represent ± 1 s.d (n = 4). Light experiment represents the mean of 2 dissolution experiments. Data from the second experiment min 480 and 720 min were excluded from the mean due to suspected contamination.	127
Figure 4.20. Effect of light in the presence of the complexing ligand DFOB on the kinetic dissolution profile of 0.5 mg L ⁻¹ of NIST 1648, a) solubility and b) released concentrations. Error bars represent ± 1 s.d (n = 4).	129
Figure 5.1. SeaWiFS image highlighting the land vegetation around the Mediterranean Sea, (September 2000), also indicated is a dust event to the west of the Eastern Levantine Basin. X indicates the location of ACD, Heraklion (Crete), + indicates the location of IMS, METU, Erdemli (Turkey) and * indicates the location of IONR, NIO, Tel-Shikmona (Israel).	136
Figure 5.2. The atmospheric sampling tower located at the Institute of Marine Sciences, Erdemli.	142
Figure 5.3. Polypropylene holding trays for the cleaning procedures of Whatman 41 filters.	146
Figure 5.4. a) High volume sampler used at Erdemli. b) Mechanism of the filtration (right).	149
Figure 5.5. a) Anodised aluminium filter holder. b) Filter ready for sampling, secured by the frame. ...	149
Figure 5.6. Example of calculated 3-day back trajectories arriving at Erdemli on the 11 th of October at 1,000; 2,000 and 4,000 m determined using HYSPLIT model.	162
Figure 5.7. Classification of 3-days back trajectories, northern and southern air masses.	162
Figure 5.8. a) Temporal variations (October 2007) in 1) Al, 2) Fe and 3) Mn aerosol concentrations (ng m ⁻³) at all sites: Erdemli (ER), Tel Shikmona (TS) and Heraklion (HE).	171
Figure 5.8. b) Temporal variations (October 2007) in 4) Ca, 5) K and 6) Ti aerosol concentrations (ng m ⁻³) at all sites: Erdemli (ER), Tel Shikmona (TS) and Heraklion (HE).	172
Figure 5.8. c) Temporal variations (October 2007) in 7) Mg, 8) Na and 9) Zn aerosol concentrations (ng m ⁻³) at all sites: Erdemli (ER), Tel Shikmona (TS) and Heraklion (HE).	173
Figure 5.9. Impacts of air mass transport on Fe aerosol concentrations as a proxy for dust events at a) Erdemli, b) Heraklion and c) Tel-Shikmona.....	175-177

Figure 5.10. Repeatability study (n = 3) of a crustally derived aerosol sample from each site. HE = Heraklion, ER = Erdemli, TS = Tel-Shikmona. Error bars = ± 1 s.d.....	179
Figure 5.11. Corresponding 3-day air mass back-trajectory arriving at the three sites for the samples collected on the 30 th October, a) Heraklion, b) Erdemli and c) Tel-Shikmona.....	180
Figure 5.12. Percentage of the iron soluble fraction against the crustal fraction contribution of iron in aerosols. a) Soluble iron fraction versus the iron crustal contribution to the aerosol population after a 2 h contact time. Open triangle = anthropogenically influenced aerosol, diamond = crustally derived aerosol. b) superimposed exchangeable (circle) and oxide / carbonate phases (diamond) for the Eastern Mediterranean marine aerosol, after Koçak <i>et al.</i> (2007).....	185
Figure 5.13. Temporal variation of iron concentrations (ng m ⁻³) for the three sites along with maximum solubility (taken at variable contact time), a) Tel-Shikmona, b) Heraklion and c) Erdemli. .	187
Figure 5.14. Percentage solubility of iron release during dissolutions of crustally derived samples from the three sites (n = 9). ER = Erdemli, HE = Heraklion, TS = Tel-Shikmona. Error bars = ± 1 s.d.	189
Figure 5.15. Percentage solubility of iron release during dissolutions of anthropogenically influenced samples from the three sites (n = 8). ER = Erdemli, HE = Heraklion, TS = Tel-Shikmona. Error bars = ± 1 s.d.....	190
 Figure 6.1. Diagram summarising the effects of chemical, physical and biological parameters on the dissolution of aerosol iron in seawater. *: factors investigated in this study.....	204

LIST OF TABLES

Table 1.1. Estimates of dusts fluxes (10^{12} g y^{-1}) to the ocean by wet and dry depositions (adapted from Jickells and Spokes 2001). Scavenging ratio of 200 was used for all oceanic basins instead of 1.000.	10
Table 1.2. Percentage of wet deposition of the total deposition of mineral aerosols (Source Hand <i>et al.</i> 2004).	10
Table 1.3. Dissolved iron concentrations (nM) in the world ocean.	16
Table 1.4. Marine aerosol iron concentrations (ng m^{-3}) in contrasting marine systems (expressed as the geometric mean).	20
Table 1.5. A summary of studies investigating the solubility of aerosol iron including the matrix and filters used, parameters considered and the adopted analytical technique. CRM: certified reference material, PC: polycarbonate membrane, PP: polypropylene filter, What.: Whatman fibrous cellulose acetate filter, 20 μm	23-24
Table 1.6. Conditional stability constants for FeL complexes for different oceanic regions. * data taken from Witter <i>et al.</i> (2000).	27
Table 1.7. The solid stage speciation signals of iron in contrasting aerosol types (expressed as a percentage of the total metal). ¹ Chester <i>et al.</i> (1994), ² Chester <i>et al.</i> (1989), ³ Koçak <i>et al.</i> (2007). S1= "exchangeable", S2= "carbonate and oxide, S3= "residual". LUAP= Liverpool Urban Aerosol particulate.	28
Table 1.8. Mineral nature, class and iron present with its solubility (from Journet <i>et al.</i> 2008)	29
Table 2.1. Timings sequence for an individual analytical cycle. Wash pump on= rinse.	52
Table 2.2. Effect of power supply voltage on signal-to-noise ratio. PMT gain D.	55
Table 2.3. Optimisation stages with corresponding analytical Figures of merit for the manual system..	57
Table 2.4. Comparison of the analytical Figures of merits of the manual and automated FI systems (n= 7), using Fe(II) standards made up in UHP de-ionised water. LoD= Limit of detection.	60
Table 2.5. Contribution of hydrochloric acid (HCl) and reducing reagent (sulphite) in ultra high purity de-ionised water (UHP water). Samples were spiked with 0.01 M HCl and 100 μM sulphite or 200 μM sulphite. LoD: Limit of detection.	60
Table 2.6. Changes in signal and baseline noise using UHP de-ionised water, depending of the gains on the PMT and software. New design of flow cell, 8-HQ micro-columns with BioVyon® F frits.	63
Table 2.7. CL emission of 5 LDPE bottles (n= 4) of acidified seawater.	65
Table 4.1. Timing sequence and operation state for each component per position of the 10-way distribution valve (cycle).	106
Table 4.2. Expected concentration (nM) of dFe in seawater equilibrated with the urban particulate material (dust concentration 0.5 mg L^{-1} assuming solubilities of 0.20, 0.50 and 1 %).	108
Table 4.3. Physiochemical parameters of Desferrioxamine B used in this study. ^a Witter <i>et al.</i> (2000), ^b Hering and Morel (1993), ^c Spasojević <i>et al.</i> (1999)	109
Table 4.4. Replicate (n=4) CL emission signals for each of the 5 separate acidified seawater samples collected from the incubation vessel using the autosampler.	111

Table 4.5. Concentrations of dFe (nM, ± 1 s.d.) in UHP de-ionised water which was passed through the autosampler lines (n = 124) and through the filter (n = 136).	112
Table 4.6. Calculated effective decrease in dFe seawater concentrations (pM) during dissolution studies (different conditions) as a result of iron adsorption onto the incubation vessel walls (n=13). Assessments were carried out under different experimental conditions (blank dissolution being seawater only: 0.5 mg L ⁻¹ NIST 1648 in seawater; DFOB additions from 20 pM to 200 nM with 0.5 mg L ⁻¹ NIST 1648 in seawater; 10nM Fe(II) spike in seawater; high volume Whatman 41 filter sample collected from Tel-Shikmona; see <i>Chapter Five</i>).	115
Table 4.7. Seawater dust loadings and their relationship to strength of natural dust events along with equivalent solubilities in seawater (%) as reported by Bonnet and Guieu (2004).	123
Table 5.1. Aerosol trace metal concentrations (ng m ⁻³) in Mediterranean marine aerosol for the southern and northern boundaries of the Eastern and Western Mediterranean, from a) Chester <i>et al.</i> (1996), b) Guerzoni <i>et al.</i> (1999a), c) Herut <i>et al.</i> (2001) and d) Koçak <i>et al.</i> (2005). Origin / classification of aerosol source were determined using air mass back trajectory analyses.	137
Table 5.2. Crustal elemental enrichment factors in Mediterranean marine aerosol originated from the southern and northern boundaries, from a) Chester <i>et al.</i> (1996), b) Guerzoni <i>et al.</i> (1999a), c) Herut <i>et al.</i> (2001) and d) Koçak <i>et al.</i> (2007).	137
Table 5.3. Geometric mean of elemental concentrations (ng m ⁻³) in Mediterranean marine aerosols at sampling stations located west and east in Northern boundary: a) Guieu <i>et al.</i> (1997) b) Koçak <i>et al.</i> (2004).	138
Table 5.4. Seasonal geometric mean variation of the crustal elemental concentrations (ng m ⁻³). Note: winter (November through to February), summer (June through to September) and transitional season: spring (March through May) and autumn (October), from Koçak <i>et al.</i> (2004).	139
Table 5.5. Atmospheric inputs of iron ($\mu\text{mol m}^{-2} \text{d}^{-1}$) to the sea surface of the world's oceans, (from Turley 1999).	140
Table 5.6. Summary of the trace elemental concentrations (ng mL ⁻¹) in an acidic (pH 4.5) UHP de-ionised water leach (25 mL for 15 min; n = 3). Operational elemental detection limits were defined as the mean (n = 3) acidic UHP water leach concentration ± 3 standard deviation.	147
Table 5.7. Summary of the techniques used for the detection of chosen analytes.	153
Table 5.8. Elemental operational blanks ($\mu\text{g mL}^{-1}$ except for Ti, Mn and Zn which are expressed in ng mL ⁻¹) for samples collected at (i) Erdemli (ii) Tel-Shikmona and (iii) Heraklion.	154
Table 5.9. Elemental contribution percentage of the operational blank concentration to the average digest elemental concentration. *Instrumental detection limit used in calculation as the operational blank was < detection limit.	154
Table 5.10. Operational detection limits ($\mu\text{g mL}^{-1}$ except for Ti, Mn and Zn which are expressed in ng mL ⁻¹) based on the operational acid washed filter blanks. nd = non-detectable.	155
Table 5.11. Observed and certified elemental concentrations of ME55-3, and NIST 1648 and their percentage recoveries using HF/HNO ₃ digestion procedure for samples from Erdemli. All elemental concentration means are presented as percentages. * concentrations in $\mu\text{g g}^{-1}$, – non detectable.	157
Table 5.12. Observed and certified elemental concentrations of CFA 1633a, ES 1646A and ME55-3, and their percentage recoveries using aqua regia digestion procedure for samples from Tel-Shikmona	

and Heraklion. All elemental concentration means are presented as percentages. * concentrations in $\mu\text{g g}^{-1}$. - non detectable.....	158
Table 5.13. Reproducibility in cutting 4 cm^2 of filter portions	160
Table 5.14. Geometric and arithmetic mean of aerosol elemental concentrations (ng m^{-3}) observed at Haifa, Erdemli and Heraklion during October 2008.	164
Table 5.15. Comparison of elemental aerosol concentrations (ng m^{-3}) for the current study ($n = 92$) and literature values representative of the Eastern Mediterranean. TS= Tel-Shikmona.	165
Table 5.16. Comparison of the geometric means of the EF_{sd} and ranges (in brackets) for the current study with those in the literature. (TS = Tel-Shikmona).....	167
Table 5.17. Geometric means and range in brackets of EF_{sd} for minor elements from samples collected at Erdemli during October 2007.	168
Table 5.18. Comparison of the geometric mean of EF_{sd} for the current study with the literature. * adapted from Kubilay and Saydam (1995).	168
Table 5.19. Rank spearman coefficient for the elements determined in the collected aerosol samples (correlations in bold significant at $p < 0.05$) for the three sites.	169
Table 5.20. Selected aerosol samples for iron dissolution studies.	178
Table 5.21. Filter blank ($n = 3$) contributions (nM) to the seawater over an 8 h dissolution study.	178
Table 5.22. Percent solubility (± 1 s.d.) of triplicate dissolutions of sample collected on the 30 th October, from each site.	180
Table 5.23. Solubility of iron in seawater from aerosols originated from the Eastern Saharan desert. Med. = Mediterranean Sea.	181
Table 5.24. Percentage solubility in crustally derived aerosols from Erdemli (ER, $n = 4$), Heraklion (HE, $n = 2$) and Tel-Shikmona (TS, $n = 3$). Error bars = ± 1 s.d.	188
Table 5.25. Percentage solubility in anthropogenically influenced aerosol samples from Erdemli (ER, $n = 3$), Heraklion (HE, $n = 3$) and Tel-Shikmona (TS, $n = 2$). Error bars = ± 1 s.d.	190
Table 5.26. Comparison of iron dry deposition fluxes expressed as $\text{mg m}^{-2} \text{y}^{-1}$ in the Levantine Basin. ¹ soluble iron fraction, ² exchangeable iron fraction.....	193
Table 5.27. Iron atmospheric dry inputs (t y^{-1}) to the Northern and Southern Levantine Basin. ¹ this study, ² Koçak <i>et al.</i> (2005). Error bars represent ± 1 s.d ($n = 7$).	194
Table 5.28. Residence time of soluble dFe over the Cretan Sea with respect to atmospheric inputs calculated from this study and from Statham and Hart (2005). Inventories of dFe for the mixed layers at different time of the year were taken from Guieu <i>et al.</i> (1997), calculated from Statham and Hart (2005).	196

GLOSSARY OF COMMONLY USED ABBREVIATIONS

8-HQ	8-hydroxyquinoline
CLE-ACSV	Competitive ligand exchange-adsorptive cathodic stripping voltammetry
dFe	dissolved Fe
DOC	Dissolved organic carbon
EM	Eastern Mediterranean
ER	Erdemli
FI	Flow-Injection
FI-CL	Flow-Injection with Chemiluminescence
HE	Heraklion
HTCO	High temperature catalytic oxidation technique
LoD	Limit of Detection
PMT	Photomultiplier tube
TdFe	Total dissolved Fe
TS	Tel-Shikmona
UHP	Ultra high purity
UV	Ultraviolet

**DISSOLUTION OF AEROSOL IRON IN SEAWATER
USING FLOW-INJECTION WITH
CHEMILUMINESCENCE DETECTION**

INTRODUCTION

1.1. MARINE BIOGEOCHEMICAL CYCLE OF IRON

1.1.1. Role of iron in marine biogeochemical cycles

The hypothesis that iron may play an essential role in phytoplankton growth and is a limiting element was first suggested by Gran (1931) and Harvey (1939). Menzel and Ryther (1961) also showed that the addition of iron stimulated the growth of phytoplankton from Sargasso Sea surface seawater. However, owing to the absence of sensitive analytical techniques, this hypothesis could not be tested efficiently before the 1980s. It is now accepted that iron is an essential micronutrient for marine organisms (Moore *et al.* 1984; Duce 1986; Martin and Fitzwater 1988; Martin and Gordon 1988; Martin *et al.* 1990). It plays an important role in phytoplankton photosynthetic and respiratory electron transport, nitrate reductase, chlorophyll synthesis and detoxification of reactive oxygen species (Falkowski *et al.* 1998; Sunda 2001). Iron influences the growth and species composition of marine phytoplankton communities (Coale *et al.* 1996; Boyd *et al.* 2000) and hence its marine biogeochemical cycling is, in turn, influenced by phytoplankton activity (Sunda 2001). For example, the production of organic chelates such as complexing ligands will change the chemical speciation of dFe (dFe) in seawater, thus potentially lowering the amount of iron oxyhydroxide precipitation. This can lead to an enhancement in its solubility and therefore decrease its loss from the water column via the production and subsequent removal of colloidal material (Sunda 2001).

Martin (1990) developed and presented the "Iron hypothesis", which linked changes in the iron supply with variations in phytoplankton primary production which in turn impacts on the carbon budget in High Nutrient Low Chlorophyll *a* (HNLC) oceanic zones (Boyd and Doney 2003). The lower than expected phytoplankton biomass in these regions was explained by iron limitation (Coale *et al.* 1996). Such zones include the Southern Ocean, Equatorial Pacific and subarctic Pacific Oceans and have been the subject of iron enrichment studies including: IronEx I in 1993 (Martin *et al.* 1994) and IronEx II in 1995 (Coale *et al.* 1996) in the Equatorial Pacific, SOIREE in the Southern Ocean in 1999 (Boyd *et*

al. 2000) and EisenEx in the Southern Ocean in 2000 (Croot *et al.* 2005). During the course of these enrichment experiments significant increases of phytoplankton productivity and abundance were observed. It has been suggested that iron could be limiting in approximately 30% of the total ocean (Falkowski *et al.* 1998; Watson 2001; Jickells *et al.* 2005) and recent studies have emphasized that iron can be co-limiting with light (e.g. Boyd *et al.* 1999; Sunda 2001), macronutrients (Boyd and Doney 2003; Mills *et al.* 2004) and trace nutrients (Co and Zn, Morel and Price 2003; Schulz *et al.* 2004).

The dominant external source of iron to the surface ocean is from the atmosphere, by aeolian dust transport (section 1.1.2, Duce *et al.* 1991; Duce and Tindale 1991; Jickells and Spokes 2001), mainly from the deserts of the northern hemisphere (North Africa and Arabian Peninsula deserts; Pye 1987; Jickells and Spokes 2001). Dust produced by these areas and deposited to the ocean has important effects on the complex inter-related mechanisms of global biogeochemical systems, owing to its relatively high content in iron ranging between ~ 2.8– 5.0 % (Duce and Tindale 1991; Spokes and Jickells 1996; Zhu *et al.* 1997; Bonnet and Guieu 2004; Milne 2007; Mendez *et al.* 2009). Atmospheric transport of dust influences major processes between the ocean and the atmosphere and indirectly affects the climate via iron enrichment by impacting upon phytoplankton productivity and decay with associated production and utilisation of important greenhouse gases, including isoprene, methane (Wingenter *et al.* 2004); dimethyl sulphide (DMS, Charlson *et al.* 1987; Zhuang *et al.* 1992a; Turner *et al.* 1996; Wingenter *et al.* 2004). Such impacts may lead to either negative (cooling) or positive (warming) effects on these systems (Charlson *et al.* 1987; Turner *et al.* 1996; Wingenter *et al.* 2004; Jickells *et al.* 2005). In addition to enhanced marine primary productivity, atmospheric inputs of dusts, enriched with iron to the surface open ocean may lead to a shift in phytoplankton species community structure depending upon the initial nutrient status and phytoplankton communities present (Coale *et al.* 1996; Boyd *et al.* 2000). For example, Baker *et al.* (2003) examined the role of N, P and Fe in the Atlantic Ocean and concluded that atmospheric inputs from the

Saharan desert could drive the system to be dominated by N₂ fixing diazotrophs (e.g. *Trichodesmium* sp.). Although the N:P ratio in aerosol inputs was considerably higher than the Redfield ratio (16:1), the overall water column ratio suggested N limitation. Once the phytoplankton communities have consumed the N, excess P and Fe can allow productivity to continue with the proliferation of diazotroph communities via N₂ fixation, providing their own N requirement for primary production. During iron enrichment in the Southern Ocean, a community shift was also observed from autotrophic flagellate community to a large diatomaceous community (Coale *et al.* 1996; Boyd *et al.* 2000). Wells *et al.* (1991) have argued that low iron conditions might limit the distribution of dinoflagellates in the Gulf of Maine. In open ocean conditions, characterized by a low seawater concentration of iron, phytoplankton require less iron by reducing their cell size or minimizing the number of iron-containing enzymes (Sunda and Huntsman 1997; Palenik *et al.* 2003). However, if iron inputs increase, the growing phytoplankton communities can become populated by a larger cell size having a less dense opal skeleton (Watson 2001). Schulz *et al.* (2004) investigated the effect of iron and zinc limitations on the coccolithophore *Emiliania huxleyi*. Under decreasing concentration of zinc, *Emiliania huxleyi* showed an increase in calcium carbonate (CaCO₃) whilst with reduced concentration of iron, the production of CaCO₃ was reduced up to sixfold, proportionally with the growth rate. A reduction in the export of CaCO₃ reduces CO₂ removal from the atmosphere (Schulz *et al.* 2004). Recently, Tortell *et al.* (2008) showed the effect of increased CO₂ concentrations on diatom species incubated with 1 nM Fe (as FeCl₃), particularly *Chaetoceros* spp which have a very high capacity for organic carbon export to the sediments. Such increased CO₂ concentrations stimulated productivity that could influence an algal species shift. In turn, this could increase the efficiency of the Southern Ocean uptake, thus contributing to a negative feedback of increased CO₂ concentrations. This then could be amplified by the addition of iron from melting ice and glaciers (Sedwick and DiTullio 1997).

1.1.2. The iron cycle

The main components of the iron cycle in marine systems are presented in Figure 1.1, along with its sources and its sinks.

Sources of dFe in seawater to the euphotic zone include both “new” sources from external inputs as well as “regenerated” sources; recycled *in situ* from various particulate forms (Wells *et al.* 1995). These sources include the atmosphere, the crust, rivers and the ocean itself (Chester 2000). In addition, iron is removed from surface waters by different mechanisms: biological assimilation; sorption; precipitation; aggregation of inorganic or organic ligands and colloids; and the sinking of mineral and biogenic particles (Wells *et al.* 1995; de Baar and de Jong 2001). However, the mechanisms and dynamics are not well understood (Wells *et al.* 1995).

Atmospheric compartment

The main source of iron to the open ocean is from the atmosphere (Duce *et al.* 1991; Duce and Tindale 1991; Jickells *et al.* 2005; Wu *et al.* 2007) by dust input. Iron is, after aluminium (Al), silica (Si) and oxygen (O), the most abundant element in crustal material. Primary sources of dusts originate from arid and semi-arid regions from the Northern hemisphere; these are mainly North Africa (Engelstaedter *et al.* 2006) and the Arabian Peninsula deserts (Pye 1987; Schutz *et al.* 1990) owing to their geographical scale and proximity to the Atlantic and Indian Oceans (Pye 1987). Moreover, dust production has been evaluated for the North Saharan desert, to be between 500 and 1,000 × 10¹² g y⁻¹ (Engelstaedter *et al.* 2006), half of the annual global production (Goudie 2008), with up to two thirds deposited in the North Atlantic Ocean (Engelstaedter *et al.* 2006).

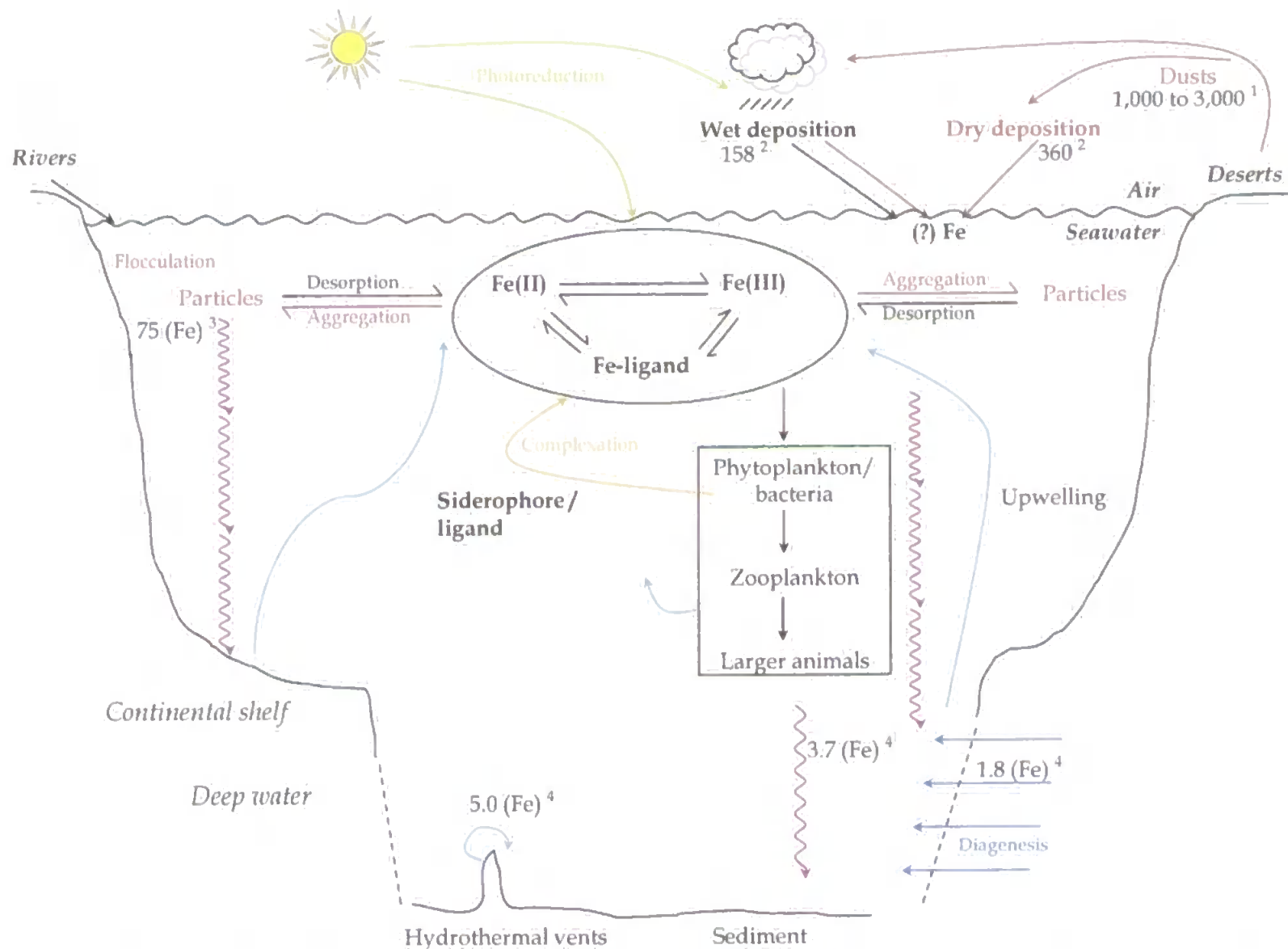


Figure 1.1. The marine biogeochemical cycle of iron. Blue arrows: resuspension, purple arrows: sedimentation. Black compartment: dFe. Brown compartment: particulate iron. Units: $10^{12} \text{ g yr}^{-1}$. ¹ Goudie (2008), ² Jickells and Spokes (2001), ³ Chester (2000), ⁴ de Baar and de Jong (2001).

Deserts from the southern hemisphere have a comparatively lower impact on iron inputs (both intensity and frequency of events) than the African and Asiatic deserts (Prospero *et al.* 1989).

In addition, anthropogenic soil disturbance has been identified as further contributing to the production of atmospheric dusts (Goudie and Middleton 1992). It has also been suggested that changing land use practices over recent decades have altered dust fluxes by up to 50 % increase (Mahowald and Luo 2003) although Tegen *et al.* (2004) suggested lower values (< 10 %). Variability in diameter for crustal dust generated from geological processes and transported over long distances has been observed (D'Almeida and Schutz 1983; Gomes *et al.* 1990; Jickells and Spokes 2001). More recently, Jickells *et al.* (2005) proposed a range, is between 0.1 and 10 μm , with the mean diameter being around 2 μm . These types of aerosols have a lifetime of hours up to weeks, allowing transportation over thousands of kilometres (Duce 1995; Prospero 1996; Ginoux *et al.* 2001), creating a strong gradient of atmospheric deposition and concentrations. For example, it has been shown that African dust can cross the tropical Atlantic Ocean and reach Barbados, Florida (Delany *et al.* 1967; Prospero *et al.* 1970; Prospero 1996), Bermuda (Chester *et al.* 1971; Sedwick *et al.* 2007), the Caribbean (Ott *et al.* 1991), as well as northwest Europe (Pitty 1968; Stevenson 1969; Borbély-Kiss *et al.* 1999). Swap *et al.* (1992) and Artaxo *et al.* (1994) also observed African dust reaching the Amazon basin in eastern Brazil in meteorological soundings. Ing (1969) observed dust deposition derived from northern and central China in the North Pacific Ocean more than 2500 km off the Chinese coast. Young *et al.* (1991) subsequently confirmed long range transport of aerosol material derived from China, across the Pacific. In addition, Jickells and Spokes (2001) reported long range (10,000 – 15,000 km) transport of dust from central Chinese desert to the Central Pacific in 8 to 14 days and Boyd *et al.* (1998) reported transports from Alaska and Asian regions to the north east subarctic Pacific ocean.

Following transport, dust (and hence iron) removal from the atmosphere occurs by two processes, dry deposition and wet deposition. During dry deposition, the particles, although they may have passed through several “wetting” and “drying” cycles during transport, reach the sea surface by gravitational settling (Chester 2000). This is a continuous process being more important for the larger particles (and their associated trace elements) in an aerosol population. Wet deposition involves the removal of particles and water soluble gases from the atmosphere by incorporation into cloud droplets (in cloud) or scavenging by falling rain droplets (below cloud), (Chester 2000). This deposition mode is spatially and temporally variable and depends upon the aerosol particle size, rainfall patterns and transport altitude.

To estimate wet deposition of dust over the ocean, the precipitation rate is necessary along with rainwater loadings. Whilst the estimation of precipitation rate is difficult owing to the lack of long term data, particularly at sea, it is common to use the scavenging ratio (Duce *et al.* 1991; Kane *et al.* 1994). The scavenging ratio relates concentrations of an element in precipitation (C_p) with that in the aerosol phase (C_a):

$$Sr = (C_p/C_a) \times \rho \quad \text{Equation 1.1}$$

Where ρ is the density of air and is used to make the equation dimensionless.

Dry deposition fluxes are calculated from:

$$\text{Dry deposition flux} = C_{\text{aerosol}} \times V_d \quad \text{Equation 1.2}$$

C_{aerosol} is the elemental concentration in aerosol and V_d is the dry deposition velocity, which is dependant upon gravitational settling, impaction and diffusion. All these processes are affected by aerosol size, wind speed, relative humidity and sea surface roughness (Duce *et al.* 1991). Duce *et al.* (1991) estimated dusts inputs to the ocean to be about $910 \times 10^{12} \text{ g y}^{-1}$ based on assigning an aerosol dust concentration for the entire world ocean and applying scavenging ratios (1,000 for the Pacific Ocean and 200 for the Atlantic ocean) and dry deposition velocities (2.0 cm s^{-1} in coastal regions and 0.4 cm s^{-1} in central

ocean regions). The difference between these two scavenging ratio is unclear, firstly it was postulated that the scavenging ratio for the Atlantic Ocean was calculated from unmatched data sets, rain and aerosol samples were collected several years apart; secondly that the vertical distribution of mineral aerosol is different between the North Atlantic Ocean and the Pacific Ocean. Moreover, using a 10 % solubility of iron in seawater from aerosols, Duce *et al.* (1991) estimated the global atmospheric deposition of iron to be $32 \times 10^{12} \text{ g y}^{-1}$. Subsequently, Duce (1995) and Prospero (1996) re-evaluated the use of the scavenging ratio, arguing that the application of a ratio of 1,000 to the entire ocean is inappropriate apart for the North Atlantic Ocean and that a value of 200 would be more realistic, based on precipitation measurements in Miami (Prospero *et al.* 1987). Kane *et al.* (1994) found scavenging ratios for iron between 90 to 390, which confirms the use of the lowest ratio value. Hence the revised total flux of dust was equal to $472 \times 10^{12} \text{ g y}^{-1}$ (de Baar and de Jong 2001; Jickells and Spokes 2001). Recently, Jickells *et al.* (2005) estimated the global production of dust to be $1,700 \times 10^{12} \text{ g y}^{-1}$. However, Goudie (2008) reported global dust production between 1,000 to $3,000 \times 10^{12} \text{ g y}^{-1}$. The efficiency of dry deposition will be influenced by the particle size (Jickells and Spokes 2001), the gravitational settling velocity and turbulent mix out, resulting in a lifetime ranging from 1.1 days for the largest size range (5.0 to $10 \mu\text{m}$) to 362 days for the smallest size range (0.1 to $1.0 \mu\text{m}$, Hand *et al.* 2004); for both particle size categories the lifetimes have previously been calculated to be 5.1 days (Luo *et al.* 2003).

Clearly there is considerable variability in the estimation of atmospheric deposition of dust and hence iron (Jickells *et al.* 2005). Duce (1995) and Prospero (1996) suggested that dry deposition exceeds wet deposition in most oceanic regions. Jickells and Spokes (2001) also stated that wet deposition contributes only 30 % of the total global atmospheric deposition of dust (Table 1.1), with an inter-oceanic basin contribution ranging from 23 % (S. Atlantic) to 34 % (N. Indian).

Hand *et al.* (2004) recently simulated the global distribution of dust in the atmosphere and predicted higher contribution of wet deposition compared with the observations (Table 1.2) using the Dust Entrainment And Deposition (DEAD) desert dust module (Mahowald *et al.* 2002; Zender *et al.* 2003), coupled with the Model of Atmospheric Transport and Chemistry (MATCH, Mahowald *et al.* 1997; Rasch *et al.* 1997).

Table 1.1. Estimates of dusts fluxes (10^{12} g y^{-1}) to the ocean by wet and dry depositions (adapted from Jickells and Spokes 2001). Scavenging ratio of 200 was used for all oceanic basins instead of 1,000.

Location	Wet deposition flux	Dry deposition flux	Percentage wet deposition flux/ total flux
North Pacific	68	140	33
South Pacific	5	14	26
North Atlantic	61	160	28
South Atlantic	3	10	23
North Indian	15	29	34
South Indian	6	12	33
Global total	158	360	33

Table 1.2. Percentage of wet deposition of the total deposition of mineral aerosols (Source Hand *et al.* 2004).

Location	Observations	Model	Reference
Bermuda	17 - 70	75 - 95	Jickells <i>et al.</i> (1998), Kim and Church (2001)
Amsterdam Island	35 - 43	75 - 95	Jickells and Spokes (2001)
Cape Ferrat, Med.	35	5 - 75	Guieu <i>et al.</i> (1997)
Enewetak Atoll	83	75 - 95	Arimoto <i>et al.</i> (1985)
Samoa	83	75 - 95	Arimoto <i>et al.</i> (1987)
New Zealand	53	75 - 95	Arimoto <i>et al.</i> (1990)
North Pacific	75 - 85	75 - 95	Uematsu <i>et al.</i> (1985)
Summit Greenland	63	50 - 75	Davidson <i>et al.</i> (1996)
Antarctica	90	50 - 95	Wolff <i>et al.</i> (1998)

The delivery of wet and dry deposition to the surface ocean therefore varies both spatially and temporally (Duce 1986). The dust flux is higher when rainfall and high atmospheric dust concentration are coincident. Wet deposition of mineral matter accounted for 80% of the total deposition measured at the SEAREX Pacific station (Uematsu *et al.* 1985). Indeed, the North Pacific and North Atlantic Oceans are the major sinks of dust by both types of depositions with 208 and 221×10^{12} g y^{-1} respectively

(Jickells and Spokes 2001) which had already been studied *in situ* by Jickells *et al.* (1998) and Sarthou *et al.* (2003). Dust production, transport and deposition processes are not only spatially variable but episodic in nature and associated with the propagation of dust storms at source (Prospero 1996). For example, Swap *et al.* (1996) estimated that 50 % of the total production of North African dust over the Eastern Mediterranean occurred during just 20 % of the year whilst Koçak *et al.* (2004) found that 74 % of dust events occurred in the same region during March – May and October whereas winter and summer accounted only for 22 and 4 % respectively. Half the annual dust depositions at Midway atoll in the North Pacific have been observed to occur in just a two week period (Prospero *et al.* 1989). However, dust production, transport and deposition depend upon climatic factors, particularly the atmospheric structure, which regulates uplift (Jickells *et al.* 2005), intensity of precipitation and wind strength (Goudie and Middleton 1992; Jickells *et al.* 2005). Dust production is proportional to the cube of wind speed (Duce 1995). Furthermore, dust production will depend on the source area, local geomorphological and climatic controls (Prospero *et al.* 2002). Details as to how dust production and transport influence global concentrations of iron in the marine aerosol are further discussed in section 1.2.

Riverine compartment

In coastal and shelf waters, substantial external inputs of iron originate from riverine sources and bottom sediments (Wells *et al.* 1995). Chester (2000) described comprehensively the river inputs of iron to the ocean and reported previous estimations of suspended sediment discharge and applied a global flux of $15.5 \times 10^{15} \text{ g y}^{-1}$ (Martin and Maybeck 1979) with the main input from Asiatic rivers (Hwang Ho and Ganges), the Amazon river being the third most important. The calculated contribution of iron to the particulate gross flux (transported to the marine boundary) was around $730 - 745 \times 10^{12} \text{ g yr}^{-1}$. Moreover, it was reported that the net flux of iron to coastal regions was 0.30 and $75 \times 10^{12} \text{ g y}^{-1}$ for dissolved and particulate iron with up to 95% of the riverine particles being

deposited in the coastal delta. In 2001, de Baar and de Jong estimated the global flux of suspended solids from rivers to be around $16 \times 10^{15} \text{ g y}^{-1}$, the distribution being regionally unbalanced: most of the fresh water entering the ocean system being represented by the Amazon, Orinoco, Congo and Mississippi inputs to the Atlantic Ocean whilst most of the bedload was accounted by the Asiatic rivers. Moreover, de Baar and de Jong (2001) reported that $6.5 \times 10^{12} \text{ mol y}^{-1}$ of iron resides within inert crystalline matrices, the remaining as metal oxide coatings on the particles and a small percentage may exist associated with organic fractions.

Hydrothermal compartment

These sources are located at mid-ocean ridges and back-arc basins and yield reductive dissolution of iron, Mn and other metals from the Mid Ocean Ridge Basalts (MORB) (de Baar and de Jong 2001). They are characterized by very high temperatures (350 – 400 °C) and pressures (~ 300 - 400 bar) and by strong reducing fluids which transfer large amounts of iron and other trace metals from the MORB (von Damm *et al.* 1985a; von Damm *et al.* 1985b; Elderfield and Schultz 1996). Typical concentrations of dFe in these extreme environments are around 1 - 3 mM. Von Damm and Bischoff (1987) reported an extremely high concentration of iron, 18.7 mM, for hydrothermal vent waters at the Juan de Fuca Ridge. However, generally lower concentrations, from 17 to 180 nM (von Damm *et al.* 1985b) and from 750 to 2,429 µM (von Damm *et al.* 1985a) of dFe can be found. Iron tends to be more concentrated in high temperature water; in lower water temperatures (200 - 300 °C), iron will have a lower removal rate from the MORB (de Baar and de Jong 2001). With the range of 1 - 3 mM, de Baar and de Jong (2001) estimated the overall inputs of iron from hydrothermal sources to be in the order of $30 - 90 \times 10^9 \text{ mol y}^{-1}$. In parallel, iron precipitates quickly, forming various mineral forms, mostly as oxyhydroxides (German *et al.* 1991) due to the mixture of ambient cold water (2 °C) and/or still within the seafloor. The result is the formation of ferromanganese deposits on the ridge crests

while very little of dFe remains in solution (de Baar and de Jong 2001). This source would therefore appear to be negligible in comparison with the other sources.

Upwelling and vertical mixing

Vertical mixing and upwelling is another important source of iron to the euphotic zone which varies markedly on spatial and temporal scales (Wells *et al.* 1995). Under upwelling conditions, iron from shelf sediments is transported to the surface (Johnson *et al.* 1999). By this transport mechanism shelf sediments are the primary source of iron to surface waters along the central Californian coast (Johnson *et al.* 1999; Fitzwater *et al.* 2003). For example, in Monterey Bay, Chase *et al.* (2005) investigated the effect of the upwelling centres in the north and south of the Bay on the concentrations of dFe and manganese in surface waters. After upwelling events, dFe concentrations doubled increasing from 3.5 nM and 0.7 nM in the north to 6 nM and 3.5 nM in the south part of the bay. In the upwelling system of central California, the amount of iron present in surface waters was found to be greater where the continental shelf is wide (north) than where it is narrow (south), (Chase *et al.* 2005). Iron supply to the surface waters in coastal upwelling systems is derived from shelf sediments and is predominantly associated with particles greater than 20 μm (Chase *et al.* 2005). In the northern and central part of the Peru suboxic upwelling system, Bruland *et al.* (2005) measured total dFe concentrations at 48 to 118 nM whilst in the southern part, values ranged from 1.4 to 4.6 nM. Moreover, Lohan and Bruland (2008) found high concentrations of total dFe off the west coast of the United States, in hypoxic upwelled waters. Off the coast of Washington, total dFe ranged from 32.2 ± 3.0 nM to 35.2 ± 7.2 nM at an inner and outer station whilst off the coast of Oregon, they observed concentrations ranging from 21.5 ± 2.1 nM to 33.5 ± 7.4 nM at an outer and inner station.

Biotic compartment

In HNLC regions, the largest reservoir of iron in the surface water may be the biota itself (Wells *et al.* 1995). This biological pool of iron is recycled within the euphotic zone by grazing, excretion and viral lysis and is then released to the deep water by bacterial degradation (Redfield *et al.* 1963) and can be reintroduced to the euphotic zone via upwelling and mixing turbulence, on a time scale of days (Hutchins *et al.* 1993). Indeed, the acidic conditions in the gut pathway of zooplankton organisms are more favourable for iron dissolution (Hutchins *et al.* 1993; Hutchins and Bruland 1994) and this may affect the external iron-oxide coating on mineral particles (de Baar and de Jong 2001) but also the external ferromanganese oxide coatings of pelagic bacteria which may be partially dissolved (Cowen and Silver 1984; Cowen and Bruland 1985). This “regenerated” iron input to surface waters is estimated to be more than an order of magnitude greater than the external supply of iron (Wells *et al.* 1995). Moreover, iron from coastal sediments can be regenerated by the acidic conditions and the enzymes present in the guts of organisms (Turner and Olsen 2000; Turner 2006). In the Sargasso Sea, despite the greater abundance of photosynthetic prokaryotes, heterotrophic bacteria appear to contribute substantially to the biological iron pool, constituting between 30 and 50 % of the iron stocks in producers (Tortell *et al.* 1999). DFe is also removed from seawater via direct assimilation by phytoplankton (Sunda 2001) and it is the largest sink of dFe from the surface ocean (de Baar and de Jong 2001). In subarctic Pacific waters, eukaryotic microalgae are responsible for 50 % of the dFe uptake and phototrophic and heterotrophic bacteria account for 30 % and 20 % (Tortell *et al.* 1996).

In summary, iron and the elements N and P can be controlled by biological uptake and regeneration cycles (Martin and Gordon 1988). After assimilation by phytoplankton and bacteria within the euphotic zone, iron is transported downwards by the settling of a portion of the standing stock of phytoplankton (e.g. for large diatom frustules, Wefer *et al.* 1988; Quéguiner *et al.* 1997) or faecal matter which reaches the seafloor (Scharek *et al.*

1999a; Scharek *et al.* 1999b). Depending on the composition of the inert mineral fraction contained within, their settling velocity will be enhanced or decreased (Ittekkot 1993).

Aggregation and precipitation

Iron complexes with inorganic and organic ligands (FeL_i) and is also present in colloidal and/or particulate forms (Bruland and Rue 2001, see section 1.1.3). Iron may sorb onto colloidal organic matter which is abundant in seawater (Wells and Goldberg 1992; 1994). Sinking macro organic particles, such as dead phytoplankton or faecal matter, can scavenge soluble iron from surface waters (Morel and Hudson 1985). However as described above, iron may also be released at depth by bacterial degradation (Redfield *et al.* 1963; Tortell *et al.* 1999) and resuspended in the euphotic zone via upwelling or turbulent mixing, on a time-scale of days (Hutchins *et al.* 1993).

1.1.3. Iron concentrations in the open ocean

Depending upon the relative contributions of the different sources and sinks, iron concentrations in the open ocean can vary spatially and / or temporally. Many studies have been carried out within different regions of the world's oceans and Table 1.3 summarises the literature of dFe concentrations in marine waters.

Table 1.3. Dissolved iron concentrations (nM) in the world ocean.

Locations	dFe concentrations (nM)	Reference
<u>Pacific Ocean</u>		
subarctic North	~ 0.5	Martin <i>et al.</i> (1989)
subtropical Central North	0.05 - 0.08	Martin and Gordon (1988)
equatorial	~ 0.2 and dissolved inorganic iron ~0.07 pM 0.4 and 1 (1000 - 5000 m) 0.05 , 0.35 (220 m)	Rue and Bruland (1995) Landing and Bruland (1987) Coale <i>et al.</i> (1996)
<u>Atlantic Ocean</u>		
northern North Sea	0.3 (20 m) to 8.5 (10 m)	Gledhill <i>et al.</i> (1998)
open ocean	0.07-0.17 to 0.9 (deeper water)	Martin <i>et al.</i> (1993), Wu and Luther (1994)
open northwest	0.15 - 0.25 (colloidal iron), 0.2 - 0.9 (dFe)	Wu and Luther (1994)
east	0.5-10 (unfiltered samples)	Powell <i>et al.</i> (1995)
north-south Atlantic Ocean	0.3 and 4.5 and 0.3 and 3.0 for (unfiltered samples)	Bowie <i>et al.</i> (2002a)
south-west	0.4-1.4, (typical values 0.6 - 0.8)	Vink and Measures (2001)
equatorial	0.28 and 0.71 (0.55 ± 0.14)	Powell and Donat (2001)
north-south transect in the eastern	0.02 to 1.1 (0.28 ± 0.21)	Sarthou <i>et al.</i> (2003)
offshore waters of the Pacific, Atlantic and Southern Ocean	0.07 ± 0.04 (< 200 m) and 0.76 ± 0.25 (> 500 m)	Johnson <i>et al.</i> (1997)
<u>Southern Ocean</u>		
Ross Sea	0.72 (base mixed layer - 2.3 surface (sea ice), 0.16 - 0.17 (ice-free)	Sedwick and DiTullio (1997)
Indian sector	0.4 (surface) and 6.2 (250 m)	Sarthou <i>et al.</i> (1997)
Kerguelen Plateau	12.6 (inshore) to 0.3 (offshore)	Bucciarelli <i>et al.</i> (2001)
Pacific sector	0.05 (surface), up to 0.2 - 0.3 (depth)	Coale <i>et al.</i> (1999)
Polar front	0.06 ± 0.02 (mixed layer), 0.04 (1000 m)	Nishioka <i>et al.</i> (2005)
Scotia front	2 (surface), 4 (100 and 400 m), 2.5 (deep water)	Nolting <i>et al.</i> (1991)
<u>Mediterranean Sea</u>		
Ligurian Sea, DYFAMED station	4.8 (autumn), < 0.13 to 0.6 at depth (spring)	Sarthou and Jeandel (2001)
Ligurian Sea, DYFAMED station	0.39 - 1.42 (exclusion of contaminated samples)	Guieu <i>et al.</i> (2002a)
Ligurian Sea, MIO station	0.13 - 1.99 (exclusion of contaminated samples)	

In seawater, iron exists in different physico-chemical forms, e.g. dFe and particulate forms which are operationally defined by membrane filtration techniques (0.2 - 0.4 μm). Iron associated with the 0.02 - 0.4 μm fraction was defined as "colloidal iron" (Wu and Luther III 1994; Wu *et al.* 2001) whilst Bruland and Rue (2001) defined it as the fraction between 10 nm and 0.2 μm . More recently Hiemstra and van Riemsdijk (2006) redefined the colloidal fraction as the fraction present between 0.025 and 0.2 / 0.4 μm . Nishioka *et al.* (2001) showed that more than 10 % of dFe in the open ocean is present in the small colloid size fraction (200 kDa - 0.2 μm). Hiemstra and van Riemsdijk (2006) compiled the data of Wu *et al.* (2001) and found that the amount of iron in the colloidal fraction contained 30 to > 50 % of the total iron that passed through a 0.4 μm filter.

Furthermore, dFe exists in two oxidation states: Fe(II) and Fe(III). Fe(III) in seawater can be reduced to Fe(II), which is more soluble but thermodynamically unstable under oxic conditions, more labile and forms much weaker organic chelates (Sunda 2001). In contrast, Fe(III) predominates in oxygenated waters but is highly insoluble owing to the formation of iron oxyhydroxides (Sunda 2001; Waite 2001). The oxyhydroxide species such as $\text{Fe}(\text{OH})_3$ are rapidly scavenged out of the water column by coagulation and adsorption onto sinking particles (Tortell *et al.* 1999). As a result, the residence time of iron in the oceans is very short, being around 100 years (Donat and Bruland 1994). Johnson *et al.* (1997) revealed that the presence of high affinity organic ligands, which specifically complex with Fe(III), increase its solubility by enhancing the dissolution of colloids, hence reducing both the scavenging rates and residence times. These organic ligands are thought to be bacterial siderophores, highly specific compounds utilized for iron acquisition (Winkelmann 1991). The chemical speciation of iron may determine the extent to which it can be taken up by phytoplankton (Hudson and Morel 1990). Indeed, diatoms are able to utilize iron bound to a number of organic chelators including siderophores via a cell surface reductase mechanism (Maldonado and Price 1999). Both autotrophic and heterotrophic plankton are apparently able to take up iron bound to desferrioxamine B

and E, and large phytoplankton species are able to reduce the iron in the chelates extracellularly (Tortell *et al.* 1999). Hence an understanding of the chemical speciation of iron is essential in defining its cycling and transport in the oceans.

Photoreduction of organic siderophore-bound iron has been investigated by Barbeau *et al.* (2001). Photolysis of certain Fe(III)–siderophore complexes (strong ligand L_1 ; $K_{\text{cond}} = 10^{12.5 \pm 0.03} \text{ M}^{-1}$) leads to the formation of a weaker ligand L^* ($K_{\text{cond}} = 10^{11.6 \pm 0.2} \text{ M}^{-1}$) and the reduction of Fe(III) to Fe(II), increasing the availability of siderophore-bound iron for uptake by phytoplankton species (Figure 1.2). This cycle involves photolysis of Fe(III)–ligand complexes, with the reduction of Fe(III) to Fe(II) and the oxidation of the ligand L to L' (oxidised form) is shown as L^* in Figure 1.2. Fe(II) may then undergo biological uptake, oxidation to Fe(III) or oxidation with subsequent complexation by strong organic ligands L' .

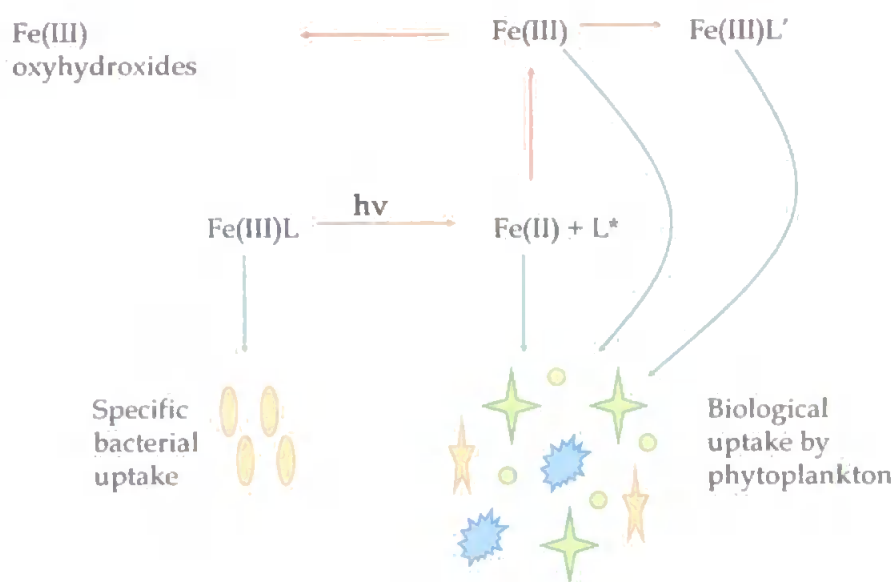


Figure 1.2. Photochemical cycling of iron in seawater (adapted from Barbeau *et al.* 2001).

Fe(III) sequestered by ligands can be released in the euphotic zone following photoreduction by ultraviolet (UV) radiation. Photoreduction of iron can increase the concentration of Fe(II) (Waite *et al.* 1995), enhance its solubility in seawater and hence its bioavailability to phytoplankton (Hong and Kester 1986; Moffett 2001). Above 99 % of

iron is reported to be organically complexed in the ocean (van den Berg 1995; Gledhill *et al.* 1998). Organic complexation increases the solubility of iron in seawater (Kuma *et al.* 1996). For example, Kuma *et al.* (1996) observed a decrease in iron solubility in coastal seawater from 1.56 to 0.52 nM and from 0.27 to 0.18 nM for oceanic seawater that was UV irradiated (pH ranging from 7.8 to 8.2). There is evidence that the higher solubility in coastal seawater is due to higher concentrations of organic ligands (Buck *et al.* 2007).

The major inputs of Fe(II) are atmospheric deposition (Zhuang *et al.* 1992b), diffusion from sediments (Hong and Kester 1986), photoreduction of iron chelates and iron hydroxides and oxides (Waite and Morel 1984; Miller *et al.* 1995; Vöelker and Sedlak 1995; Waite *et al.* 1995), bioreduction at cell surfaces (Maldonado and Price 1999; 2000) and chemical or microbiological reduction in reducing environments. After photoreduction, Fe(II) is less strongly bound to chelates and/or oxyhydroxides and organic ligands are degraded (Faust and Zeep 1993) and have a lower binding affinity. After its release, inorganic Fe(II) can be reoxidized by O₂ or photochemically produced H₂O₂ (Millero and Sotolongo 1989). Fe(III) resulting from this process may then be chelated once more with organic ligands or precipitated as iron hydroxides.

1.2. SPATIAL AND TEMPORAL VARIABILITY OF IRON IN THE MARINE AEROSOL

Generally, the overall composition and concentration of any trace element in an aerosol population is controlled by, (i) the predominant type of aerosol source (anthropogenic or crustal), (ii) the emission strengths of the contributing sources, (iii) chemical and physical (wet and dry deposition) modifications of the aerosol population during transport and (iv) atmospheric transport processes (influenced by meteorological processes). These influences have been confirmed by a large body of work defining aerosol concentrations both in coastal and open ocean environments (e.g. Duce *et al.* 1991; Yaaqub *et al.* 1991; Chester *et al.* 2000; Spokes *et al.* 2001). The concentration of iron in the marine aerosol is directly related to the transport of mineral dust to the open ocean

atmosphere and hence exhibits both large spatial and temporal gradients (see section 1.1.2). Not surprisingly highest recorded concentrations of iron in the marine aerosol are associated with marine systems bordering / surrounded by arid continental regions, e.g. Red Sea (Orif 2008), Western Mediterranean (Chester *et al.* 1991) and Eastern Mediterranean (Koçak *et al.* 2004). Therefore concentrations exhibit spatial gradients as a result of such influences, for example iron aerosol concentrations in regions influenced by northern Saharan dust show a decrease in the order Atlantic North East Trades > Red Sea > Southern Levantine Basin > Northern Levantine Basin > Western Med. (Table 1.4).

Table 1.4. Marine aerosol iron concentrations (ng m^{-3}) in contrasting marine systems (expressed as the geometric mean).

Location	Iron aerosol concentrations (ng m^{-3})	Seasonal variations	Reference
Atlantic North East Trades (n= 7, open ocean sampling)	3,865		Murphy (1985)
Red Sea (coastal sampling)	2,262	Winter = 1470 Summer = 3150	Orif (2008)
Eastern Med. South. Levantine Basin (coastal sampling)	787		Herut <i>et al.</i> (2001)
Eastern Med. North. Levantine Basin (coastal sampling)	407	Winter = 251 Transitional = 751 Summer = 568	Koçak <i>et al.</i> (2004)
Western Mediterranean	320		Chester <i>et al.</i> (1990)
Irish Sea	159		Fones (1996)
English Channel	115		Wells (1999)
North Pacific	17 (Enewatek)		Duce <i>et al.</i> (1983)
South Atlantic	2.6		Murphy (1985)
South Pacific	0.21 (Samoa)		Arimoto <i>et al.</i> (1987)

Within these regions, temporal / seasonal differences have been detected as a result of dust disturbance and transport being influenced by meteorological processes. For example Orif (2008) observed iron aerosol concentrations at the Saudi Arabian coast (Jeddah) to be $3,150 \text{ ng m}^{-3}$ and $1,470 \text{ ng m}^{-3}$ for the summer and winter respectively,

representing a seasonal enrichment of 2.1. Peak activity and dust re-suspension in the Arabian Peninsula occurred during June-July.

Over the Northern Levantine of the Eastern Mediterranean iron aerosol concentrations are greatest during the transitional period (March - May, October) compared with those detected in the summer and winter months: transitional period 751 ng m⁻³; winter 377 ng m⁻³, summer 568 ng m⁻³, Koçak *et al.* 2004). African mineral dust is transported over the Mediterranean with northward winds generated by depressions (Alpert *et al.* 1990; Moulin *et al.* 1998). Studies have shown that the frontal region of these depressions can generate intense dust mobilization over North Africa and are able to transport dust over long distances to the eastern Mediterranean (Kubilay and Saydam 1995; Kubilay *et al.* 2000; Koçak *et al.* 2004), and beyond; e.g. south-eastern United States (Prospero 1999), Italy (Bonelli *et al.* 1996). Moulin *et al.* (1998) has summarized this cyclogenesis such that during the spring and early summer Saharan thermal lows (or Saharan cyclones) develop south of the Atlas mountains, under the influence of the strong thermic contrast between the temperature of the cold marine waters and the warm continental surfaces. Such cyclones move eastward along this thermal gradient just south of the North African coast and finally cross the Mediterranean and transport large quantities of desert dust to Libya and Egypt.

The open ocean exhibits generally much lower iron aerosol concentrations with the lowest being detected in the Southern Atlantic and Pacific oceans, 2.6 and 0.21 ng m⁻³ respectively (Murphy 1985; Arimoto *et al.* 1987). In contrast however the Northern Atlantic periodically experiences intense Saharan dust events, elevating the open ocean marine aerosol iron concentrations, e.g. > 3,000 ng m⁻³, Murphy 1985; > 1,500 ng m⁻³ (Chen and Siefert 2004). The mineral dust plumes are transported by trade winds from the Sahel region of North Africa (Gao *et al.* 2001; Chen and Siefert 2004); and lie around 20 °N in the summer moving to 5 °N in the winter months (Husar *et al.* 1997; Moulin *et al.* 1997). The

impact on primary productivity and phytoplankton community structure in the surface of the North Atlantic of such dust events have been the focus of previous studies (Baker *et al.* 2003; Mills *et al.* 2004).

The spatial and temporal aerosol iron concentrations in the marine aerosol, as discussed above, will therefore have an impact on both the wet and dry deposition of iron from the atmosphere to the sea surface. As a result of these variable inputs, balanced by particulate removal through the water column, surface seawater iron concentrations will also exhibit spatial and temporal gradients (Table 1.5, Wells *et al.* 1995). In addition to aerosol iron loadings and subsequent deposition, the contribution of atmospheric inputs of dust to the dFe pool in surface seawater will also depend upon the solubility of the aerosol associated iron. Literature values of the soluble iron (and Fe(II)) from aerosol material are presented in Table 1.5 respectively.

It is apparent from Table 1.5 that a high degree of variation in the percentage of seawater soluble iron from aerosol material has been reported. Solubilities range from <1 to 30 %. This variability is a result of, (i) environmental factors and (ii) different experimental approaches adopted by different authors. These factors are reviewed in detail in sections 1.3. and 1.4. The uncertainty in the “correct” seawater solubility of iron in the marine aerosol is as important as the uncertainty in the variability of dust fluxes in determining the atmospheric bioavailable inputs of iron to the open ocean (Mahowald *et al.* 2005). Thus a better understanding of the processes influencing the solubility of aerosol iron is essential both during atmospheric transport and subsequent post-deposition to the sea surface (Jickells *et al.* 2005).

Table 1.5. A summary of studies investigating the solubility of aerosol iron including the matrix and filters used, parameters considered and the adopted analytical technique. CRM: certified reference material, PC: polycarbonate membrane, PP: polypropylene filter, What.: Whatman fibrous cellulose acetate filter, 20 µm.

Matrix / Filter	Parameters	Technique	Solubility range (%)	Origin, conditions	References
seawater/ What. 40	incubation for 3 h	FAAS	< 1 % 1 %	mixed, Mexican urban, N. American	Hodge <i>et al.</i> (1978)
seawater/ coal fly ash	incubation for 1 and 24 h, constinuously stirred, temperature and pH controls	gamma counted on Ge(Li) diode	7.5 ± 0.5 % 3.5 ± 0.5 %	marine, N. American, 1 h incubation marine, N. American, 24 h incubation	Crecelius (1980)
seawater/ What. 41 and CRM	neutron activation of particulate and incubation for 1h, light/dark, continuously stirred	liquid scintillation counter	6 % 1 %	urban N. American NIST 1648	Hardy and Crecelius (1981)
seawater/ What. 41	incubation for 1 h	FAAS	< 1 % < 1 % 6 % (1 to 18 %) 2 % (1 to 2 %)	West Africa, crustal mixed, west. Med. And Cape Verde urban-rich from UK west. Mediterranean	Chester <i>et al.</i> (1993)
Milli-Q water/ What. 41	shaken for 1 h	GFAAS	1 % (0.1 to 13 %)	west. Mediterranean	Guernozi <i>et al.</i> (1999a)
seawater/ dust and CRM	particle concentration effect, incubation 24 h to 7 days	FI-CL	0.04 - 1.6 % 0.45 - 2.2 %	Saharan, 7 days, 10 - 0.01 mg L ⁻¹ NIST, 7 days, 10 - 0.01 mg L ⁻¹	Bonnet and Guieu (2004)
seawater/ PP	instantaneous solubility	ICP-MS	6 ± 5 % (0.26 to 26.3 %)	Asian	Buck <i>et al.</i> (2006)
Milli-Q water/ PP			9 ± 8 % (0.20 to 52.3 %)	Asian	
ammonium acetate leach, pH 4.7/ What. 41	release in upwelled waters	ICP-OES and GFAAS	1.2 % (0.5 - 4.1 %)	Saharan	Baker <i>et al.</i> (2006a)
			2.7 % (1.9 to 54 %)	S. Atlantic	Baker <i>et al.</i> (2006c)

Continued

Matrix / Filter	Parameters	Technique	Range solubility		References
Milli-Q water/ PC seawater/ PC	30 min sonication	ICP-OES	5 % (0.5 to 19 %) 0.7 % (0.003 to 2 %)	Saharan/ Arabian Pen. Saharan/ Arabian Pen.	Chen <i>et al.</i> (2006)
Milli-Q water/ PC	instantaneous solubility, particle concentration effect	FI-CL	0.44 % to 19 % (~ 0.5 to ~ 5 nmol m ⁻³)	Saharan and N. Am., ~ 0.5 to ~ 5 nmol m ⁻³	Sedwick <i>et al.</i> (2007)
seawater/ dust and CRM	incubation 24 h to 8 days, particle effect concentration	FI-CL	0.001 to 0.04 %	6 Saharan-type, 10 to 0.1 mg L ⁻¹	Milne (2007)
seawater/ PC	semi-continuous flow- through reaction chamber	ID-ICPMS	0.05 to 2.4 % 1.9 to 5.9 % 2.4 to 9.5 %	Trop. Atlantic N. Atlantic N. Pacific	Wu <i>et al.</i> (2007)
seawater/ dust	incubation from 1 to 35 days	ICP-MS	0.03 to 15 % (Saharan) 0.2 to 30 %	Saharan American	Mendez <i>et al.</i> (2009)
Milli-Q water/ PC seawater/ PC	semi-continuous flow- through reaction chamber	ID-ICPMS	1.3 % to 19.6 % 1.3 to 1.4 %, to 13.1 %	Gulf of Alaska and N. Pacific N. American urban and N. Pacific	Aguilar-Islas <i>et al.</i> (2009)
UV-seawater/ PC seawater/ PP	instantaneous solubility	ICP-MS	1.6 % 9 ± 5 %	N. American urban N. Atlantic	Buck <i>et al.</i> (2009)
Milli-Q water/ PP			15 ± 8 % (3 to 47 %)	N. Atlantic	
Milli-Q water /What.41	shaken 0.5 h/rest 0.5 h	ICP-MS	7.7 ± 4.5 %	Asian	Hsu <i>et al.</i> (2009)

1.3. FACTORS IMPACTING ON SOLUBILITY

Bioavailability of atmospherically delivered iron, as stated above, is dependent on its aerosol solubility in seawater, which is potentially controlled by a number of different factors. These may be divided into three broad categories: chemical, physical and biological. The following sections review how each of these factors may impact upon the aerosol iron solubility in seawater. Where data are lacking on the impact of these parameters on the solubility of aerosol iron in seawater, others metals are discussed.

1.3.1. Chemical factors

A well established factor affecting aerosol metal solubility in seawater is the particle concentration. This has been highlighted in a number of recent studies (Spokes *et al.* 1994; Spokes and Jickells 1996; Biscombe 2004; Bonnet and Guieu 2004; Milne 2007). For example, Bonnet and Guieu (2004) highlighted a decrease in the seawater solubility of iron with increasing particle concentration. Aerosol iron seawater dissolution studies maintained over a period of 7 days produced the highest solubilities in seawater of 1.6 % and 2.2 % of dFe for Saharan and urban particles respectively when the particle concentration was at its lowest (0.01 mg L^{-1}). In contrast the lowest iron solubilities in seawater, 0.04 % and 0.45 %, for Saharan and urban aerosols, respectively were observed at the highest particle concentration (10 mg L^{-1}). The importance of scavenging of dFe onto particle surfaces at enhanced dust concentrations was described, such that the rate of re-adsorption can be equal to the rate of dissolution and so induce a net dissolution rate of zero. Spokes and Jickells (1996) also indicated a decrease in the solubility of iron with increased dust particle concentrations using de-ionized water. With aerosol concentrations less than 0.5 mg L^{-1} , the solubility of iron present in the aerosol material was 7 % and decreased to ~1.4 % at an aerosol particle concentration $> 0.12 \text{ g L}^{-1}$. More recently Milne (2007) carried out *in situ* incubation studies of a range of Saharan dusts in seawater. The dust concentrations varied from 0.1 to 10 mg L^{-1} for 24 h and 8 days exposure times. Owing to a limited release of iron in seawater from the dusts after 24 h,

the solubilities were calculated for the dusts after 8 days exposure. Solubilities varied from 0.02 % at 0.1 mg dust L⁻¹ seawater to 0.001 % at 10 mg dust L⁻¹ seawater. The effect of particle concentrations was clear within this range of dust concentrations. Therefore, it is crucial, when carrying out iron seawater dissolution studies, that the lowest practical particle concentration (0.25 – 0.5 mg L⁻¹) is applied, as it is more representative of natural conditions and hence yields more realistic solubility data.

Following atmospheric deposition aerosols encounter the sea surface micro-layer, rich in organic matter which may complex strongly with trace metals. Lead (Musani *et al.* 1980; Maring and Duce 1990), aluminium, copper (Maring and Duce 1987; 1989), iron (Zhuang *et al.* 1990) have all shown enhanced solubilities up to 50 % in surface seawater containing relatively high concentrations of organic material. The presence of organic matter, in aerosols and seawater, has the potential to increase the rate of Fe(III) photoreduction and hence enhance its solubility but also, through Fe(II) complexation, diminish its rate of re-oxidation (Theis and Singer 1974, see section 1.1.3). Dissolved organic carbon (DOC) is variable, both in its concentration and its chemical composition in marine systems (Cauwet 1994; Chester 2000), over both temporal and spatial scales. Previous metal aerosol dissolution experiments have been conducted under high ($389 \pm 7 \mu\text{mol kg}^{-1}$) and low ($33 \pm 2 \mu\text{mol kg}^{-1}$) dissolved organic carbon concentrations (Maring and Duce 1987; 1989; 1990). Their results indicated that dissolved organic material complexed lead and copper, enhanced the aerosol solubility of these metals and also increased the trace metal dissolution rates (Maring and Duce 1989; 1990). The presence of strong iron complexing ligands in seawater has been shown after fertilization experiments (e.g. Rue and Bruland 1997; Boye *et al.* 2005). Rue and Bruland (1997) pointed out that an enhancement of the phytoplankton activity leads to a greater degree of complexation of iron by two broad groups of organic ligands: (i) stronger ligands L_1 having conditional complexation stability constants of the order of $K' = 5 \times 10^{12} \text{ M}^{-1}$ and (ii) weaker ligands L_2 , $K' = 6 \times 10^{11} \text{ M}^{-1}$.

In addition, the complexation of iron by organic ligands has been observed during other studies, including those initial studies of Haygood *et al.* (1993) and Gledhill and van den Berg (1994). For example Maldonado and Price (1999) and Barbeau *et al.* (2001) have shown that it is likely that siderophores contribute to the complexing capacity of iron in seawater; these complexing ligands are characterized by strong conditional stability constants (Table 1.6). Furthermore, Kraemer (2004) confirmed that the presence of natural siderophores enhanced the solubility of iron oxide surfaces, via organic complexation. Aguilar-Islas *et al.* (2009) more recently has investigated the effect of the iron complexing ligand Desferal (Desferrioxamine B) on the dissolution rate of iron from urban material collected in north America and found a twofold increase compared to the control without addition of Desferal.

Table 1.6. Conditional stability constants for FeL complexes for different oceanic regions. * data taken from Witter *et al.* (2000).

Location	Stability constant log K'	Reference
Menai Straits, Wales	21.2 ± 2.3	Gledhill and van den Berg (1994)
Atlantic Ocean	from 18.8 ± 0.1 to 19.7 ± 0.5	
S. and Eq. Atlantic Ocean	surface: 12.2 ± 0.9 depth: 13.0 ± 0.7	Powell and Donat (2001)
NW. Atlantic Ocean	23.22 ± 0.27 and 23.38 ± 0.27	Wu and Luther III (1995)
NW. Atlantic Ocean	from 20.8 to 23.0 ± 0.2	Witter <i>et al.</i> (2000)
northern North Sea	21.4 ± 0.3	Gledhill <i>et al.</i> (1998)
central N. Pacific Ocean	23.1 ± 0.6 for L ₁ 21.5 ± 0.6 for L ₂	Rue and Bruland (1995)*
Eq. Pacific Ocean	23.7 for L ₁ and 22.8 for L ₂	Rue and Bruland (1997)*
W. Mediterranean Sea	surface: 21.3 ± 1.3 (n= 4) depth: 21.4 ± 0.6 (n= 23)	van den Berg (1995)
Arabian Sea	from 21.6 ± 0.1 to 22.5 ± 0.9	Witter <i>et al.</i> (2000)
Southern Ocean	from 21.1 to 22.2	Nolting <i>et al.</i> (1998)

Aerosol associated iron dissolution in seawater may also be influenced by the aerosol solid phase association (i.e. its solid state speciation, Table 1.7). For example, urban aerosol material exhibits generally higher iron solubilities compared with crustal dominated aerosols; around 10 % and less than 4 % respectively (Chester *et al.* 1993; Spokes and Jickells 1996; Bonnet and Guieu 2004). Chester *et al.* (1993, 1994) and Koçak *et*

al. (2007) attributed this enhanced dissolution to the nature of the trace metal solid phase association in the aerosol material. Using a three stage sequential leach scheme it has been possible to differentiate, chemically, iron associated between three different aerosol solid phases: “exchangeable”, “carbonate/oxide” and “residual” (Chester *et al.* 1989; Chester *et al.* 1994; Koçak *et al.* 2007).

Table 1.7. The solid stage speciation signals of iron in contrasting aerosol types (expressed as a percentage of the total metal). ¹ Chester *et al.* (1994), ² Chester *et al.* (1989), ³ Koçak *et al.* (2007). S1= “exchangeable”, S2= “carbonate and oxide, S3= “residual”. LUAP= Liverpool Urban Aerosol particulate.

	North Sea ¹	LUAP ²	Saharan Crust ²	Eastern Med. "Saharan" ³	Eastern Med. "Anthropogenic" ³
S1	6.5	9.9 ± 6.2	0.03 ± 0.003	0.9 ± 0.6	2.6 ± 1.1
S2	11	31.9 ± 11.8	9.5 ± 2	2.9 ± 1.6	7.2 ± 3.2
S3	82.5	58.2 ± 12.2	90.5 ± 2	96.2 ± 2.2	90.2 ± 3.2

It is apparent from Table 1.7. that urban dominated aerosol material is characterized by having greater “exchangeable” (2.6 to 9.9 %) and “carbonate / oxide” (7.2 to 32 %) phases in comparison with aerosols dominated by Saharan dust, 0.03 to 0.9 % in the “exchangeable” and 2.9 to 9.5 % in the “carbonate / oxide” phases respectively. A similar trend was observed by Baker *et al.* (2006c) in aerosol samples collected from the North Atlantic. Using a leach solution of 1 M ammonium acetate (pH= 4.7, equilibrating filters for 1 - 2 h) they observed contrasting solubilities between Saharan and non-Saharan dominated aerosol populations: Saharan population mean = 1.7 % (range 1.4 - 4.1%); non-Saharan population, mean = 7.8 (range 4 - 19, with 3 samples peaking at 21, 15 and 54 %). Bonnet and Guieu (2004) used iron-rich Saharan mineral soil and anthropogenic particles (4.5 and 3.9 % of iron respectively) in their studies. They attributed the greater solubility of iron (and other metals) in urban aerosols to the higher association of iron with the exchangeable and oxide solid phases located on the surface of urban particles, whereas for crustal material, iron is predominantly found chemically bound with the refractory aluminosilicate solid phase.

Moreover, the nature of the mineral, e.g. clay, feldspar or iron oxide, impacts on the potential release of iron in seawater and rainwater. Journet *et al.* (2008) investigated the dissolution of various minerals in rainwater (Table 1.8). Iron bonded with oxygen (Magnetite, Goethite and Hematite) have the lowest solubilities whereas the highest solubilities were observed in feldspar, iron present as impurities.

Table 1.8. Mineral nature, class and iron present with its solubility (from Journet *et al.* 2008)

Mineral	Class	Case	Fe fraction (% w/w)	Fe soluble (%)
Case A				
Magnetite	Iron oxide	Fe in strong O-Fe lattice bonds	77.4	0.003
Goethite	Iron hydroxide		62.9	0.005
Hematite	Iron hydroxide		57.5	0.010
Case B				
Nontronite	Clay	Fe located in Al and Si layers	23.0	0.34
Beidellite	Clay		6.5	0.34
Case C				
Orthoclase	Feldspar	Ionic bonds hold Fe in lattice	0.13	5.25
Illite	Clay		3.38	1.39
Montmorillonite	Clay		2.55	2.6
Case D				
Oligoclase	Feldspar	Fe in form of impurities	0.54	0.76

During atmospheric transport aerosols are exposed to condensation and evaporation cycles, which can lead to very low pH due to HNO_3 and H_2SO_4 uptake and SO_2 oxidation; values as low as pH 2.2 in clouds have been observed (New York State), (Spokes *et al.* 1994). Aerosols typically experience ~ 10 condensation / evaporation cycles in clouds before rainout (Spokes *et al.* 1994). The final pH of precipitation ranges between 4 and 7 but may not reflect the pH conditions in the atmosphere (Spokes and Jickells 1996). Maring and Duce (1987, 1989, 1990) investigated the effect of pH on aluminium, copper and lead solubilities in Barbados aerosol particles. Rainwater, characterized by lower pH than seawater, increased the dissolution of aerosol metals, aluminium and lead (Maring and Duce 1987, 1990), by up to 17 % (Colin *et al.* 1990). For Saharan dust, the greatest dissolution of iron was observed at pH 2 (4.7 ± 0.2 %) whilst an increase of pH to

5.5 decreased the solubility to 0.3 %. DFe concentrations decreased further on increasing the pH to 8 (~0.01 %, Spokes and Jickells 1996). This pH-dependant release is consistent with the findings of Spokes *et al.* (1994) who observed an urban aerosol released 12 % of its total iron at a pH 2, whilst Saharan material released 5.5 %. Indeed, the solubility for Saharan particles in cloudwater increased to ~5 % (Spokes & Jickells 1996) and 17 % for urban particles (Dedik *et al.* 1992). Recently, Theodosi *et al.* (2008) investigated the solubility of iron by dissolving aerosol samples in polluted rain (pH 4 – 5) and Saharan-influenced rain at a pH close to 8 (Mahowald *et al.* 2005). They observed contrasting solubilities of 27.2 % in polluted rain and 0.5 % in Saharan-influenced rain.

1.3.2. Physical factors

Biscombe (2004) investigated the effect of seawater temperature and stirring rates on the dissolution of aerosol associated metals in seawater. Lead (Pb) and zinc (Zn) solubilities in seawater were shown to increase with temperature. The observed solubility of Zn was at least 5 % higher for equatorial oceanic temperatures than for high latitude temperatures (25 °C and 5 °C respectively). Moreover, low mixing rates increased the solubility of both zinc and lead whilst higher mixing rates lowered their solubilities. This was explained by the frequency of collisions between dissolved species and particle surfaces which would enhance the probability of metal particle re-adsorption. Based on this study, the solubility of iron in seawater could be impacted by the temperature and the stirring rate, with increasing solubility with increasing temperature and low stirring rate.

Light may also affect iron dissolution by photoreduction. A number of studies have investigated this effect on dFe in seawater (Hong and Kester 1986; O'Sullivan *et al.* 1991; Johnson *et al.* 1994) using mineral particulates from the atmosphere (Zhu *et al.* 1997). Indeed, the photochemical process (or photoreduction), taking place in mineral particles suspended in the atmosphere, may reduce Fe(III) to Fe(II) and increase its solubility in seawater and hence its bioavailability for phytoplankton (Hong and Kester 1986; Moffett

2001). This process can occur at low pH (~ 3.5) through the hydrated forms of Fe^{3+} and FeOH^{2+} . The reaction provides an important source of Fe^{2+} but also OH radicals (Graedel *et al.* 1985). Under certain conditions, Fe(II) complexation by organics can retard the rate of its reoxidation to Fe(III) and so prolong iron availability in aqueous environment (Theis and Singer 1974). Spokes and Jickells (1996) used natural sunlight and a solar simulator during their photoreduction solubility experiments in Milli-Q water using Saharan and urban dusts. They simulated light and dark conditions and found an enhancement of Fe(II) production in the light compared with the dark but this also depended on the origin of dust. Indeed, soluble Fe(II) comprised 0.9 % in the light and 0.25 % of the total iron in the aerosol in the dark for the Saharan dust whilst in urban originated dusts, soluble Fe(II) was present at 8.4 % in the light and 2.1 % of the total iron in the aerosol in the dark. Subsequently, Zhu *et al.* (1997) evaluated the effects of light on soluble ferrous iron (FeI_s) and total soluble iron (FeT_s) concentrations from aerosol filter samples collected in Barbados, using acidified sodium chloride solution, during day/night cycles. They found higher ($\text{FeI}_s / \text{FeT}_s$) ratios during the daytime compared with the night samples. The mean FeI_s concentration in daytime (3.67 ng m^{-3}) was more than twice as high as that observed for the night samples (1.45 ng m^{-3}). However, when placed in the dark, Fe(II) was rapidly re-oxidized. More recently, Borer *et al.* (2005) investigated the effect of both the presence of siderophores and light on goethite and lepidocrocite dissolutions. In their laboratory study, they added two types of siderophores, a non-photo-reductive molecule, desferrioxamine B (DFOB), and a second organic ligand, aerobactin, acting as an electron donor. At 32°C , no significant thermal dissolution of lepidocrocite was observed in the absence of these siderophores, even in deaerated (oxygen-free by purging N_2 through the suspensions), irradiated lepidocrocite solution. However, an acceleration of dissolution rates was observed in the presence of DFOB and aerobactin; 2.0 and $2.8 \text{ nmol min}^{-1} \text{ m}^{-2}$ respectively. Irradiation caused further acceleration of dissolution rates relative to thermal dissolution by a factor of four and six: 8.2 and $11.5 \text{ nmol min}^{-1} \text{ m}^{-2}$ in the presence of

DFOB and aerobactin respectively. Thermal or photodissolution of goethite with DFOB as the only organic ligand under aerated or deaerated conditions however was not observed. They concluded that the synergistic effect of siderophores and light may be an important process in the dissolution rates of colloidal Fe(III) (hydr)oxides in marine systems. However, a relatively limited number of studies have shown that natural complexing ligands are an important factor for the dissolution of aerosols into seawater (Kuma *et al.* 1996; Borer *et al.* 2005).

1.3.3. Biological factors

Biscombe (2004) carried out lead, copper and zinc seawater solubility experiments in the presence and absence of bacteria. It was noted that all trace metal solubilities were increased with higher bacteria concentrations (around 6 % more), indicating uptake of dissolved trace metal onto the bacteria surface. It is possible that iron solubility may also be impacted by this process. Moreover, siderophores are produced by bacteria. As previously discussed they are Fe(III)-binding chelators characterized by very high complexation constants 10^{23} - 10^{52} (Crumbliss 1991). Indeed, siderophores enhance aerosol iron solubility in seawater (Waite 2001). Ligand concentrations in seawater have been shown to vary from 0.1 to 40 nM (Witter *et al.* 2000 and references therein).

1.4. PRACTICAL APPROACHES ADOPTED TO DETERMINE THE SOLUBILITY OF AEROSOL IRON

Studies that have investigated the solubility of aerosol iron have adopted different approaches in both experimental methodology and analytical detection systems. Table 1.5 summarises previous iron dissolution studies, the range of solubilities obtained, the practical approach adopted, parameters considered, dissolution medium with the filter / membrane used and the analytical techniques used. It is clear that a range of approaches have been adopted which can be broadly categorised by, (i) semi-continuous flow through a reaction chamber (Wu *et al.* 2007; Aguilar-Islas *et al.* 2009), (ii) incubation

(Bonnet and Guieu 2004; Milne 2007; Mendez *et al.* 2009) and (iii) instantaneous solubility (Buck *et al.* 2006; Sedwick *et al.* 2007; Buck *et al.* 2009). Time scales considered in such studies range from instantaneous dissolution (Buck *et al.* 2006; Sedwick *et al.* 2007) to intermediate (hours to several days; Milne 2007; Bonnet and Guieu 2004) and long term kinetic dissolution studies (weeks, Mendez *et al.* 2009). Leach solutions used include ammonium acetate (Baker *et al.* 2006a; Baker *et al.* 2006c); Milli-Q water (Buck *et al.* 2006; Sedwick *et al.* 2007) and seawater (Bonnet and Guieu 2004; Buck *et al.* 2006; Milne 2007; Sedwick *et al.* 2007; Wu *et al.* 2007; Mendez *et al.* 2009).

It is apparent from the majority of studies using discrete bulk aerosol material that a dominant factor affecting the solubility of an aerosol is the particle concentration effect (see *previous section*); lower solubilities being observed with low dust / seawater concentrations (Bonnet and Guieu 2004, Milne 2007). Therefore it was suggested (*section 1.3.1.*) that dissolution studies should always be designed to use particle concentrations as low as is practically possible to lower this effect and mimic natural conditions as closely as possible. Those studies which have used low dust concentrations however have not considered other factors simultaneously with the same bulk aerosol material which may impact upon the extent and rate of dissolution of iron in seawater. Bonnet and Guieu (2004) and Milne (2007) only considered different types of aerosol material: Bonnet and Guieu (2004) considered urban and Saharan “end-member” dusts; whereas Milne (2007) considered sieved Saharan soils of different origin as well as atmospherically “processed” Saharan dust. Recently Aguilar-Islas *et al.* (2008) adopted different incubation times for two types of aerosol sources, urban and marine, but also considered the addition of complexing ligands. Therefore, there is a real gap in the community knowledge of the relative importance of chemical, physical and biological factors on the dissolution of iron in seawater at realistic natural dust concentrations.

To be able to carry out such studies requires the application of an analytical technique which is sensitive enough to measure dFe in seawater at pM /nM concentrations. It is also apparent that there is not a consensus on the best length of time for such studies (hours - days). Release of iron has been shown to be rapid (within minutes to hours) but intermediate (hours) and long term (days) release have also been reported. Therefore rapid and intermediate kinetics should both be included in aerosol release studies.

1.5. FLOW INJECTION WITH CHEMILUMINESCENCE DETECTION

Several techniques have been developed to detect iron in seawater (Achterberg *et al.* 2001b). One of the most suitable for automated chemical analysis is Flow Injection (FI) analysis. Indeed this approach can be used in the laboratory and on board ship. However, in order to work at nanomolar concentrations, a preconcentration stage is necessary by addition of a solid phase cation exchange column, e.g. an 8-hydroxyquinoline (8-HQ) micro-column (Obata *et al.* 1993; Bowie *et al.* 1998). The detection can then be carried out using spectrophotometry (Hong and Kester 1986; Measures *et al.* 1995) or chemiluminescence (Obata *et al.* 1993; Obata *et al.* 1997; Bowie *et al.* 1998).

1.5.1. Flow Injection (FI)

Flow injection (FI) analysis is a simple technique based on the rapid and reproducible liquid mixing of sample and reagents. Flow injection techniques incorporate on-line sample treatment, mixing and on-line detection in an enclosed continuous flow system. Relatively inexpensive equipment that is easy to automate allows a rapid throughput of samples with good precision (see *Chapter Two*). A typical FI system is composed of, (i) propelling system (pump), (ii) injection system, (iii) reactor and (iv) detector. Additional elements such as mixing coils, preconcentration columns and 3-way switching valves can easily be incorporated. For the determination of iron in seawater, the high ionic strength of the seawater matrix can severely interfere with the quantitative

relationship between iron concentrations and CL emission and its removal is essential (Achterberg *et al.* 2001b). To achieve sub-nanomolar concentration detection in open-ocean samples, the analyte requires preconcentration of up to an order of magnitude prior to analysis. The concept of solid-phase extraction using a chelating resin was first presented by Riley and Taylor (1968) using Chelex-100 resin and since then similar methods have been developed and applied to matrix removal and preconcentration of various analytes (Nickson *et al.* 1995). The most commonly used extraction phase is 8-hydroxyquinoline (8-HQ) immobilised on an inert resin support (Landing *et al.* 1986; Bowie *et al.* 1998; Laes 2004; Ussher 2005; Milne 2007). 8-HQ is selective for transition and heavy metal cations (e.g. Fe, Co, Mn, Cu, Al, Zn, Cd, Ni, Pb) relative to alkali and alkaline earth metals (Landing *et al.* 1986; Nickson *et al.* 1995). 8-HQ was previously immobilized onto silica substrates offering good mechanical strength, resistance to swelling and rapid exchange kinetics but was unstable at high pH. Landing *et al.* (1986) used the porous, chemically stable organic resin gel Toyopearl TSK as the solid support. It has subsequently been used extensively for the determination of Fe (Elrod *et al.* 1991; Powell *et al.* 1995; Bowie *et al.* 1998; Bowie *et al.* 2002b), Mn (Chapin *et al.* 1991), Co (Sakamoto-Arnold and Johnson 1987) and Cu (Coale *et al.* 1992) in seawater.

1.5.2. Chemiluminescence detection (CL)

Chemiluminescence (CL) is the emission of light without emission of heat as the result of a chemical reaction. During the process, the chemiluminescence reagent is oxidised into an electronically excited state which then goes back to the ground state emitting photons and light (Figure 1.3). Therefore the light emitted is proportional to the number of photons produced. Elrod *et al.* (1991) developed a flow injection analysis method with chemiluminescence detection for the determination of Fe(II) in seawater, using brilliant sulfoflavin. Obata *et al.* (1993) reported the development of a flow injection system for the determination of Fe(III) in seawater using luminol as the reagent. Methods for Cu, Fe, Co, and Cr detection have been reported also using luminol (Seitz and

Hercules 1972 and references therein) and it is the most common reagent used in CL for the determination of iron in seawater (O'Sullivan *et al.* 1995; Bowie *et al.* 1998; Bonnet and Guieu 2004; Ussher 2005; Milne 2007; Séguret *et al.* 2008). Luminol is a 5-amino-2,3-dihydro-1,4-phthalazidedione (Figure 1.3) which is oxidized in the presence of dissolved oxygen (Seitz and Hercules 1972) or hydrogen peroxide (Obata *et al.* 1993; Obata *et al.* 1997).

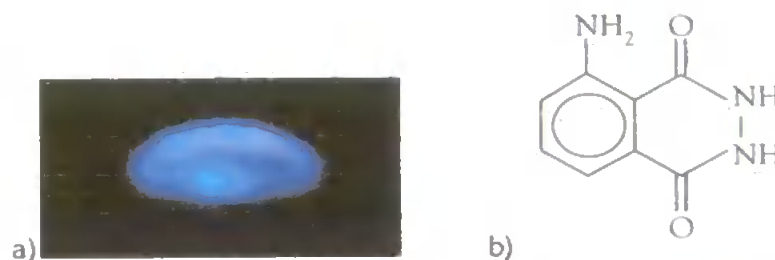


Figure 1.3. Chemiluminescence reaction of Fe(II). a) 1 M solution. b) chemical formula of luminol (5-amino-2,3-dihydrophthalazine-1,4-dione).

This oxidation reaction can be catalysed by the action of iron in basic solution (pH 10.5 - 11, Seitz and Hercules 1972; Laes 2004). Rose and Waite (2001) described three steps (Figure 1.4) during which an electron oxidation reaction (1) needs a trace metal e.g. Fe, Co, Cu or Mn as oxidant; followed by a secondary oxidation of the luminol radical (2), the third reaction (3) is dependant of the deprotonation of the α -hydroxyhydroperoxide species and the optimum pH is approximately 10.5.

1.5.3. FI-CL

The combination of an FI manifold with CL detection presents many advantages, including:

- (i) Good sensitivity with nanomolar detection limits: detection limit ranging between 40 to 100 pM have been reported by O'Sullivan *et al.* (1995), Powell *et al.* (1995) and Bowie *et al.* (1998).
- (ii) High temporal resolution (seconds / minutes) of the FI technique is attractive for studying rapid responses and processes occurring in the marine environment. The

kinetics of marine biogeochemical processes are often rapid and storage of samples may influence the chemical speciation e.g. Fe(II)/Fe(III), (Ussher 2005).

(iii) Contamination free: the manifold tubing diameter is narrow (0.75 mm), the FI system and PMT are suitable to be placed outside a laminar flow hood while the reagents and samples are stored inside.

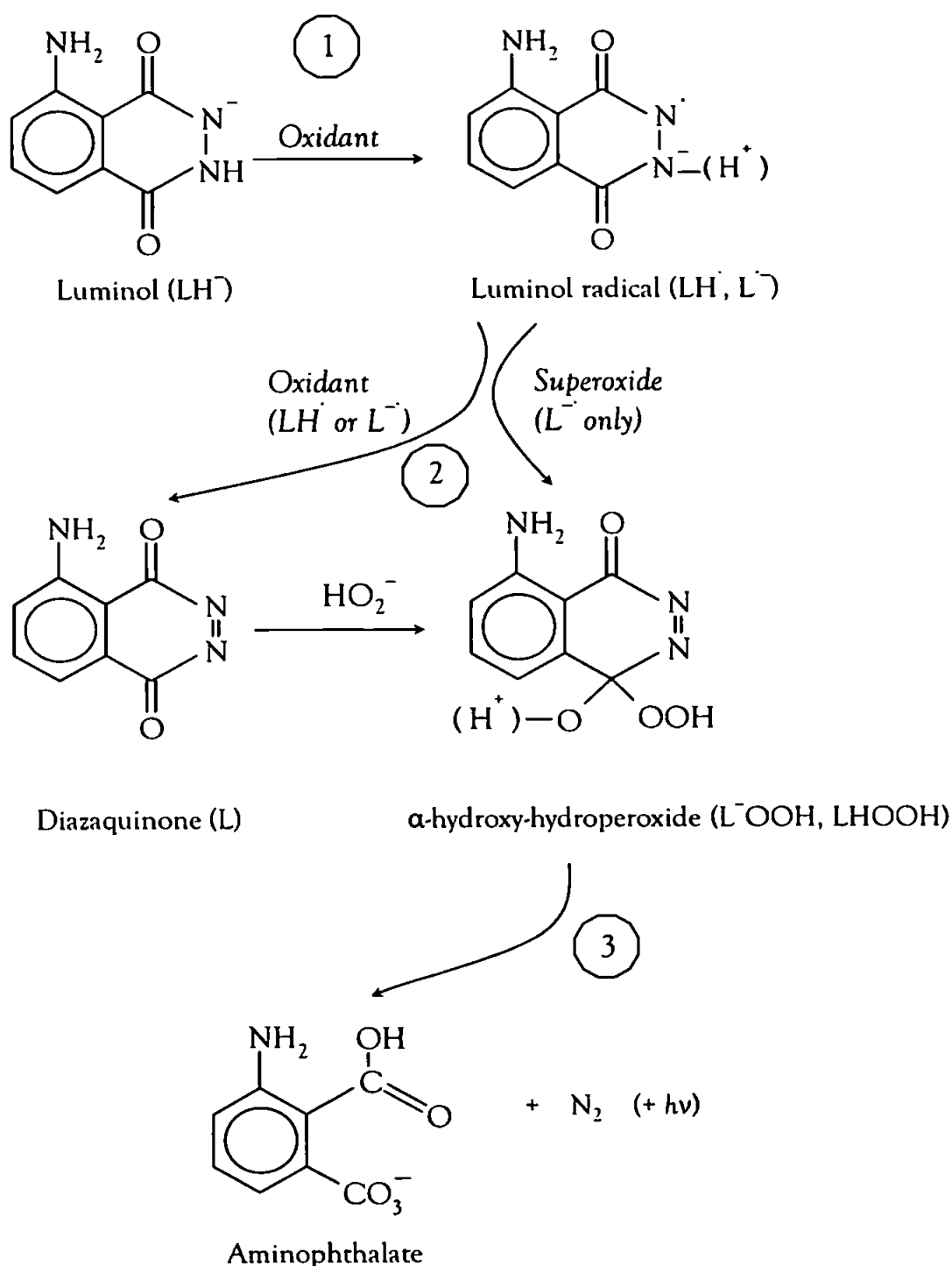


Figure 1.4. Major pathways in the oxidation of luminol (source Rose and Waite 2001).

(iv) Robustness, portability, low cost, simple to maintain, manual or automated instrument: suitable for laboratories and shipboard deployment for *in situ* real time analyses (Achterberg *et al.* 2001, Bowie *et al.* 1998, Ussher 2005).

(v) Automated technique: suitable for analysing numerous samples, particularly advantageous when associated with a 10-port distribution valve.

(vi) In line preconcentration of trace metals by the addition of an 8-hydroxyquinoline micro-column (Obata *et al.* 1993). Therefore, FI-CL was the preferred analytical technique for the purpose of this study, to determine dFe released from aerosols in seawater.

1.6. AIMS AND OBJECTIVES

The main aim of this research was to carry out a comprehensive study to determine the factors which impact upon the dissolution of aerosol iron in seawater at environmentally relevant concentrations. Hence this work was designed to contribute to our understanding of the solubility of aerosol iron by determining the kinetics of dissolution of total dFe in surface seawater during the post deposition process. These new data on the solubility of aerosol iron via dry deposition will help future studies to determine more accurately dry deposition fluxes to the ocean, particularly in the euphotic zone, and subsequently our ability to model the global iron cycle. To ensure successful completion of the study, two challenges were defined: (i) determination of ultra trace Fe concentrations (pM) in seawater, allowing the simulation of more realistic natural concentrations (i.e. low particle concentrations); (ii) quantifying the effects of a range of factors physical, chemical and biological (e.g. presence of model ligands and light) on the dissolution process at low particle concentrations.

In order to achieve this overall aim, the objectives were:

(i) Optimise a reliable flow injection with chemiluminescence detection system for the determination of trace and ultra-trace concentrations of dFe in seawater (with and

without 8-HQ preconcentration columns) and automate the system to allow detection of sub-nanomolar concentrations of dissolved Fe(II) in seawater.

(ii) Assemble, assess and optimise a seawater treatment system for the production of low dissolved organic carbon (DOC) and dFe concentrations in seawater.

(iii) Design, construct and validate an aerosol seawater dissolution system with an automated sampling system.

(iv) Assess the effect of chemical and physical parameters on the extent and kinetics of the dissolution of aerosol iron in seawater under carefully controlled experimental conditions.

(v) Modify the dissolution/incubation system to investigate the solubility of iron in seawater from the Eastern Mediterranean marine aerosol and to estimate the atmospheric dry inputs of soluble iron in seawater to the Levantine Basin.

**DETERMINATION OF IRON IN SEAWATER
USING FLOW INJECTION WITH
CHEMILUMINESCENCE DETECTION**

2.1. INTRODUCTION

The aim of the work presented in this chapter was to optimise a reliable flow injection with chemiluminescence detection system for the determination of iron in seawater (Bowie 1999; Ussher 2005; Milne 2007), suitable for samples from aerosol dissolution experiments. Automation of the system was employed to allow a more reliable detection of sub-nanomolar concentrations of dissolved Fe(II + III) in seawater and lowered the risks of contamination during dissolution studies of aerosol iron in seawater (see *Chapter Four*).

The objectives therefore were (i) to optimise a manual FI-CL system for the determination of dissolved Fe(II) in ultra high purity (UHP) de-ionised water, (ii) to assemble and optimise an automated FI-CL system for the determination of total dissolved Fe(II+III) in seawater and (iii) to document protocols for the effective utilisation of the FI-CL technique.

2.2. EXPERIMENTAL

2.2.1. Reagents and standards

Chemicals were obtained from Fisher Scientific (Loughborough, UK), unless otherwise stated; reagents and standards were prepared in ultra high purity (UHP) de-ionised water ($18.2 \text{ M}\Omega \text{ cm}^{-1}$, Elgastat Maxima, High Wycombe, UK). Plasticware was cleaned by soaking in different baths: for 24 h in hot 0.25% (v/v) micro-detergent (Decon), then in 50 % (v/v) hydrochloric acid (Analytical reagent grade) for one week and finally in 20 % (v/v) nitric acid (Trace analysis grade) for one week. Between each bath, labware was rinsed thoroughly with UHP de-ionised water and stored containing diluted acid (0.1 M high purity HCl, SpA grade, Romil, Cambridge, UK) and placed in re-sealable plastic bags. To avoid any risks of contamination, handling of iron concentration standards and reagents was carried out under a class-100 laminar flow hood (model K6, Bassaire Ltd., Southampton, UK).

Reagent solution: A 0.01 M luminol (5-amino-2,3-dihydro-1,4-phthalazinedione, Fluka, Sigma-Aldrich, Gillingham, UK) stock was prepared by dissolving 0.089 g of luminol in 50 mL of borate buffer followed by sonication for 30 min. A working 1×10^{-5} M luminol stock was prepared by adding 1 mL to 1 L UHP de-ionised water, 16 g of sodium carbonate (Na_2CO_3 , Trace analysis grade) and adjusted to pH 12.2 by adding 5 mL of 2 M sodium hydroxide (NaOH, Analytical reagent grade). For the cleaning of the reagent, the solution was passed through a column containing Chelex-100 chelating resin to reduce the baseline noise generated by any impurities. Chelex-100 resin remove metal cations including Fe^{3+} and Fe^{2+} by complexation with its carboxylic acid groups (see section 3.3.1.). The luminol solution was prepared and cleaned at least 24 h before use to maximise sensitivity and was stable for at least one month. Different batches of luminol were mixed at least 24 h to stabilise to prevent differences in the baseline noise.

Eluent: A 0.06 M solution of hydrochloric acid (HCl) was prepared by diluting 5 mL of 12 M hydrochloric acid solution (HCl, Trace analysis grade) to 1 L with UHP de-ionised water for the manual system. The eluent solution for the automated FI-CL system was prepared by diluting 10 mL of high purity hydrochloric acid (SpA grade, Romil, Cambridge, UK) to 1 L with UHP de-ionised water.

Ammonium acetate buffer: Ammonium acetate (NH_4OAc) stock solution (2 M) was prepared by adding 30 mL of high purity acetic acid (CH_3COOH , Romil) to 100 mL of high purity ammonia solution (SpA grade, Romil) and diluting to 250 mL with UHP de-ionised water. A working buffer solution (0.4 M) was prepared by diluting 20 mL stock solution to 100 mL with UHP de-ionised water and adjusted to pH 5.5 with high purity acetic acid. The buffer was cleaned in-line using an 8-hydroxyquinoline micro-column.

Reducing reagent: A stock solution (0.04 M) of reducing reagent for Fe(III) was prepared by dissolving 0.1008 g of Na_2SO_3 (extra pure, Merck, Oxford, UK) in 15 mL of UHP de-

ionised water and 5 mL of 0.4 M ammonium acetate buffer (pH 5.5). This stock reagent was cleaned by passing through one 8-hydroxyquinoline column. Aliquots of 25 μL were added per 10 mL of acidified seawater, 8 h prior to analysis, to achieve a final concentration of 100 μM in the sample.

Iron standards: A 0.02 M Fe(II) stock was prepared monthly by dissolving 0.3191 g of di-ammonium ferrous sulphate hexahydrate ($\text{Fe}(\text{NH}_4)_2(\text{SO}_4)_2 \cdot 6\text{H}_2\text{O}$) in 50 mL of a 0.12 M hydrochloric acid solution (HCl, Trace analysis grade, Fisher). Then high purity hydrochloric acid (SpA grade, Romil) was used and spiked with 125 μL of reducing reagent. A 40 μM stock solution of Fe(II) was prepared weekly.

Certified reference material: NASS-4 was purchased from the Institute for National Measurement Standards (Ottawa, Canada). This seawater was collected in the North Atlantic Ocean, at a depth of 10 m, 35 km southeast of Halifax (Canada) and filtered with 0.45 μm acrylic copolymer filters and acidified to pH 1.6. The assigned concentration was $0.105 \pm 0.016 \mu\text{g L}^{-1}$ (± 2 s.d.) of iron (equivalent to $1.880 \pm 0.286 \text{ nM}$). SAFe samples were not analysed owing to the difference in pH, 1.7 instead of 2.

In-house reference material: this 20 L surface seawater was collected in the Canary Basin (2002) and was filtered in-line using 0.2 μm pore size cartridge filters (Sartobran™, Sartorius Stedim. Biotech., Aubagne, France).

Acid wash: An acid wash solution (1.2 M) was prepared by diluting 25 mL of high purity hydrochloric acid (SpA grade, Romil) to 250 mL with UHP de-ionised water.

Seawater: the seawater was collected in the Atlantic Ocean (salinity 37.3, open ocean seawater) during the AMT 16 cruise, at 14°0' S and 25°0' W (2005) by Dr Simon Ussher (University of Plymouth, UK). The sample was filtered from a tow fish, in-line using 0.2 μm pore size cartridge filters (Sartobran, Sartorius Stedim. Biotech., Aubagne, France) into

an 50 L acid washed HDPE (High Density Polyethylene) carboy and stored in the dark for 2 years before use.

2.2.2. Instrumentation

Manual FI-CL system without/with 8-hydroxyquinoline column(s)

For preliminary experiments, calibrations of iron standards were carried out with simple instrumentation: a manual switching valve linked to a photomultiplier tube (PMT) and a chart recorder (Figure 2.1). Standards and reagents were propelled by a peristaltic pump (Minipuls 3, Gilson, Villiers le Bel, France) at a flow rate of 2.0 mL min^{-1} (grey-grey 2-stops tubing, Elkay, Basingstoke, UK) through a narrow bore PTFE tubing (polytetrafluoroethylene, 0.75 mm i.d., Fisher, Loughborough, UK). Then, the standards were passed through a 17 μL spiral PTFE coil, mounted in a manual valve (Cheminert Valve NCW0004) which had two operating positions: elution and loading of the samples/standards (Figure 2.2).

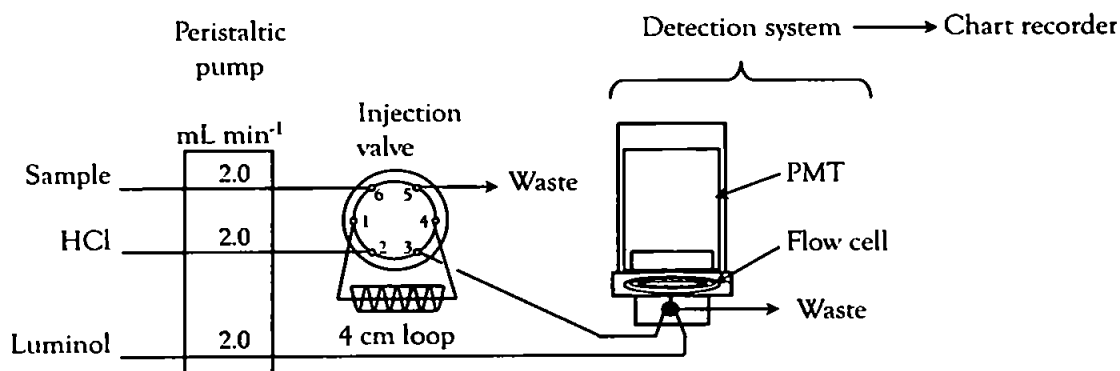


Figure 2.1. Flow injection with chemiluminescence detection manifold for the determination of Fe(II).

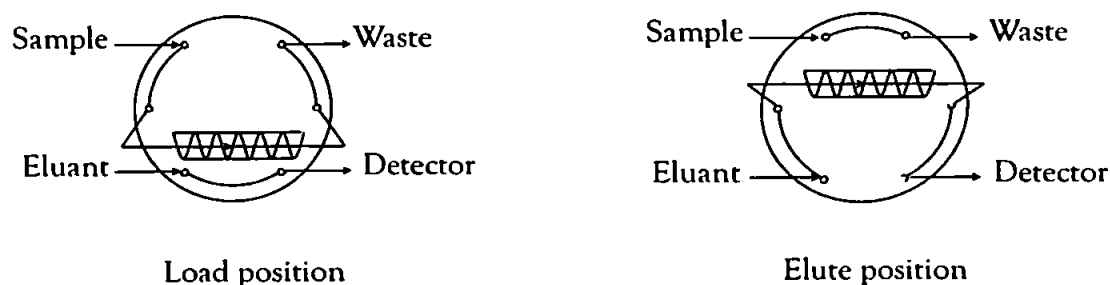


Figure 2.2. Manual switching valve, showing load and elute positions of the sample.

The detection system consisted of a quartz glass spiral flow cell opposite to an end-window photomultiplier tube (Thorn EMI, 9798 QA), contained in a μ -metal shield for magnetic insulation (MS52D), connected to a built-in current-to-voltage amplifier (C634, with 4 gain settings, from A to D) and protected in an ambient temperature shielded housing (Electron tubes, B2F/RFI). The photomultiplier tube was powered by a 1.1 kV power supply (Thorn EMI, PM28B). The C634 amplifier was supplied with 15 V from an independent power supply (BBH, RS Components Ltd, Corby, UK).

An essential component of the detection system was the quartz flow cell (Figure 2.3a) connected to a T-piece which mixes buffered samples and reagent. The flow cell allowed the detection of the rapid chemiluminescence reaction (blue light 350 - 500 nm, 1-10 s) by the end-window of the photomultiplier tube (Figure 2.3b). The flow cell used had one inlet and 3 spirals of a tightly wound quartz glass spiral coil (tubing i.d. 1.1 mm; o.d. 3.0 mm; internal volume 130 μ L; diameter 20 mm; Baumbach and Co. Ltd, Ipswich, UK). The length of tubing between the T piece and the flow cell was minimised (volume = 4.4 μ L) to ensure that the chemiluminescence reaction occurred in the coil.

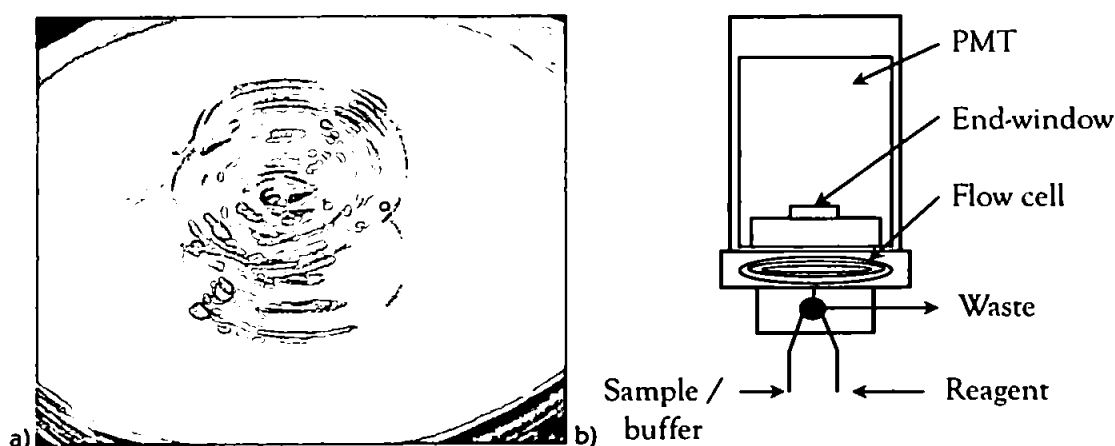


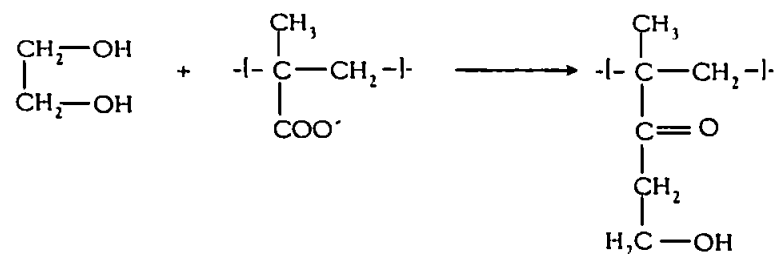
Figure 2.3. a) Picture of the quartz flow cell, b) flow cell and end-window in the housing.

To enhance the limit of detection, the PTFE coil on the injection valve was then replaced by an 8-hydroxyquinoline (8-HQ) micro-column. 8-HQ resin is highly selective for trace metals, complexing strongly with both Fe(II) and Fe(III) ions (high stability constants of $\log K_1 = 8.71$ and 13.69 respectively (Sillén and Martell 1964)), allowing

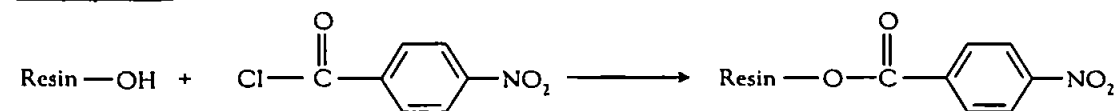
unwanted components to pass through the column to waste. The preconcentrated analyte is then desorbed by elution from the resin using a weak acid (0.12 M HCl). The chelating 8-HQ resin was immobilised on TSK gel (Toyoparl HW-75F, 32-63 micron, TosoHaas Co., supplied through Anachem, Luton, UK) according to the method used by Bowie (1999), adapted from Landing *et al.* (1986). This consisted of 5 steps (Figure 2.4): removal of fine particles and wash of the support resin; substitution of a secondary alcohol group from the resin with an aromatic acid chloride, p-nitrobenzoylchloride (esterification); reduction by sodium dithionite; diazotization by sodium nitrite and acetic acid finishing by attachment of 8-HQ group. The total preparation time was 25 h and the synthesis provided enough resin to pack more than 200 columns.

Micro-columns were initially built from Perspex® (1 cm long, 1.5 mm i.d., Figure 2.5.a) and sealed (Figure 2.5.b) with nylon frits and polyester fibre pads, maintained by standard union screws (Figure 2.6). To overcome problems due to clogging, nylon frits and pads were replaced by BioVyon® T frits made from ultra high molecular weight polyethylene (1 mm thickness, 9-18 µm pore range, Porvair Filtration Group Ltd., Fareham, UK). Due to backpressure problems, thinner frits were subsequently made from BioVyon® F (high density polyethylene, HDPE, 0.75 mm thickness, 22-57 µm pore range, Porvair Filtration Group Ltd., Fareham, UK). A cleaning 8-HQ micro-column was also added into the buffer line (Figure 2.7). In order to buffer the samples in-line, a buffer solution was prepared to achieve a pH of 5.0 after mixing with samples/standards acidified at pH 1.7 (Obata *et al.* 1993). A second peristaltic pump (Minipuls 3) propelled samples/standards at 1.6 mL min⁻¹ (yellow-blue 2-stops tubing, Elkay, Basingstoke, UK) and buffer at 0.23 mL min⁻¹ (orange-white 2-stops tubing). Reagent and eluent were propelled at 2.0 mL min⁻¹ (grey-grey 2-stops tubings).

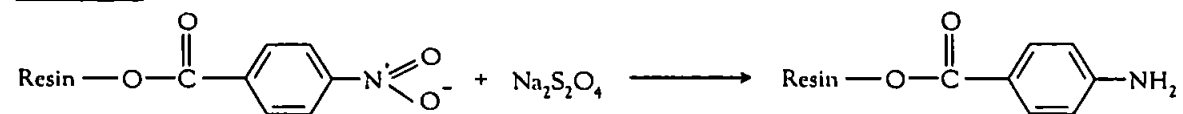
The resin



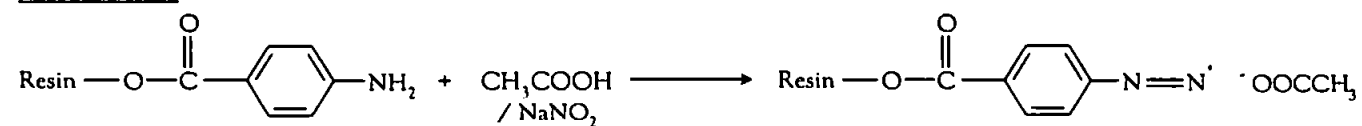
Benzoylation



Reduction



Diazotisation



8-HQ immobilisation

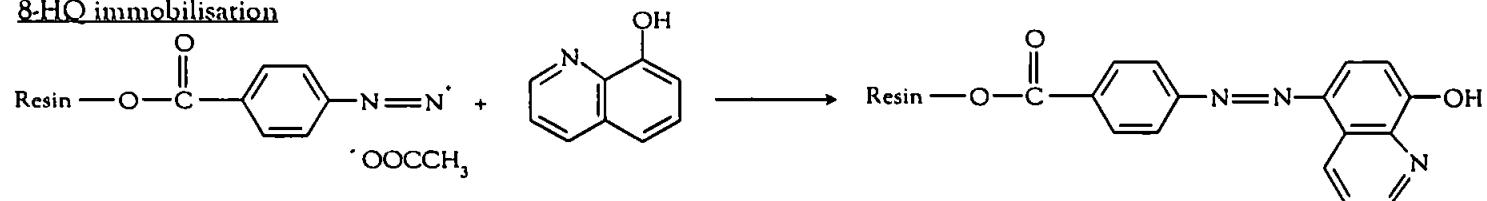


Figure 2.4. Reaction scheme for the immobilisation of 8-hydroxyquinoline onto TSK resin.

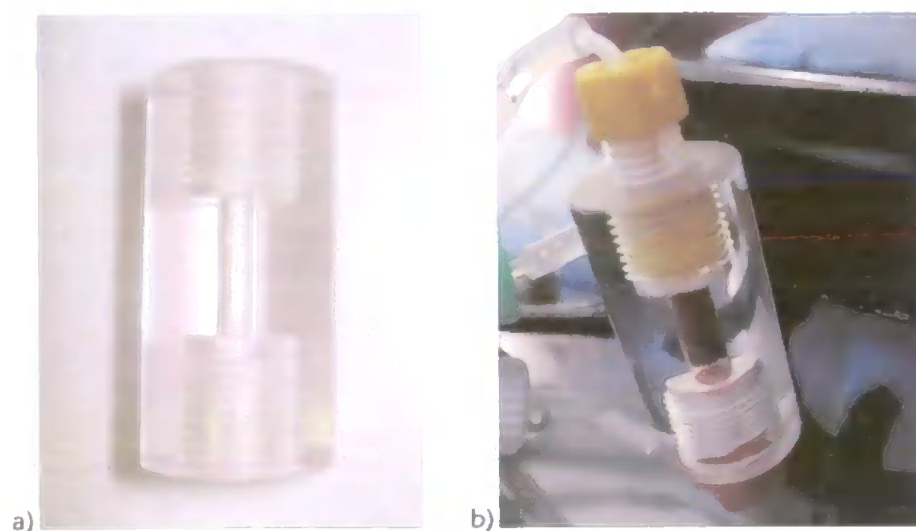


Figure 2.5. Perspex micro-column: a) empty, b) packed with 8-hydroxyquinoline coated resin and mounted onto the injection valve.

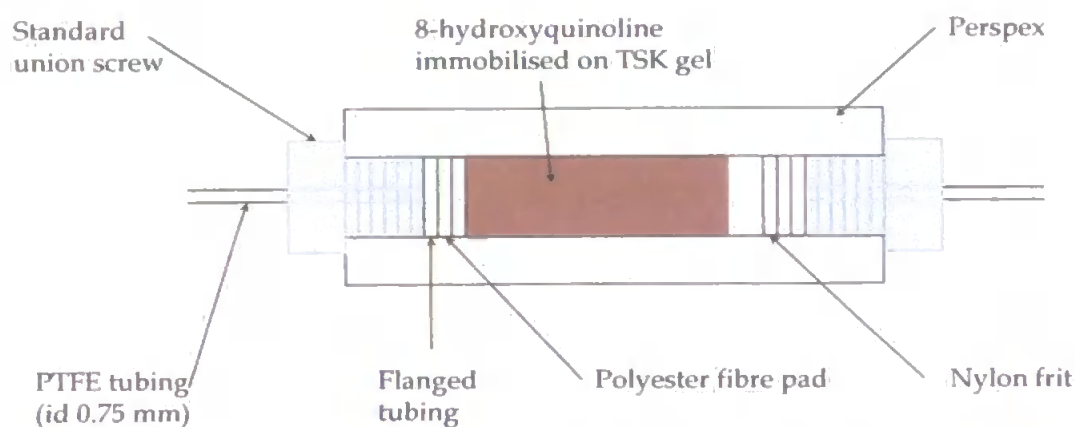


Figure 2.6. Preconcentration micro-column containing 8-HQ immobilized on TSK, with a space allowing the resin to move when changing from elution to load.

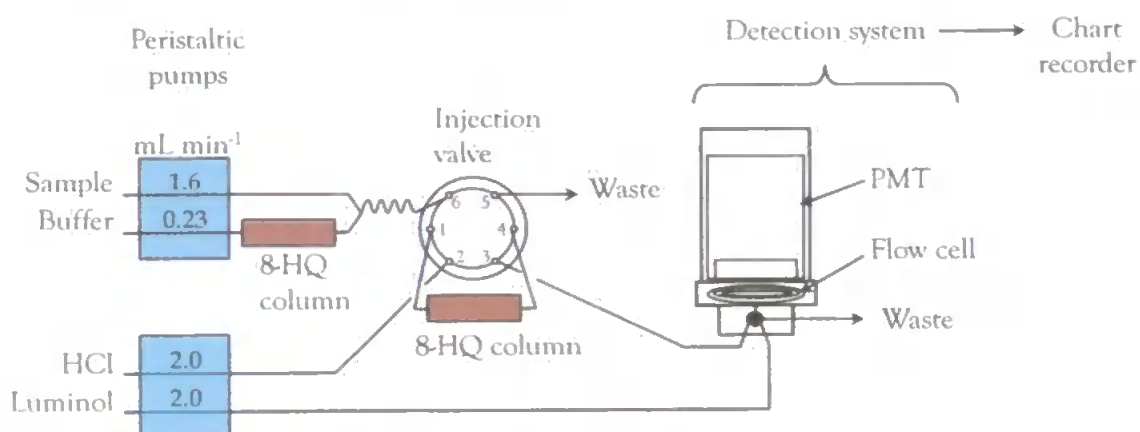


Figure 2.7. Final manual FI manifold, with two 8-hydroxyquinoline micro-columns: on the buffer line and the switching valve.

Automated FI-CL system with three 8-hydroxyquinoline columns

FI components

An automated FI-CL system was assembled for the determination of dFe in seawater (Figure 2.8).

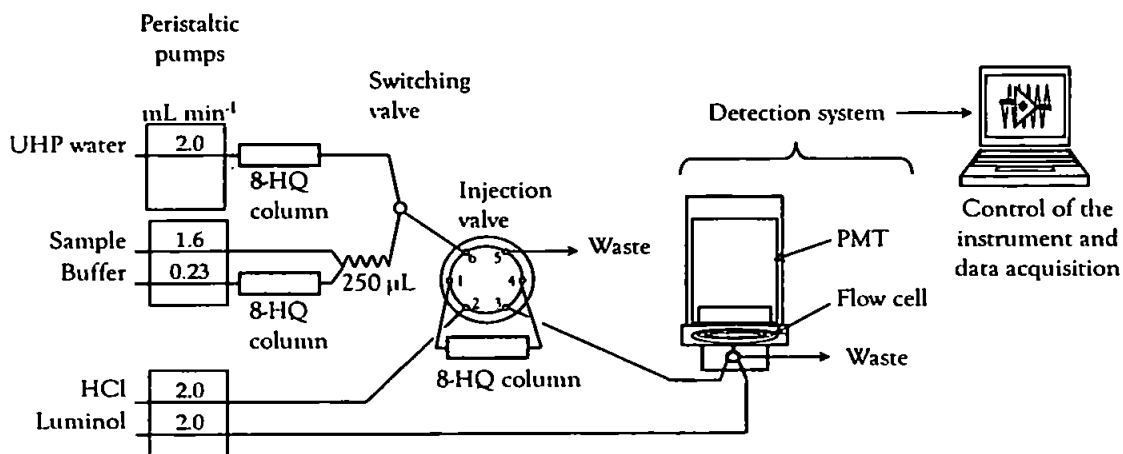


Figure 2.8. Automated FI system, with three 8-hydroxyquinoline micro-columns: on the buffer line and UHP water rinse and mounted onto the switching valve.

A third peristaltic pump (Minipuls 3) was added to the manual system to propel an UHP de-ionised water rinse line at 2.0 mL min^{-1} (grey-grey 2-stops tubing) onto the preconcentration micro-column. Three 8-HQ micro-columns were incorporated in the system: in the injection valve, on the buffer line and on the rinse line. Samples/standards were buffered in-line and mixed by passing through a $250 \text{ }\mu\text{L}$ PTFE coil (0.75 mm i.d.), achieving a final pH of 5.5. Pumps, photomultiplier tube, switching valve and injection valve were automated via an interface (*see Interface section*). Sample and rinse pumps were alternatively switched on and off: buffered samples/standards and UHP rinse passed through a switching valve and were loaded or eluted onto the 8-HQ micro-column in the injection valve. Solutions were then detected by the photomultiplier tube. The switching valve was 3-way PTFE, with a 2 position solenoid valve (EW-01367-72, Cole-Palmer, London, UK). The injection valve was an electronic rotary injection valve (NDV0008, Valco AG International, Schenk, Switzerland) automated by a micro-electric actuator (EHCACE, Valco AG International, Schenk, Switzerland) powered by a power supply

(DPS55, Astec, Didcot, UK). Data were acquired and collected on a laptop with the software LabVIEW version 7.1.

Interface

Process control was developed during this study and achieved using a control and data acquisition instrument (Ruthern Instruments, Bodmin, UK). This instrument was based on a NI USB-6008, multifunction data acquisition device (National Instruments Corp. Ltd., Newbury, UK) with 12 digital input/output TTL lines, 12-bit analogue input resolution at up to 10 kS s⁻¹ (10,000 samples per second). NI-DAQmx Base is a software multiplatform driver with a subset of the NI-DAQmx programming interface (National Instruments Corp. Ltd., Newbury, UK). Virtual instrument (VI) software (Ruthern Instruments, Bodmin, UK) was written in LabVIEW version 7.1 (National Instruments Corp. Ltd., Newbury, UK). The control instrument had five modules, one for the USB system controller, one for the solenoid and relay controlling switching valves, one for the photomultiplier tube (PMT) integrator and amplifier, one for the TTL output controlling the pumps and one for the sample pump (Figure 2.9).

Graphical interface

The LabVIEW VI front panel (version 14, Figure 2.10) contained the virtual switches, buttons, controls and graphical displays. The timing in the cycle (580 s) but also percentage progress of the analysis, gain of the interface and position of the injection valve loading or eluting were displayed on the right hand side. The current analysis was on the top left hand side and the historical analysis on the bottom left hand side of the screen. Each element was graphically connected using a wiring diagram which included timing of operations (Figure 2.11).

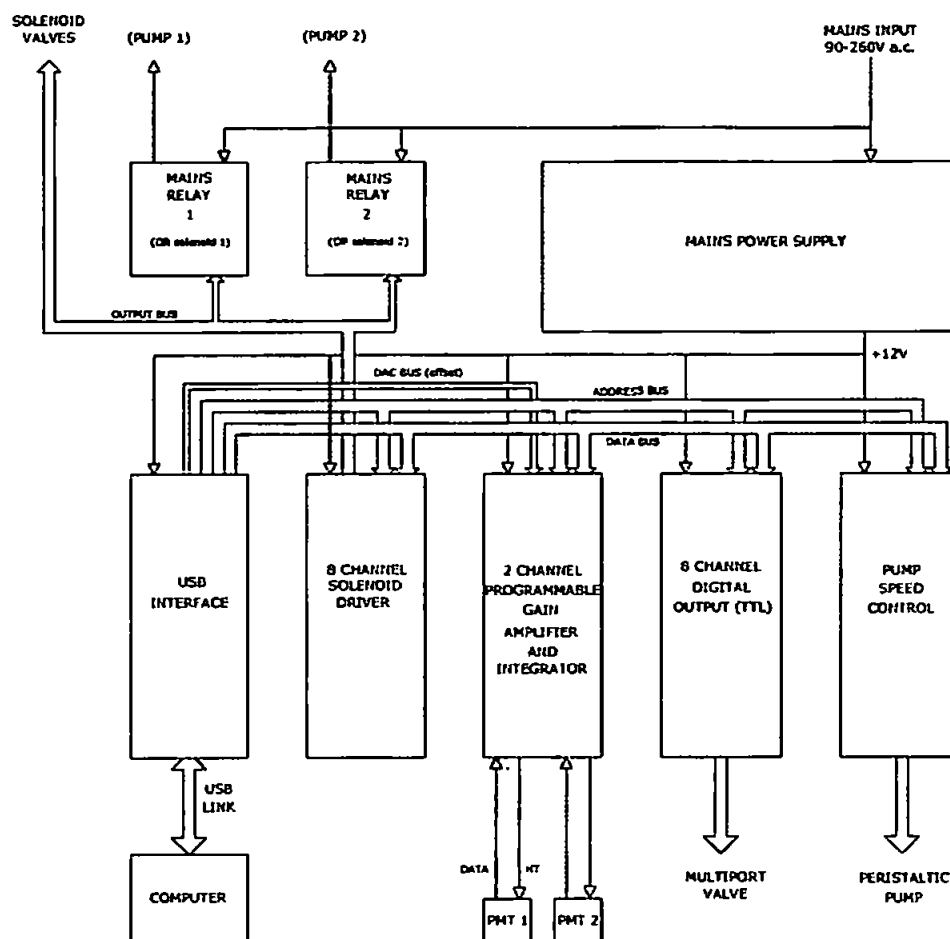


Figure 2.9. Block diagram of the interface, incorporating the 5 units: USB system controller, solenoid and relay controlling switching valves, PMT integrator (2 channels), TTL output and pump.

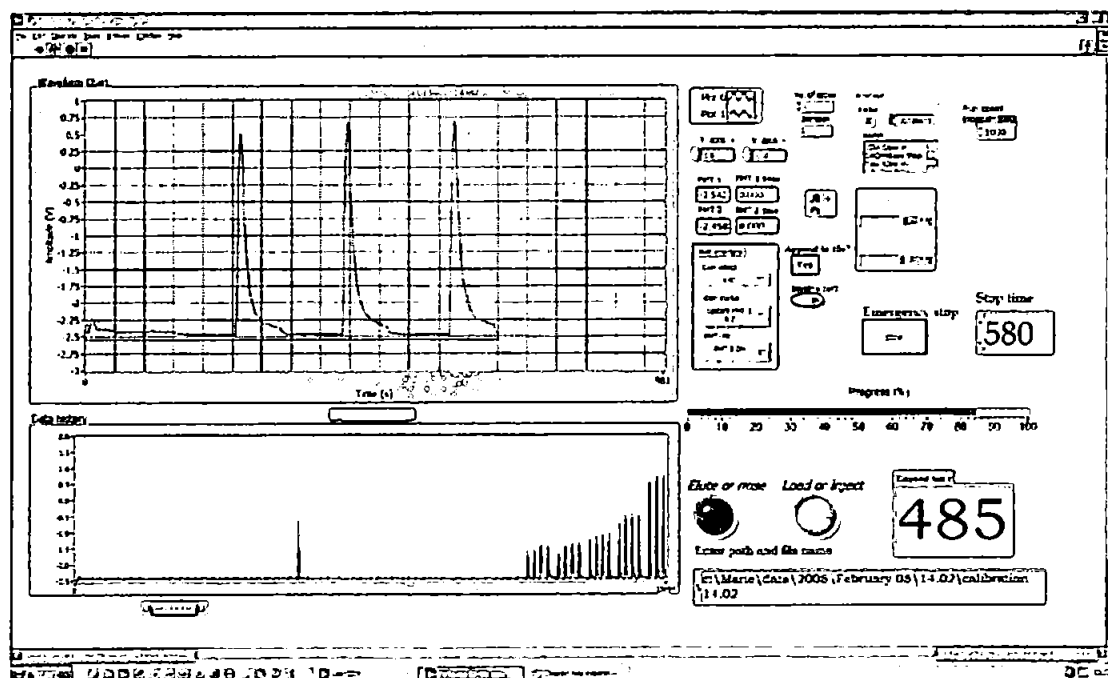


Figure 2.10. LabVIEW front panel (version 14) for the virtual instrument, with current analysis, data history, elapsed time and position of the injection valve.

Each analytical cycle (Table 2.1) consisted of 4 replicate measurements including sample/buffer loads (43 s each) and elutions (27 s each) with 0.12 M HCl, followed by a UHP de-ionised water rinse. The total time taken for one analytical cycle was 10 min.

Table 2.1. Timings sequence for an individual analytical cycle. Wash pump on= rinse.

Elapsed time (s)	Injection valve	Sample pump	Wash pump	Switching valve
0	Elute	ON	OFF	OFF
100	Load	✓		
143		OFF	ON	ON
170	Elute		✓	✓
205		ON	OFF	OFF
225	Load	✓		
268		OFF	ON	ON
295	Elute		✓	✓
330		ON	OFF	OFF
350	Load	✓		
393		OFF	ON	ON
420	Elute		✓	✓
455		ON	OFF	OFF
475	Load	✓		
518		OFF	ON	ON
545	Elute		✓	✓
580		OFF	ON	ON

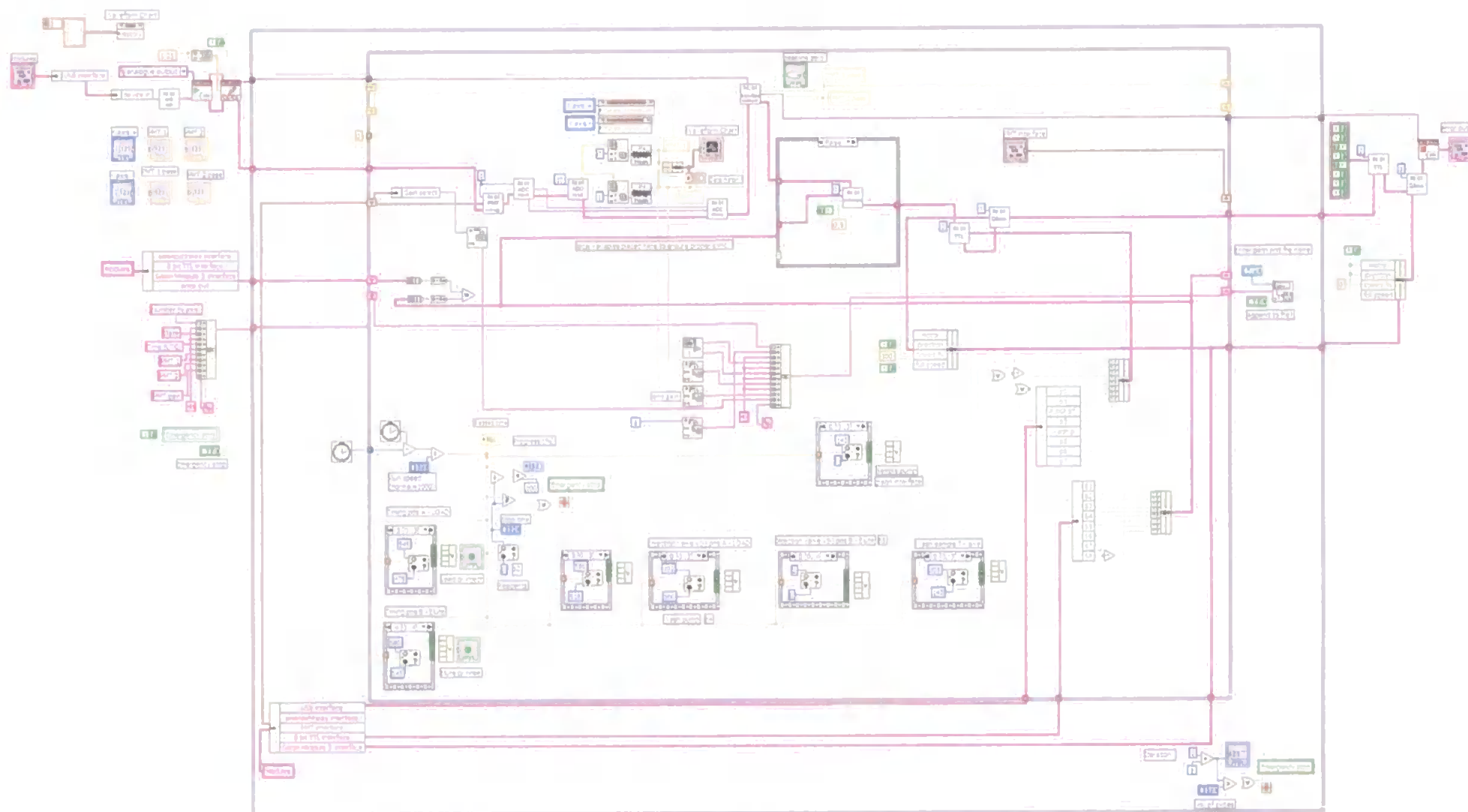


Figure 2.11. Wiring diagram showing the graphical code for instrument control and data acquisition. This code controls the front panel presented in Figure 2.10.

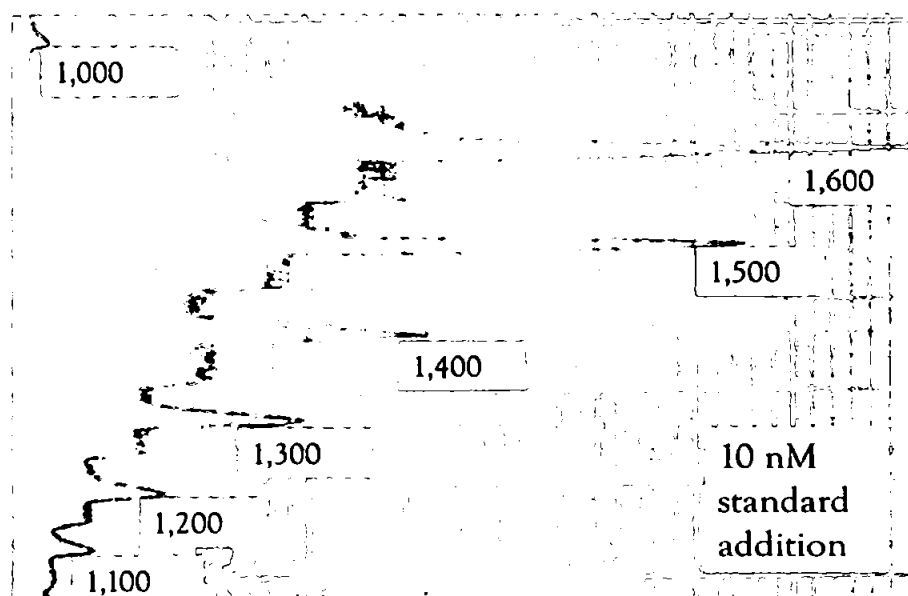


Figure 2.12. Effect of changing power supply voltage on standard additions 10 nM of iron(II) to UHP de-ionised water.

Table 2.2. Effect of power supply voltage on signal-to-noise ratio, PMT gain D.

Voltage (V)	Baseline noise (mm)	Signal (mm)	Signal-to-noise ratio
1,000	0.25	2	8.0
1,100	0.5	5	10.0
1,200	1	10	10.0
1,300	2	17	8.5
1,400	3	23	7.7
1,500	4	47	11.8
1,600	6	56	9.3

In the final stage of the optimisation, an 8-hydroxyquinoline micro-column was mounted in the injection valve, replacing the loading coil. Preconcentration is an effective means of lowering the limit of detection (Fang 1995). Therefore, calibrations were performed using standards ranging from 0.5 to 10 nM iron(II). Furthermore, a second preconcentration micro-column was inserted in the buffer line and used to carry out calibrations from 1 to 10 nM; solutions were prepared and stored in a class-100 laminar flow hood. The 8-HQ micro-columns used were 10 mm long and 1.5 mm i.d. (17 μ L, Cannizzaro *et al.* 2000; Sandford 2001; Ussher 2005; Milne 2007). Different laboratories use different geometries, e.g. de Jong *et al.* (2000) reported a column of 40 mm long and 3 mm internal diameter representing an internal volume of 283 μ L whilst Measures *et al.* (1995) used, for the determination of iron in seawater, the same dimensions of columns as Resing

and Mottl (1992) used for the determination of manganese in seawater (70 mm long and 3.3 mm i.d., volume 600 μL).

Owing to low sensitivity and the high concentration of iron in the acid used initially (12 M HCl, Aristar), high purity hydrochloric acid (SpA grade) was used for samples and eluent and for storage (0.06 M). In a further effort to reduce the blank signal the luminol reagent was cleaned by passing it through a Chelex-100 chelating resin column (Sigma-Aldrich, St Louis, U.S.A., see *Complexing resins* in *Chapter Three*, Figure 2.13). The column consisted of a polyethylene tube (30 cm long, 1.5 cm o.d.), closed at each end by a polypropylene fittings (15 cm long) connected to small bore tubing to retain all particles of Chelex resin and to avoid the use of glass wool / filter which could be moved by the high flow or create backpressure.

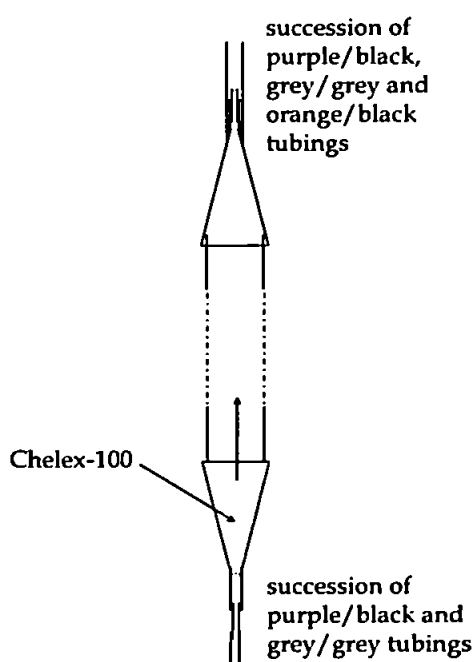


Figure 2.13. Chelex-100 column for cleaning the luminol reagent: bottom section with the chelating resin and top section preventing the loss of Chelex.

The column was 60 cm long and was 20 % filled with Chelex-100 allowing expansion of the resin (up to ~ 30 cm) during the cleaning of the luminol. The resin was cleaned with 125 mL of high purity HCl (1 M, SpA) and rinsed with 800 mL of UHP de-

ionised water. Luminol was then passed through and the first 200 mL discarded before collection.

Analytical Figures of merit of the optimised system

During the optimisation of the manual FI system, the linear range, linearity and precision were compared (Table 2.3) to assess improvements made.

Table 2.3. Optimisation stages with corresponding analytical Figures of merit for the manual system.

Standards (nM)	Linearity (R^2)	Precision (%)	Settings
10 - 50	0.8976	6.2 - 36	17 μ L PTFE coil
10 - 30	0.9572	6.2 - 28	Preconcentration 8-HQ micro-column
2 - 10	0.9701	2.6 - 7.5	Buffer line with 8-HQ micro-column, laminar flow hood
1 - 4	0.9933	2.9 - 12	SpA HCl, clean luminol

With the original manual assembly (17 μ L PTFE coil) calibrations were performed from 10 to 50 nM Fe(II), exhibiting relatively poor linearity ($R^2 = 0.8976$) and precision, ranging from 6.2 to 36 % ($n = 3$). The subsequent incorporation of a preconcentration 8-HQ micro-column improved linearity $R^2 = 0.9572$ and slightly improved precision, from 6.2 to 28 % ($n = 3$). Moreover, incorporation of a second 8-HQ micro-column onto the buffer line substantially improved precision, ranging from 2.6 to 7.5 %. The utilisation of high purity hydrochloric acid and clean luminol reduced the level of impurities and lowered both the baseline signal and the baseline noise. During the course of the optimisation, the linearity improved from $R^2 = 0.8976$ to $R^2 > 0.97$. The blanks were systematically investigated using the automated FI system (see *Analytical Figures of merit*, in section 2.3.2).

The limit of detection ($3 \times \text{standard deviation of the sample} / \text{slope}$), at the final stage of the optimisation was 0.2 nM, an order of magnitude higher than that the 40 pM reported by Bowie *et al.* (1998), and was not low enough to achieve the aims of the current study.

2.3.2. Automated FI-CL system

Optimisation of the system

The automated FI system (Figure 2.8) consisted of three pumps, the injection valve, the photomultiplier and the computer and was controlled through a digital interface (see *Instrumentation, section 2.2.2*). The development of such a system was a challenging process and required systematic optimisation of the key variables.

In UHP de-ionised water: Once the virtual instrument and interface were in full control of the system and recording data, calibrations were carried out using standards ranging from 0.1 to 0.6 nM Fe(II). A fresh 8-HQ resin, new containers and Sterilin™ vials instead of volumetric flasks were used. Samples were spiked with reducing reagent immediately prior to analysis and the effect of sulphite addition and the contribution of acid to the blank were investigated. The final stage of the optimisation for Fe(II) in UHP de-ionised water was the preparation and storage of the samples and reagents in a class-100 laminar flow hood (Bassaire Ltd., Southampton, UK). The analytical cycle was reduced in time by running 4 replicates for each sample instead of 8.

During the final stage of the optimisation of Fe(II), standards were prepared in the range of 0.1 to 0.6 nM using an interface gain of 100 and a gain setting on the PMT of 1,000 (D). The calibration line exhibited a good linearity of $R^2 = 0.9811$, with a precision ranging from 2.3 to 10 % ($n = 4$). The calculated limit of detection for iron in UHP de-ionised water was 20 pM which was in good agreement with the 40 pM reported by Bowie *et al.* (1998). The automation of the manifold and the use of a laminar flow hood greatly improved the limit of detection of the system (Table 2.4.) compared with 200 pM for the manual system. The precision improved slightly and varied from 2.3 - 10 %, compared with 2.9 - 12 % for the manual system. The automated system allowed the measurement of a range of Fe(II) standards from 0.1 to 0.6 nM whilst with the manual system allowed detection in the range from 1 to 4 nM.

Troubleshooting

During the optimisation, UHP de-ionised water blanks gave “negative” peaks (Figure 2.14) which suggested that the luminol reagent was less clean than the injected sample. Therefore, the reagent was cleaned by passing through a Chelex-100 column, to remove any impurities, and the acid was changed to a high purity hydrochloric acid (Figure 2.15). The limit of detection was 3.4 nM before optimisation and was lowered to 0.2 nM using clean reagent and acid.

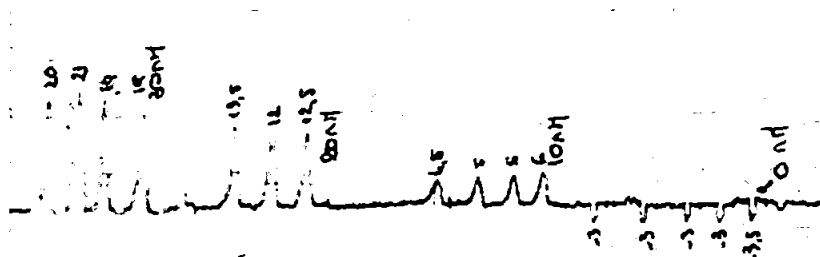


Figure 2.14. Chart showing peaks of a calibration of iron(II) from 0 to 30 nM. UHP de-ionised water peaks showed the negative peaks of injection.

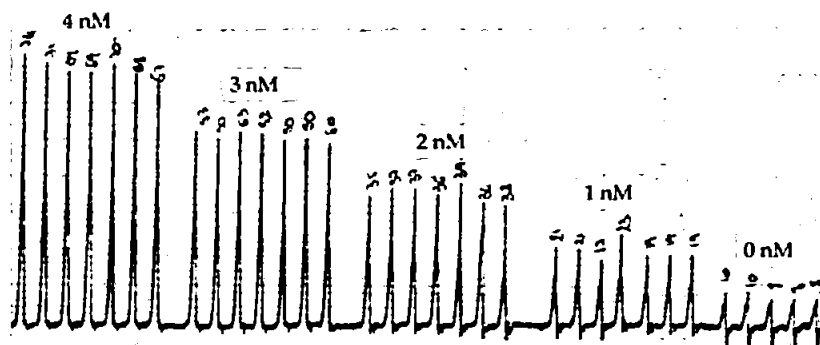


Figure 2.15. Chart showing a peak calibration of iron(II) from 0 to 4 nM in UHP de-ionised water.

Addition of an 8-HQ micro-column was found to increase the resistance of the flow in the tubings and occasionally result in leaks and disconnections due to backpressure. A well-packed column allowed the movement of the resin depending on the elution and loading position. It was found that a column packed ~ 90 % full reduced backpressure.

Due to poor precision and inadequate detection limits, it was decided that an automated flow injection system would be assembled and analyses conducted in a laminar flow hood, aiming for a precision of < 10 % RSD and a limit of detection of 40 pM (Bowie *et al.* 1998).

Table 2.4. Comparison of the analytical Figures of merits of the manual and automated FI systems (n= 7), using Fe(II) standards made up in UHP de-ionised water. LoD= Limit of detection.

	Manual FI	Automated FI
Range (nM)	1 - 4	0.1 - 0.6
LoD (pM)	200	100
Linearity	0.9933	0.9811
Precision (%)	2.9 - 12*	2.3 - 10

The contributions made to the blank signal by the acid (SpA grade) and reducing reagent were determined by analysing: (i) UHP de-ionised water only, (ii) 0.01 M HCl made in UHP de-ionised water, (iii) 0.01 M HCl and 100 μ M reducing reagent made in UHP de-ionised water and (iv) 0.01 M HCl and 200 μ M reducing reagent made in UHP de-ionised water (n = 4, Table 2.5).

Table 2.5. Contribution of hydrochloric acid (HCl) and reducing reagent (sulphite) in ultra high purity de-ionised water (UHP water). Samples were spiked with 0.01 M HCl and 100 μ M sulphite or 200 μ M sulphite. LoD: Limit of detection.

Sample	Mean CL emission (V)	Standard deviation (V)	Concentration (pM)
UHP water	0.098	0.008	< LoD
0.01 M HCl	0.106	0.006	< LoD
0.01 M HCl + sulphite	0.107	0.011	< LoD
0.01 M HCl + 2 x sulphite	0.103	0.005	< LoD

The limit of detection for this analysis was 106 pM (n = 4). The signal of UHP de-ionised water was 0.098 ± 0.008 V (n = 4, 7.8 % RSD) while the sample with the addition of HCl gave a signal of 0.106 ± 0.006 V (n = 4, 5.9 %). Samples spiked with the reducing reagent exhibited signals of 0.107 ± 0.011 V (n = 4, 10 %) and 0.103 ± 0.005 V (n = 4, 4.6 %) for 100 and 200 μ M respectively. No increase in the signal was observed between UHP de-ionised water and UHP de-ionised water and HCl. Moreover, the detected signal did not change between UHP de-ionised water and samples containing different concentrations of sulphite. Hence, the contributions of HCl and sulphite were negligible compared with UHP de-ionised water only. To confirm this, an ANOVA test (analysis of variance) was performed to separate and estimate any potential causes of variation, using StatGraphics Plus, version 5.1. The P-value was 0.5944 (> 0.05) which indicates that there was not a

statistically significant difference between the mean values from one level of treatment to another at the 95.0% confidence level.

In seawater: The next step of the optimisation was to measure dissolved Fe(II) in filtered seawater. Sub-samples of seawater were acidified to pH 2.0, for at least one month, providing a stable concentration of dFe concentration (as a result of reduction of Fe(III) to Fe(II)), sulphite was added just prior to analysis. The Fe(II) seawater standards were made up to volume in Sterilin™ vials (20 mL) instead of volumetric flasks (25 mL), using pipettes, from 0.2 to 2 nM (gain of 10 on the interface). The calibration graph exhibited good linearity $R^2 = 0.9704$ with a precision between 7.4 and 15.6 %, the limit of detection was 0.080 nM, being higher than that observed for standards made in UHP de-ionised water. Further modifications were made to the procedures to improve the precision and lower the limit of detection and changes in the equipment were carried out. 30 mL LDPE bottles (Low Density PolyEthylene, Fisher) were used to replace the Sterilin™ vials (Ussher 2005; Milne 2007). The reducing reagent was spiked at least 8 h prior to analysis to allow the total reduction of iron(III) to iron(II) (Bowie *et al.* 1998). As a result of those modifications the calibration was linear (lower slope compared with UHP de-ionised water) over the range 0.5 to 8 nM ($R^2 = 0.9979$), the precision ranged from 1.5 to 6.6 % ($n = 4$) and the limit of detection was 40 pM, in total agreement with the 40 pM reported by Bowie *et al.* (1998). This improvement in linearity, precision and limit of detection supported the view that the reducing reagent should be spiked at least 8 h prior analysis but also that the sample containers should be chosen with care.

In order to improve the precision further, the loading time of the sample onto the 8-HQ micro-column mounted onto the injection valve was increased from 30 s to 43 s (version 14 of the VI). The concentration of the eluent was also increased from 0.06 to 0.12 M of HCl (SpA grade). BioVyon® F (high-density polyethylene) frits were used for the micro-columns at the end of the optimisation process. The PMT housing was regularly

opened for inspection. On one occasion, the surface of the mirror was damaged around the edge but mainly below the quartz flow cell (Figure 2.16.a) which contained white deposits. The mirror was changed to a 1 mm thickness mirror-silver styrene (Raboesch® Super Sheets, Zeewolde, The Netherlands) and the flow cell was also replaced (Baumbach & Co., Ipswich, UK, Figure 2.16.b)

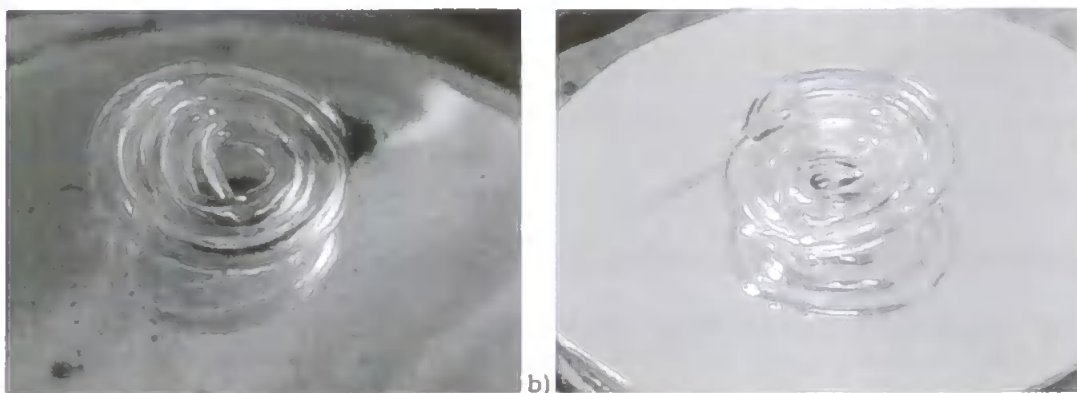


Figure 2.16. a) PMT opened with flow cell. b) detail of flow cell and mirror.

Furthermore, erosion at the base of the PMT indicated previous leaks suggesting backpressure problems. The mixing sample/buffer or UHP de-ionised water rinse with luminol passed through a T-piece to a flow cell (1.1 mm i.d., Figure 2.17.a). The new design of the outlet of the flow cell was the addition of peristaltic pump tubing blue-blue 2-stops (Elkay), on the flow cell outlet (1.6 mL min⁻¹) and purple-white 2-stops (Elkay) on the waste line of the PMT (3.90 mL min⁻¹, Figure 2.17.b) to allow a higher outlet flow rate, reducing resistance and backpressure through the flow cell and the waste line.

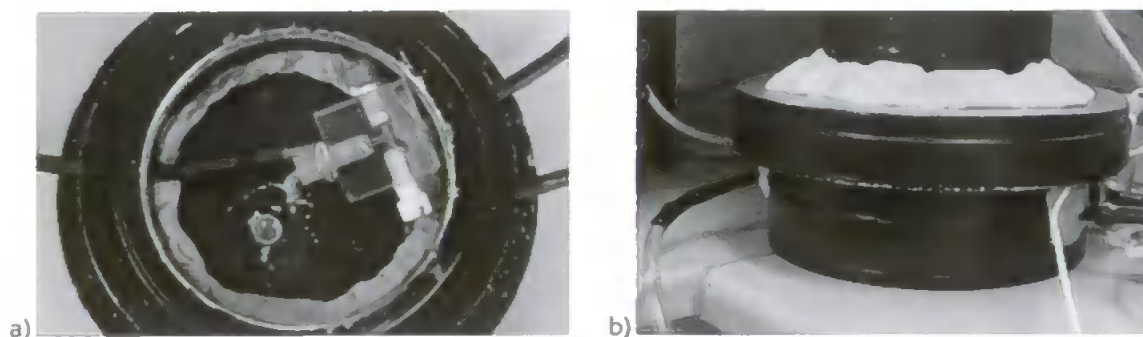


Figure 2.17. a) Detail for the T-piece and its connections. b) Insulation of the PMT from light.

nM, the limit of detection was 0.04 ± 0.04 nM ($n = 3$) and the precision ranged from 6.5 to 9.4 % ($n = 4$).

Accuracy

To test the accuracy of the system, an inter-comparison was carried out using an in-house reference material (surface water from the Canary Basin). To do this, two subsamples were analysed in quadruplicate ($n = 4$) then standard additions were prepared from 0.4 to 2.4 nM. The measured concentration was 0.85 ± 0.07 nM, which was in good agreement with the in-house "reference" value, 0.85 ± 0.02 nM, measured by Dr Simon Ussher. As a further check of the accuracy of the system, the certified reference material NASS-4 was analysed. The standard addition had a good linearity ($R^2 = 0.9666$) and the measured concentration of $1.95 \text{ nM} \pm 0.10$ was in agreement with the certified concentration of $1.88 \text{ nM} \pm 0.28$ nM. To test for statistical agreement for the NASS-4 sample, a comparison of the measured result with the certified value was carried out using the recommended method from the European Reference Material Commission (Linsinger 2005). The absolute difference between the mean measured value and the certified value was calculated as:

$$\Delta_m = |c_m - c_{CRM}| \quad \text{Equation 2.1}$$

Where Δ_m is the absolute difference between the mean of the measured value and the certified value, C_m the mean of the measured value and c_{CRM} the certified value. Each measurement has an uncertainty, expressed as the standard deviation. The uncertainty of Δ_m is calculated from the uncertainty of the measured value and the certified value as:

$$u_\Delta = \sqrt{u_m^2 + u_{CRM}^2} \quad \text{Equation 2.2}$$

Where u_Δ is the combined uncertainty of the measured value and the certified value, u_m is the uncertainty of the measured value and u_{CRM} is the uncertainty of the certified value. Then the expanded uncertainty U_Δ corresponding to a confidence interval of approximately 95 %, is calculated as:

Interface settings with new design of flow cell

The interface contained a 16-position switched gain amplifier, providing gain settings from 1 to 8000, selectable by the control VI software while the PMT had 4 gains from A (1) to D (1,000). To estimate the increase in sensitivity, 2 nM Fe(II) in UHP de-ionised water was analysed (gain 20 on the interface) using the two gains of the PMT used during analyses, from D to B (Table 2.6).

Table 2.6. Changes in signal and baseline noise using UHP de-ionised water, depending of the gains on the PMT and software. New design of flow cell, 8-HQ micro-columns with BioVyon® F frits.

Design	PMT gain	Software gain	Total gain	2 nM Fe(II)	Baseline noise (V)	Ratio
original	D – 1,000	20	20,000	1.165	0.0153	76.2
new	B – 10	20	200	1.012	0.0061	166

With the original flow cell design and original parts of the PMT, the total gain of the PMT and the interface was 20,000 and the ratio of the signal of 2 nM Fe(II) standard to baseline noise was 76.2. The signal-to-noise ratio with the new design and optimised settings was 166. With the new design and replacements of parts, gain on the PMT and software were decreased to a total gain of 200 instead of 20,000, demonstrating the enhanced sensitivity due to the design and operational changes made. The calibration was linear over the range 2 to 12 nM ($R^2 = 0.9965$), the precision ranged from 3.5 to 10 % ($n = 4$).

Analytical figures of merit using the optimised system

Over a period of 18 months, calibrations of Fe(II) were regularly run from 0.8 to 16 nM (gain 20 on the interface) with seawater. Typical linearity was $R^2 > 0.985$, the precision ranged from 0.2 to 10.8 % ($n = 26$) and the limit of detection was 0.041 ± 0.034 nM ($n = 26 \pm 1$ s.d.) in seawater. This variation was due to day to day changes in sensitivity of the system, mainly due to new batches of reagents and temperature in the laboratory. In UHP de-ionised water, calibrations showed good linearity ($R^2 > 0.985$) over the range 0.2 to 4

$$U_{\Delta} = 2 \times u_{\Delta} \quad \text{Equation 2.3}$$

To evaluate the difference between the measured value and the certified value, Δ_m is compared with U_{Δ} . If Δ_m is $\leq U_{\Delta}$ there is no significant difference between the measurement and the certified value. As $\Delta_m = 0.07$ was $< U_{\Delta} = 0.59$, there was no significant difference between the measured value and the certified reference value.

Variability between bottles

The errors associated with sample handling and the measurement technique for 5 LDPE bottles filled with acidified seawater collected from the Canary Basin, were investigated. Table 2.7 shows CL emission replicates ($n = 4$), their means and the precision for each bottle.

Table 2.7. CL emission of 5 LDPE bottles ($n = 4$) of acidified seawater.

Emission (nM)				Mean (nM)	RSD (%)
1.36	1.64	1.50	1.70	1.55 ± 0.15	7.68
1.44	1.77	1.77	1.93	1.73 ± 0.21	9.66
2.01	2.14	2.10	2.25	2.12 ± 0.10	3.92
1.66	1.86	1.73	1.94	1.80 ± 0.13	5.80
1.66	1.59	1.97	2.12	1.83 ± 0.25	11.11

The precision for the 5 bottles ranged from 3.9 to 11.1 %, indicating good reproducibility for analysis of individual samples. The overall precision between the bottles was 9.3 % ($n = 5$) suggesting a good reproducibility of handling and analysis. To confirm this, an ANOVA test (analysis of variance) was performed using StatGraphics Plus, version 5.1. The P-value was 0.0061 (< 0.05) which indicates that there was a statistically significant difference between the mean values from one level of treatment to another at the 95 % confidence level. A further ANOVA test identified bottle n° 3 (0.8783 V) to be significantly different from the others. The P-value was 0.2130 (> 0.05) for the 4 remaining bottles. The mean values for these four bottles was not significantly different at the 95 % confidence level and the precision was lowered to 5.8 % ($n = 4$). This shows that

2.3. RESULTS AND DISCUSSION

A manual FI-CL manifold was initially assembled to understand the chemistry of the method and optimised to minimise the blank signal. The system sensitivity was increased by integration of 8-HQ micro-columns. These columns preconcentrated the analyte, reducing interferences from major matrix cations Ca(II) and Mg(II), and removed the seawater matrix, preventing any precipitation of sea-salt ions at the reaction pH (Bowie *et al.* 1998; Cannizzaro *et al.* 2000). Due to limitations of the manual system, an automated FI-CL system was then assembled to improve reproducibility, limit of detection and sample throughput.

2.3.1. Manual FI-CL system without/with 8-hydroxyquinoline columns

Optimisation of the system

The manual system (Figure 2.1, section 2.2.2) comprised of a peristaltic pump, manual injection valve, photomultiplier tube and chart recorder. Calibrations were carried out in UHP de-ionised water, from 10 to 50 nM of iron(II), by loading a coil mounted onto the injection valve. Samples and reagents were initially prepared outside a class-100 laminar flow hood and were stored close to the system, resulting in poor linearity and precision. To improve the protocol, plastic bags and a perspex container to store reagent, eluent and samples and the installation of plastic protection above the analytical system were used to limit suspected atmospheric contamination. Furthermore, in order to optimise the signal-to noise ratio, the effect of changing the power supply voltage to the PMT was investigated. A 10 nM standard was passed through the system and the voltage was changed from 1,000 V to 1,600 V (gain D on PMT, Figure 2.12, Table 2.2). The signal-to-noise ratio varied from 7.7 to 11.8 depending on the power supply voltage used. A voltage of 1,500 V had the highest ratio (11.8) while voltages of 1,100 and 1,200 V showed a ratio of 10.0. However, 1,500 V was too high to give a linear response up to 50 nM. Therefore, a voltage of 1,200 V was chosen for all subsequent experiments.

Moreover, for a period of time, the system was positioned next to a laboratory with a strong magnetic field. The profile in this case was characterised by a baseline below - 2.5 V (typically between - 2.5 and -2.4 V) followed by an oscillation. The system was stopped and left to settle down for several hours.

A chemical interference was observed and variable profiles were recorded (Figure 2.19.a to e). An increase of the signal was observed when the sample was loaded onto the column followed by a decrease during the elution (Figure 2.19.a), oscillations of the baseline and of the analytical peaks which presented a secondary peak (Figure 2.19.b and c) but also oscillating peaks with oscillating baseline (Figure 2.19.d and e). It was concluded that the 8-HQ micro-column mounted on the injection valve was the origin of the variable profiles. After repacking the micro-column several times, the frits were replaced due to partial blockage by particles, reducing the flow and decreasing the capacity of the resin to preconcentrate Fe(II). The nylon frits were replaced by BioVyon® F (high density polyethylene, HDPE, 0.75 mm thickness, 22 - 57 µm pore range, Porvair Filtration Group Ltd., Fareham, UK).

2.3.3. Recommended protocols and maintenance

During the optimisation of the manual and automated FI-CL systems, analyses were preceded by an operational maintenance check. The temperature in the laboratory was checked regularly and the system was not used if the temperature was > 30 °C, which caused a variable signal due to the production of air bubbles, particularly in the luminol line.

Maintenance

Each analytical sequence was preceded by running the system for at least one hour with UHP de-ionised water in the sample line to give a stable baseline and reproducible peaks. The blank measurement for the determination of dFe was then determined as the

there is generally good reproducibility between bottles but that great care should be taken to monitor potential contamination of bottles.

Troubleshooting

Some challenges were experienced at the beginning of the assembly and operation of the automated system. The connection between the interface and the computer was lost randomly during analysis and hence control of the system was lost, the pumps turned in the opposite direction and the software showed an error message (bus control error). When this happened the computer and system had to be rebooted for more tests. The USB cable connecting the interface to the computer was changed due to corrosion but a faulty component of the hardware, a USB adapter type A (female) to type B (male) inside of the USB interface module, was responsible of this intermittent disconnection and was replaced.

During the optimisation, the system showed variable outputs due to electrical and chemical interferences. The electrical interference (Figure 2.18.a and b) appeared as random negative peaks on the baseline and on the analytical peaks (Figure 2.18.a) along with a noisy baseline while rinsing the system, followed by a loss of signal (Figure 2.18.b). It was concluded that the system was very sensitive to electrical interferences due to building work on the campus and this was limited by adding an anti-surge plug.

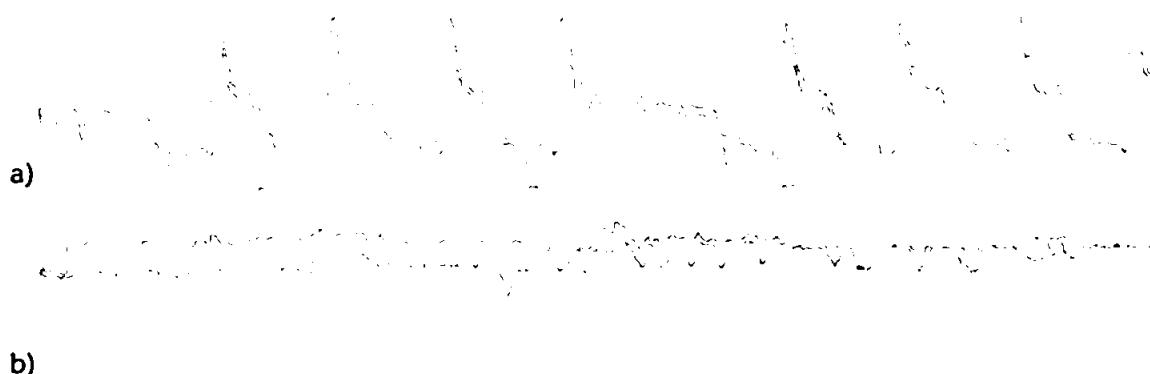


Figure 2.18. Chart showing electric interferences a) during analysis. b) during rinse of the system.

mean of the height of CL emission of 8 injections of ammonium acetate buffer (Figure 2.20).



Figure 2.19. a) increase of the signal when loading column. b and c) oscillations of the baseline and secondary peak. d and e) oscillating peaks and baseline.

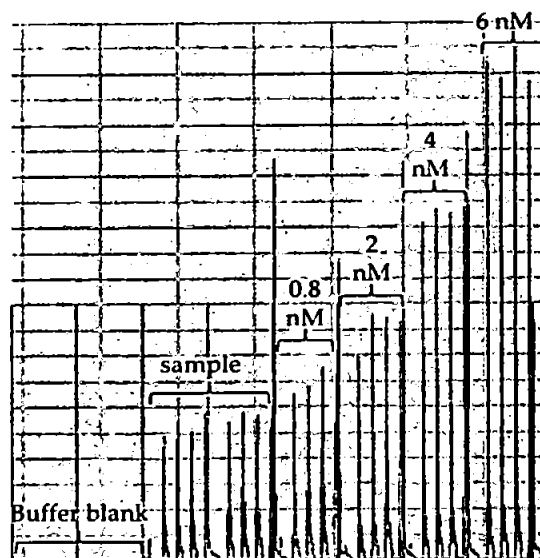


Figure 2.20. Typical output of standard additions in seawater between 0.8 and 6 nM.

The sample line to the T-piece was closed and the tubing disconnected from the head of the pump, while the buffer was injected through the T-piece and 8-HQ micro-column in the injection valve. The ammonium acetate buffer was injected at least 12 times and the last 8 replicates were used for the determination of the mean of the blank which was subtracted from the signals for the samples and standards. The limit of detection was calculated:

$$3 \times \text{standard deviation of the blank/slope} \quad \text{Equation 2.4.}$$

During analysis, the movement of the 8-HQ resin in the micro-column mounted onto the injection valve was checked during elution and loading. At the end of each analytical sequence, a final rinse of the sample line with UHP de-ionised water avoided any precipitation of salts from seawater. The pump tubes were then released from the head of the pumps to avoid any distortion of the tubes and ensure a constant flow rate. When the system was not in use, the lines were left in UHP de-ionised water to avoid precipitation in the lines and, particularly, in the flow cell.

Recommended protocols

Reagents and samples/standards

It is recommended to prepare the reagents as follows. New batches of luminol should be prepared at least 24 hours prior to use. Clean batches of luminol should be processed by passing through a clean Chelex-100 chelating resin column. The Chelex-100 column (approximately 200 mL) should be cleaned by passing 125 mL of high purity hydrochloric acid (1.2 M, SpA grade), rinsing with 800 mL of UHP de-ionised water, then discarding the first 200 mL of luminol solution prior to collection (the mixing of two batches of clean luminol was made at least the day before analysis in order to have an equilibrated mixing for stable baseline and sensitivity). The luminol should be kept for a maximum of one month. New batches of the ammonium acetate buffer solution should be prepared at least one day before use as freshly prepared buffer appears to greatly

decrease the sensitivity. Each batch of reducing reagent should be cleaned by passing twice through an 8-HQ micro-column and used at least one day later. Samples and standards should be prepared with the same matrix, at pH 2.

FI-CL components

For the PMT housing, all joints should be covered with black tape and PTFE tubing wrapped with black tubing and then sealed with rubber sealing compound. All tubing and connections in the FI-CL manifold should be checked regularly for leaks and wear and for light penetration into the PMT.

All manifold lines should be as short as possible, particularly the mixing line after the T-piece in the PMT to allow the fast (1 to 10 s) chemiluminescence reaction to take place within the detector window (Bowie 1999). For this reason, the T-piece should be situated as close as possible to the flow cell. The quantity of resin in the micro-column in the injection valve should be checked regularly; a well packed micro-column should be filled with ~ 90 % of 8-HQ resin to avoid backpressure.

Furthermore, it is highly recommended to have a reflective mirror in the PMT and a clean flow cell in order to maximise the sensitivity. Quartz is preferred to plastic for the flow cell due to better optical properties and inertness but the replacement of quartz flow cell is a delicate operation and requires great care. Moreover, it is crucial to condition the LDPE bottles before use, with acidified seawater, to avoid contamination.

Electrical issues

All connections should be checked regularly for corrosion. To avoid interferences it is recommended to use anti-surge plugs, particularly for the interface, computer and PMT tube. It is important to minimise any potential electric interferences and it is crucial to isolate the system from strong magnetic fields.

2.4. CONCLUSIONS

A manual FI-CL system was assembled and optimized for the determination of dissolved Fe(II) in UHP de-ionised water. Owing to its poor limit of detection (0.2 nM) and precision (from 2.9 to 12 %), an automated system was assembled and optimised for the determination of total dissolved Fe(II+III) in seawater at sub-nanomolar concentrations, suitable for aerosol dissolution experiments. Automation and optimisation of the system (e.g. cleaning of the reagents, use of LDPE bottles) allowed a more reliable determination of dFe concentrations, inducing improved limit of detection of 0.041 ± 0.034 nM ($n = 26$) in seawater, the precision ranging from 0.18 to 10.8 % ($n = 156$), and a lower risk of contamination during analysis. Moreover, the accuracy of the system was tested with a certified reference material NASS-4 ($1.94 \text{ nM} \pm 0.16$) and an in-house reference material (0.85 ± 0.07 nM). A good agreement with the certified values ($1.88 \text{ nM} \pm 0.28$ nM and 0.85 ± 0.02 nM respectively) was found. Furthermore, during the development of the automated manifold, protocols, maintenance and troubleshooting sections have been documented for effective utilisation of the FI-CL technique.

**DEVELOPMENT AND ASSESSMENT
OF THE EFFICIENCY OF A
SEAWATER TREATMENT SYSTEM**

3.1. INTRODUCTION

To evaluate the role played by organic ligands on the kinetics of aerosol iron dissolution, seawater with a low concentration of dissolved organic carbon (DOC) was required. The introduction of model complexing ligands in a series of defined experiments and comparison with non-UV irradiated seawater was deemed important to assess the role of natural organic complexes (see *Chapter Four*). Moreover, because dusts are mainly deposited in open ocean regions, low in iron and DOC (see *Chapter One*), it is crucial to mimic this natural environment by having a low background iron concentration in order to determine iron released from aerosols in seawater. For this reason, open ocean seawater with low DOC and iron was required as a matrix for the experiments described in this thesis to study the impact of iron complexing ligands. However, open ocean seawater (low in DOC / Fe concentrations) may not be always readily available, so an on-line system which can efficiently remove DOC and iron, by UV irradiation, was investigated.

Organic complexation of metals is known to prevent scavenging by suspended particles and formation of insoluble inorganic metal complexes, enhancing dissolved trace metal concentrations in seawater (Rijkenberg *et al.* 2006; Hunter and Boyd 2007). As trace metal concentrations in open ocean seawater are low (i.e. down to fM level), UV irradiation prior to analysis is a preferred method for the breakdown of dissolved metal-organic complexes, as contamination is kept at a minimum. UV digestion can be done "cleanly", does not require oxidants and is commonly used for destruction of organic matter before analysis (e.g. Achterberg and van den Berg 1994; Nimmo and Fones 1994; Achterberg *et al.* 2001a; Biscombe *et al.* 2004). Commonly, a mercury vapour lamp (medium or low pressure) is used as a source of UV radiation (Achterberg *et al.* 2001a; Sandford 2001; Konhauser *et al.* 2007).

Donat and Bruland (1988) developed a seawater treatment system for the removal of trace metals and DOC in seawater. The seawater was filtered by passing it through a 0.4 μm polycarbonate filter at 2 mL min^{-1} to remove particulates. Then, the filtered seawater was passed through different resins: Duolite S-587 to remove organics, Sumichelate Q-10R and Chelex-100 resins to remove trace metals cations. The seawater was then exposed to an UV irradiation for 5 h to destroy residual organics and passed through two Chelex-100 resins and finally a C18 resin to remove any remaining organics.

The aim of the work presented in this chapter was therefore to develop and assess the efficiency of an on-line UV photo-oxidation system coupled with ion exchange and C18 columns to produce low DOC and dFe seawater for model dissolution studies (see *Chapter Four*) from coastal seawater. The specific objectives of this chapter were (i) to assemble a variation of the on-line photo-oxidation system for the production of low DOC and Fe seawater by integrating a series of extraction columns, previously described by Donat and Bruland (1988), (ii) to assess its efficiency to breakdown DOC, (iii) to assess its efficiency to remove iron, (iv) to assess the efficiency of a simpler system with only a UV lamp (and no extraction columns) to breakdown DOC and to remove iron and (v) to determine the concentration of complexing ligands in treated seawater samples.

3.2. EXPERIMENTAL

3.2.1. Seawater treatment system

A variation of the system proposed by Donat and Bruland (1988) was constructed and is shown in Figure 3.1. The system was composed of a container of unfiltered seawater which was filtered in-line through a polycarbonate cartridge (0.2 μm , Supor Cap 50, PALL Gelamn Laboratory, VWR International Ltd., Lutterworth, UK) by a peristaltic pump (Minipuls 3, Gilson) at a flow rate of 1.0 mL min^{-1} (grey-grey 2-stops tubing, Elkay,) through a narrow bore PTFE tubing (polytetrafluoroethylene, 0.75 mm i.d., Fisher). The seawater was then pumped through a series of four columns: (i) Duolite A7, (ii) Amberlite

GT73, (iii) Amberlite XAD-16 and (iv) Chelex-100. The seawater was then passed through a UV irradiation system (400 W medium pressure mercury vapour lamp, Photochemical Reactors, Reading, UK) to destroy residual dissolved organics, then through two Chelex-100 resin columns in series followed by two Sep-Pak C18 resin columns to remove any remaining organic compounds. The resins were easily regenerated with 100 mL of 1 M HCl (Trace analysis grade), followed by 1 L of UHP de-ionised water, then 100 mL of 1 M NaOH and finally rinsed with 5 L of UHP de-ionised water. The Sep-Pack C18 columns were activated by passing 30 mL of UHP de-ionised water followed by 15 mL of high purity methanol (SpS grade, Romil), rinsed with 30 mL of UHP de-ionised water, then 15 mL of 1 M high purity HCl (SpA grade, Romil) and finally by 30 mL of UHP de-ionised water.

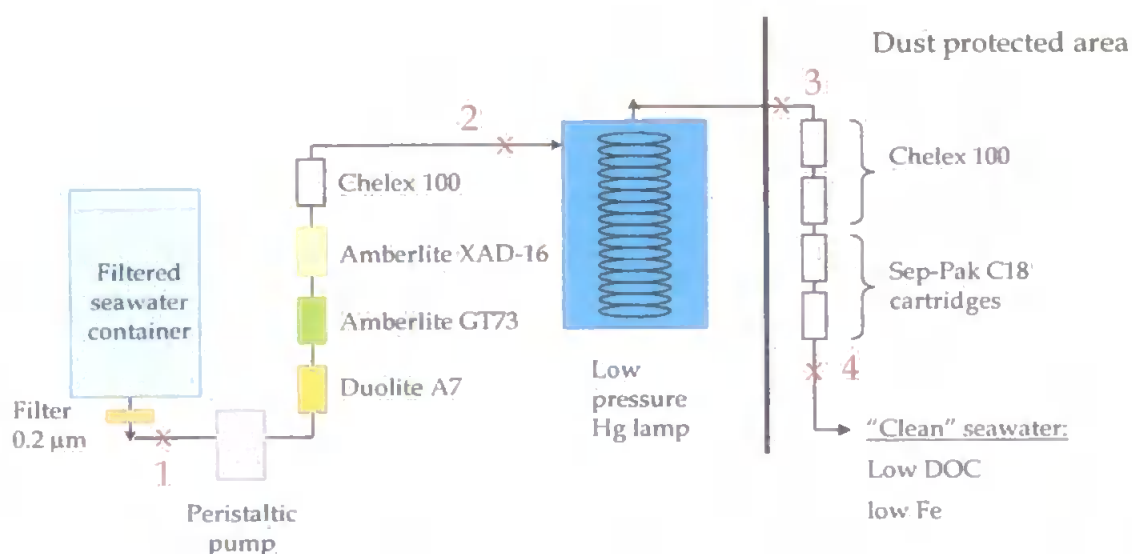


Figure 3.1. In-line UV photo-oxidation system coupled with complexing resins. X shows the four strategic sampling points: (1) filtered seawater, (2) after the first series of resins, (3) after the UV mercury lamp and (4) the final product.

Seawater was collected from station L4 (Eddystone Rocks, 50°10.80'N 4°15.90'W) 14 km south west of Rame Head (Cornwall, UK) by personnel from the Marine Biological Association of the United Kingdom in 2003 (salinity ~ 35). The seawater was then used for assessing the performance of the seawater treatment system and was stored in a carboy. The system was further assessed using two open ocean seawaters. One was collected in the Atlantic Ocean (open ocean seawater, salinity 37.3) during the AMT 16 cruise (see

section 2.2.1) whilst the other was collected in the Canary Basin (coastal ocean seawater, 2006, salinity 33.2) by Dr Micha Rijkenberg (at the National Oceanography Centre, Southampton, UK). Both seawaters were filtered from a tow fish, in-line using 0.2 μm pore size cartridge filters (Sartobran™, Sartorius Stedim. Biotech., Aubagne, France) and stored in the dark for 2 years before use.

3.2.2. UV irradiation system

The UV irradiation source used was a 400 W, medium pressure mercury vapour lamp (model 3040, Photochemical Reactors) shown in Figures 3.2 – 3.3 (Achterberg *et al.* 2001a; Sandford 2001). The lamp was encapsulated in an aluminium-housing and surrounded by a double walled quartz water jacket built in-house (Figure 3.2 – 3.3, Sandford 2001). This cooled the UV lamp using a submersible pump in a cool water reservoir. The 400 W medium pressure lamp emitted discrete Hg atomic lines at 365 and 313 nm with lower intensities at the shorter UV wavelengths of 254, 265, 270, 280, 289, 297, 302 and 334 nm and also in the visible regions at 436 and 405 – 408 nm (Figure 3.4). A photoreactor coil was constructed using fluoro-ethylene polymer (FEP) tubing (2.4 mm i.d., 3.2 mm o.d., 8 m length, 36 ml volume, Adtech Polymer Engineering Ltd., Stroud Glos, UK) wound around the quartz water jacket to enable on-line irradiation of the pumped sample. A light-tight lid was fitted over the lamp, immersion well and photoreactor coil and covered by a plastic container to minimise the loss of UV radiation and to eliminate exposure to UV radiation. The water jacket prevented excessive heating of the UV lamp by circulation of distilled water via a submersible pump contained in a large container, hence avoiding any risks of burning the coil or boiling the seawater samples. High voltage power for the lamp was provided by a 400 W reactive type supply with a large inductance (model 3140, Photochemical Reactors).

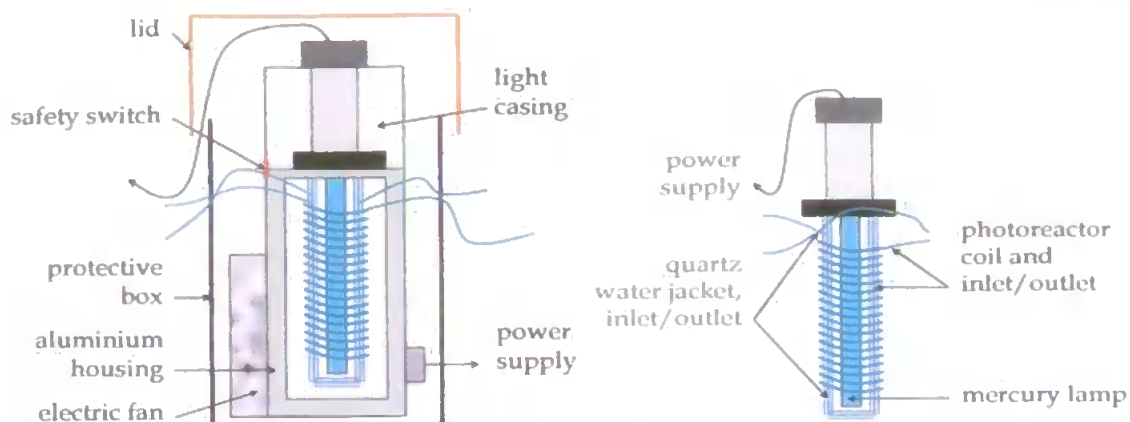


Figure 3.2. Main components of the mercury vapour lamp and of the UV photo-oxidation system.

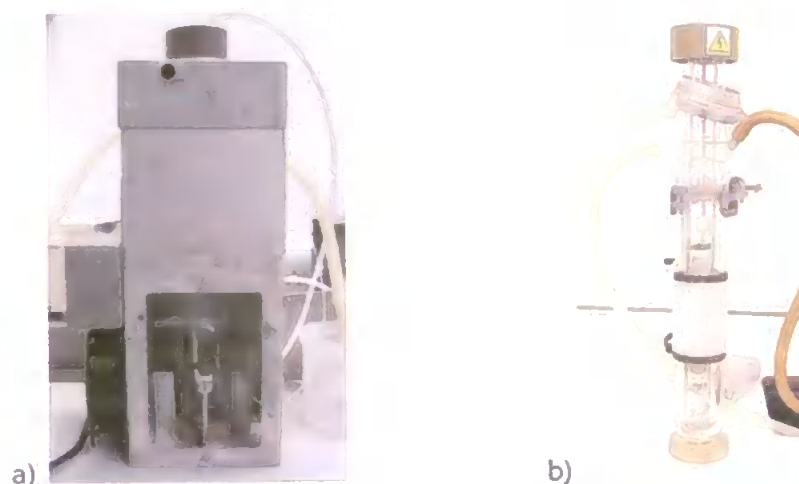


Figure 3.3. Mercury lamp. a) aluminium-housing encapsulating the UV lamp. b) UV lamp with water jacket and photo-reactor coil.

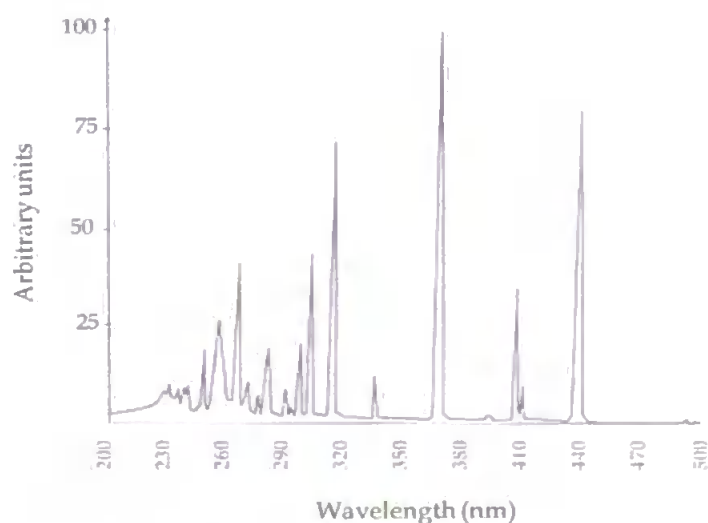


Figure 3.4. Spectral irradiance of the Model 3040 mercury lamp.

Once the system had been constructed, its efficiency was checked by determining the dFe and DOC concentrations in the coastal seawater at various stages in the treatment. Seawater samples were analysed for iron concentrations using the optimised FI-CL

detection system (see *Chapter Two*) and for DOC by a high temperature catalytic oxidation technique (HTCO, Sugimura and Suzuki 1988). Seawater Fe complexing capacity titrations were performed by Dr. Micha Rijkenberg using competitive ligand exchange-adsorptive cathodic stripping voltammetry (CLE-ACSV), developed by Croot and Johansson (2000), at the National Oceanography Centre (Southampton, UK) using the ligand 2-(2-thiazolylazo)-p-cresol (TAC, 10^{-5} M).

3.2.3. Determination of dissolved organic carbon (DOC)

Description of the analytical technique

Total organic carbon (TOC) was determined using a Shimadzu TOC-5000A analyser coupled with an ASI 5000A autosampler (Figure 3.5). The initial dissolved DOC was measured after filtration of the seawater (0.2 μm , polycarbonate filter). Determination of DOC concentrations in samples involved the full oxidation of organic matter to CO_2 by high temperature catalytic oxidation using a platinum based catalyst (Figure 3.6). Dissolved inorganic carbon (DIC) concentration is greater than DOC in seawater ($\sim 10^{18}$ g C, McCarthy *et al.* 1996), hence it is necessary to remove it prior to DOC analysis (sample decarbonation) by purging with CO_2 -free oxygen. Purification of the carrier air stream is achieved by passing it through hydrocarbon and organic filters (Fisons Scientific, Loughborough, UK), followed by a moisture trap, prior to delivery to the instrument at a regulated flow rate of 150 mL min^{-1} .

Aliquots of seawater samples (100 μL) were automatically injected onto the catalyst column, consisting of 0.5 % platinum on an aluminium oxide substrate (Pt on Al_2O_3). The catalyst has 98 % efficiency for converting total hydrocarbons and CO to CO_2 under net oxidising conditions whilst being maintained at a high temperature ($> 680^\circ\text{C}$). The combustion products (CO_2 , H_2O and radicals) are passed through a H_3PO_4 solution (25 %) in the inorganic reaction chamber, preventing the CO_2 being absorbed by the water vapour. The stream of gas is then dried by passing through a dehumidifier and purified

by a halogen scrubber and particle filters before analysis. Halogens have to be removed owing to their interferences with the infrared gas analyser (IRGA) during the detection of CO_2 . The signal (voltage) from the IRGA is recorded using Shimadzu TOC software which collects and integrates the peaks. Three replicate injections were conducted for each sample, followed by the automated calculation of the relative standard deviation. If this was $> 2\%$, then 2 more injections were carried out.

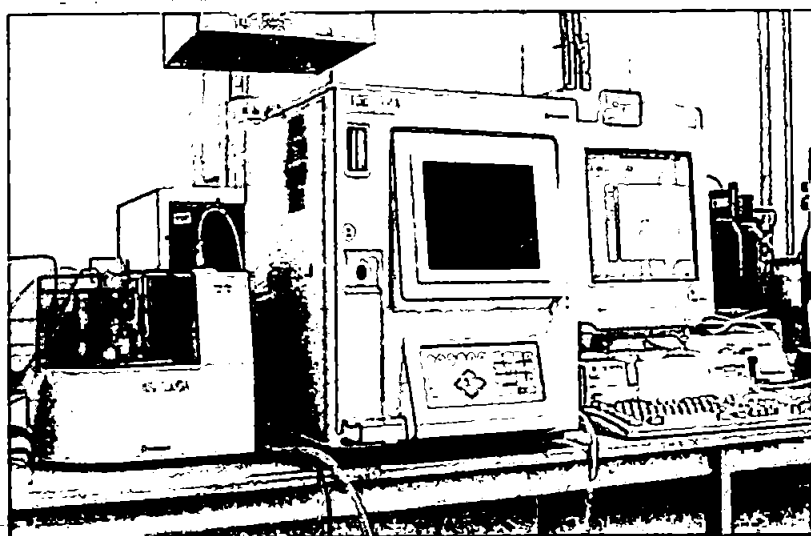


Figure 3.5. Shimadzu TOC 5000A analyser / ASI 5000A auto analyser, from left to right: autosampler, DOC analyser and computer for the acquisition of the data.

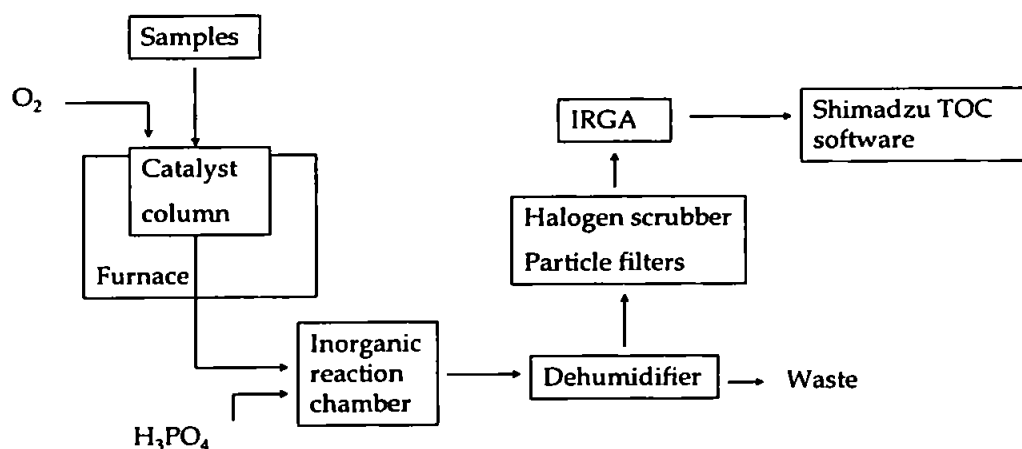


Figure 3.6. Schematic diagram of the main components of the Shimadzu DOC analyser.

Sample collection and preparation

All glassware was cleaned using a hot DeconTM detergent wash for 24 h, then a UHP water rinse, followed by an acid wash (50 % Trace analysis grade HCl, Fisher) for 5 days. Finally glassware was rinsed with copious volume of UHP de-ionised water, followed by

ashing at 450 °C in a muffle furnace for 4 h. Filtered seawater samples were collected in a dust protected area, using 60 mL acid washed glass bottles and were stabilised with 10 µL of 50 % v/v high purity HCl (SpA grade, Romil) per 10 mL of sample and stored in the fridge before analysis.

For each seawater batch treatment, the following procedure was used: the UV lamp was first switched on for 4 min (burning time, T_{0min}) to allow the lamp to reach its optimal temperature, then the submersible pump was turned on for 2 min (T_{4min}) to equilibrate the temperature in the water jacket and finally at T_{6min} the sample pump was switched on. Non-adherence to the burning time greatly decreases the efficiency of the UV lamp (Sandford 2001).

DOC standard preparation

One 6000 µM C stock solution was prepared from potassium hydrogen phthalate ($C_6H_4(COOK)(COOH)$) in UHP de-ionised water (DOC concentration < LoD), from which a series of 25 mL standards ranging from 60 µM C to 600 µM C were prepared by dilution. The blanks were below the calculated limit of detection which was 12 µM ($n = 4$) from:

$$((Blank + 3 * standard deviation) - intercept) / slope \quad \text{Equation 3.1}$$

3.2.4. Flow injection with chemiluminescence detection

All plasticware was cleaned in 20 % hydrochloric acid (Trace analysis grade, Fisher) for 48 h and then rinsed with UHP de-ionised water and stored in re-sealable plastic bags. Samples for the determination of dFe in seawater were treated as reported in *Chapter Two* whilst UV irradiated seawater batches were stored frozen. Calibrations were run with 10 mL standards, from 0.2 to 4 nM in UV-irradiated seawater. Analyses were conducted with an automated FI-CL detection system. The analytical performance (detection limits, linearity and blank) and hardware are discussed in *Chapter Two*.

3.3. RESULTS AND DISCUSSION

A photo-oxidation system was developed and its efficiency to remove DOC, dFe and iron complexing ligands in seawater was assessed using HTCO, FI-CL and CLE-ASCV respectively. Seawater was passed through the in-line system and sub-samples were taken for analysis at strategic collection points (Figure 3.1).

3.3.1. Complexing resins

Ion exchange resins are formed from a matrix, made from a polymeric material, to which ionic functional groups of an acidic, basic or chelating nature are attached. Resins are distinguished on the basis of this functionality: cationic (e.g. $-\text{SO}_3^-$ and $-\text{COO}^-$ active groups), anionic (e.g. $-\text{N}^+-\text{R}_3$ active group) and chelating (e.g. iminodiacetate, carboxylate, aminophosphonate groups) (Fernández *et al.* 2005). In this system, a series of five different resin columns were used to remove DOC and dFe (Figure 3.2):

(i) Duolite A7 is a weakly basic anion exchange resin (obtained from Sigma-Aldrich, St Louis, U.S.A.) and its functional group is a secondary amine. The highly porous structure of this hydrophilic granular resin makes it useful for the reversible adsorption of large organic molecules and de-acidification (Vera *et al.* 2003), and the removal of high molecular weight organic acid colourants (e.g. in wine processing, Porcal *et al.* 2004) and metal ions (Zhao *et al.* 2005). The effective pH range for this resin varies from 0 to 6 for de-acidification and from 0 to 8 for decolourisation. The resin has a longer service life when regenerated with Na_2CO_3 or ammonia rather than with NaOH, and is subject to attack by oxidants such as chlorine, chromic acid, peroxides and chlorates.

(ii) Amberlite GT73 is a weakly acidic exchange resin (obtained from Supelco, Bellefonte, U.S.A.) and its active functional group is a thiol (dithiol) ($[\text{R}-(\text{SH}_2)]$) which makes this resin useful for the selective removal of trace metals: $\text{Hg} > \text{Ag} > \text{Cu} > \text{Pb} > \text{Cd} > \text{Ni} > \text{Co} > \text{Fe} > \text{Ca} > \text{Na}$. This resin can be regenerated very efficiently with hydrochloric acid. Amberlite GT 73 is insoluble in common solvents and stable over the entire pH range.

(iii) Amberlite XAD-16 is a non-ionic and hydrophobic phase which derives its adsorptive properties from its high surface area and the aromatic nature of its surface (obtained from Sigma-Aldrich). This adsorbent is efficient for removing organic compounds of relatively low to medium molecular weight. Organic solvents (e.g. methanol, ethanol) are used to regenerate the resin for hydrophobic compounds whilst diluted bases (0.1 – 0.5 % NaOH) are used for weak acidic compounds.

(iv) Chelex-100: is a weakly chelating ion exchange resin (obtained from Sigma-Aldrich) which removes trace metal cations, with a high preference for copper, iron and other heavy metals. The selectivity depends upon the pH, ionic strength and the presence of other complex-forming species. Its selectivity in chloride solutions is $\text{Cu}^{2+} > \text{Pb}^{2+} > \text{Fe}^{3+} > \text{Al}^{3+} > \text{Cr}^{3+} > \text{Ni}^{2+} > \text{Zn}^{2+} > \text{Co}^{2+} > \text{Cd}^{2+} > \text{Fe}^{2+} > \text{Mn}^{2+} > \text{Ca}^{2+} > > > \text{Na}^{+}$. Exchange is very low below pH 2, increases sharply from pH 2 to 4, and reaches a maximum above pH 4. At very low pH; the resin acts as an anion exchanger and is stable over the entire pH range and functionally active from 2 to 14.

After passing through the columns described above, the seawater was then irradiated by the UV photo-oxidation system to destroy residual dissolved organic compounds; after which the seawater was passed through two more Chelex-100 resin columns followed by:

(v) Sep-Pak C18 is a resin (obtained from Waters Associates, Milford, USA) which removes refractory dissolved organics. The C18 Sep-Pak extraction technique was first reported by Mills and Quinn (1981) for the determination and characterization of organic copper complexes. It gained an increasing popularity and has been applied by many authors (e.g. Mackey 1983; Elbaz-Poulichet *et al.* 1994). However, Donat *et al.* (1986) showed that the cartridges may not extract all complexing organic ligands, isolating only a small fraction (< 12 %) of organic copper from seawater within the upper 100 m of the water column and between 11 and 30 % at depths between 125 and 5,000 m at a central

North Pacific Gyre station. The retained fraction on C18 bonded silica with methanol extraction is mostly composed of non-polar hydrophobic organic matter (Mills *et al.* 1982).

3.3.2 DOC concentrations

The dissolved organic carbon pool in the ocean is approximately 10^{18} g C (McCarthy *et al.* 1996), which represents the most important organic reservoir in the oceans (Spyres *et al.* 2000). DOC is fundamental to oceanic processes but its nature and function are not well defined in trace metal geochemical and biological cycles (Spyres *et al.* 2000). Prior to the late 1980s, DOC was presumed to be of refractory nature and was analysed by wet chemical oxidation techniques using e.g. hydrogen peroxide, nitric acid (Achterberg and van den Berg 1994; Achterberg *et al.* 2001a; Sandford 2001). Then Sugimura and Suzuki described the high temperature catalytic oxidation method for DOC determination in seawater (Sugimura and Suzuki 1988). The technique is rapid and precise for the determination of non-volatile organic compounds in seawater. In this work, the linear correlation (R^2) was typically > 0.99 over the range 60 to 600 $\mu\text{M C}$ whilst the observed precision ($n = 3$) ranged from 1 % to 7 % for the three seawaters (72 to 560 $\mu\text{M C}$), 10 % for the standard solution (100 $\mu\text{M C}$) and 40 % for the standard solution after UV treatment (6 $\mu\text{M C}$) from section 3.2.3.

Initial set up

The seawater treatment system was used to produce low DOC seawater in order to investigate the effect of the ligands on the dissolution of aerosol iron. The initial set up allowed the evaluation of the efficiency of the seawater treatment system with the initial set up for DOC breakdown, using coastal seawater with a DOC concentration of 560 μM . The objective was to lower the treated coastal seawater DOC concentration to the typical level of open ocean seawater ($\approx 40 \mu\text{M C}$). Some preliminary experiments were carried out with a flow rate of 1.1 mL min^{-1} . Samples were collected from four strategic sampling points in the treatment system: filtered seawater (1), after the first series of resins (2), after

the UV mercury lamp (3) and the final product (4, see Figure 3.1); two vials were collected for each sample. Figure 3.7 shows the detected DOC concentrations (μM).

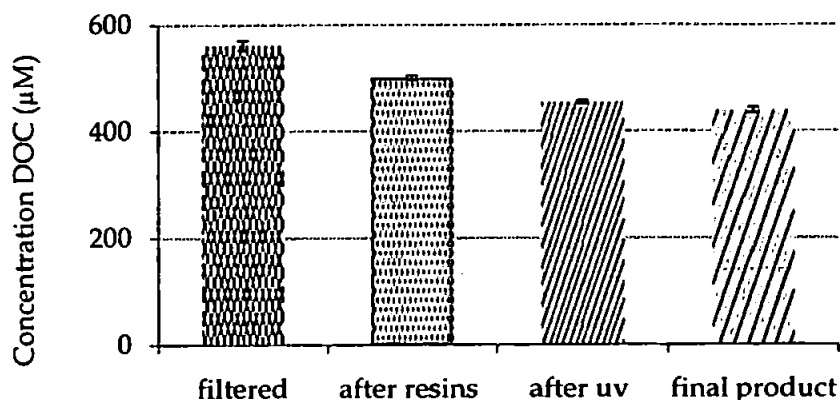


Figure 3.7. DOC concentrations (μM) in seawater through the different stages of the UV photo-oxidation system. Error bars = ± 1 s.d.

DOC concentrations decreased from 560 μM after the filter to 440 μM in the final product which represents a removal of 22 %. There was removal of DOC in the samples at each stage of the system but it was less efficient than expected. Achterberg *et al.* (2001a), for example, showed a 90 % DOC decrease in low carbon seawater with an on-line UV photo-oxidation system coupled with a Sep-Pak C18 column. Addition of hydrogen peroxide (H_2O_2) to Tamar estuary water (2.27 mg L^{-1} C / 0.189 mM) showed a net diminution of 77 % DOC within 11.2 min of UV exposure and H_2O_2 addition (15 mM). The low removal efficiency was probably due to the age of the lamp (6 years, black deposits on each extremity of the lamp) which may decrease the efficiency of the breakdown of organic compounds as a result of the lower intensity of emitted UV radiation. Furthermore, the high DOC concentrations found (Fry *et al.* 1996; Peltzer *et al.* 1996) can result from storage of unfiltered coastal seawater for a long period of time which can encourage bacterial populations in the seawater to thrive, using the particulate material as a food source (Fukami *et al.* 1983; Grossart *et al.* 2003). The high DOC concentrations would also have led to a lowering of the efficiency of the resins by rapidly saturating the columns.

Optimisation

Owing to a low breakdown efficiency and high DOC concentration, the system was optimised first by regeneration of the resins and secondly, by replacement of components in the system. A new batch of freshly collected coastal seawater of lower DOC concentration was passed through the seawater treatment system once the resins had been regenerated and samples were collected from the following points: initial filtered seawater (1), after the UV lamp (2) and the final product (4). The DOC concentrations found are presented in Figure 3.8.

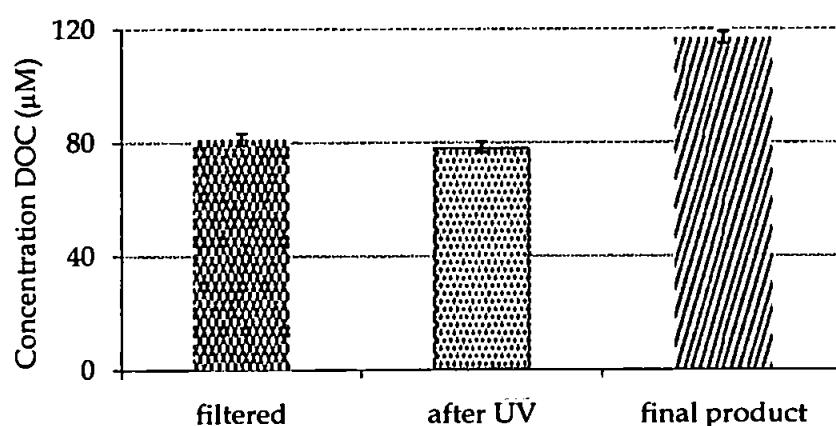


Figure 3.8. Effect on the DOC concentrations (μM) in a new batch coastal water and regeneration of the resins. Error bars = ± 1 s.d.

The initial concentration of DOC in the new batch of coastal seawater was 81.4 ± 2.1 μM (0.98 ± 0.03 mg C L^{-1}), which was in the typical range of concentrations for coastal waters (Fry *et al.* 1996; Peltzer *et al.* 1996). A small decrease in the concentration was observed between the filtered seawater and after the UV lamp but the final product exhibited an increase of 33 % in the concentration of DOC, going up to 117 ± 2 μM (1.40 ± 0.02 mg C L^{-1}). It was concluded that the last stage of the treatment process increased the DOC due to the elution of organic ligands from the Chelex-100 and Sep-Pak C18 columns and that the resins should be regenerated regularly (every 10 L treated) and the system used to process small batches of seawater.

Owing to its poor efficiency, the system was inspected and crucial elements were changed. Firstly, the lamp had significant deposits of mercury on the extremities of the

glass casement, most likely due to its age and past usage. Therefore a new medium pressure mercury lamp was purchased. Moreover, the water jacket had deposits on its walls, indicating photo-reactions between the UV lamp and the contents of the cooling water. Treatment with 50 % v/v HCl (Trace analysis grade) removed these deposits (Figure 3.9).

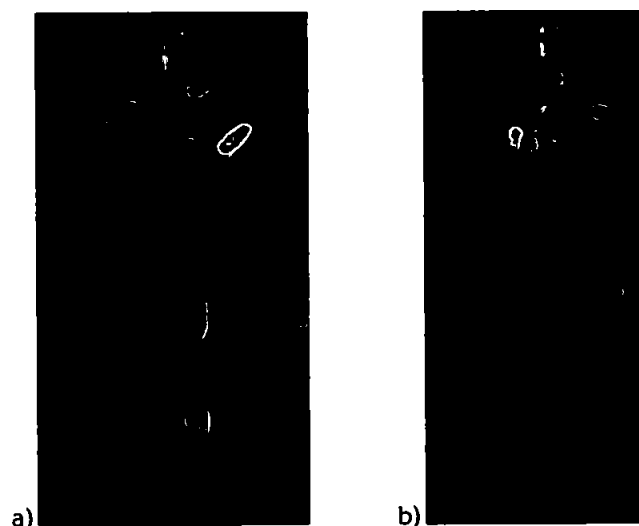


Figure 3.9. Water jacket a) before and b) after cleaning with 50% v/v HCl.

Finally, the fluoro-ethylene polymer (FEP) tubing coil on the water jacket was changed to a smaller diameter (0.8 mm i.d., 1.6 mm o.d., 9 m length, 3.98 mL volume, Adtech Polymer Engineering Ltd., Stroud Glos, UK), to improve exposure of the sample to the UV irradiation. The aim of this final optimisation was to process large volumes of seawater, with potentially high initial DOC concentrations, in order to provide suitable water for the dissolution experiments described in *Chapter Four*. Therefore the columns were removed because they became saturated quickly under the conditions used and the system performance was re-evaluated using only the UV lamp. Two ocean seawaters (open Atlantic Ocean and coastal Canary Basin) and a standard solution (100 μM C of potassium hydrogen phthalate in UHP de-ionised water) were used to evaluate the efficiency of the lamp. Water was passed through the coil at 1.1 mL min^{-1} (equating to a sample exposure to the lamp of 5 min). The observed DOC concentrations are presented in Figure 3.10.

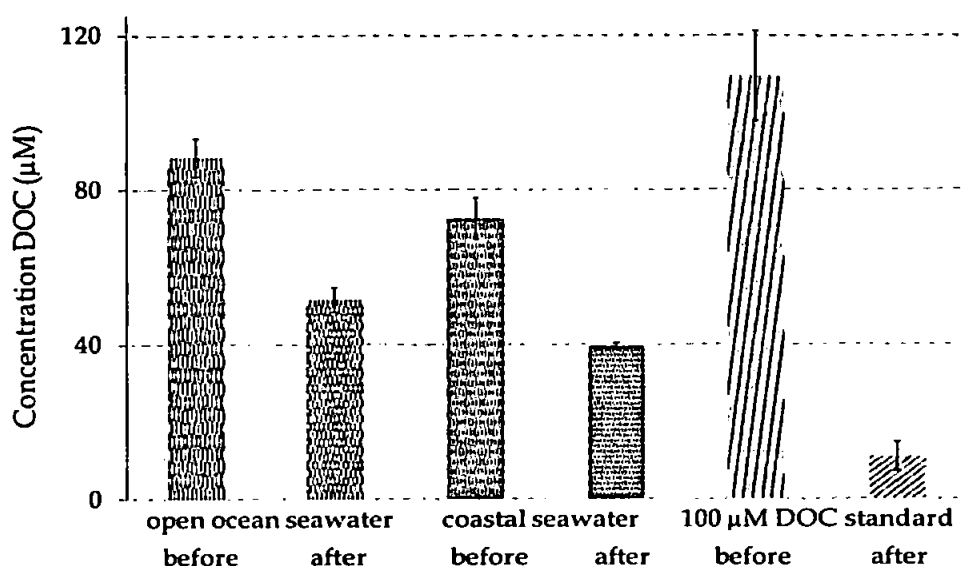


Figure 3.10. The effect of the UV lamp treatment alone on the DOC concentration in two ocean seawaters, (a) open ocean seawater (Atlantic Ocean) (b) coastal ocean (Canary Basin), and (c) 100 µM DOC standard at 1.1 mL min⁻¹. Error bars = ± 1 s.d.

The open Atlantic Ocean seawater contained $88.4 \pm 4.9 \mu\text{M}$ ($1.06 \pm 0.06 \text{ mg C L}^{-1}$) whilst the Canary Basin seawater had $72.5 \pm 5.4 \mu\text{M}$ ($0.87 \pm 0.07 \text{ mg C L}^{-1}$) of DOC initially, decreasing to $51.5 \pm 3.2 \mu\text{M}$ ($0.62 \pm 0.04 \text{ mg C L}^{-1}$) and $39.5 \pm 0.8 \mu\text{M}$ ($3.3 \pm 0.1 \mu\text{g C L}^{-1}$) respectively after treatment. The percentage breakdown of DOC was therefore 42 % for the Atlantic Ocean sample and 46 % for the Canary Basin sample. Similar studies have investigated the breakdown of DOC in seawater and Milli-Q (MQ) water spiked with humic acid which was chosen as an indicator compound for UV digestion due to its refractory nature (Achterberg and van den Berg 1994; Achterberg *et al.* 2001a). These studies showed that humic acid solutions in non acidified MQ water exhibited a breakdown of > 99 % for 3.8 mg C L^{-1} (within 100 s), 7.75 mg C L^{-1} (after 275 s) and 15.5 mg C L^{-1} (after 275 s). Under the same conditions seawater collected from the Mediterranean Sea achieved > 98 % of 15.5 mg C L^{-1} humic acid with an exposure time of 275 s. However, lower breakdowns in this study were probably due to the fact that seawater is composed of a variety of complexing ligand categories which would be more or less refractory to UV irradiation.

Furthermore, the standard solution decreased from $109.4 \pm 11.7 \mu\text{M}$ ($1.31 \pm 0.14 \text{ mg C L}^{-1}$, RSD = 10 %) to $10.9 \pm 3.8 \mu\text{M}$ ($0.13 \pm 0.05 \text{ mg C L}^{-1}$, RSD = 30 %). The striking increase in breakdown of DOC obtained (90 %) with $100 \mu\text{M}$ standard solution compared with the two open ocean seawaters might be due to the simple matrix of the standard, UHP de-ionised water only, and a single photoreactive DOC compound. The seawater matrix is complex, with an ionic strength of 0.7 M, which will reduce the effect of the UV irradiation. Moreover, a significant fraction of natural organic ligands present in seawater are not thought to be photochemically reactive, e.g. Desferioxamine B (Barbeau *et al.* 2003).

Effect of flow rate

In order to increase the breakdown efficiency of the new system the flow rate was decreased from 1.1 to 0.5 mL min^{-1} , giving exposure times of 5 and 10 min respectively. The results are given in Figure 3.11 and show an improvement in breakdown efficiency from 90 % to 95 % with the slower flow rate, using UHP de-ionised water.

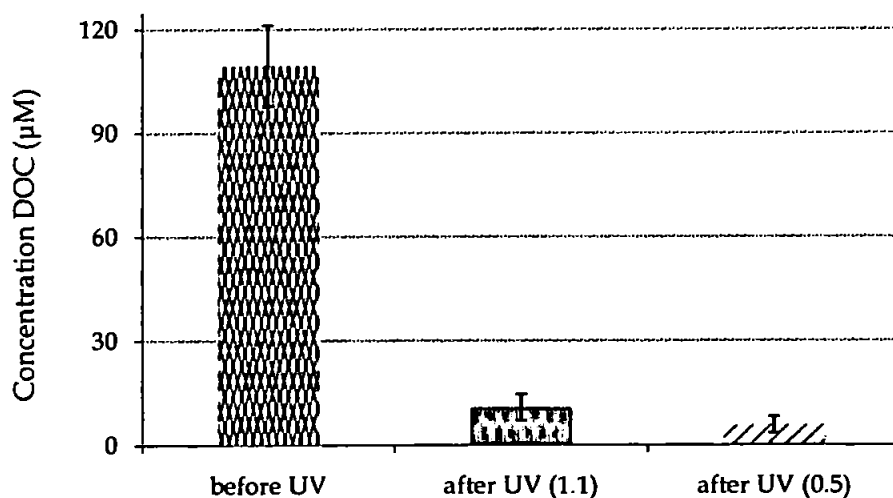


Figure 3.11. The effect of flow rate on DOC concentration in $100 \mu\text{M}$ DOC standard, 1.1 and 0.5 mL min^{-1} . Error bars = $\pm 1 \text{ s.d.}$

Sandford (2001) investigated the breakdown of DOC using humic acid standard (3 mg L^{-1}) in UHP de-ionised water passed through a medium pressure mercury lamp with and without the addition of nitric acid (pH 2) and hydrogen peroxide (10 mM). The

breakdown of the non-spiked standard was 63 % for an exposure time of 400 s whilst the spiked standard had a breakdown of 96 % for 400 s exposure time. In this study, the standard solution (100 μM C) had a comparable breakdown efficiency for a similar exposure time. The lamp was therefore highly efficient in the breakdown of potassium hydrogen phthalate in UHP de-ionised water, particularly at 0.5 mL min^{-1} , due to the replacement of the lamp, smaller diameter of the coil and clean water jacket. The lower flow rate (0.5 mL min^{-1}) was used for all future treatments.

3.3.3. Dissolved Fe concentrations

The seawater treatment system was also tested to produce low iron seawater to mimic natural open ocean regions for dissolution studies of aerosol iron in seawater (see *Chapter Four*). The objective was to lower the treated non acidified coastal seawater dFe concentration to the level typical of open ocean seawater (picomolar concentrations).

Initial set up

The first assessment of dFe concentration was carried out simultaneously with the DOC determination using coastal seawater collected in the English Channel, and passed through the entire seawater treatment system at 1.1 mL min^{-1} . Samples were taken at three strategic points (Figure 3.1): filtered seawater (1), after UV lamp (2) and the final product (4). Two vials were collected for each sample, the results are shown in Figure 3.12. Concentrations of dFe decreased from 0.77 ± 0.06 nM in filtered seawater to below the limit of detection after the UV lamp and final product (0.23 nM), the calculated concentration was 0.02 ± 0.02 nM after the UV lamp. The instrumental precision for replicate samples ($n=2$) ranged from 7.3 to 13 %. The system incorporating the different resins was therefore extremely effective in removing iron from the seawater samples with an efficiency of > 98 %.

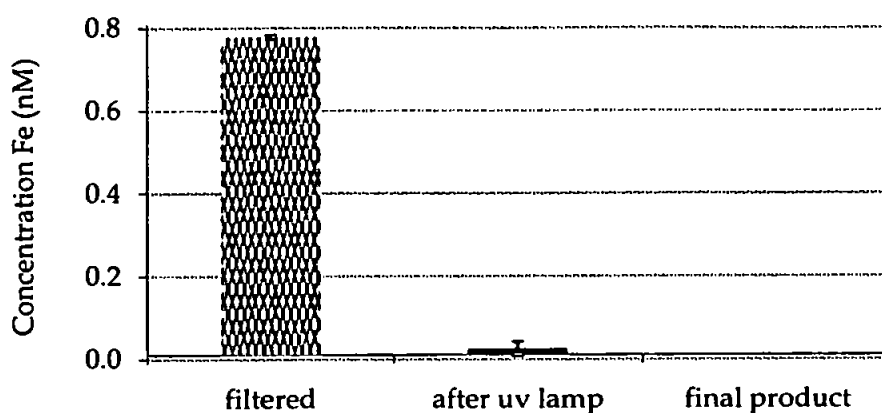


Figure 3.12. Concentrations of Fe (nM) in seawater at different stages of the treatment, error bar = ± 1 s.d.

Optimisation

In order to be compatible with the optimum conditions for DOC removal the efficiency for dFe removal was re-evaluated at a flow rate of 0.5 mL min^{-1} . Once the modification had been made and the optimum flow rate established, Atlantic Ocean (open ocean) and Canary Basin (coastal ocean) seawaters were treated using the lamp only (Figure 3.13), their initial dissolved Fe concentrations being 0.70 ± 0.12 and 2.19 ± 0.27 nM respectively. The dFe concentration in both seawaters decreased after UV irradiation to 0.27 ± 0.05 nM and 0.05 ± 0.02 nM for the coastal water and open ocean seawaters respectively. This was equivalent to removals of 88 % and 93 % for the Canary Basin and Atlantic Ocean seawaters. A decrease of 30 % in dFe concentrations in estuarine waters using Philips UV-A, B and VIS lamps (280 – 680 nm) has been observed by Rijkenberg *et al.* (2006). They explained the decrease by the degradation of the Fe(III) chelators and the increase of free iron which might have increased the inorganic Fe(III), inducing precipitation of particulate iron. In this study, adsorption of dFe onto the FEP coil tubing could have occurred due to the use of non acidified seawater, inducing an apparent decrease in dFe concentrations. Rinsing of the coil with weakly acidified UHP de-ionised water or seawater and its measurement by FI-CL would have confirmed this hypothesis. Acidification of the seawater before treatment would have prevented any adsorption onto the walls and this is recommended for future study. Moreover, generation of hydrogen

peroxide and radicals during irradiation might have interfered in the signal of the FI-CL manifold.

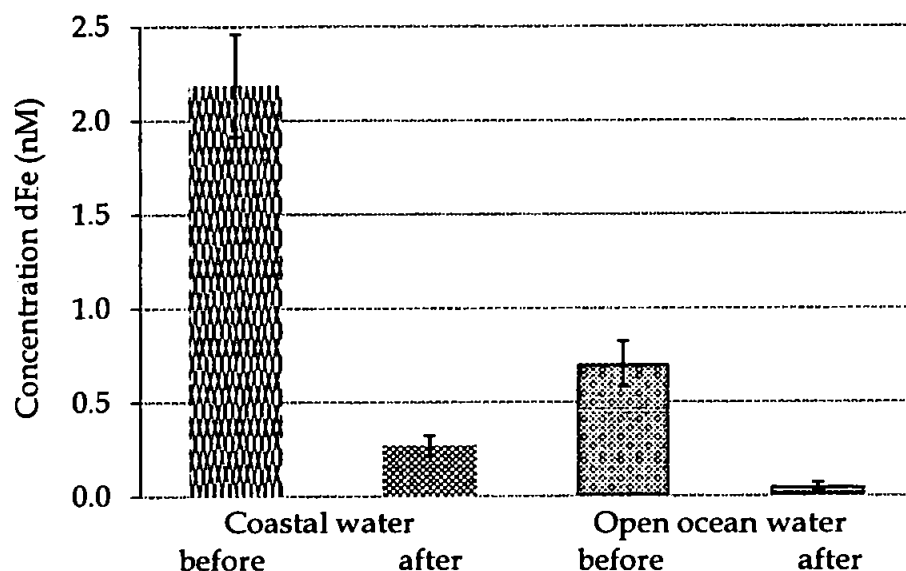


Figure 3.13. Concentration of dFe in coastal ocean (Canary Basin) and open ocean (Atlantic Ocean) seawaters before and after UV irradiation. Error bar = ± 1 s.d.

3.3.4. Complexing ligands titration

Due to the varying efficiency of the UV lamp for breaking down different fractions of the DOC pool, titration of total and free (difference between total binding ligands added and ligands complexed with Fe) iron binding ligands was carried out in the coastal seawater collected in the Canary Basin and the open ocean seawater collected in the Atlantic Ocean (stored frozen and used for dissolution studies, see *Chapter Four*), at the National Oceanography Centre (Southampton, UK) using CLE-ACSV and the ligand 2-(2-thiazolylazo)-p-cresol (TAC, 10^{-5} M). The concentrations are reported in Figure 3.14.a and b.

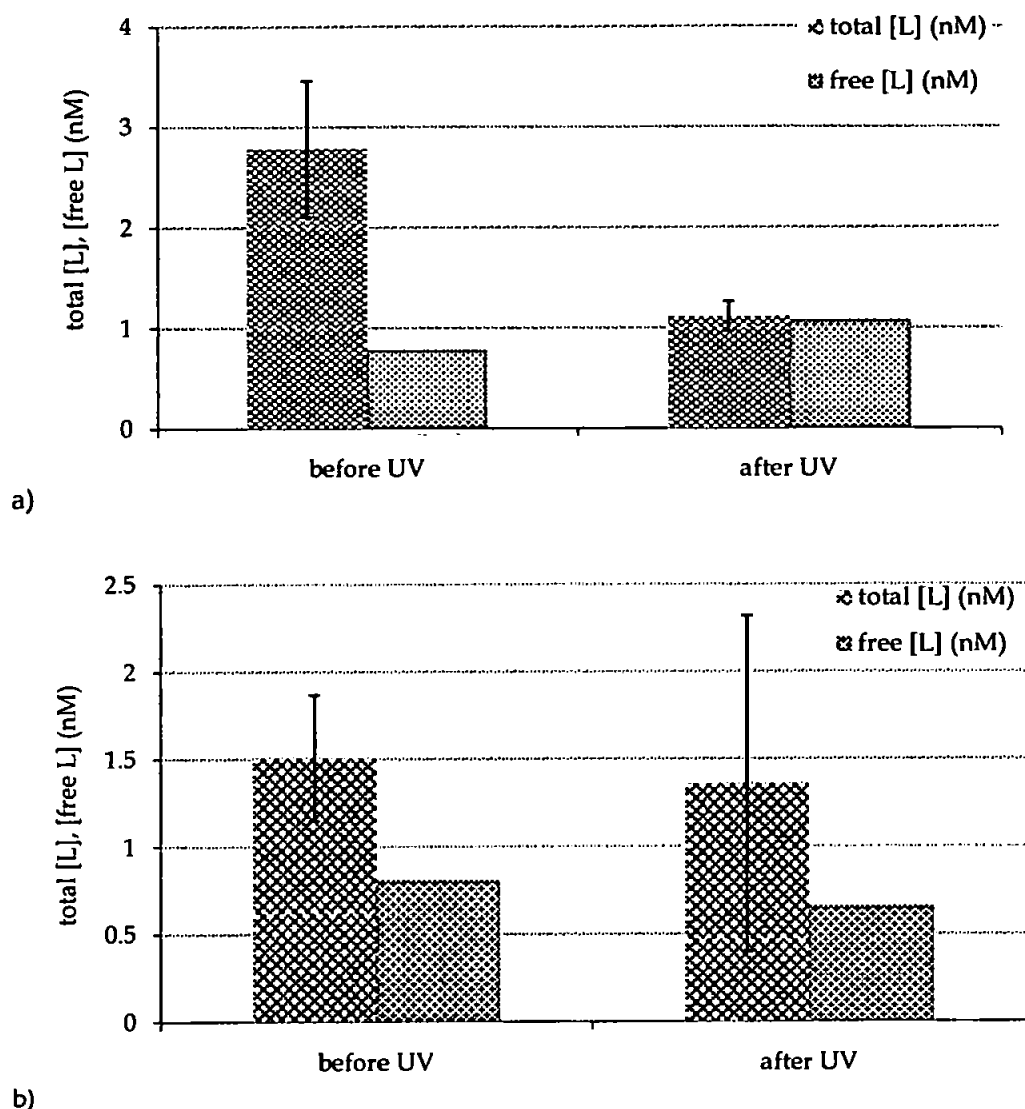


Figure 3.14. Concentrations of total and free ligands before and after UV irradiation in seawaters collected from (a) the Canary Basin and (b) the Atlantic Ocean.

In the Canary Basin seawater, the concentration of total ligands was 2.78 ± 0.68 nM initially and decreased to 1.11 ± 0.15 nM after irradiation whilst in the Atlantic Ocean seawater, the concentration was 1.51 nM and decreased to 1.36 nM after irradiation. However, the free Fe-binding ligand concentration increased slightly from 0.78 to 1.08 nM in the Canary Basin seawater whilst in the Atlantic Ocean the concentration decreased from 0.81 to 0.66 nM after irradiation which indicated in both that there were still Fe-binding ligands present after UV irradiation. Moreover, the logarithm of the conditional stability constant of the ligands was $\log K' = 23.34$ before and $\log K' = 22.75$ after UV irradiation in the Canary Basin seawater and $\log K' = 23.34$ before and $\log K' = 23.18$ after

UV irradiation in the Atlantic Ocean seawater. The breakdown of Fe complexing ligands was 60 % in the Canary Basin seawater and only 10 % in the Atlantic Ocean seawater. Similarly, Rijkenberg *et al.* (2006) investigated the effect of light on the destruction of Fe complexing ligands in two Dutch estuarine waters, using Philips UV-B, A and VIS lamps (280 - 680 nm). The initial concentrations of ligands were ~ 23 nM and after UV irradiation, the samples contained ~ 18 nM. The breakdown was 21 %. The higher breakdown in this study might be due to the origin and the storage of the seawater which was, in this study, open ocean water aged for more than two years in the dark. The ligands might have been (i) destabilised with ageing of the seawater whilst Rijkenberg *et al.* used freshly collected estuarine waters, with higher concentration in complexing ligands and (ii) different in character to estuarine ligands.

3.4. CONCLUSIONS

A photo-oxidation system was developed to produce low DOC and dFe seawater and its efficiency was assessed using HTCO, FI-CL and CLE-ASCV. The seawater treatment system showed an improvement in the removal of DOC concentrations once the optimisation was carried out, i.e. new UV lamp, water jacket cleaned and diameter of coil reduced. The final efficiencies were measured by passing seawater through the UV lamp only due to potential leak of DOC from the last Chelex-100 columns. The removal of organic compounds were 42 % and 46 % for Atlantic Ocean and Canary Basin seawaters respectively and up to 95 % for a 100 µM DOC standard made up in UHP de-ionised water. DOC removal in seawater was relatively poor compared with literature data. This was probably due to a combination of the following: nature of seawater, saturation of the Sep-Pak C18 columns, also incomplete oxidation by UV irradiation and bacterial leaching from filter and resins. The apparent removal of dFe was 88 % and 93 % for Canary Basin and Atlantic Ocean seawaters respectively. This decrease should not have occurred and the concentrations should have remained the same or an increase in dFe concentrations should have been determined after exposure to UV radiation. This apparent removal

could have occurred due to adsorption of dissolved iron onto the walls of the FEP coil tubing or interferences in the signal of the FI-CL manifold by generation of hydrogen peroxide and radicals. The use of acidified seawater would have prevented adsorption of dFe onto the wall of the FEP tubing. Adsorption of dFe would have been verified by rinsing with weakly acidified UHP de-ionised water or seawater. Finally, the breakdown of the iron binding-complexing ligands accounted for 60 % and 10 % of the total ligand concentration in the Canary Basin and Atlantic Ocean seawaters respectively. The low breakdown efficiency of the complexing ligands might be due to the utilisation of FEP tubing instead of quartz coil, lowering the light transmitted through the coil and samples.

In order to improve the removals, the system should include the different resins: Duolite, Amberlites, Chelex, followed by the UV lamp and finishing by Chelex. The Sep-Pak C18 should be included in the first series of resins to avoid contamination in the final product. Moreover, the coil should be made of quartz, suspended or placed onto the bottom of the aluminium housing to avoid breaks, allowing a higher exposure of the samples at the low wavelengths.

**FACTORS IMPACTING UPON THE DISSOLUTION
OF AEROSOL IRON IN SEAWATER**

4.1. INTRODUCTION

Different methods have been adopted to investigate and constrain the solubility of aerosol iron in seawater (as discussed in *Chapter One*), including the use of (i) discrete end-member aerosol material in incubation systems whilst extracting sub-samples over time (from 1 to 35 days) to garner information on the kinetic response (e.g. Bonnet and Guieu 2004; Milne 2007; Mendez *et al.* 2009), (ii) a single equilibration time using high / low volume aerosol collected samples and (iii) a semi-continuous flow system. For (i) the sub-samples, after collection, are filtered, terminating the reaction between the particles and seawater, and subsequently analysed for iron. The limitations of this approach (i) are that the temporal resolution of sample collection at the start of a dissolution process is limited due to a low temporal resolution, which may mask potential fast release of iron, and also increases the sample handling, which enhances the risk of contamination. Another limitation of the studies by Bonnet and Guieu (2004), Milne (2007) and Mendez *et al.* (2009) was that, although low dust concentrations were used, only a limited range of experimental / environmental conditions, potentially impacting upon the dissolution process, were investigated. The limitation of the approach (ii) is a lack of information in the kinetic of the dissolution of iron from the aerosols; one single equilibration time could either under or over-estimate the maximum solubility (e.g. Hodge *et al.* 1978, Crecelius 1980, Chester *et al.* 1993, Bonnet and Guieu 2004). The utilisation of a semi-continuous (iii) flow system (Wu *et al.* 2007; Aguilar-Islas *et al.* 2009) might over-estimate the solubility of iron over time due to input of new batches of seawater are introduced into the system for subsequent sub-samples. Low particle concentrations are essential to mimic the dissolution of aerosol elements in the open ocean and hence nanomolar/ sub nanomolar concentrations of dFe would need to be measured during such studies. Therefore minimising the risk of sample contamination is essential.

The aim of the work presented in this chapter was to investigate the impact of various factors (physical and chemical) on the dissolution of aerosol iron in seawater.

Therefore, the objectives were to (i) design, construct and validate an aerosol seawater dissolution system with an automated sampling system and (ii) apply the system to assess the effects of chemical and physical parameters on the extent and kinetics of the dissolution of aerosol iron in seawater under carefully controlled conditions.

The criteria for the automated sampler were to collect discrete samples, over short periods of time, during the first few hours of a study to define the short term dissolution kinetics and also have the ability to collect over an extended period (i.e. several days) to monitor medium term kinetic processes. Owing to the low concentrations expected, the determination of dFe was carried out using FI-CL (see *Chapter Two*). Preliminary validation of the integrated incubation / sampling system was carried to assess the system blanks and potential adsorption of dFe onto the incubation vessel walls. The effects of seawater treatment (stirring and cooled UV irradiated seawater) were also investigated.

As the extent and kinetics of the seawater solubility of aerosol iron are influenced by a complex array of processes (see *section 1.3*), once the incubation/sampling system had been validated, the impacts of physical (light intensity) and chemical parameters (dissolved organic ligands) on the dissolution process were investigated. Dust was introduced into the incubation system containing seawater at concentrations ranging from 0.25 to 2 mg L⁻¹, the lower dust concentration being representative of a medium to strong Saharan dust event over a 10 m mixed surface layer (Bonnet and Guieu 2004). This range of concentration was applied to investigate the particle effect amongst the physical and chemical factors. During dissolution studies seawater samples were extracted from the incubation vessel using a peristaltic pump, in-line filtration system and 10-way distribution valve. Samples were taken over a 1-day period for short term to 7 days for long term kinetics and total dFe(II+III) was determined by FI-CL after acidification and sulphite reduction. Instrument control, sample collection and data processing were

facilitated by a graphical programming environment (LabVIEW) which is discussed in detail below.

4.2. EXPERIMENTAL

4.2.1. Autosampler coupled with an incubation vessel

Figure 4.1 illustrates the set up of the automatic sampler integrated with an aerosol incubation vessel. The pump was a peristaltic pump (MS/CA4-E/8-100C, Ismatec, Glattbrugg, Switzerland) placed in a IP62 pump housing (Ruthern Instruments, Bodmin, UK), powered by an AC/DC switch mode power supply (type 9921, Mascot, Norway) and operated at 5 V dc (TTL). The 10-way distribution valve was a multi-position micro-electric valve (EMHMA-CE, Valco Instruments Co. Inc., USA) automated by a multi-position actuator control module (P/N EMHCA-CE, Valco Instruments Co. Inc., USA) and assembled in a IP62 valve housing (Ruthern Instruments).

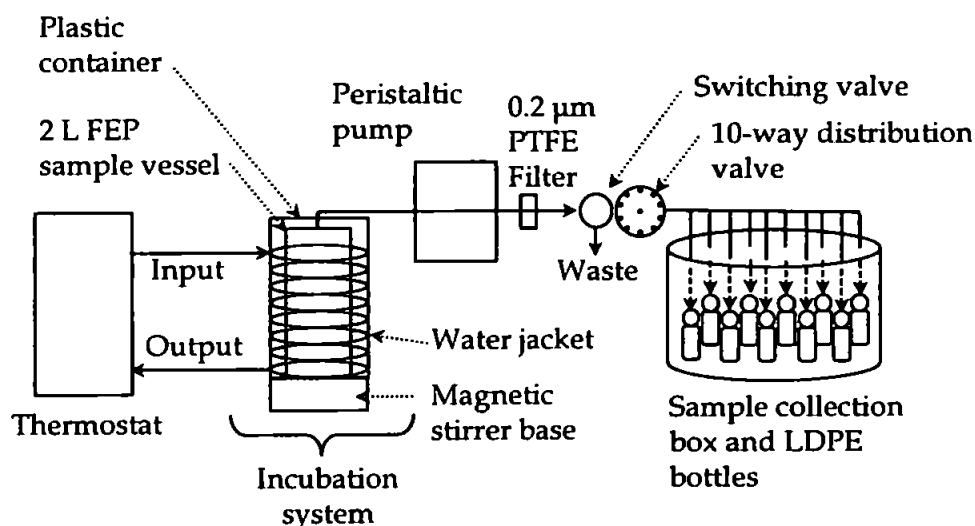


Figure 4.1. Components of the sampler-incubation vessel for the sampling of dFe released in seawater during model dissolution studies.

The actuator of the 10-way distribution valve was powered by a power adapter (FSA46A240-B2, Fortron Source, UK). The switching valve was a PTFE 3-way valve, with 2 position solenoids (EW-01367-72, Cole-Palmer, UK) and operated at 12 V dc. 30 mL LDPE bottles (Low Density PolyEthylene, Nalgene, Fisher) were placed in sealed plastic bags and positioned inside a sealed box. The temperature of the incubation vessel was

controlled using a heater/chiller system (Endocal RTE-100; Neslab Instruments Inc., USA) via a water jacket which consisted of a rubber tube which was coiled (1 m long and 2 cm i.d.) around the incubation vessel; a 2 L Teflon FEP (fluorinated ethylene-propylene) bottle (Nalgene). The incubation vessel and water jacket were placed in a plastic container filled with water to equilibrate faster the temperature of the incubation vessel with the temperature of the water jacket. Seawater was mixed by a PTFE magnetic stirrer rotating at its lowest practical setting (Stuart, Barloworld Scientific, UK) and set at 25 ± 0.2 °C, to represent marine systems at low latitudes. In-line filtration of seawater was carried out by acid washed PTFE acrodisc syringe membrane filters (0.2 µm pore size, Pall Corporation) via PTFE manifold tubing (0.75 mm i.d., Fisher Scientific) and flow-rated tubing (~ 6.5 mL min⁻¹, 3 stops, yellow-blue, Elkay).

Samples for the determination of dFe in seawater were treated as reported (see section 2.2.2. in *Chapter Two*). Calibrations were run with 20 mL standards made up in UV-irradiated seawater, from 0.8 to 16 nM. Analyses were conducted with an optimised automated FI-CL detection system. The analytical performance (detection limits, linearity and blank) and hardware are discussed in *Chapter Two*.

4.2.2. Interface

Process control was achieved using a control and data acquisition instrument (see *Chapter Two*). The LabVIEW VI front panel (Figure 4.2) contained ready-to-use switches, buttons, controls and graphical displays. The main elapsed time of the dissolution process was displayed on the left hand side while elapsed time of sub-sample collection in the cycle (150 s) and percent progress of the sampling appeared in the centre. Positions of the 10-way distribution valve were shown at the top right hand side with control buttons. Each function was linked in the software via the wiring diagram (Figure 4.3) which also controlled the timing of operations.

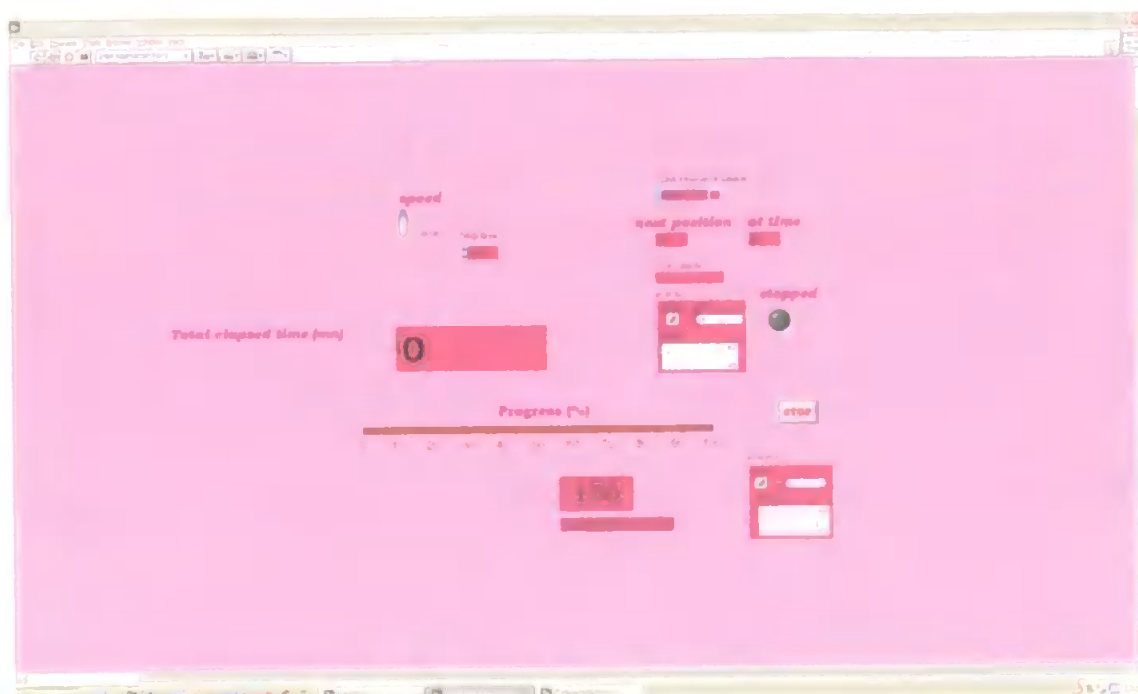


Figure 4.2. LabVIEW front panel with main elapsed time of the dissolution process, elapsed time of sub-sample collection and indication of the position of the 10-way distribution valve.

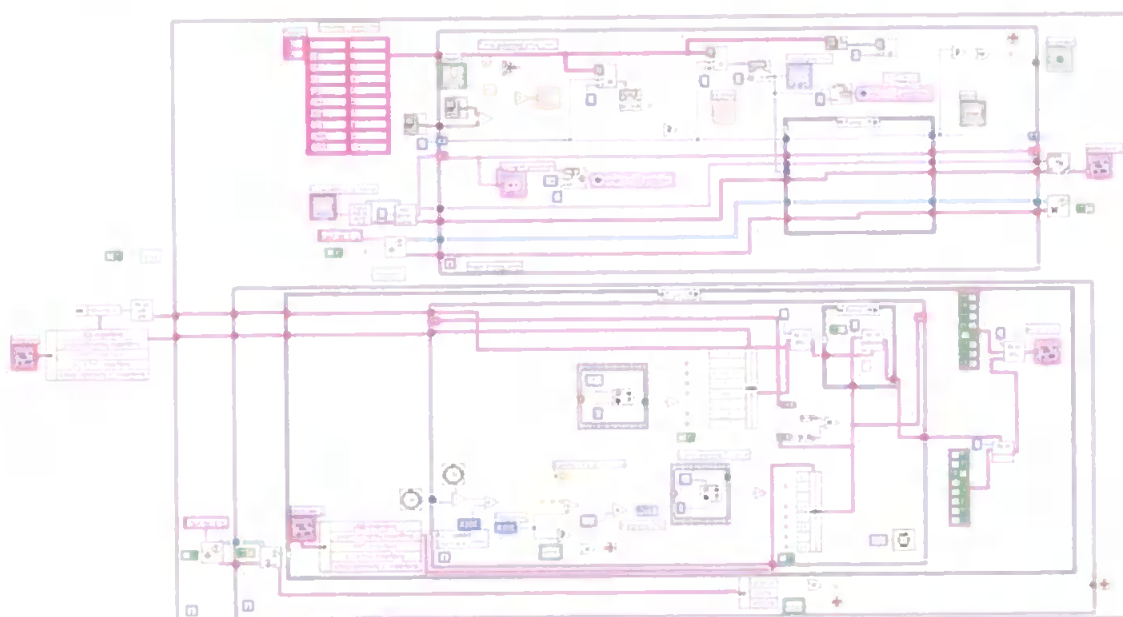


Figure 4.3. Wiring diagram showing the graphical code for instrument control.

4.2.3. Experimental dissolution settings: dark and light

Dark settings

To make sure the incubation vessel was fully darkened, the magnetic stirrer and incubation vessel encapsulated into the plastic container were placed in the polystyrene box and covered by the lid (Figure 4.4). The system was positioned in a class-100 laminar flow hood (model K6, Bassaire Ltd.) whilst the interface and computer were positioned

outside. The chiller was set at 26 °C (to adjust for loss of heat through the water jacket and the water bath, giving a final seawater temperature of 25 ± 0.2 °C) and the incubation vessel was equilibrated for 30 min before dissolution. Once equilibrated, the temperature remained constant over time (± 0.2 °C, measured with an alcohol thermometer, placed in the water bath of the chiller).

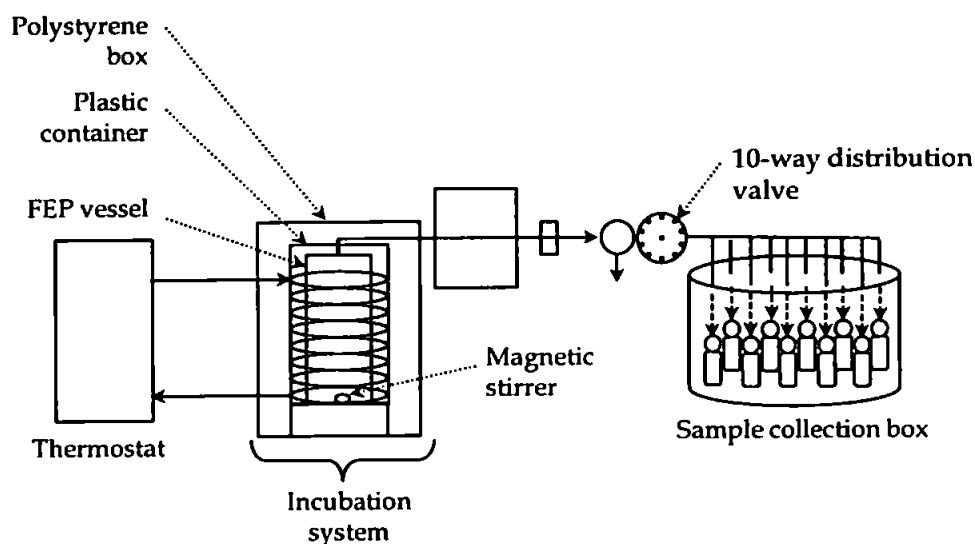


Figure 4.4. Integration of the incubation vessel with the sample collection box for dissolution in dark.

Light settings

For dissolution experiments carried out in the light, the incubation vessel had to be adapted, owing to a poor transmission of light through the FEP vessel (Figure 4.5, Morel *pers. comm.*, ThermoFisher, Belgium), particularly in the UV region (with a decrease in the transmission of up to 90 % at 250 nm). This was achieved by removing the top section of the 2 L FEP incubation vessel (0.6 mm thickness) and replacing it with a quartz disc (\varnothing 14 cm, 1 mm thickness, Baumbach & Co.). A notch at the top of the bottle allowed the PTFE tubing to be inserted and secured whilst the quartz was laid flat (Figure 4.6), to reduce the risks of contamination of the seawater.

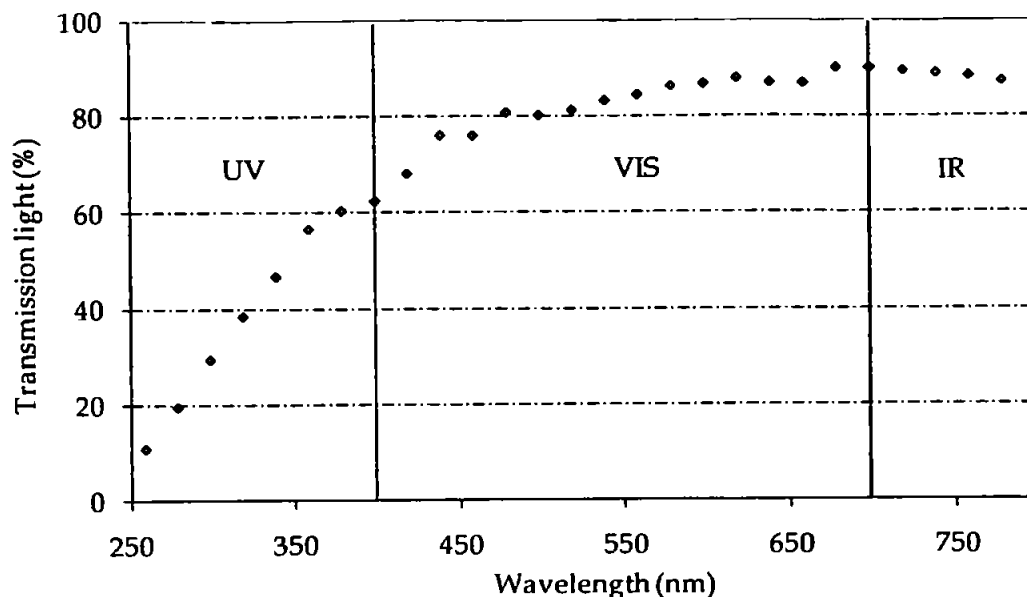


Figure 4.5. Transmission of light (between 250 - 800 nm) of the FEP incubation vessel.

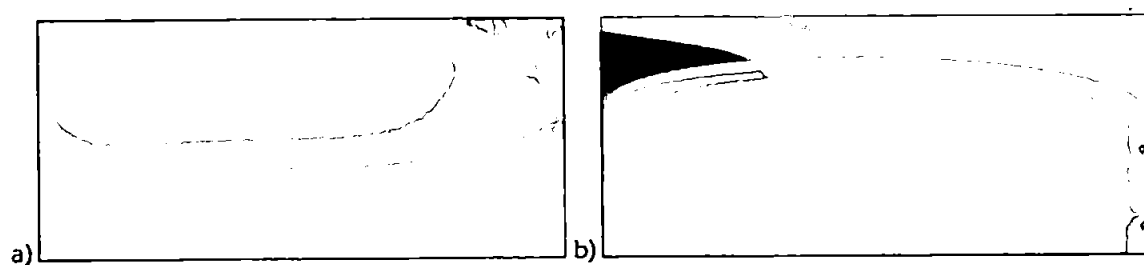


Figure 4.6. Incubation vessel with the (a) quartz mounted on the top and (b) detail of the notch.

The water jacket was coiled around the FEP incubation vessel and placed in the plastic container which was then placed on the magnetic stirrer base. The assemblage was then positioned under a xenon lamp (model Suntest CPS, Heraeus, Hanau, Germany, Figure 4.9). The xenon lamp irradiated from the top and the light emitted was reflected to the sides of the chamber. Owing to the presence of the non transparent plastic container, light received into the incubation vessel was originated from the top part only. This system has been previously used to study the effect of natural daylight on the photochemical decomposition of organic components (Yager and Yue 1988; West 2007). The main advantages of this lamp are: (i) the radiation profile is similar to that of natural sunlight which makes the results comparable with outdoor irradiation in Florida, (ii) irradiance can be changed by using an irradiance control, allowing investigation of the impact of contrasting irradiances (and hence mimic diurnal changes). Intensities and spectral characteristics of the xenon lamp (with filter) are very close to those of sunlight

(Figure 4.7) and by using this type of lamp, the conditions experienced by the dust added to the incubation vessel were as close as possible to those experienced during daylight in the oceans (upper cm of the euphotic zone).

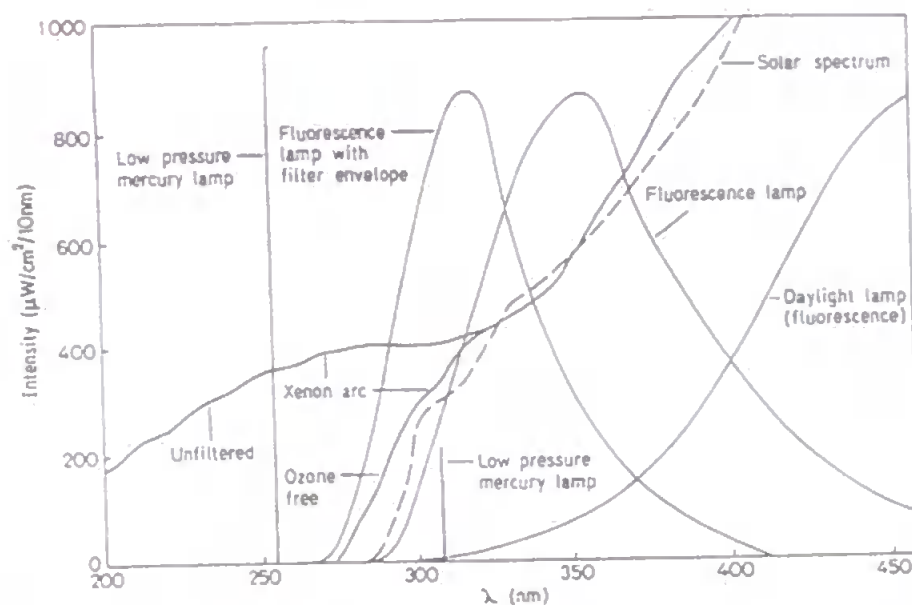


Figure 4.7. Comparison of the spectral intensities of different laboratory light sources with natural light (Roof 1982).

The xenon lamp was positioned on plastic coated blocks to allow the assemblage to be placed securely whilst transferring it from the laminar flow cabinet (Figure 4.8 and 4.9). The chiller was set at 17 °C to balance the heat produced by the lamp and the lamp was switched on for at least 30 min before the start of a dissolution experiment, to equilibrate the seawater temperature in the incubation vessel. The temperature remained constant over time (± 0.2 °C).



Figure 4.8. Equipment set-up for dissolution studies investigating the effects of light.

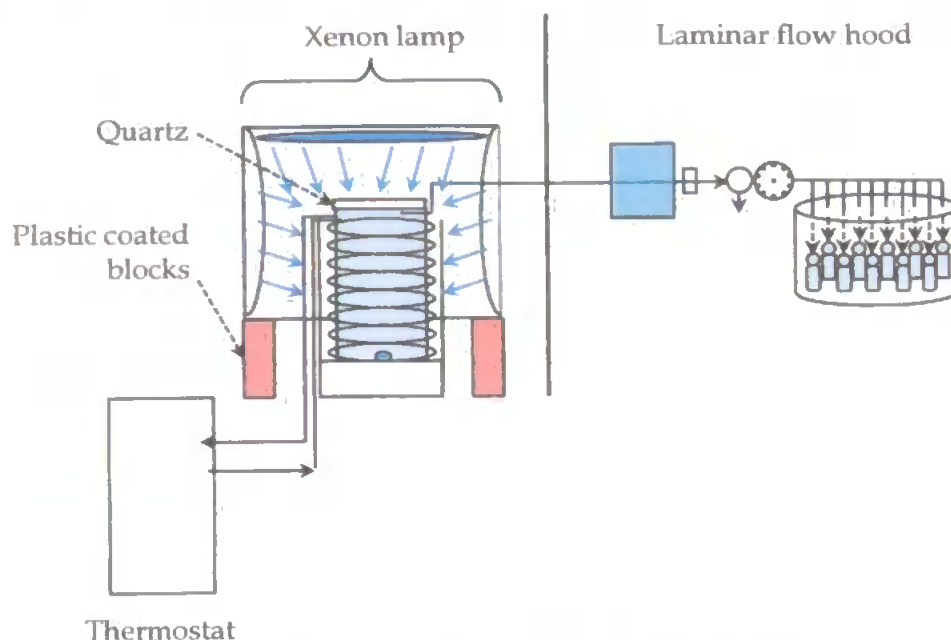


Figure 4.9. Schematic diagram of the incubation vessel with the Xenon lamp.

Preliminary tests were carried out to quantify the transmission of light from the xenon lamp at different heights above the incubation vessel (Figure 4.10). The transmission was measured at position just under the quartz cover of the incubation vessel (i.e. it represents the light reaching the surface of the seawater in the incubation system) and the bottom of the vessel using a spectroradiometer (model SR9910, Macam Photometrics Ltd., Livingston, UK). The spectroradiometer software integrated the measurements of the irradiation emitted at each wavelength (resolution 1 nm), from 280 to 800 nm.

The xenon lamp showed a good irradiance through the quartz cover and to the bottom of the vessel, particularly in the visible region (from 400 to 700 nm). The integral irradiance received at the position of the quartz cover was 514 W m^{-2} and 189 W m^{-2} at the bottom of the vessel. The radiant flux density of solar irradiation received perpendicularly at the top of the atmosphere is accepted to be about 1366 W m^{-2} (World Radiation Center, Switzerland). Ignoring clouds, the average surface irradiance is approximately 250 W m^{-2} , taking into account the lower radiation intensity in early morning and evening, and its near-absence at night. In this study, the average irradiance received from the quartz to the

bottom of the vessel was 350 W m^{-2} . Therefore the system used in the study was representative of both the spectral profile and irradiance of natural daylight.

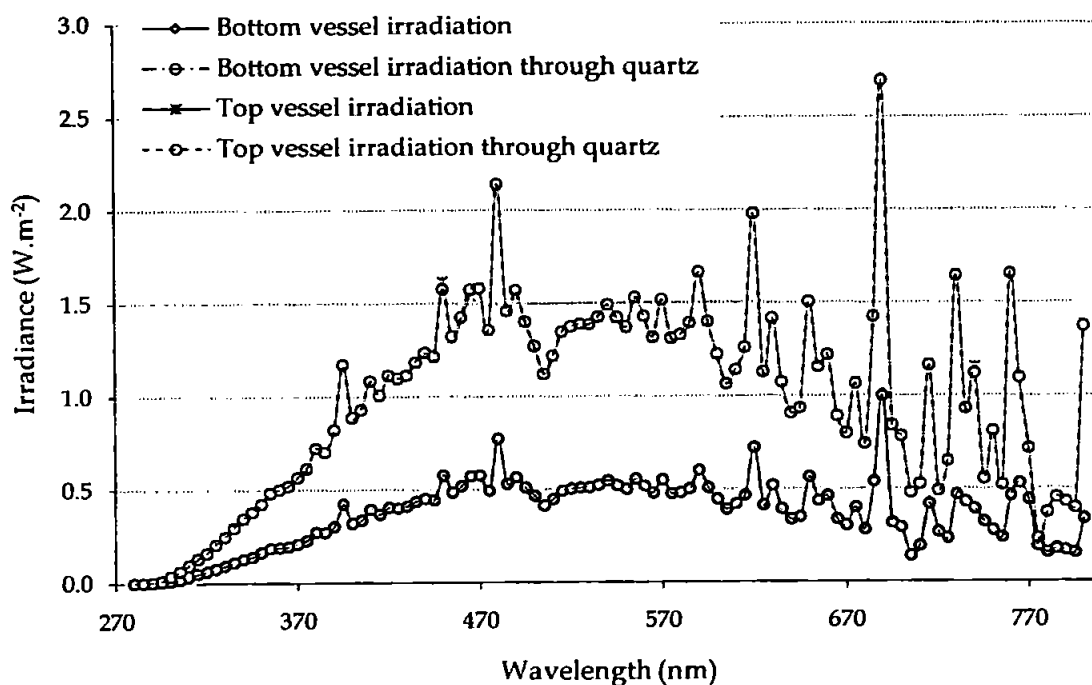


Figure 4.10. Irradiance measured at the positions of the quartz cover and magnetic stirrer in W m^{-2} .

4.2.4. Dissolution procedures and material used

Cleaning procedure

Chemicals were obtained from Fisher Scientific (Loughborough, UK), unless otherwise stated; reagents and standards were prepared in UHP de-ionised water. To avoid any risks of contamination, handling of standards and reagents was carried out under a class-100 laminar flow hood. The 2 L incubation vessel was cleaned in a separate hydrochloric acid bath (6 M, Analytical reagent grade) while the magnetic stirrer was cleaned for 8 h in 20 % (v/v) nitric acid (2 M, Trace analysis grade). Between each bath, labware was rinsed thoroughly with UHP de-ionised water. LDPE bottles were cleaned as described in *Chapter Two* and stored in 0.1 M high purity HCl (SpA, Romil) in re-sealable plastic bags. The PTFE membrane filters were activated by soaking in high purity methanol (5 mL, SpS, Romil) for 5 min, followed by a 20 mL UHP de-ionised water rinse and 10 mL of high purity HCl (1 M, SpA). Once activated, the filters were stored wet in re-sealable bags to avoid drying out. For each dissolution experiment, flow lines, fittings,

activated PTFE filter and connectors of the autosampler were cleaned with 1 M HCl acid (SpA) and 4 volumes of UHP de-ionised water prior to use. Preparation of the samples, standards and cleaning procedures for the FI manifold were as described in *Chapter Two*.

Dissolution procedure

Each dissolution study was preceded by the following rigorous controls to assess the contribution of dFe from the autosampler and the 0.2 μm filter: 2 UHP de-ionised water blanks (water through the lines), 2 filter blanks (water passing through the filter) and 3 sub-samples of the seawater in the incubation vessel before addition of the aerosol material (i.e. T_0 seawater) were collected. The aerosol material was weighed (AT 201, Mystic Mettler Toledo) in an acid washed Sterilin™ and introduced to the incubation vessel. Then the wall of the Sterilin™ was rinsed by adding 10 mL of seawater from the same batch of seawater and shaken for a maximum of 5 s and poured into the incubation vessel. This step was repeated three times, to bring the volume of seawater back to 2 L. The addition of the aerosol material was carried out in less than 30 s. Then ten sub-samples were collected at T_{Dust} , $T_{15 \text{ min}}$, $T_{30 \text{ min}}$, $T_{60 \text{ min}}$, $T_{90 \text{ min}}$, $T_2 \text{ h}$, $T_4 \text{ h}$, $T_8 \text{ h}$, $T_{12 \text{ h}}$ and $T_{24 \text{ h}}$. Each sample was automatically collected over a period of 150 s (Table 4.1) with the first 12 s discarded to waste, between T_0 to $T_{24 \text{ h}}$ at a flow rate of $\sim 6.5 \text{ mL min}^{-1}$.

Table 4.1. Timing sequence and operation state for each component per position of the 10-way distribution valve (cycle).

Elapsed time (s)	Pump	Switching valve	Operation
0	On	On	Sample goes to waste
12	On	On	Start collection of sample
150	Off	Off	End collection of sample

Seawaters

Two open ocean seawaters were used for the dissolution studies: one from the Atlantic Ocean (salinity 37.3) and one from the Canary Basin (salinity 33.2, see *sections 2.2.1 and 3.2.1*).

End member aerosols

NIST 1648: The urban particulate reference material was purchased from the National Institute of Standards and Technology (Gaithersburg, USA). The material was collected over a 12-month period (1977 - 78) from St. Louis, Missouri, using a specifically built baghouse system. The material was removed from the filter bags, sieved through a fine mesh and thoroughly homogenised. It was then packaged into sequentially numbered glass bottles. The urban reference material was adopted for this study due to the potential long transport of this material to the surface ocean and also to enable future comparisons to be made and to compare the results from this study with those from previous studies which have also used NIST 1648 as a proxy for an urban/ anthropogenically influenced aerosol end-member (e.g. Bonnet and Guieu 2004).

Scanning electron microscopy (SEM) enables the examination of the surface structure of particles with high resolution. Samples are fixed onto separate sticky carbon stubs and then gold-coated. Energy dispersive X-ray analysis (EDAX) provides useful qualitative information on the elemental composition of aerosol particles, e.g. C, O, Fe. Samples are carbon-coated on carbon-mounted stub. Biscombe (2004), using SEM and EDAX, found that the average particle diameter of NIST 1648 was c. 10 µm. "Cameo" software (Oxford Instrument) was used to assign different colours to the elements: the particles contained primarily calcium sulphate and silicates, organic material, aluminosilicates and sodium chloride. Some fly-ash particles (5 - 40 µm) were observed along with spherical aluminosilicate particles, indicative of anthropogenic high temperature processes (Guieu *et al.* 1994).

The concentration of iron released, during dissolution studies, from the aerosols in seawater was converted to percent solubility by:

$$\text{Solubility} = \left(\frac{\text{amount of Fe released into seawater}}{\text{total Fe present in added aerosol}} \right) \times 100 \quad \text{Equation 4.1}$$

Table 4.2 presents the total iron concentrations (mg kg^{-1}) for 0.5 mg L^{-1} of the particulate material added and the expected concentrations for 0.20, 0.50 and 1 % solubility.

Table 4.2. Expected concentration (nM) of dFe in seawater equilibrated with the urban particulate material (dust concentration 0.5 mg L^{-1} assuming solubilities of 0.20, 0.50 and 1 %).

	Total iron dust concentration (mg kg^{-1})	Expected dFe concentration (nM)		
		0.20%	0.50%	1%
NIST 1648	$39,100 \pm 1,000$	0.70	1.75	3.50

Complexing ligand (siderophore)

The model ligand desferrioxamine B (DFOB, Figure 4.11), a hydroxamate, was chosen owing to its wide utilisation (e.g. Witter *et al.* 2000; Ussher *et al.* 2005; Milne 2007). Hydroxamate compounds are a category of iron complexing ligand which has been found in the ocean (Martinez *et al.* 2001; Mawji *et al.* 2008). Siderophores are chelates produced by bacteria as part of a highly specific iron uptake mechanism. They are thought to be important in the bacterial acquisition of iron in seawater and to influence iron biogeochemistry in the ocean.

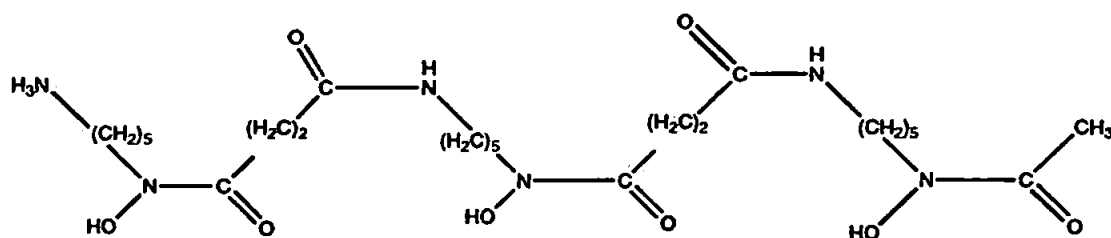


Figure 4.11. Chemical structure of the ligand Desferrioxamine B.

Complexing ligands are characterised by high stability constants with iron, a highly negative redox potential (Table 4.3) and their molecular structure is composed of fatty acid side chains with either hydroxamate (Figure 4.11) or mixed α -hydroxycarboxylic acid/hydroxamate functional group that may affect the ability of an organism to acquire iron from seawater.

Table 4.3. Physiochemical parameters of Desferrioxamine B used in this study. ^a Witter *et al.* (2000).
^b Hering and Morel (1993). ^c Spasojević *et al.* (1999)

$\log K_{\text{Fe}^{3+}\text{L}^{\text{a}}}$	$\log K_{\text{Fe}^{2+}\text{L}^{\text{b}}}$	$E^{\circ} \text{ (mV)}^{\text{c}}$
21.6	20.32	-460

A stock solution of DFOB (10 mM) was prepared by diluting 66.5 mg in 10 mL of UHP de-ionised water only (Gledhill *pers. comm.*), 2 mL of 20 μM solution in UHP de-ionised water was spiked in 2 L of seawater during dissolutions of dusts and left to equilibrate for 5 min to give a final concentration of 20 nM DFOB (12 DFOB : 1 dFe) in seawater, to mimic the potentially fast response of the complexing ligands, produced after inputs of iron to the surface ocean.

It has been reported by Ussher *et al.* (2005) that ligands interfere on the signal of FI-CL by masking up to 40 % the signal of Fe(II). To investigate the potential effects of DFOB, unacidified seawater was spiked with 2 nM of Fe(III) prepared by dilution of a 17.9 mM atomic absorption standard (1000 ppm Spectrosol solution, equivalent of Primar grade, Fisher Scientific) and increasing DFOB concentrations from 20 pM to 200 nM overnight and then acidified for at least 2 weeks before analysis. This approach enabled the study of potential interferences of the complexing ligand on the FI-CL signal; equilibration overnight allowed the stabilisation of the complexes Fe-DFOB and the comparison with Ussher *et al.* (2005).

4.3. RESULTS AND DISCUSSION

4.3.1. Experimental performances of the autosampler and incubation vessel

Preliminary experiments were required to validate the analytical performances of the autosampler over time. Its reliability and reproducibility were tested and the sub-samples analysed using the optimised FI-CL system (see *Chapter Two*). Thus, further controls were carried out: blank controls, blank dissolutions, colloid formation, adsorption onto the walls, effect of DFOB on the FI-CL signal, and pH changes during the equilibration of dust in seawater.

Hardware control

Preliminary experiments were carried out using a relatively high concentration of NIST 1648. Figure 4.12 presents a typical temporal change in dFe concentration following the addition of 1.97 mg L^{-1} of NIST 1648 dust to Atlantic Ocean seawater (dark conditions, low DOC concentration $81.35 \pm 0.96 \text{ } \mu\text{M}$; $25 \pm 0.2 \text{ } ^\circ\text{C}$). A fast release of dFe was observed (up to 6.2 nM), reaching a maximum solubility of 0.45% within 2 h , from the aerosol material into the seawater. Subsequently, dFe concentrations decreased (down to 1.0 nM), equivalent to a solubility of 0.07% after five days.

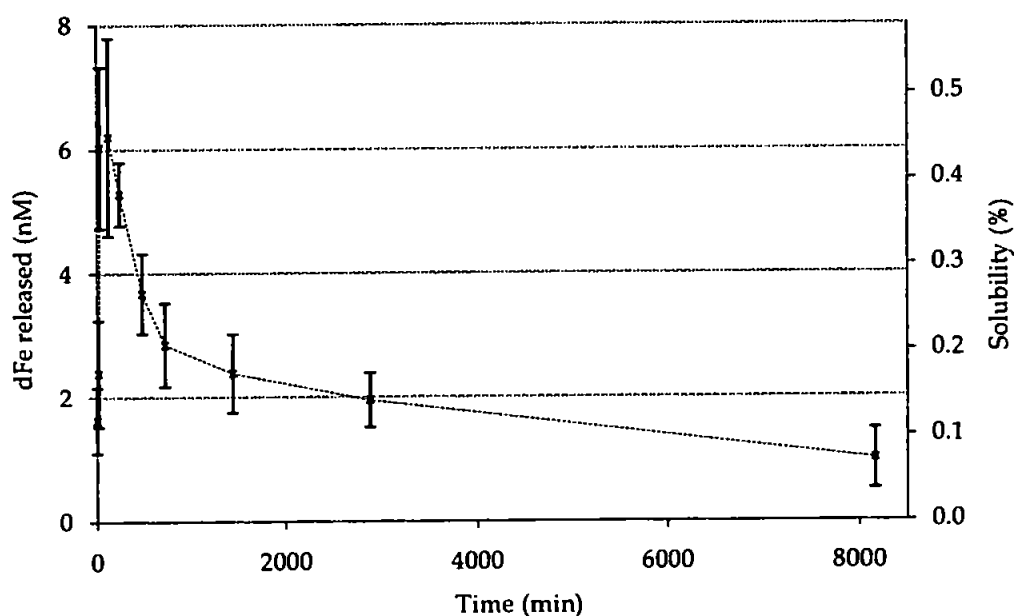


Figure 4.12. Percentage solubility of 1.94 mg L^{-1} NIST 1648 in seawater (Atlantic Ocean).

The fast release of trace metals, in particular iron, is consistent with previous studies which involved the use of aerosol material (Crecelius 1980; Statham and Chester 1988; Chester *et al.* 1993; Chester *et al.* 1994; Guernozi *et al.* 1999a). The decrease in dFe ($> 2 \text{ h}$) may have been as a result of one or more of the following (i) re-adsorption onto the incubation vessel walls (ii) re-adsorption of dFe onto the aerosol particles (iii) changes in the chemical speciation of dFe to a less soluble form. Subsequent sections will discuss studies carried out to investigate the relative importance of those processes involved in decreasing the dFe concentrations. In addition, more details of the kinetic character and

interpretation of the dissolution process will be presented when considering the different experimental conditions.

The initial dissolution profiles obtained, however, demonstrate the reliability of the integrated system, developed during the study period, over a period of 5 days for monitoring the kinetics of Fe dissolution with no downtime. The user friendly nature of the software allowed flexibility in controlling the time of sample collection.

Cumulative errors in dFe concentration from the autosampler and FI-CL system

The errors associated with sample collection by the different lines ($n = 10$) of the autosampler, sample handling and the FI-CL measurements were assessed by taking 5 discrete seawater samples (Atlantic Ocean; 0.85 ± 0.11 nM, $n = 20$) from the incubation vessel using the autosampler, followed by dFe detection (see *Chapter Two*). Prior to analyses samples were stored acidified in LDPE bottles. Table 4.4 presents the CL emissions ($n = 4$), for each of the replicate samples along with the corresponding means and precisions. The precisions of measurement for each of the 5 separate samples ranged from 4.4 to 15.5 %. The overall precision from the bottles was 9.2 % ($n = 5$) suggesting a good reproducibility of sampling, handling and analysis. To confirm this, an ANOVA test (analysis of variance) was performed using StatGraphics Plus, version 5.1. The P-value was 0.0302 (< 0.05) which indicates that there was a statistically significant difference between the mean values from one level of treatment to another at the 95 % confidence level.

Table 4.4. Replicate ($n=4$) CL emission signals for each of the 5 separate acidified seawater samples collected from the incubation vessel using the autosampler.

LDPE bottle N°	CL emission (nM)				Mean (nM)	RDS (%)
1	0.745	0.803	0.732	0.819	0.775 ± 0.043	5.10
2	0.755	0.833	0.858	0.806	0.813 ± 0.044	5.04
3	0.778	0.837	0.873	0.819	0.827 ± 0.040	4.44
4	0.630	0.851	0.872	0.952	0.826 ± 0.138	15.5
5	0.823	1.005	1.027	1.107	0.990 ± 0.120	11.4

A further ANOVA test identified bottle n° 5 to be significantly different from the others and the P-value was 0.7601 (> 0.05) for the 4 remaining bottles. The mean values for these four bottles was not significantly different at the 95 % confidence level and the overall precision of collection and measurement was 2.8 % ($n = 4$). This shows that the autosampler and the analyses were very reproducible between bottles but that care should be taken when preparing and handling samples.

Blank controls and dissolutions

Rigorous blank assessment during every dissolution study was carried out. This consisted of the collection of two UHP de-ionised water blanks (labelled autosampler line blank) to investigate the contamination of the autosampler, followed by two filter blanks to examine the contamination from the filter once installed on the sampling line (Table 4.5). The two UHP de-ionised water blanks and two filter blanks were taken from a 60 mL LDPE bottle and collected through the autosampler lines.

Table 4.5. Concentrations of dFe (nM, ± 1 s.d.) in UHP de-ionised water which was passed through the autosampler lines ($n = 124$) and through the filter ($n = 136$).

	Autosampler line blank	Filter blank
dFe (nM)	0.09 ± 0.11	0.08 ± 0.11

The concentrations of dFe were 0.09 ± 0.11 nM and 0.08 ± 0.11 nM in the UHP de-ionised water blanks and filter blanks respectively. The overall precision ranged from 2.7 to 16.3 % with some exceptions (5 samples), peaking at 26.8 % for samples with concentrations below the limit of detection. The variability in dFe concentrations ($n = 65$) from the autosampler line and filter blank were due to the low concentrations and the majority of the blank controls ($n = 41$) were below the limit of detection (0.059 ± 0.032 nM) in UHP de-ionised water.

Moreover, preliminary blank dissolutions using Atlantic Ocean seawater were carried out to investigate the potential risk of contamination from the incubation vessel,

the 10-port valve and the settings of the system during the lifetime of a typical dissolution study (Figure 4.13).

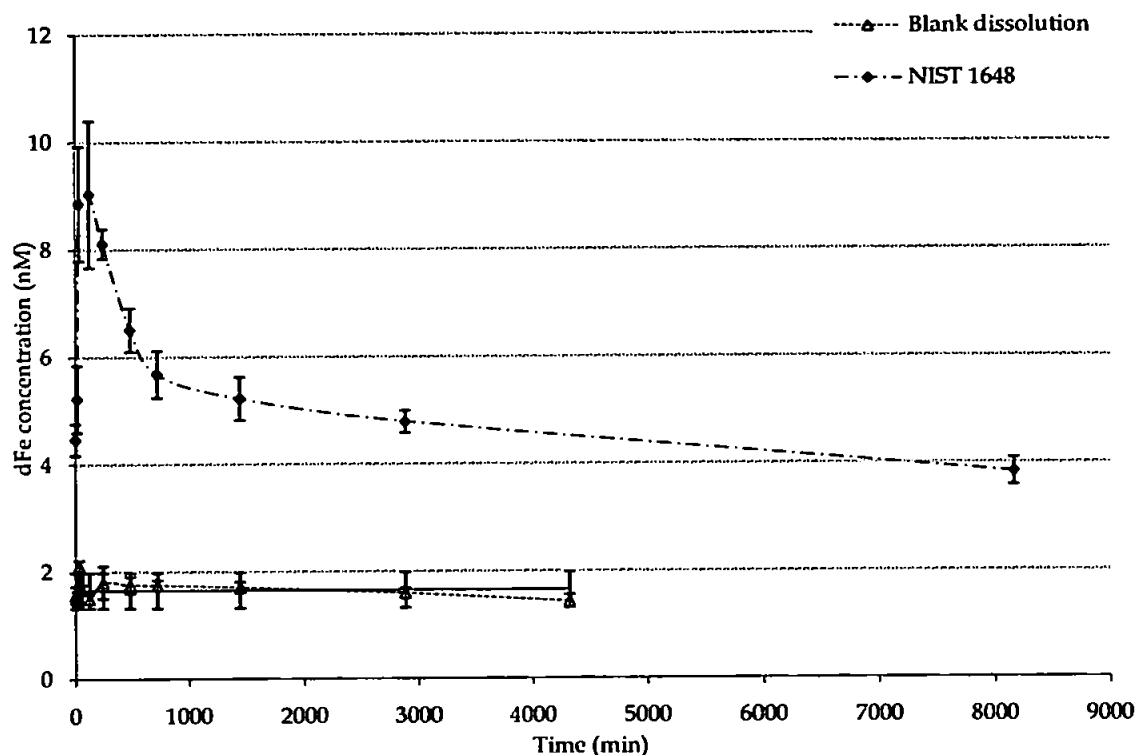


Figure 4.13. Blank dissolution profile (± 1 s.d.), along with the mean line (± 1 s.d.) and a typical dissolution profile of NIST 1648, 1.94 mg L^{-1} .

The concentration of dFe was $1.65 \pm 0.33 \text{ nM}$ ($n = 16$) in the Atlantic Ocean seawater over a 3-day kinetic study. No contamination was detected from the incubation vessel or the magnetic stirrer over this time period, however a higher dFe concentration in the 50 L carboy was detected, due to handling and storage outside the laminar flow hood. These results also suggest minimal adsorption of dFe onto the incubation vessel walls. This potential interference effect is further discussed in the next section.

Therefore contribution of dFe from the autosampler lines, filter, incubation vessel and magnetic stirrer was very low. The autosampler and incubation vessel therefore produced controlled and reproducible results over an extended period of time (up to 5 days).

Adsorption effect

During a number of dissolution studies ($n = 13$) an assessment of dFe which had undergone adsorption onto the incubation vessel walls was made. This was carried out in response to observations made from initial kinetic profiles obtained during the equilibration of NIST 1648 with Atlantic seawater (i.e. a significant decrease in dFe concentrations after > 2 h contact time). Several possible mechanisms for this can be proposed, one of which is the adsorption of dFe onto the incubation vessel walls. This was evaluated in the following manner; at the end of each dissolution study, the remaining seawater was discarded after which the walls and the magnetic stirrer were rinsed twice with 30 mL of UHP de-ionised water and a final rinse was carried out with 30 mL, 0.012 M HCl (pH= 2; SpA, Romil) prepared in UHP de-ionised water, the aim being to remove any potentially adsorbed dFe. The dFe concentrations were then determined by FI-CL and converted, using equation 4.1, to the equivalent decrease in the dFe concentration that would be observed in the 2 L of seawater during dissolution studies as a result of any adsorption:

$$[dFe]_{adsorption} = [dFe]_{acidic\ leach} / (2,000 / 30) \quad \text{Equation 4.1}$$

Where (2,000/30) represents the dilution factor from the 30 mL leach solution to the 2000 mL volume of seawater used in the dissolution studies. The calculated effective decrease in dFe concentrations as a result of adsorption onto the incubation vessel walls are reported in Table 4.6. The adsorption was assessed for 13 experiments in total and the concentrations ranged between 13.3 and 109 pM. The effective decrease in dFe concentrations as a result of adsorption onto the incubation vessel walls, taking into account their respective precisions, were all (except after a 10 nM Fe (II) spike; see *next section*) below the reported limit of detection (60 ± 32 pM). The FEP bottles were therefore a good choice owing to low / no adsorption of dFe onto their walls. This is in opposition with Fischer *et al.* (2007) who investigated the adsorption of ^{55}Fe onto the walls of different types of container and observed an increasing adsorption onto the walls from:

polymethylmethacrylate, polytetrafluoroethylene and high-density polyethylene (40 % of iron adsorbed) < polycarbonate and polyethylene (50 %) < glass and quartz (60 %).

Table 4.6. Calculated effective decrease in dFe seawater concentrations (pM) during dissolution studies (different conditions) as a result of iron adsorption onto the incubation vessel walls (n=13). Assessments were carried out under different experimental conditions (blank dissolution being seawater only; 0.5 mg L⁻¹ NIST 1648 in seawater; DFOB additions from 20 pM to 200 nM with 0.5 mg L⁻¹ NIST 1648 in seawater; 10nM Fe(II) spike in seawater; high volume Whatman 41 filter sample collected from Tel-Shikmona; see *Chapter Five*).

Experiment	Concentration (pM)	s.d.	replicates
Blank dissolution	24.7	25.8	4
1 mg NIST 1648	32.7	12.4	3
DFOB addition	69.7	14.0	3
10 nM Fe(II) spike	109	36.8	2
Filter sample	13.3	-	-

Effect of DFOB on FI-CL signal

The effect of DFOB concentration on the FI-CL signal was determined to investigate the impact of organic ligand additions to seawater during the Fe dissolution process. A range of DFOB concentrations were added to natural unacidified Atlantic Ocean seawater spiked with 2 nM Fe(III), ranging from 20 pM to 200 nM (Figure 4.14), with the upper concentrations representing extreme conditions (≥ 100 nM). The samples were equilibrated overnight, acidified for at least 2 weeks and spiked with reducing reagent 8 h prior to analysis.

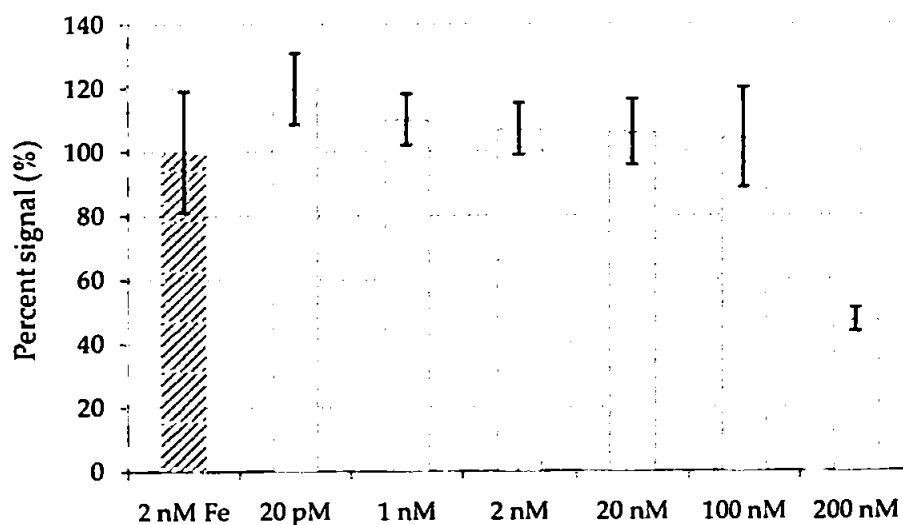


Figure 4.14. Effect of the addition of different DFOB concentrations on the FI-CL signal of 2 nM of Fe(III). Error bars represent ± 1 s.d. (n = 4).

No effect of the complexing ligand on the signal was observed up to 100 nM DFOB spike, whilst the FI-CL signal for the sample containing 200 nM DFOB was quenched by ~ 50 %. Consistent FI-CL signals, ($\text{DFOB} \leq 100 \text{ nM}$), clearly suggested no analytical interference from DFOB. To confirm this, an ANOVA test was performed using StatGraphics Plus, version 5.1. The P-value was 0.0000 (< 0.05) which indicated that there was a statistically significant difference between the mean values from one level of treatment to another at the 95 % confidence level. A further ANOVA test identified the sample spiked with 200 nM of DFOB to be significantly different from the others and once excluded the P-value was 0.4807 (> 0.05) for the remaining bottles. The concentrations of dFe for these bottles was not significantly different at the 95 % confidence level and the complexing ligands did not affect the FI-CL signal of Fe(III) from 20 pM to 100 nM. Ussher *et al.* (2005) investigated the effect of various ligands among other DFOB on Fe(III) signal by equilibrating, for 48 h, 100 nM ligands (DFOB) with 2 nM Fe(III). The samples were then acidified and spiked with sulphite (reducing reagent, 100 μM). After 72 h of acidification and reduction, over 40 % of Fe(III) were still undetectable. The samples in this study were left acidified for storage in dark for 2 months to make sure the reduction step reached equilibrium and the percent recoveries were above 100 %.

pH changes

For aerosol iron dissolution studies in seawater it is essential to ensure that the seawater pH remains constant. Therefore the variation in pH following the addition of the urban end member aerosol material (1.0 mg L^{-1}) into the Atlantic Ocean seawater was investigated over a one day period. The pH reading fluctuated around 8.09 ± 0.02 ($n = 19$). This amount of dust, therefore, did not impact on the pH of the seawater over time. This amount corresponds to a very strong Saharan dust event input to the ocean (Bonnet and Guieu 2004) and was a greater dust concentration that was used in subsequent dissolution studies. Furthermore, after UV irradiation treatment, the pH of Atlantic Ocean seawater (see Chapter Three) was 8.08, showing that there was no impact from the UV irradiation

process on the pH of seawater. In addition, the pH of seawater equilibrated with a crustally derived high volume collected Whatman 41 filter sample from Tel-Shikmona (see Chapter Five) was depressed only slightly to 7.98 after 8 h contact time.

4.3.2. Development of the aerosol dissolution experimental protocol in seawater

The development of a strict dissolution experimental protocol, prior to investigating key factors (light / dark; presence / absence of complexing ligands), is crucial to ensure reproducible and meaningful observations, allowing comparisons within and between (literature) studies. Moreover, it is important to apply experimental conditions that are as close as possible to those encountered in the environment, for a better understanding of the factors impacting upon the dissolution process. Therefore this section discusses the impact of changing the experimental conditions including the effects of the UV irradiation of seawater, stirring and dust concentrations.

Mixing: stirred and non-stirred

Biscombe (2004) recently highlighted the impact of stirring the seawater during kinetic aerosol trace metal seawater dissolution studies. Typically lower solubilities were determined at higher stirring rates. To study the impact of stirring the seawater matrix on the aerosol iron dissolution process, two experiments were carried out with 0.5 mg L⁻¹ of NIST 1648 in the Atlantic Ocean seawater, with seawater stirred at the lowest practical rate and with no stirring (Figure 4.15). The profile of the stirred solution was characterised by an increase in the solubility within 90 min, up to 0.36 % (1.25 ± 0.41 nM released) followed by a decrease down to - 0.11 % after 12 h (i.e. overall adsorption of released dFe, 0.39 ± 0.19 nM adsorbed). The non-stirred solution exhibited a more variable profile, increasing within the first 15 min up to 0.24 % (0.82 ± 0.25 nM released) followed by fluctuations between 0.14 and 0.27 % (from 0.48 ± 0.69 nM to 0.95 ± 0.16 nM released, after 2 h), with a final solubility of 0.14 % (0.50 ± 0.45 nM released). The non-stirred solution maintained iron in solution at a variable solubility, particularly after 8 h.

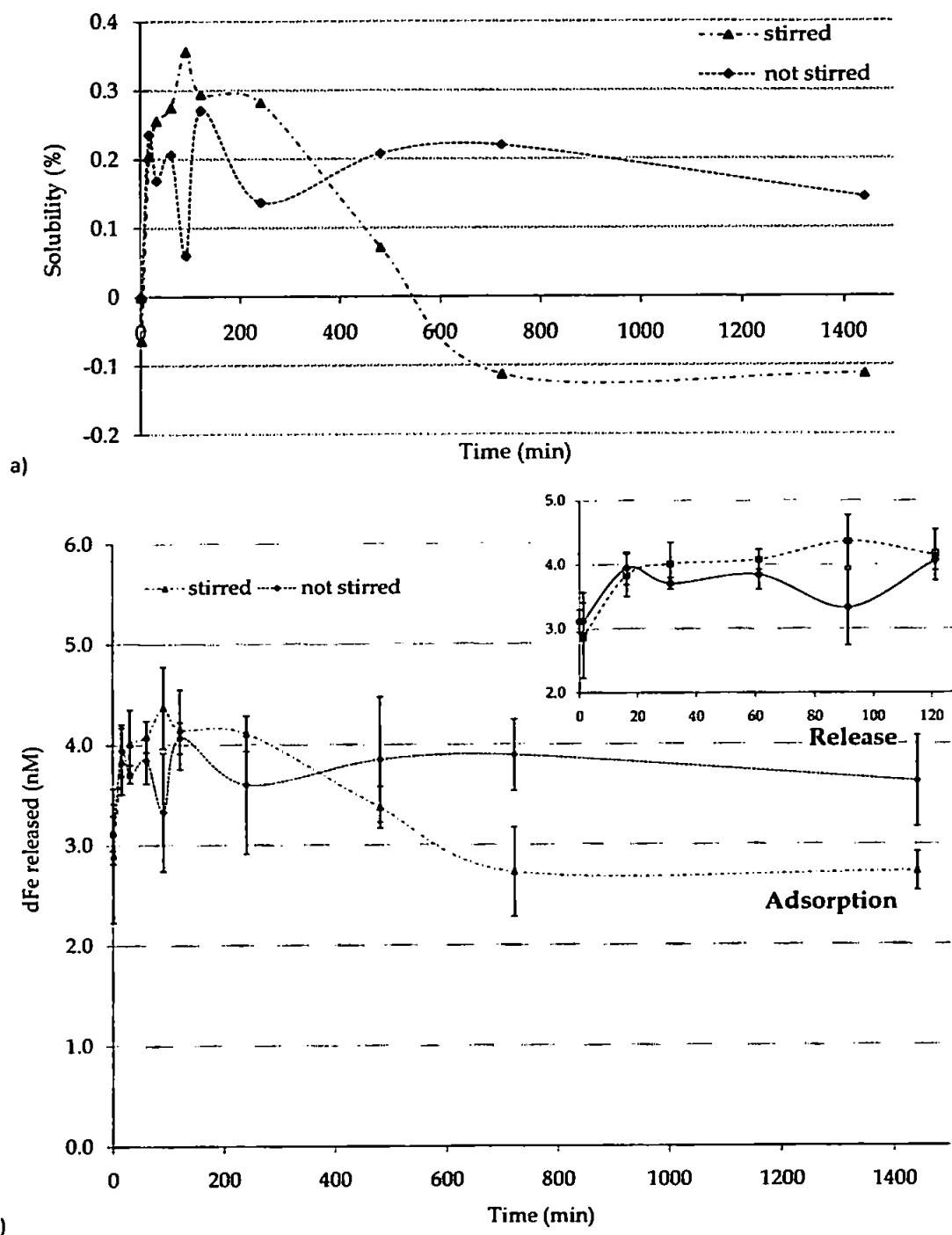


Figure 4.15. Effect of stirring and not stirring the seawater on iron a) solubility and b) released concentration (nM, inset: focus on the first 2 h), from NIST 1648 (0.5 mg L^{-1} , non UV irradiated Atlantic Ocean seawater) over a 1-day period. Error bars represent ± 1 s.d. (n = 4).

Biscombe (2004) observed a higher impact of stirring on the solubility of zinc (Zn), lead (Pb), copper (Cu) and cadmium (Cd) using different stirring rates and different dust loadings from 14 to 800 mg L^{-1} . Using 300 mg L^{-1} and different stirring rates, the decreases in solubilities at faster speeds ranged from 15 % for Cd to 93.5 % for Pb, with medium

effect on Zn and Cu solubilities. Biscombe (2004) proposed that the stirring rate determines the kinetic energy of the suspension (Morel and Hering 1993); therefore increasing the seawater mixing rate increases the frequency of collisions between the aerosol particles and the analyte, hence the adsorption is increased and the apparent solubility of the analyte is reduced. However, Biscombe (2004) used higher particulate material concentrations compared with this study, up to 1,600 times. At this level of concentration, less collision would occur and diffusion from the surface area would be, more than collision rate, a potential source of dissolved iron in seawater.

The question to stir or not to stir therefore is critical in the experimental design. For this study and for others (Biscombe 2004) it is clear that stirring will impact upon the dissolution process. This impact increases with both greater stirring rate and higher particle concentration (Biscombe 2004), as both lead to a decrease in the apparent metal solubility in seawater. From the above discussion and Figure 4.15, it is apparent that short term kinetic dFe profiles indicate a small affect on the short term maximum observed solubility. However the long term kinetic profiles are different, with stirring producing an enhanced removal of dFe after several hours of contact between the aerosol and seawater. Iron aerosol dissolution studies in seawater reported in the literature have not been clear as to how, and how long for, the seawater has been agitated (Bonnet and Guieu 2004; Wagener *et al.* 2008; Aguilar-Islas *et al.* 2009). The main aim of this study was to mimic the natural conditions as closely as possible, therefore it is unrealistic to apply no stirring as the marine system is always in motion, although this will vary both spatially and temporally. Therefore for subsequent studies a constant stirring rate (lowest setting) was applied to the seawater / aerosol mixture to mimic natural disturbance of the seawater. In addition, the unstirred solution exhibited a comparatively more variable kinetic profile of dFe (Figure 4.15) which might be due to the higher heterogeneity of the seawater in the incubation vessel.

Seawater matrix (i.e. UV and non-UV-irradiated) and dust concentrations

To determine the impact of natural organic complexing ligands and dust particle concentration on the apparent iron solubility (and released concentration) in seawater dissolution studies were carried out with low (0.25 mg L^{-1}) and high (2 mg L^{-1}) NIST 1648 concentrations in both UV-irradiated (no ligands) and non-UV-irradiated (ligands) seawater (Canary Basin). The results are presented in Figure 4.16.

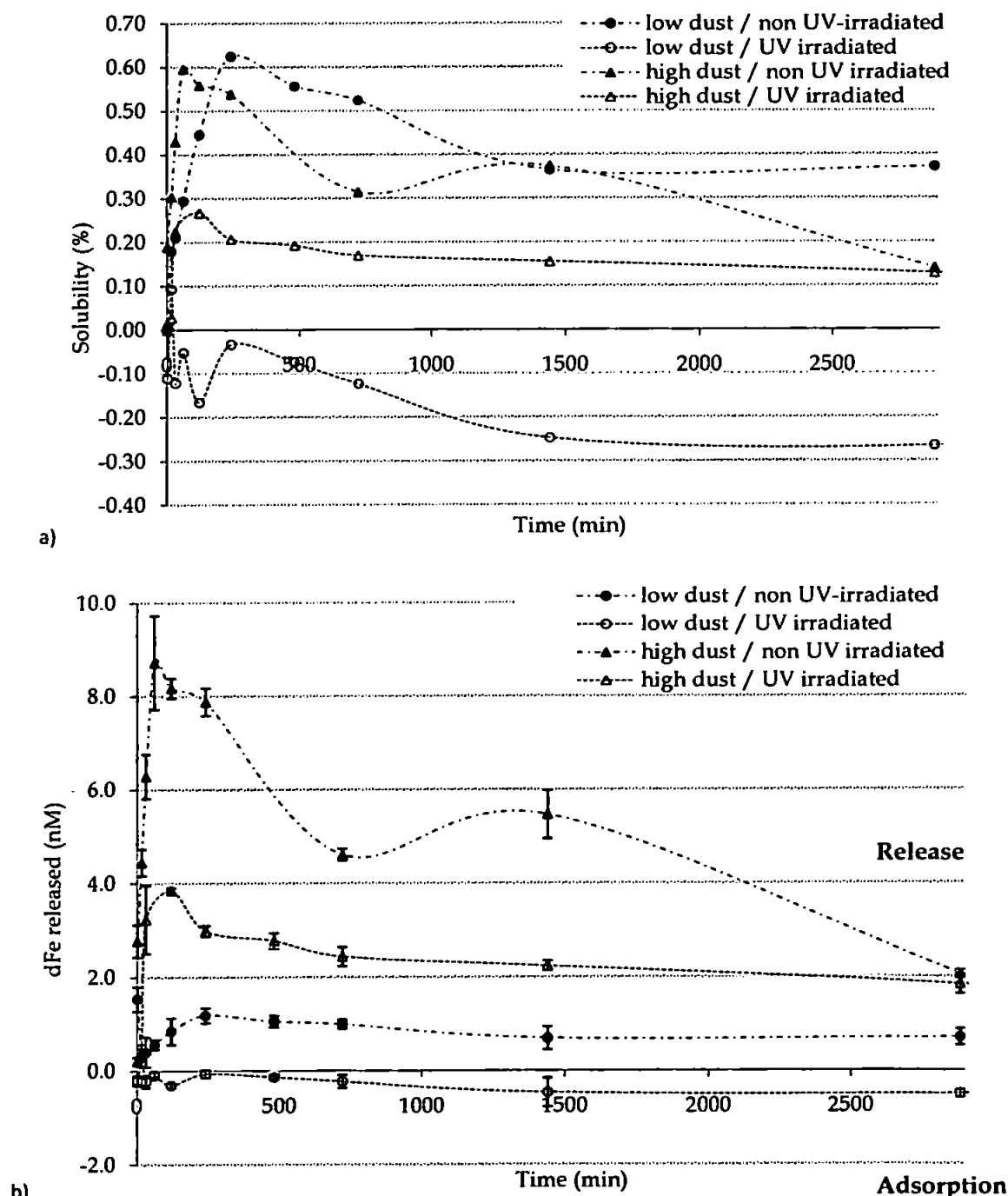


Figure 4.16. Effect of UV irradiation on iron a) solubility and b) released concentration (nM) from low and high NIST 1648 loadings (0.25 and 2 mg L^{-1}). Error bars represent $\pm 1 \text{ s.d.}$ (n = 4).

Solubilities in non-UV-irradiated seawater were significantly higher than those observed in UV-irradiated seawater for both dust concentrations. The maximum solubility at the low dust loading decreased from 0.62 ± 0.07 % (at 240 min, 1.18 ± 0.09 nM released) to 0.37 ± 0.06 % (at 24 h, 0.70 ± 0.10 nM released) whilst with high dust loadings the maximum solubility decreased from 0.60 ± 0.07 % (at 1 h, 8.72 ± 0.06 nM released) to 0.14 ± 0.01 % (at 48 h, 2.05 ± 0.01 nM released). In UV-irradiated seawater, a significant decrease was observed for both dust loadings. The maximum solubility decreased from 0.60 ± 0.07 % (8.72 ± 0.06 nM released, no UV-irradiation) to 0.27 ± 0.01 % (3.85 ± 0.01 nM released) in UV-irradiated seawater with a dust concentration of 2 mg L^{-1} . For a dust concentration of 0.25 mg L^{-1} minimal short term (16 min) release coupled with re-adsorption of iron released from the particles and adsorption of background dFe from the seawater matrix induced net negative solubilities. These observations clearly highlight the importance of natural complexing ligands in seawater on dFe release from aerosol material. A low natural ligand concentration is likely to lead to low aerosol iron solubilities as a result of the formation of insoluble colloidal $\text{Fe}(\text{OH})_3$ (lower effective solubility product). The importance of natural organic complexing ligands has been discussed recently by Wagener *et al.* (2008) and Aguilar-Islas (2009). Wagener *et al.* (2008) observed a positive correlation between the concentrations of the free organic Fe-binding ligands in the seawater and changes in dFe concentrations, and suggested that Fe-binding ligands in seawater control atmospheric iron dissolution. Aguilar *et al.* (2009) concluded from their matrix of experiments that the presence of free organic ligands with high affinity for iron helps in the mobilization of iron from the particulate to the solution phase. It is also clear, from this study, that the use of non-UV irradiated seawater is necessary for the determination of dFe release from aerosol material particularly at low dust concentrations (0.25 mg L^{-1}). As mentioned in *Chapter Three*, the apparent removal of iron from seawater was suspected to be due to adsorption of dFe onto the FEP coil or interferences in the FI-CL signal due to production of radicals and hydrogen peroxide, masking the release of dFe from dusts at low loading.

Moreover, difference in the release of iron from the aerosol particles in natural (non-UV irradiated) seawater, from the kinetic profile, was observed between the two dust loadings during the first two hours (Figure 4.17).

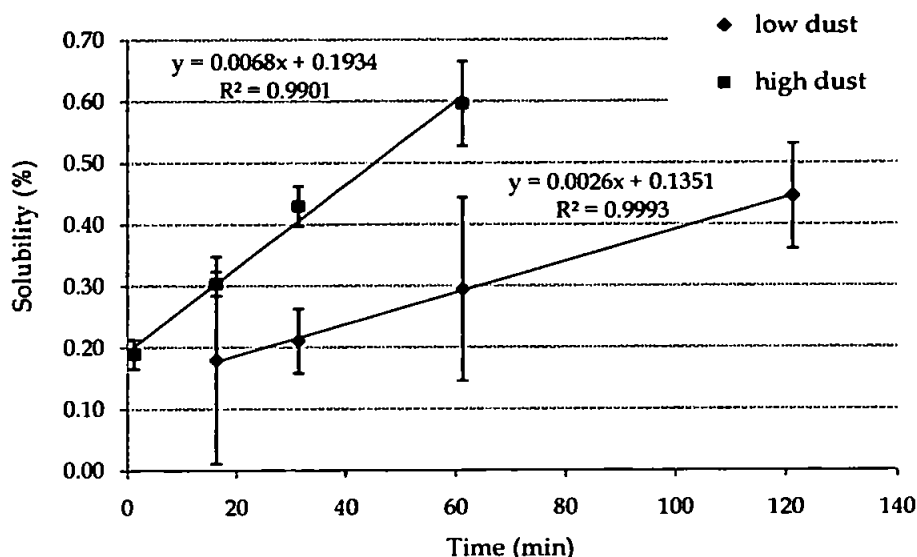


Figure 4.17. Rate of release of iron from the aerosol particles in natural seawater at two different dust loadings, high 2 mg L⁻¹ and low 0.25 mg L⁻¹. Error bars represent ± 1 s.d.

From Figure 4.17, it is apparent that the release of iron from high dust loading was carried out at faster dissolution rate, 0.0068 % min⁻¹ whilst the dissolution rate for low dust loading was 0.0026 % min⁻¹. The linearity in both cases was $R^2 > 0.99$ (loss of the first sample for the low loading dissolution) and significantly correlated at 99.9 %. It was apparent that the maximum solubilities at both high and low dust loadings were not significantly different: the ANOVA test P-value was 0.9184 (> 0.05) which indicated that there was not a statistically significant difference between the mean values of the two dust loading from one level of dust loading to another, at the 95 % confidence level. This suggested that the applied dust concentrations were low enough that the “particle effect” on the apparent solubility observed in other studies (e.g. Spokes and Jickells 1996; Biscoombe 2004; Bonnet and Guieu 2004; Milne 2007) was of limited importance. However it should be noted that the long term solubilities were comparatively lower for the high dust loadings with those observed for low dust loadings, 0.37 ± 0.06 % and 0.14 ± 0.01 %

respectively, at 24 h. This suggested an enhanced re-adsorption of dFe onto the aerosol particle surfaces following its initial release.

Therefore it is clear that using dust loadings $< 2 \text{ mg L}^{-1}$ is preferred to ensure no particle concentration effects (both short and long temporal scales) on the observed solubilities in seawater (and also to ensure a realistic dust concentration is applied). Dust concentrations lower than 0.25 mg L^{-1} , however, are not advisable owing to the low dFe concentrations (i.e. analytical constraints) that would be encountered (even in non-UV irradiated seawaters). How the dust concentration in surface seawater relates to the strength of natural dust events is presented in Table 4.7 (Bonnet and Guieu 2004).

Table 4.7. Seawater dust loadings and their relationship to strength of natural dust events along with equivalent solubilities in seawater (%) as reported by Bonnet and Guieu (2004).

Magnitude of the event	Dust concentration (mg L^{-1})	Solubility (%)
Extremely low	0.001	7.2
Very low	0.005	2.9
Low	0.01	2.0
Medium	0.1	0.5
Strong	0.5	0.2

Therefore as a compromise between applying a realistic dust seawater concentration and analytical practicalities it was decided, for the model dissolution studies reported in the next section, to use a dust concentration of 0.5 mg L^{-1} .

4.3.3. Chemical and physical factors impacting upon the dissolution of aerosol iron

The following section discusses the results from a series of model studies to investigate the impact of (i) dark /light conditions as well as the (ii) absence and presence of a model complexing ligand (DFOB) on the extent and kinetics on the dissolution of aerosol iron in seawater. Based on the result from the previous section, tightly controlled experimental conditions were adopted and are summarised as follows: (i) urban end member NIST 1648 was used at a seawater concentration of 0.5 mg L^{-1} (ii) all studies were carried out in non-UV irradiated seawater (at a constant natural ligand concentration) (iii)

the seawater was stirred (at the lowest practical stirrer setting) and (iv) the temperature was kept constant ($25 \pm 0.2^\circ\text{C}$).

Dark experiment

This section describes the dissolution profiles of 0.5 mg L^{-1} NIST 1648 under dark conditions with and without the addition of DFOB (20 nM and 200 nM, Figure 4.18). The aim of this experiment was to investigate the potential effect of extreme concentrations of complexing ligands (Mawji *et al.* 2008) and to show the potential of the system to investigate kinetic dissolutions of aerosol particles under different conditions with high temporal resolution. The dissolution profile of 0.5 mg L^{-1} NIST 1648 in the absence of DFOB, was characterised by an increase within the first 90 min to a maximum solubility of $0.36 \pm 0.12\%$ ($1.47 \pm 0.48\text{ nM}$ released), followed by a decrease to $-0.11 \pm 0.06\%$ (i.e. net adsorption, $0.46 \pm 0.23\text{ nM}$ adsorbed) after 24 h. It has already been shown (section 4.3.1) that the decrease of dFe, leading to a net adsorption, was not as a result of adsorption of dFe onto the incubation vessel walls. The formation of iron oxy(hydroxides) might lead to a loss by precipitation / adsorption on the aerosol particle surface. However it is also possible that a fraction of the released dFe from the aerosol material complexes with the natural organic ligands present in the seawater and then these complexes undergo adsorption onto the aerosol particle surfaces. The addition of 20 nM DFOB induced an enhancement in the dFe solubility within the first 200 min followed by relatively constant solubilities ($0.76 \pm 0.11\%$, $2.65 \pm 0.29\text{ nM}$ released). Post 214 min the solubilities with the addition of 20nM of DFOB were all higher compared with those observed in the absence of DFOB. To confirm this, an ANOVA test was performed using StatGraphics Plus, version 5.1. The P-value was ≤ 0.0001 (< 0.05) for 480 – 1440 min sub-samples which indicated that the two sets of data were significantly different at the 95 % confidence level. Moreover, addition of 200 nM DFOB triggered a higher maximum solubility of iron released from the aerosol particles, $1.6 \pm 0.08\%$ ($5.51 \pm 0.37\text{ nM}$ released) compared with $0.90 \pm 0.27\%$. The presented results take in account of the quenching of the FI-CL signal

discussed in section 4.3.1 by doubling the concentrations of dFe in seawater in the different sub-samples, assuming ~ 50 % decrease in the FI-CL signal as previously observed (section 4.3.1). This implies that higher concentrations of complexing ligands induce a higher maximum solubility of iron.

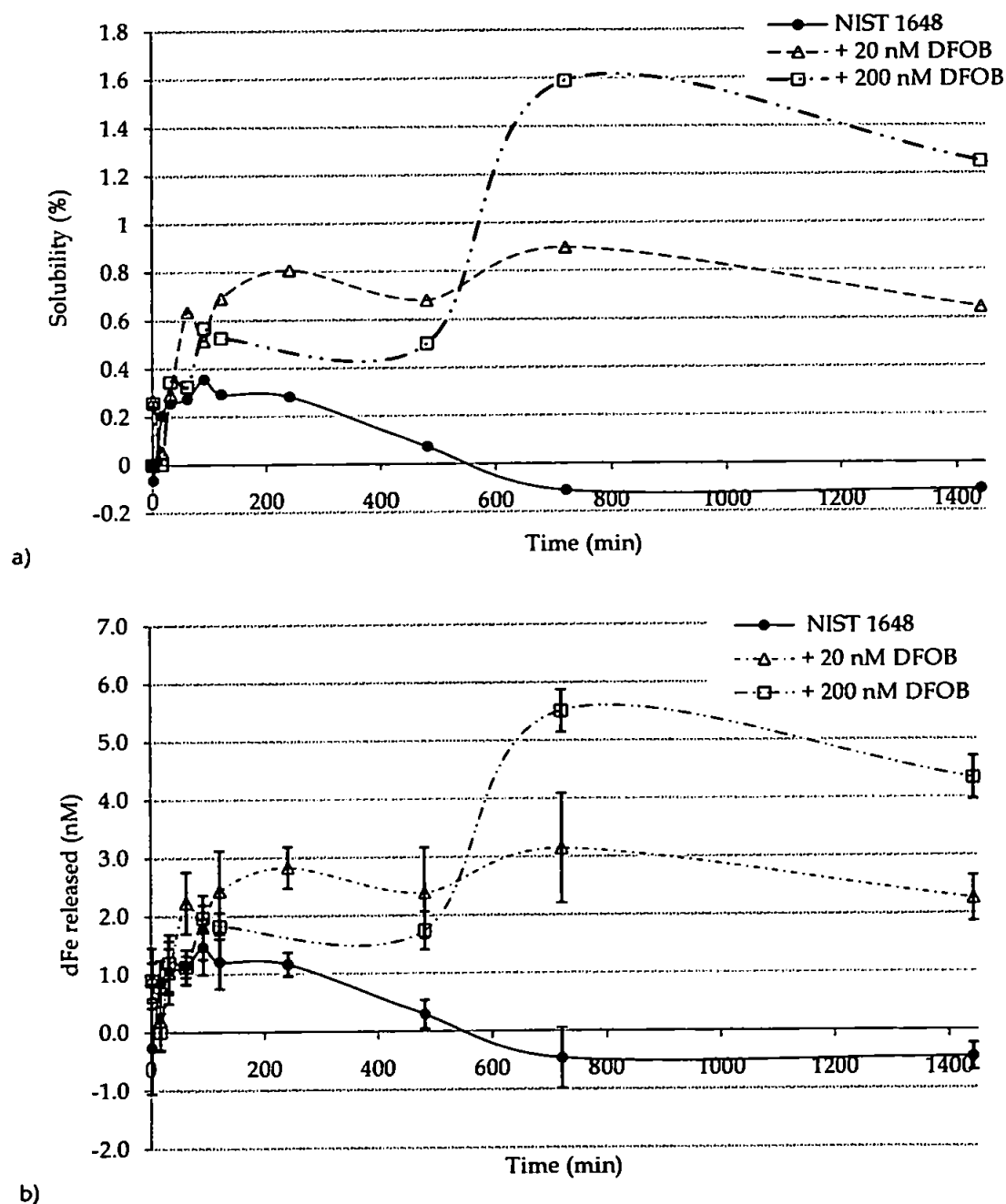


Figure 4.18. Effect of complexing ligand concentration DFOB (20 nM, 200 nM) on the kinetic dissolution profiles of 0.5 mg L^{-1} NIST 1648 under dark conditions. a) solubility and b) released concentration. Error bars represent ± 1 s.d.

From these kinetic profiles, it is evident that the presence of the model iron complexing ligand DFOB had two impacts upon the dissolution of iron from NIST 1648;

(i) an enhancement in its solubility in seawater and (ii) preservation of dFe in solution, preventing the re-adsorption of dFe which was observed in the absence of DFOB. Aguilar-Islas *et al.* (2009) also observed an increase in the solubility of inland urban aerosol iron, collected at Fairbanks, in seawater with the addition of a complexing ligand. They used seawater which was UV-irradiated (labelled, for this discussion, "control") and divided into two batches; 2 nM of DFOB was then added to one. After 1 min of contact time, the solubility of iron from the urban aerosol used was 1.6 % in the UV-irradiated seawater and 2.6 % in the batch of seawater spiked with DFOB. After 90 min contact time, the solubility was 1.8 % in the UV-irradiated seawater compared with 3.2 % in the UV-irradiation seawater spiked with DFOB. The utilisation of 2 nM of DFOB induced an increase in solubility by a factor of 1.7 compared with the control. In this study, solubility enhancement factors of 2.5 for 20 nM of DFOB and 4.4 for 200 nM DFOB were observed. Using Western Mediterranean Sea water, Wagener *et al.* (2008) has also recently observed an increase in the dFe concentration in seawater equilibrated with soil composites, collected from the South Algerian Hoggar Region, with an increase in the concentration of complexing ligands (as a result of enhanced biological activity), suggesting that complexing ligands in seawater influence aerosol iron dissolution.

The results from this study showed a consistent trend with the literature in observing an enhancement of the solubility of iron in seawater by complexing ligands and hence the stabilisation of dFe in solution. Therefore they are likely to have an important impact on a large spatial scale when dust enters the euphotic zone in the open ocean (Rijkenberg *et al.* 2008).

Light experiments

This section describes the dissolution profiles of NIST 1648 under light conditions compared with dark, with and without the addition of DFOB (20 nM). Figure 4.19 shows the effect of light on the kinetics of iron dissolution, using 0.5 mg L⁻¹ NIST 1648 only, in

seawater and Figure 4.20 highlights the effect of light/dark on the iron solubility with the added complexing ligand.

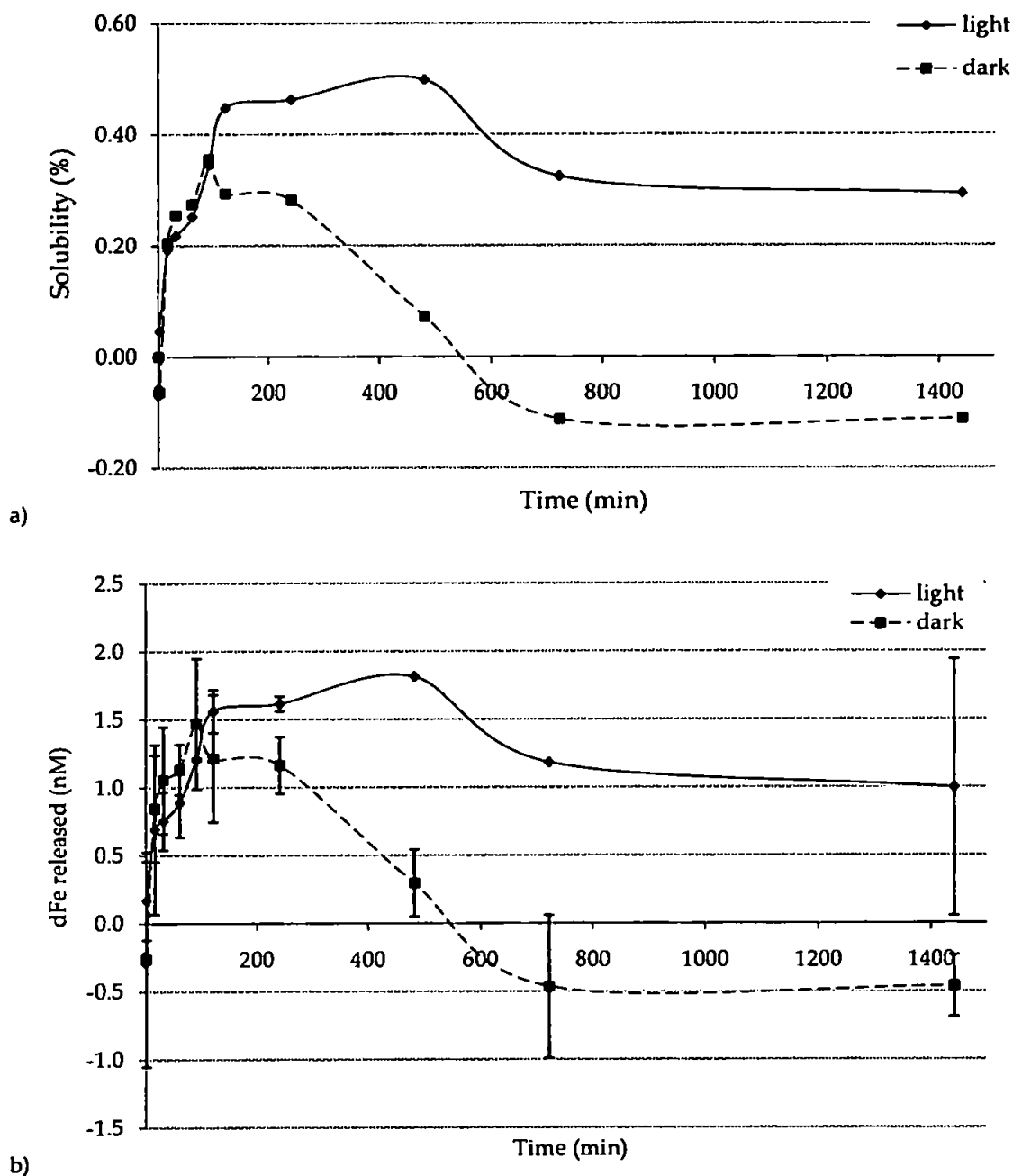


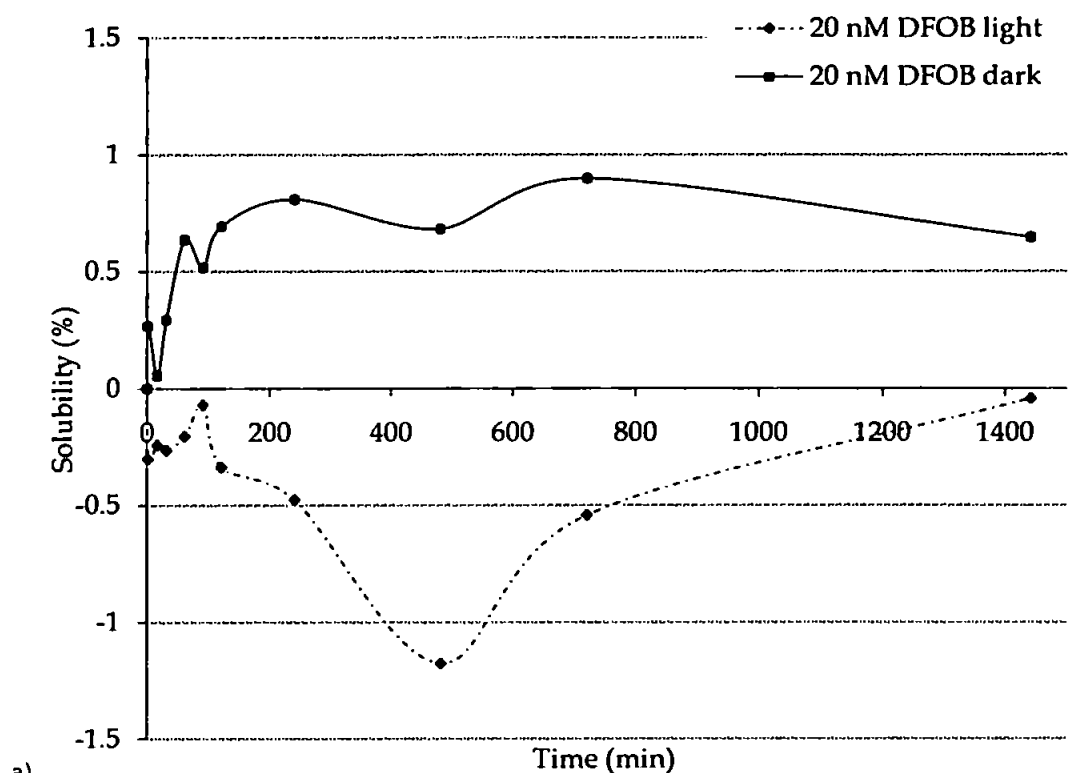
Figure 4.19. Effect of light on the kinetic dissolution profile of 0.5 mg L⁻¹ of NIST 1648. a) solubility and b) released concentrations. Error bars represent ± 1 s.d. (n = 4). Light experiment represents the mean of 2 dissolution experiments. Data from the second experiment min 480 and 720 min were excluded from the mean due to suspected contamination.

Both kinetic profiles of NIST 1648 in the absence of ligands, in dark and light conditions, were characterised by a fast release of iron followed by a decrease, with net adsorption for the experiment carried out in the dark and consistent dFe values in the

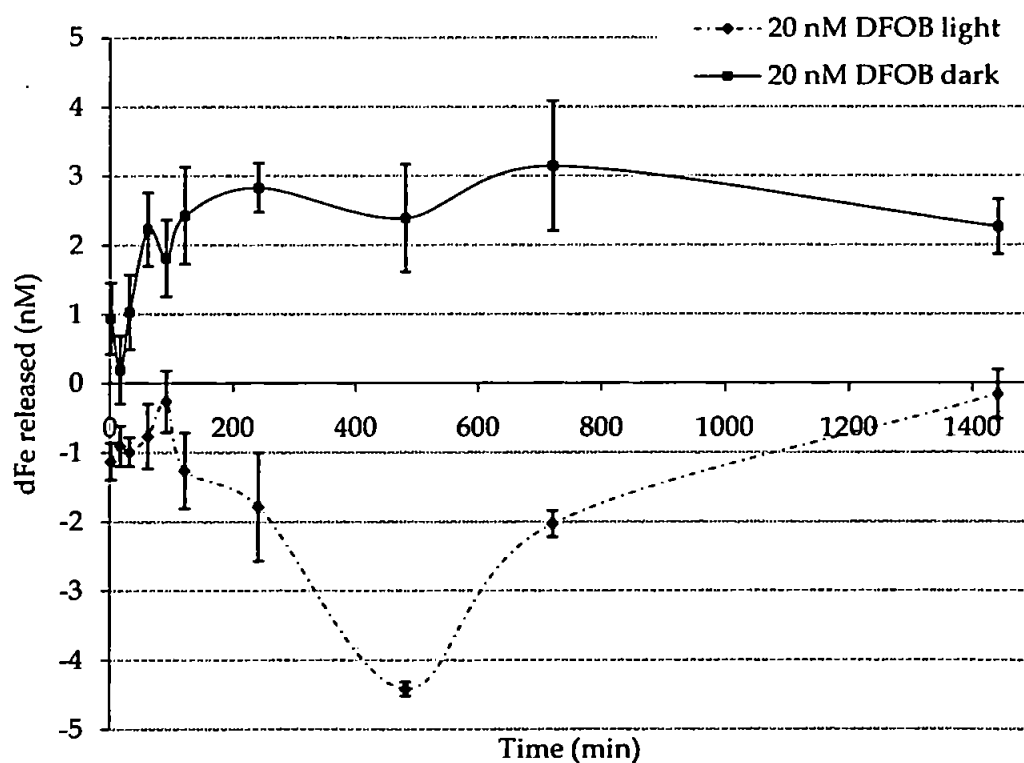
experiment carried out with light (>721 min). The maximum solubility of iron in the seawater exposed to light was reached after 480 min whilst in the dark it was reached after 90 min. The exposure to light induced an increase in the solubility of Fe of up to 0.50 % compared with 0.36 ± 0.12 % for the dark experiment. The final sub-sample exhibited a solubility of -0.11 ± 0.06 % in the dark and 0.29 ± 0.29 % in the light. Fe(III) in seawater can be reduced to Fe(II) via photoreduction which forms much weaker organic complexes (Sunda 2001). Photoreduction of Fe(III) leads to the dissociation of iron chelates or to the dissolution of Fe(III) (oxy)hydroxides. The Fe(II) produced is more weakly complexed with these degraded ligands and Fe(II) is highly soluble (Sunda 2001). As the degraded ligands have a lower complexation stability constant this may promote the dissociation of Fe(II). Fe(II) may then be re-oxidised and the Fe(III) produced bound by organic ligands or precipitated as iron (oxy)hydroxides. Photoreduction, in this experiment, would have lead to the production of Fe(II), enhancing the maximum solubility; in addition the degraded natural or weaker complexing ligands may then have complexed with the iron present in solution, but as a result of photochemical modification, would appear to have an apparent lower adsorptive character than those natural ligands complexing with iron under dark conditions.

The effect of light in the presence of the complexing ligand DFOB on the kinetic dissolution of dFe is presented on Figure 4.20. As mentioned earlier in this section, the kinetic profile under dark conditions was characterised by a fast (within 30 min) enhancement of the maximum solubility of iron released and by the stabilisation of dFe. Under light conditions, the kinetic profile was characterised by a net adsorption of the iron present from the start of the experiment and throughout the duration of the experiment. Although an increase (within a net adsorption) from T_0 was observed up to 91 min indicating that the competing processes were (i) release of iron from the NIST 1648 and (ii) an initial immediate adsorption of background dFe in the seawater on introduction of NIST 1648 to the seawater which had previously been equilibrated with

DFOB. The net adsorption increased to 1.18 ± 0.01 % after 480 min, followed by a decrease in adsorption, -0.04 ± 0.02 % at 1,400 min. The observed net adsorption was unexpected.



a)



b)

Figure 4.20. Effect of light in the presence of the complexing ligand DFOB on the kinetic dissolution profile of 0.5 mg L^{-1} of NIST 1648. a) solubility and b) released concentrations. Error bars represent ± 1 s.d. (n = 4).

In sunlight, an enhancement of the maximum solubility by complexing ligand has been suggested (Sunda 2001). For example, Barbeau *et al.* (2003) investigated the effect of sunlight on various complexing ligands. The seawater matrix was first UV-irradiated and spiked with up to 5 nM of DFOB only, the solution was then exposed to natural sunlight for 5.5 h. Seawater was also spiked with 20 to 40 μ M of DFOB and UV-irradiated and finally exposed to 6 – 8 h of natural sunlight. DFOB was not degraded and they concluded that this hydroxamate binding group was photo-stable in UV-visible light. Moreover, Borer *et al.* (2005) investigated the dissolution of lepidocrocite and goethite with DFOB under light conditions, using a xenon lamp. They observed dissolution of lepidocrocite in the presence of DFOB, enhanced under light conditions whilst no photodissolution was observed for goethite with DFOB (time of exposure 350 min). Barbeau *et al.* (2003) investigated the effect of light of the structure of DFOB only, without iron present. The results, from this study however, suggest that the DFOB / Fe-DFOB complex was photochemically modified, with the final Fe-DFOB becoming more adsorptive onto the NIST 1648 particles (in comparison with Fe-DFOB complexes in the dark), inducing a net decrease of dFe (net adsorption). This has important implications for iron marine cycling and the potential contrasting roles played by organic ligands coupled with the effect of light and therefore warrants further investigation.

4.4. CONCLUSIONS

An automatic sampler composed of a 10-way distribution valve and peristaltic pump was designed and integrated with an aerosol incubation vessel, for the extraction of sub-samples during dissolution experiments of aerosol iron in seawater. Analyses were carried out using flow injection with chemiluminescence detection for the determination of iron in seawater (at pM / nM concentrations). The incubation vessel coupled with the autosampler had low iron contamination, no adsorption onto the walls and low contribution of iron from the autosampler lines and filter. This is an inexpensive and robust system suitable for the laboratory as well as for shipboard deployment, within a

clean environment that minimises the risk of contamination. The automatic sampler allows the monitoring of the fast release of iron from aerosol material into seawater, particularly within the first two hours. The interface allows easy and full control of the sampling strategy: collection time (i.e. T_{0min} , T_{5min} , T_{10min}), number of samples (from 1 to 10 without additional rinsing of the lines), and the duration of sampling (i.e. 30 s, 200 s, 1000 s), ensuring high precision of sampling. In addition, although this study focuses on the dissolution of iron from aerosols into seawater, the user friendly software and reliable interface makes the sampler adaptable and suitable for studying other important environmental dissolved/particle interactions.

Moreover, the autosampler was applied successfully to studying the effect of chemical and physical parameters on the extent and kinetics of the dissolution of aerosol iron in seawater under carefully controlled experimental conditions. Experiments were carried out using the end-member urban particulate NIST 1648, simulating long range transport, in dark and light conditions, with and without addition of a model siderophore Desferrioxamine B (DFOB), at 25 ± 0.2 °C. Dissolution experiments enabled some conclusions to be drawn:

(i) There was a non-negligible effect of the stirring rate on the kinetic dissolution profile of release, and hence dissolution studies were carried out with constant stirring rate (lowest settings).

(ii) Consistent dissolution kinetic profiles were observed using the NIST 1648 end-member at different concentrations. An increase in the solubility of iron released from the aerosol particles in seawater was observed within the first 120 min followed by a decrease in solubility, with potential net adsorption of the dFe onto the aerosol particles.

(iii) The presence of natural complexing ligands increased the solubility of iron by a factor of ≥ 2 , whilst the absence of complexing ligands (UV irradiated seawater) induced absorption at low particle concentration, probably due to the poor efficiency of the UV photo-oxidation system to remove dFe.

(iv) There were contrasting dissolution rates for low and high dust loading dissolutions; a higher rate of release of dFe being observed with higher dust loading.

(v) There was no apparent “dust concentration effect” on the maximum solubility of iron released from seawater, at the dust concentrations used in this study.

(vi) Under dark conditions, with the additions of DFOB, there was an enhancement in the solubility of iron, and no net adsorption was observed.

(vii) Under light conditions, the maximum solubility was increased up to 0.50 % compared with 0.36 ± 0.12 % (dark) and iron was maintained in solution. With the addition of DFOB, a net adsorption of iron was observed, possibly as a result of photochemical induced structural changes of the DFOB /Fe-DFOB complex.

**SOLUBILITY OF IRON IN SEAWATER FROM
THE EASTERN MEDITERRANEAN
MARINE AEROSOL**

5.1. INTRODUCTION

Natural and anthropogenic sourced aerosols play an important role in many biogeochemical global processes and may supply macro (N and P) and micro (Fe) nutrients to the ocean surface (Jickells *et al.* 2005) that have a significant impact on the rate of primary productivity as well as phytoplankton community structure in the world's ocean (Coale *et al.* 1996; Boyd and Abraham 2001; Baker *et al.* 2003; Herut *et al.* 2005 and see also *Chapter One*). The main source of particulate material to the atmosphere in the northern hemisphere is from the Saharan and the Arabian Peninsula deserts (Pye 1987; Jickells *et al.* 2005). Long and medium range transport of Saharan dusts has been confirmed across the northern Atlantic Ocean (Prospero *et al.* 1987; Sedwick *et al.* 2005; Sedwick *et al.* 2007), towards the Black Sea (Kubilay *et al.* 1995), the Amazon Basin (Swap *et al.* 1992), the Netherlands (Reiff *et al.* 1986), Western Mediterranean (Loÿe-Pilot *et al.* 1986; Guieu *et al.* 1997; Chester *et al.* 1999) and Eastern Mediterranean (Kubilay and Saydam 1995; Kubilay *et al.* 2000; Herut *et al.* 2001; Koçak *et al.* 2004; Koçak *et al.* 2005; Kubilay *et al.* 2005).

During this study, there was the opportunity to contribute to a NATO funded collaborative project (NATO CLG 982862) involving three marine institutes in the surrounding of the Levantine Basin of the Eastern Mediterranean Sea (Figure 5.1) and the University of Plymouth (UoP, UK). These were the Institute of Marine Science (IMS) based at Erdemli (Middle East Technical University (METU), Turkey); the Israel Oceanographic and Limnological Research (IOLR), based at Tel-Shikmona (National Institute of Oceanography (NIO), Israel) and the Atmospheric Chemistry Division (ACD), located at Heraklion (University of Crete, Crete). The overall aim of the project was to define the spatial variability of the chemical composition of marine aerosols during Saharan dust events over the Eastern Mediterranean, by simultaneous sampling at the three sites during a transitional period (October 2007). The specific objectives were to (i) collect simultaneous high volume aerosol samples at Erdemli, Tel-Shikmona and

Heraklion; (ii) carry out total digestion of aerosol samples collected at Erdemli and subsequent analyses for major and minor elements (ICP-OES); (iii) determine major elemental concentrations using ICP-OES, in total digestion solutions of aerosol samples collected from Heraklion and Tel-Shikmona and (iv) determine the solubility of iron in seawater from selected samples from the three sites influenced predominantly by anthropogenic and Saharan sources. It will be then possible to present a first approximation of the atmospheric deposition of soluble Fe to the Levantine Basin of the Eastern Mediterranean (with an emphasis on the impact of Saharan dust events).

5.2. THE MEDITERRANEAN SEA AND ATMOSPHERIC INPUTS

The Mediterranean Sea is a small semi-enclosed sea, with narrow connections with the Atlantic Ocean at the Straits of Gibraltar, the Red Sea via the Suez Canal and the Black Sea via the Bosphorus Straits (Figure 5.1). The Straits of Gibraltar restricts the exchange between the Mediterranean Sea and the North Atlantic Ocean surface seawater which has an important influence on the circulation and also on the productivity of the Mediterranean Sea (e.g. Turley 1999). Indeed, the Mediterranean Sea is one of the most oligotrophic seas in the world (Dugdale and Wilkerson 1988; Kress and Herut 1998), with the eastern Basin being ultra-oligotrophic (Kress and Herut 2001; Herut *et al.* 2005). Depleted in nutrients by the uptake of phytoplankton, the warm North Atlantic surface seawater flows through the Straits of Gibraltar and moves eastward in an anticlockwise direction, and in doing so increases the nutrient-depleted character of surface seawater (Bethoux 1980; Achterberg and van den Berg 1997). The lack of significant nutrient rich deep-water mass upwelling, induces low productivity in the Levantine Basin (Azov 1991). There is clearly a gradient west-east in productivity, with on average a three times lower productivity in the eastern Basin compared with that observed in the north-western Basin (Turley *et al.* 2000).



Figure 5.1. SeaWiFS image highlighting the land vegetation around the Mediterranean Sea, (September 2000), also indicated is a dust event to the west of the Eastern Levantine Basin. X indicates the location of ACD, Heraklion (Crete). + indicates the location of IMS, METU, Erdemli (Turkey) and * indicates the location of IONR, NIO, Tel-Shikmona (Israel).

The Mediterranean coastline has large population centres, with two contrasting regions (Chester *et al.* 1996). The northern boundary is surrounded by industrialized and semi-industrialized nations (Western and Eastern Europe), which provide a continuous background of anthropogenic aerosols to the Mediterranean marine aerosol enriched in certain trace metals such as lead (Pb), zinc (Zn), cadmium (Cd), copper (Cu), (Tables 5.1 and 5.2). In contrast sources from the south contribute relatively higher inputs of crustally derived elements (orders of magnitude) such as aluminium (Al), iron (Fe) and manganese (Mn) due to the proximity of the arid and desert areas.

The degree to which a trace metal in a particulate aerosol is enriched or depleted, relative to a specific source, can be assessed by the crustal enrichment factor (EF):

$$EF_{\text{crust}} = (C_{xp}/C_{Alp}) / (C_{xc}/C_{Alc}) \quad \text{Equation 5.1.}$$

Where C_{xp} and C_{Alp} are the concentrations of the trace metal x and Al, in the aerosol, and C_{xc} and C_{Alc} are their concentrations in an average crustal material. The crustal enrichment factor (EF_{crust}) is generally applied (Rahn *et al.* 1979; Chester *et al.* 1999). Anthropogenic-rich components have high values of EF_{crust} (> 10) and crust-rich components have low EF_{crust} (< 10) (Chester *et al.* 1997; Chester *et al.* 1999; Herut *et al.* 2001). The elemental EF_{crust} for Mediterranean marine aerosol are summarised in Table 5.2

using the aerosol elemental concentrations quoted in Table 5.1 and using equation 5.1 (Appendix B). The presented elemental EF_{crust} values confirms the enrichment of elements Cd, Pb, Zn and Cu (i.e. $EF_{\text{crust}} > 10$) in Mediterranean marine aerosol from populations derived from northerly (anthropogenic) sources whereas EF_{crust} in aerosol populations derived from the southern boundary of the Mediterranean Sea were order(s) of magnitude lower.

Table 5.1. Aerosol trace metal concentrations (ng m^{-3}) in Mediterranean marine aerosol for the southern and northern boundaries of the Eastern and Western Mediterranean, from a) Chester *et al.* (1996), b) Guerzoni *et al.* (1999a), c) Herut *et al.* (2001) and d) Koçak *et al.* (2005). Origin / classification of aerosol source were determined using air mass back trajectory analyses.

Elements	Southern boundary origin				Northern boundary origin			
	a	b	c	d	a	b	c	d
Al	2,000	2,929	865	1,143	112	210	318	475
Fe	1,249	1,138	787	891	117	84	275	439
Cd	0.31	0.08	0.24	0.24	0.44	0.17	0.7	0.21
Cr	4.9	3.3	2.4	-	1.0	0.5	2.9	-
Pb	7.4	25.3	34.2	27.4	11	11.7	40	17.6
Mn	18.5	-	15.7	19.9	4.3	-	11	10.9
Zn	8.4	-	89	27.4	12	-	41	18.5
Cu	2.7	-	5.7	7.4	2.0	-	5	5.0

Table 5.2. Crustal elemental enrichment factors in Mediterranean marine aerosol originated from the southern and northern boundaries, from a) Chester *et al.* (1996), b) Guerzoni *et al.* (1999a), c) Herut *et al.* (2001) and d) Koçak *et al.* (2007).

Elements	Southern boundary origin				Northern boundary origin			
	a	b	c	d	a	b	c	d
Al	1.0	1	1.0	1.0	1.0	1	1.0	1
Fe	0.92	1.7	2.3	1.5	1.7	8.3	2.2	1.9
Cd	96	12	228	4.1	1,219	80	1,806	35.2
Cr	2.9	1.1	6.4	-	8.6	3.3	21	-
Pb	46	66	159	19.4	767	550	506	215
Mn	0.84	-	2.4	1.3	3.5	-	4.6	2
Zn	5.6	-	117	3.4	120	-	146	12.2
Cu	5.6	-	21	5.3	28	-	51	21.7

Moreover, within the northern boundary, a gradient in the aerosol elemental concentrations has been observed moving from the Western Mediterranean to the Levantine Basin of the Eastern Mediterranean (Table 5.3).

Table 5.3. Geometric mean of elemental concentrations (ng m^{-3}) in Mediterranean marine aerosols at sampling stations located west and east in Northern boundary: a) Guieu *et al.* (1997) b) Koçak *et al.* (2004).

Elements	Cap Ferrat (Western Mediterranean) ^a	Erdemli (Eastern Mediterranean) ^b	Tel-Shikmona (Eastern Mediterranean) ^b
Al	370	567	952
Fe	320	407	724
Mn	11	7.9	16.7
Cr	2.5	3.9	2.3
Cu	6.2	8.9	5.9
Cd	0.36	0.17	0.22
Zn	40	15.9	22.4
Pb	58	21.5	24.9

Table 5.3 clearly shows a substantial increase in crustally derived elemental aerosol concentrations (Al, Fe, Mn) with a concomitant decrease in predominantly anthropogenic derived elemental aerosol concentrations from west to east of the Mediterranean Sea. This reflects the greater influence of the Saharan inputs (southern boundary) on the eastern Mediterranean marine aerosols. Moreover, Table 5.3 demonstrates a southerly increase in crustally derived elemental concentrations within the Levantine Basin. This has been observed by Kubilay *et al.* (2000) who showed that total dust deposition flux exhibits a clear gradient across the eastern Mediterranean and was confirmed by Koçak *et al.* (2004). Moreover, Kubilay *et al.* (2000) calculated the annual dust deposition rate at Erdemli to be approximately $13 \text{ t km}^{-2} \text{ y}^{-1}$. Ganor and Foner (2001) estimated the annual deposition rate in Israel from 37 to $91 \text{ t km}^{-2} \text{ y}^{-1}$ at Tel Aviv (south) and Jerusalem (south - east) respectively, with exceptional deposition rate during March equivalent to $413 \text{ t km}^{-2} \text{ y}^{-1}$.

The southern and eastern boundaries are characterized by arid and desert regions, including the Sahara, Saudi Arabian and Syrian deserts. These areas are sources of crustal originated aerosols which are transported as seasonal episodic pulses occurring in the Eastern Mediterranean, predominantly during the Spring and Autumn period or during the "Transitional" period which include the months March, April, May and October (Kubilay *et al.* 2000; Ganor and Foner 2001; Koçak *et al.* 2005, Table 5.4). The dust events

originating from North Africa influencing the Eastern Mediterranean occur mainly during the spring, whilst in autumn such events are mainly derived from the Middle East (Kubilay *et al.* 2000). In contrast, Moulin *et al.* (1998) showed that dust transport from North Africa to the western and central Mediterranean occurs mainly during the summer. Thus, the Mediterranean Sea is influenced mainly by a mix of these contrasting aerosol populations; anthropogenic originating from Europe and crustal type aerosols from the desert belt, formed by the Saharan and Arabian Peninsula deserts (Kubilay and Saydam 1995; Guernozi *et al.* 1999a; Guerzoni *et al.* 1999b; Kubilay *et al.* 2000; Herut *et al.* 2001; Kubilay *et al.* 2005).

Table 5.4. Seasonal geometric mean variation of the crustal elemental concentrations (ng m^{-3}). Note: winter (November through to February), summer (June through to September) and transitional season: spring (March through May) and autumn (October), from Koçak *et al.* (2004).

Elements	Transition	Summer	Winter
Al	813	759	316
Fe	537	525	251

In terms of global marine systems, the Mediterranean Sea has one of the largest fluxes of mineral dust due to its close proximity with the Saharan desert (Guerzoni *et al.* 1999b, Table 5.5) whilst sea-salts, biomass burning and volcanic activity represent a negligible contribution to the trace metals concentrations in the aerosol populations (Chester *et al.* 1996). Aeolian inputs of iron into the Mediterranean are amongst the highest in the world (Guerzoni *et al.* 1999b) and are important for phytoplankton metabolism and hence primary production (Krom *et al.* 1991; Bonnet *et al.* 2005; Herut *et al.* 2005). Moreover, the Mediterranean receives, along with iron, other trace metals such as Al, Mn, Zn and Pb (Guernozi *et al.* 1999a; Guieu *et al.* 2002b; Bonnet and Guieu 2004) and nutrients, N and P (Krom *et al.* 1991; Herut *et al.* 1999; Ridame and Guieu 2002; Sarthou *et al.* 2003; Carbo *et al.* 2005; Herut *et al.* 2005).

Table 5.5. Atmospheric inputs of iron ($\mu\text{mol m}^{-2} \text{d}^{-1}$) to the sea surface of the world's oceans. (from Turley 1999).

Oceanic region	Atmospheric Iron Flux
West African Coast	3.13 – 31.3
Mediterranean	2.50 – 21.5
Central Africa	0.46 – 5.40
Pacific	0.09 – 1.09

The impact of these inputs are not negligible (Guerzoni *et al.* 1999b; Kubilay *et al.* 2000; Guieu *et al.* 2002a; Kubilay *et al.* 2002; Ridame and Guieu 2002; Bonnet *et al.* 2005; Herut *et al.* 2005). Dusts from the Saharan desert have a relatively high content of bioavailable phosphorus (Herut *et al.* 2002; Herut *et al.* 2005). Phosphate can leach out of dust to the surface seawater depleted in phosphate, which may stimulate the growth of phytoplankton at the surface (Krom *et al.* 1991) but iron in deeper water can also scavenge phosphate (Krom *et al.* 1991), reducing the N:P ratio in eastern Mediterranean waters. Indeed, a recent study (Herut *et al.* 2005) has clearly shown a short-term response of Eastern Mediterranean surface seawater, which is characterized by low nutrient low chlorophyll (LNLC) regions by the addition of Saharan dust. In microcosm incubations, a linear increase in Chl *a* and primary productivity, up to fivefold, was observed with fresh dust added (4.88 mg L^{-1} > being above a strong Saharan event dust concentration), (Bonnet and Guieu 2004). A Chl *a* increase corresponded to approximately 32 ng L^{-1} whilst primary production corresponded to $0.1 \text{ mg C m}^{-3} \text{ h}^{-1}$ for $1 \text{ mg fresh dust L}^{-1}$ added.

It is important to determine the soluble fraction of the key nutrients associated with the Mediterranean aerosol because: (i) elements in the dissolved phase will undergo geochemical cycling more readily via adsorption / desorption reactions and precipitation / dissolution reactions; and (ii) it is generally postulated that typically only dissolved forms of trace metals are available for uptake by marine phytoplankton (Sunda 2001). Therefore, atmospheric inputs may exert many different effects on the marine environment, and it is necessary to understand the magnitude and geographical distribution of atmospheric fluxes of these materials to both coastal and open seas.

Aerosols from this area are strongly impacted by sporadic intense Saharan dust events, occurring during transition periods in March – May and October (Kubilay *et al.* 2000; Herut *et al.* 2001) and from the Middle East in autumn (Kubilay *et al.* 2000). Therefore as part of the aims highlighted in *section 5.1*, the seawater soluble fraction of aerosol iron in contrasting aerosol population (Saharan and anthropogenic dominated) types collected from different locations around the Eastern Mediterranean was evaluated. This unique dataset will enhance our ability to model atmospheric inputs of iron.

5.3. EXPERIMENTAL

5.3.1. Description of sampling sites

During October 2007, high volume aerosol samples were collected from three rural coastal sites (i) IMS, METU, Erdemli, Turkey, (ii) ACD University of Crete, Heraklion, Crete and (iii) IOLR, Tel-Shikmona, Haifa, Israel), (Figure 5.1).

IMS, Erdemli

Erdemli is located on the northern coastline of the Levantine Basin of the Eastern Mediterranean, (36°33'54" N and 34°15'18" E, Turkey). The immediate surrounding area of the sampling site is mainly semi-arid agricultural land, citrus groves and market gardening. The nearest town is Erdemli, located approximately 7 km away with 49,103 inhabitants and Mersin 45 km away to the east, being a city of 641,133 inhabitants in 2007. Mersin is one of the busiest cities, spreading out along the coast. It has a petroleum refinery and a number of factories manufacturing glass, detergents, fertilizers, chromium and soda. A thermic power plant is situated along with extensive coastal developments in the surrounding hills. To the west of the sampling site, 45 km away, pulp and paper industries are in operation (Biscombe 2004; Koçak 2006).

Bulk aerosol filter samples were collected using the high volume sampler GMVL - 2000 (Sierra Anderson, Mequon, USA), positioned at the top of a designed sampling tower 22 m high (Figure 5.2) located ~ 20 m from the shore.



Figure 5.2. The atmospheric sampling tower located at the Institute of Marine Sciences, Erdemli.

IOLR, Tel-Shikmona

Tel-Shikmona is located on the eastern coastline of the Levantine Basin of the Eastern Mediterranean ($32^{\circ}49'34''$ N and $34^{\circ}57'24''$ E, Israel). This urban site is on a headland pointing out to sea, 0.5 km away from urban conurbations. To the east is Mount Carmel, which peaks at 546 m, and its slopes are covered with luxuriant vegetation, including oaks, pines, olives and laurels. Haifa, the largest city in northern Israel and third-largest city in the country having 270,500 inhabitants. The harbour is the leading passenger ferry port in the country and is also a major cargo port. The industrial region is to the north of the city and located here is one of the two oil refineries in Israel, large petrochemical plants, an oil-fuelled power station, a large cement factory, fertilizer production plant and small industries and workshops (Ganor *et al.* 1998).

Bulk aerosol filter samples were collected using a high volume sampler (HiVol 3000, Enviro Technology Services plc.), situated on the roof of the National Institute of Oceanography (NIO), located partly in the inter-tidal zone, 22 m above sea level.

ACD, Heraklion

Heraklion is located in the western part of the Levantine Basin of the Eastern Mediterranean (35°18'29" N and 25°04'48" E, Island of Crete). The immediate surrounding area of the sampling site is composed of semi-arid agricultural land, olive trees, with no important barrier between the sampling site and the sea. The nearest city is Heraklion located 6 km north-east of the sampling site, with a population of 250,000. Industry has not developed in the region, the airport being east of the city. There is a power plant 6 km away to be north-west.

Bulk aerosol samples were collected using a high volume sampler (Sierra Anderson, Mequon, USA), located on the roof of the University of Crete, Voutes campus, on the north coast of Crete, 20 m above ground and 96 m above sea level (3.3 km from the shore).

5.3.2. Sampling procedures

Choice of filter

The most common method used to collect aerosols for the determination of trace metals is by high volume sampling using fibrous filters (Chester *et al.* 1981; Kubilay and Saydam 1995; Biscombe 2004; Koçak 2006; Koçak *et al.* 2007). Contrasting filter materials have been used, including cellulose membrane (0.45 µm) filters (e.g. Yaaqub *et al.* 1991), fibrous glass fibre filters (e.g. Herut *et al.* 2001) and Whatman 41 fibrous cellulose acetate filters (e.g. Chester *et al.* 1993; Herut *et al.* 2001; Baker *et al.* 2003; Koçak *et al.* 2004). For this project, it was decided to use Whatman 41 cellulose acetate filters (Whatman Int. Ltd., London, UK), being the most common filter medium for the sampling of trace metals associated with marine aerosol populations.

This type of filter material is most suitable for the following reasons:

- (i) Low metal contamination of filter blanks in contrast to the high level of impurities present in quartz filters.
- (ii) Easily digested in mineral acids in contrast to quartz filters.
- (iii) Causes minimal restriction to air flow, allowing high volume collection to be carried out in contrast to cellulose nitrate membrane filters which greatly restrict flow rates and are brittle.
- (iv) Reasonably inexpensive and readily available (Lowenthal and Rahn 1987).
- (v) High retention efficiency (> 95 %) for most elements in fine ($d < 2.5 \mu\text{m}$) and coarse ($d > 2.5 \mu\text{m}$) particles (Lowenthal and Rahn 1987).
- (vi) Mechanical stability as it is flat in the sampler, remains in one piece and gives a good seal with the filter holder to minimize air leaks.
- (vii) High temperature stability, which is important because filters must maintain their physical properties (porosity and structure) over ambient temperature ranges.
- (viii) All collaborating partners possessed high volume sampling systems.

Clearly all of the above factors are important, however in terms of collection of a representative sample, high retention efficiency is the most important factor. Whatman 41 filter collection efficiencies have been tested by Stafford and Ettinger (1972), who found that at low filter velocities, their efficiency never dropped below 95 % for particles down to $0.18 \mu\text{m}$ diameter. During sampling, filters are likely to become loaded with material which will further enhance the collection efficiency of the filters. The main limitation of the Whatman 41 filters is their hygroscopic nature, leading to errors in gravimetric analysis. Accurate measurements of total suspended particulate concentrations (generally collected with low volume samplers) are therefore unreliable with Whatman 41 filters (e.g. Herut *et al.* 2001).

As part of the analytical development of this work, high volume sample dissolutions in seawater were investigated using FI-CL, allowing (i) low particle / seawater concentrations and (ii) repeat studies of the same aerosol sample.

Filter cleaning procedures

Due to a low seawater solubility of iron ($< 1\%$, see *Chapters One and Four*), particularly in Saharan dust dominated aerosol populations (Bonnet and Guieu 2004), it was decided that all samples for the three sites should be collected using pre acid-washed Whatman 41 filters, ensuring as low as possible blank concentrations. A slightly different procedure from the one suggested by Baker *et al.* (2006c) was adopted. All manipulations of filters and baths were carried out in a class-100 laminar flow cabinet (Mac 10 XL, Fan filter unit, Cleanroomshop, Lancaster, UK) to minimise contamination during cleaning. Due to the fragility of the filters once wet and to prevent disintegration, specially designed holding trays (Figure 5.3) were made “in house” from high density polyethylene (thickness 6 mm, Plastics Direct, Tameside, UK) onto which polypropylene meshes (size 3 mm, Plastok, Merseyside, UK) were glued on the top with epoxy resin. Five trays were held one above the other with *ca.* 1 cm gap, being held together using polypropylene dowels (0.5 mm diameter; Plastics Direct, Tameside, UK) at each corner of the frames (Figure 5.3).

The trays were cleaned by soaking in a hot 5% (v/v) micro-detergent (Decon) overnight and then in a 10% (v/v) hydrochloric acid (1.2 M, Analytical reagent grade, Fisher Scientific) bath for 2 days. Between each soak, the trays were rinsed with copious volume of UHP de-ionised water. Once the trays had been cleaned, filters were placed onto each layer of the tray using acid washed plastic tweezers and then soaked in 0.6 M hydrochloric acid (Analytical reagent grade, Fisher Scientific) for an hour and then in 0.1 M hydrochloric acid (Trace analysis grade, Fisher Scientific) for another hour. Between each acid bath soaks, filters were rinsed with a copious volume of UHP de-ionised water

and then soaked for 15 min in a UHP de-ionised water bath; the final UHP de-ionised water bath being followed by a final UHP de-ionised water rinse. The filters were then left to dry overnight and placed in re-sealable plastic bags ready to be sent to the three sites for use. The acid washed filters were sent to the sampling sites unfrozen and once sampled, the filters were sent, for analysis, frozen in a cool bag.

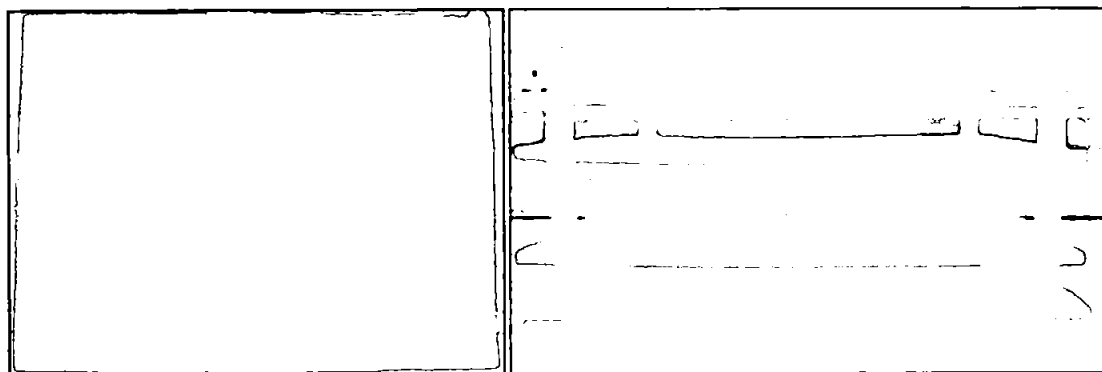


Figure 5.3. Polypropylene holding trays for the cleaning procedures of Whatman 41 filters.

Validation of the filter cleaning procedure

To assess the efficiency of the cleaning technique a simple acidic UHP de-ionised water leach (pH 4.5) was carried out on both acid washed and non-acid washed Whatman 41 filters, followed by elemental analyses of the leach solutions for Fe by graphite furnace atomic absorption spectrometry (GFAAS, Perkin-Elmer), for Ca, Na, Mg and Mn by inductively coupled plasma optical emission spectrometry (ICP-OES), and for Zn, Ni, Pb, Cd, Co and Cu by inductively coupled plasma mass spectrometry (ICP-MS). The handling of the filters was carried out in a class-100 laminar flow cabinet (model K6, Bassaire Ltd., Southampton, UK) to ensure minimal contamination. A quarter of an acid washed ($n = 3$) and non-acid washed ($n = 3$) Whatman 41 filter, cut with ceramic scissors (Aegis Advanced Materials Ltd., Bewdley, UK), were placed in 30 mL polycarbonate "sterilins" bottles (Fisher), previously acid washed in 50 % v/v HCl for a week and rinsed with copious volume of UHP de-ionised water. Then 25 mL of UHP de-ionised water, acidified to a pH of 4.5 using high purity HCl (Romil, Cambridge, UK) was added to the filters. The leach solutions were shaken for 1 h (SSL1, orbital shaker, Stuart Scientific) and then centrifuged at 3,000 rpm for 15 min (Centaur 2, MSE, SANYO). The solutions were finally

transferred to clean acid washed sterilins via micropipetting and acidified to pH = 2 prior to analyses (SpA HCl, Romil). Blanks to assess the contribution of the added HCl ($n = 3$) and from the sterilins with UHP de-ionised water ($n = 3$) were also prepared.

The non-acid washed and acid washed filter elemental dataset represents the mean of three separate acidic leaches (Table 5.6).

Table 5.6. Summary of the trace elemental concentrations (ng mL^{-1}) in an acidic (pH 4.5) UHP de-ionised water leach (25 mL for 15 min; $n = 3$). Operational elemental detection limits were defined as the mean ($n = 3$) acidic UHP water leach concentration ± 3 standard deviation.

Elements	Non-acid washed	Acid washed	Detection limits
Fe	4.20 ± 0.2	< 0.60	0.60
Ca	118 ± 6	< 14.4	14.4
Na	530 ± 10	< 40.0	40.0
Mg	16.0 ± 0.8	< 2.00	2.00
Mn	1.04 ± 0.2	< 0.60	0.60
Zn	0.50 ± 0.2	< 0.20	0.20
Ni	0.39 ± 0.02	< 0.31	0.31
Pb	0.14 ± 0.02	< 0.10	0.10
Cd	0.10 ± 0.1	< 0.08	0.08
Co	0.07 ± 0.01	< 0.06	0.06
Cu	1.48 ± 0.2	< 1.12	1.12

The release of metals in the acid washed filters were all below the defined operational limit of detection whilst in the non-acid washed filters they were all detectable. Even though a weak acidic leak was used and not a total digest, this clearly validates the washing procedure of the Whatman 41 filters for the determination of trace metals in aerosols. To investigate the total elemental contributions, total digests were carried out on the operational blank filters, collected during sampling, in parallel as the filter samples. The limits of detection were calculated, from the mean of acidic UHP de-ionised water leach ($n = 3$), as follows:

$$\text{Mean of blank solutions} + 3 \times \text{standard deviation} \quad \text{Equation 5.2.}$$

Collection and storage of filter samples

High volume sampling requires the forcing of the air sampled through the filter substrate over a specific time using an air pump. High volume systems have been used in the past (Zhuang *et al.* 1990; Kubilay and Saydam 1995; Spokes *et al.* 2001; Koçak *et al.* 2004; Wieprecht *et al.* 2004; Koçak *et al.* 2005; Baker *et al.* 2006c; Koçak *et al.* 2007) and are the most common systems currently used, allowing an approximate flow rate of 1,000 L min⁻¹. Owing to the dynamic nature of the atmosphere and changing aerosol trace metal concentrations over very short time periods, it is crucial to adopt a high temporal resolution sampling strategy. For example, Koçak *et al.* (2004) found that just three Saharan dust events (spanning only several days) occurring over the Eastern Mediterranean in 2001 contributed about 25 % to the total annual dry deposition fluxes for crustally derived elements (Al, Fe and Mn). Thus, such events could easily be missed if a low temporal resolution sampling approach was adopted, leading to significant errors in elemental dry deposition flux calculations.

Samples were collected using a high-volume sampler (Figure 5.4), over a collection time of 24 h (Ganor and Foner 2001). The sampling campaign commenced on 7th October 2007 in Erdemli and Heraklion and on the 11th October 2007 at Tel-Shikmona and continued until the end of the month. Simultaneous sampling at all three sites was carried out in October as it is one of the documented transitional months when Saharan dust events are likely to take place (Kubilay and Saydam 1995; Koçak *et al.* 2004). In total, 60 samples were collected. As part of the NATO collaborative work, sampling at the three sites continued during Spring 2007. However, owing to time constraints for this study only the sampling campaign of October is discussed in this chapter.

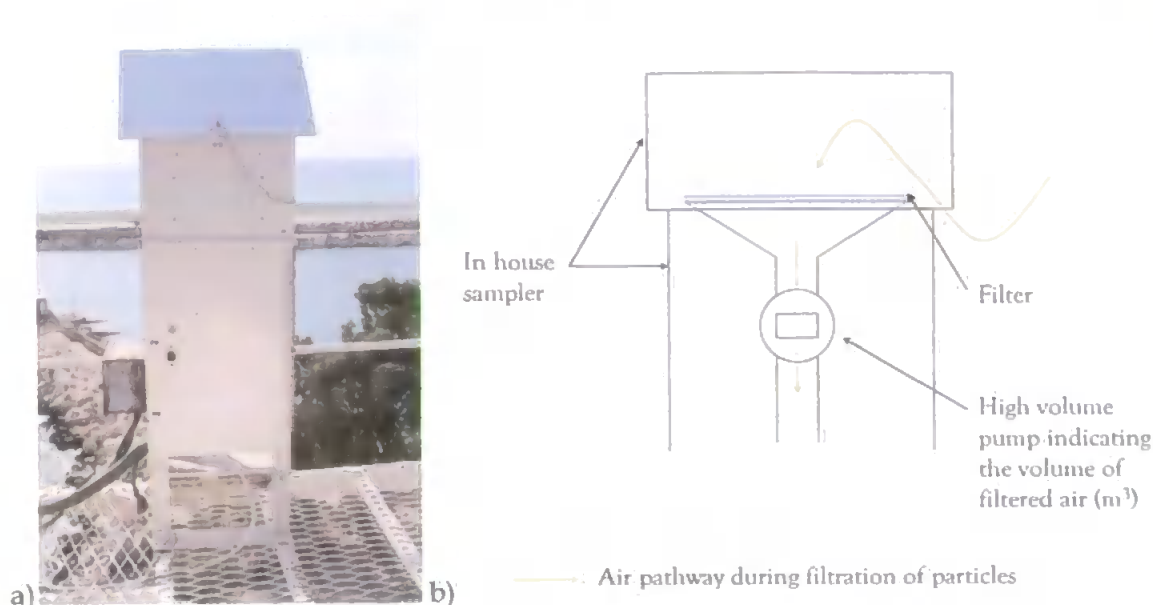


Figure 5.4. a) High volume sampler used at Erdemli. b) Mechanism of the filtration.

The filters were transported to the sampler in re-sealable bags and were then mounted on an anodised aluminium filter holder, using acid washed tweezers, and secured by a frame screwed above the filter holder (Figure 5.5). After sampling, the filters were folded into quarters, the exposed side facing inside and replaced in the re-sealable storage bag, and placed in a second labelled re-sealable bag.



Figure 5.5. a) Anodised aluminium filter holder, b) Filter ready for sampling, secured by the frame.

Back at the laboratory, the filters were separated into quarters using an acid-washed nylon string, in a laminar flow cabinet (Clan LAF, HF 906, Claus Damm, Allerød, Denmark). Samples from Erdemli were taken back to the University of Plymouth to undergo dissolutions for the determination of the solubility of iron in seawater using FI-CL and total digestions for the determination of major and minor elements (ICP-OES). An eighth of the samples from Tel-Shikmona and Heraklion were digested in Tel-Shikmona

and sent to the University of Plymouth for the determination of the major elements by ICP-OES; whereas the minor elements and water soluble chemical constituents were analysed at the ACD, Heraklion along with a three stage sequential leach to determine the aerosol trace elemental solid state speciation (Chester *et al.* 1989). Before and during transport, samples were kept frozen / cool as in a previous study (Buck *et al.* 2006) has shown that the iron solubility of filter collected aerosol may decrease with time if stored at room temperature. Two operational blanks were set aside for each batch of acid washed filters. A filter was placed onto the anodised aluminium filter holder using acid-washed tweezers, the secured frame put back and the sampler closed for about one minute. Then, the filter was removed and folded into quarters, the exposed side facing inwards, and placed back in a re-sealable bag. In addition a blank filter was set aside, without being exposed on the sampler, to assess the contribution of the sampler to the cleaning procedure.

5.3.3. Digestion procedure for major and minor elemental concentrations

For the determination of total concentrations of metals in bulk aerosols using ICP-MS or ICP-OES, it is essential to mineralise the particulate material into solution. Consequently, a total digestion procedure (HNO₃ and HF digestion, Biscombe 2004; Koçak 2006) was applied to solubilise aerosol material from Whatman 41 filters. Plasticware was cleaned by soaking in different baths: the digest PTFE (polytetrafluoroethylene, 30 mL, Savillex, Minnetonka, USA) beakers and the centrifuge tubes (50 mL, sterilin Nalgene, Fisher, Loughborough, UK) for digest solution storage were soaked for 3 days in hot 0.25% (v/v) micro-detergent (Decon). Then the PTFE beakers were placed in a 20 % v/v nitric acid (HNO₃, Trace analysis grade) bath for a week whilst the centrifuge tubes were placed in a 40 % v/v hydrochloric acid bath (Trace analysis grade) for a week. Between the acid baths and final rinse, labware was rinsed thoroughly with UHP de-ionised water and stored in re-sealable plastic bags. To avoid any risks of contamination, handling and preparation of standards were all carried out

under a class-100 laminar flood hood (model K6, Bassaire Ltd., Southampton, UK). The PTFE beakers were refluxed with 5 mL of concentrated nitric acid (Trace analysis grade) overnight on an hotplate at 100 °C (SH3, Stuart, Barloworld Scientific, Stone, UK) and then rinsed with UHP de-ionised water.

Samples collected from Erdemli were digested at the University of Plymouth (UK) using concentrated nitric acid (HNO₃) and hydrofluoric acid (HF). A quarter of the filters were transferred into 30 mL PTFE beakers and covered with 18 mL of concentrated nitric acid (Trace analysis grade), and the lids were tightly secured. The preparation of the samples was in a class-100 laminar flow cabinet (model K6, Bassaire Ltd., Southampton, UK). The contents of the beakers were left to reflux on a hotplate (SH3, Stuart, Barloworld Scientific, Stone, UK) in a fume hood at 100 °C for 48 h. Once the solution was clear of the filter material, suprapur 40 % hydrofluoric acid (5 mL, HF, Merck, Oxford, UK) was added with a disposable acid washed Pasteur pipette (5 mL) and left to reflux for further 48 h at 100 - 120 °C to dissolve any remaining material, in particular the silicate matrix. Due to the reaction with hydrofluoric acid, silicon (Si) evaporates as SiF₄ (e.g. silicon tetrafluoride) and is lost. Therefore aluminium (Al) is used as the indicator of the presence of mineral dust. Once the solutions were clear, the lids were removed and the mixture allowed to evaporate to near dryness (~ 6 h). Concentrated nitric acid (2 mL, Trace analysis grade) was then added, followed by evaporation to near dryness. This step was repeated twice more to remove any residual volatile fluorides, which could damage the nebulizer of the ICP instrument. After the final evaporation, 5 mL of 1 % nitric acid (Trace analysis grade) was added to the digestion vessel contents. The lids were then replaced and the PTFE beakers transported to the laminar flow cabinet where the samples were transferred into the 50 mL centrifuge tubes for storage and were accurately made up to volume (25 mL) with 0.1 M nitric acid. Reagent blanks (n = 3), operational blank filter blanks (n = 4) and acid washed filter blanks (n = 2) were carried out applying the same procedure. Moreover, digests of certified reference materials MESS-3 (50 mg, n = 3) and

NIST 1648 (100 mg, $n = 3$) were carried out in the same batch. 5 mL of 1 % nitric acid was added to the urban aerosol material and made up to volume using 0.1 M nitric acid whilst 5 mL of 2 % nitric acid was spiked to the sediment material and made up to volume using 1 % nitric acid. All blanks, certified reference materials and samples were kept in a refrigerator at 4 °C. Owing to the toxic and corrosive nature of concentrated HF all digestion procedures were performed in a specially designed HF fume cabinet in the presence of a trained HF first aider.

High volume samples from Heraklion and Tel-Shikmona were digested using an HF / aqua regia procedure developed at the National Institute of Oceanography at Tel-Shikmona. An eighth of the filters was placed into 100 mL polyethylene bottles (Nalgene) and covered with 3 mL of concentrated HF (40 %, GR for analysis) and 3 mL of aqua regia (1 part concentrated HNO_3 + 3 parts concentrated HCl). The bottles were then heated to 70 °C on a sand bath for approximately 1 h until complete dissolution of the filters had occurred. Once cool, 30 mL of saturated boric acid was added to the contents and then transferred into 50 mL glass bottles and made up to volume with UHP de-ionised water. The digest contents were then filtered through Whatman 42 filters and stored in 50 mL polyethylene bottles (Nalgene) and placed in the fridge. Moreover, digests of certified reference materials were carried out in the same batch: sediment MESS-3 ($n = 2$, National Research Council of Canada, Institute for National Measurement Standards, Ottawa, Canada), coal fly ash 1633a ($n = 2$) and estuarine sediment 1646a ($n = 2$, National Institute of Standards and Technology, Gaithersburg, USA).

5.3.4. Analytical techniques and performance characteristics

Techniques for elemental analysis were chosen for their detection limit, sensitivity, precision, accuracy, and time and cost of analysis. Depending of these criteria, FI-CL detection and ICP-OES were used during this study for the determination of the solubility

of iron in seawater and the total aerosol major and minor elemental concentrations respectively (Table 5.7).

Table 5.7. Summary of the techniques used for the detection of chosen analytes.

Analytical technique	Analysed elements
FI-CL	Fe
ICP-OES	Al, Fe, Ca, Na, K, Mg, Mn, Ti, Zn,

A Varian 725ES (ICP-OES instrument, Varian, Yarnton, UK) was used for the determination of the major Al, Fe, Ca, Na, K, Mg, Mn, Ti and Zn elemental concentrations. Over the last 25 years, atomic emission spectrometers, also referred to as optical emission spectroscopy with inductively coupled plasma (ICP) excitation sources, have become an indispensable tool for chemical elemental analysis. Their ease of use, high sensitivity and good precision, plus relative freedom from interferences, have made ICP-OES systems the analytical method of choice for a wide range of applications. In addition, ICP-OES has a linear range covering ~ 5 orders of magnitude, but the limit of detection is very element specific.

Filter and operational blank contributions

Operational blanks were determined by taking an acid washed Whatman 41 filter and processing it through exactly the same sampling and digestion procedures as discussed previously (section 5.3.3) to define the level of contamination introduced. Table 5.8 summarises the operational blanks for all three sampling sites. The operational blank values were then compared with the average digest concentrations and these are presented as percentages in Table 5.9. It is apparent that a degree of contamination exists, increasing from Erdemli to Heraklion. Blank contributions from Erdemli were undetectable, except for K (0.5 %) whilst contributions for Tel-Shikmona were generally ≤ 5 % for Al, Fe, Ti, Mg and Na, and < 10 % for the remaining elements except for K. Contributions for Heraklion were higher than for the other two sampling sites and were ≤ 11 % for all elements except for K. The contributions of Na and Zn were overestimated as

the values used in the calculation for the data presented on Table 5.8 were the instrumental detection limits. This was due to the operational blank concentrations being non-detectable.

Table 5.8. Elemental operational blanks ($\mu\text{g mL}^{-1}$ except for Ti, Mn and Zn which are expressed in ng mL^{-1}) for samples collected at (i) Erdemli (ii) Tel-Shikmona and (iii) Heraklion.

Element	Erdemli	Haifa	Heraklion
Al	< 0.12	0.05 ± 0.05	0.31 ± 0.18
Fe	< 0.03	0.09 ± 0.04	0.1 ± 0.04
Mn	< 0.67	3.9 ± 2.6	2.5 ± 3.0
Ti	< 0.78	6.2 ± 2.5	13.3 ± 12.5
Zn	< 1.82	< 5.3	< 5.3
Ca	< 0.02	0.6 ± 0.2	0.6 ± 0.5
Mg	< 0.003	0.02 ± 0.02	0.13 ± 0.06
Na	< 0.07	< 0.35	< 0.35
K	< 0.14	< 0.22	0.45 ± 0.11

Operational detection limits

Operational detection limits (as described in *equation 5.2*) can be determined from the mean of the operational filter blank and the corresponding standard deviation (Table 5.8). Thus, the operational elemental detection limits take into account the variability in the sample digestion procedure and the previous handling of the filters. Operational detection limits are presented in Table 5.10.

Table 5.9. Elemental contribution percentage of the operational blank concentration to the average digest elemental concentration. *Instrumental detection limit used in calculation as the operational blank was < detection limit.

Element	Erdemli	Tel-Shikmona	Heraklion
Al	nd	2.2	9.1
Fe	nd	5.1	4.5
Mn	nd	9.9	5.7
Ti	nd	4.1	6.9
Zn	nd	6.4*	11*
Ca	nd	7.5	7.8
Mg	nd	0.8	6.5
Na	nd	5.3*	12*
K	0.5	23*	33

Elemental operational detection limits for Tel-Shikmona and Heraklion are significantly greater than the corresponding instrumental detection limits except for K. The enhancement in the operational detection limits is typically up to an order of magnitude. Poorer operational detection limits are not unexpected owing to the introduction of contamination during filter handling, sampling, storage and total digestion. Any elements having a digest solution concentration lower than the operational detection limits were deemed to be non-detectable.

Table 5.10. Operational detection limits ($\mu\text{g mL}^{-1}$ except for Ti, Mn and Zn which are expressed in ng mL^{-1}) based on the operational acid washed filter blanks. nd = non-detectable.

Elements	Erdemli	Tel-Shikmona	Heraklion
Al	nd	0.21	0.84
Fe	nd	0.19	0.24
Mn	nd	10.6	4.15
Mg	nd	0.07	0.31
Ca	nd	0.98	2.23
K	nd	nd	0.80
Na	nd	0.21	1.06
Ti	nd	12.2	20.7
Zn	nd	13.3	59.4

Assessment of the experimental and analytical accuracy

To ensure that the applied digestion procedures, HF / aqua regia for samples from Heraklion and Tel-Shikmona and HF/HNO₃ for samples from Erdemli, were efficient at liberating elements from the “residual” phase of the aerosol populations and to ensure that the analyses were accurately performed, three (Tel-Shikmona $n = 2$, Heraklion $n = 1$) and two (Erdemli, $n = 3$) certified reference materials were processed and analysed in the same batch. A summary of the obtained recoveries for the analyses of the CRMs total digest solutions are presented in Table 5.11 for Erdemli and Table 5.12 for Tel-Shikmona and Heraklion. The elemental percentage recoveries obtained using the UoP total digestion method yielded generally slightly lower recoveries (Table 5.11), however for the NIST 1648 (urban aerosol) for “residual” elements Al, and Fe, the recoveries were good ($\approx 88 \%$) which indicates efficient breakdown of this solid phase. Mn, Na, and Ti had

recoveries > 90 % whilst the other elements had recoveries > 80 %, except for Cr (52.9 %). In the sediment material (MESS-3), the recoveries were > 90 % except for Al, Ca, Na and Cu which had recoveries > 80 %, Zn and Ni had recoveries > 65 %. Lead was undetectable within the sediment material.

It is clear from Table 5.12 that most of the elements had excellent recoveries, in particular for the coal fly ash which is more representative of the chemical character of aerosol material than the sediment CRMs. Considering Table 5.12, recoveries were typically above 95 % for all elements except Na, Ti and Zn (although the recoveries for Ti and Zn for all considered CRMs were > 80%). Sodium exhibited the poorest recoveries ranging from 50.0 (MESS-3) to 64.9 % (Est. Sedm. 1646a), and was undetectable in the coal fly ash. The low recovery for Na should be considered when interpreting the aerosol datasets.

Therefore, it is clear that, generally, the two digestion procedures (HF/aqua regia and HF/HNO₃) were efficient for different CRMs of contrasting composition, even though higher recoveries were obtained using aqua Regia. Furthermore, the analyses carried out by UoP were of good analytical quality, thereby allowing accurate environmental interpretation of the aerosol datasets.

Table 5.11. Observed and certified elemental concentrations of MESS-3, and NIST 1648 and their percentage recoveries using HF/HNO₃ digestion procedure for samples from Erdemli. All elemental concentration means are presented as percentages. * concentrations in $\mu\text{g g}^{-1}$, – non detectable.

Element	MESS -3			NIST 1648		
	observed	certified	% recovery	observed	certified	% recovery
Al	6.92 ± 0.28	8.59 ± 0.23	80.6	2.98 ± 0.07	3.42 ± 0.11	87.2
Fe	3.92 ± 0.21	4.34 ± 0.11	90.3	3.45 ± 0.09	3.91 ± 0.10	88.2
Ca	1.27 ± 0.05	1.47 ± 0.06	86.7	5.19 ± 0.15	-	-
K	2.4 ± 0.1	2.6	92.3	0.91 ± 0.03	1.05 ± 0.01	86.7
Mg	1.6 ± 0.1	1.6	100	0.7 ± 0.0	0.8	87.5
Mn	294 ± 11	324 ± 12*	90.7	716 ± 23	786 ± 17*	91.1
Na	1.4 ± 0.0	1.6	87.5	0.495 ± 0.176	0.425 ± 0.002	116
Ti	0.41 ± 0.02	0.44 ± 0.06	93.2	0.4 ± 0.0	0.4	100
Zn	123 ± 7	159 ± 8*	77.4	0.412 ± 0.013	0.476 ± 0.014	86.6
Ni	30.8 ± 4.8	46.9 ± 2.2*	65.7	67 ± 4	82 ± 3*	81.7
Pb	-	21.1 ± 0.7*	-	0.534 ± 0.019	0.655 ± 0.008	81.5
Cd	0.38 ± 0.48	0.24 ± 0.01	158	66 ± 2	75 ± 7*	88.0
Cr	95 ± 3	105 ± 4*	90.5	213 ± 19	403 ± 12*	52.9
Cu	27.6 ± 2.3	33.9 ± 1.6*	81.4	544 ± 10	609 ± 27*	89.3

Table 5.12. Observed and certified elemental concentrations of CFA 1633a, ES 1646A and MESS-3, and their percentage recoveries using aqua regia digestion procedure for samples from Tel-Shikmona and Heraklion. All elemental concentration means are presented as percentages. * concentrations in $\mu\text{g g}^{-1}$, - non detectable.

Elements	coal fly ash 1633a			Estuarine sediment 1646a			MESS-3		
	observed	certified	% recovery	observed	certified	% recovery	observed	certified	% recovery
Al	14.7 ± 0.8	14.3 ± 1	102	2.158 ± 0.104	2.297 ± 0.018	104	8.25 ± 0.25	8.59 ± 0.23	97.0
Fe	9.8 ± 0.4	9.4 ± 0.1	105	1.962 ± 0.123	2.008 ± 0.039	97.7	4.17 ± 0.13	4.34 ± 0.11	96.0
Ca	1.17 ± 0.07	1.11 ± 0.01	106	0.511 ± 0.030	0.519 ± 0.020	98.0	1.45 ± 0.06	1.47 ± 0.06	98.3
K	1.87 ± 0.13	1.88 ± 0.06	99.3	0.784 ± 0.052	0.864 ± 0.016	90.8	2.5 ± 0.1	2.6	97.1
Mg	0.476 ± 0.024	$0.455 \pm 0.010^*$	105	0.387 ± 0.17	0.388 ± 0.009	99.7	1.7 ± 0.1	1.6	107
Mn	181 ± 6	$179 \pm 8^*$	101	236.4 ± 17.3	$234.5 \pm 2.8^*$	101	318 ± 14	$324 \pm 12^*$	98.2
Na	-	0.17 ± 0.01	-	0.375 ± 0.318	0.741 ± 0.017	50.6	1.0 ± 0.2	1.6	64.5
Ti	0.8 ± 0.0	0.8	105	0.413 ± 0.027	0.456 ± 0.021	90.6	0.35 ± 0.08	0.44 ± 0.06	79.3
Zn	216 ± 31	$220 \pm 10^*$	98.4	39.4 ± 4.4	$48.9 \pm 1.6^*$	80.6	143 ± 12	$159 \pm 8^*$	89.8

Determination of the seawater solubility of iron in selected aerosol samples

A quarter of each selected sample from the three sites were set aside to undergo dissolution experiments for the determination of the aerosol seawater solubility of iron using a modified version of the incubation system described in *Chapter Four* with FI-CL detection. Selected samples were placed into the incubation vessel (Figure 4.1) and seawater sub-samples were taken at T_{2h} , T_{4h} and T_{8h} , established from dissolution of a crustally derived sample and previous dissolution studies (Séguret *et al.* 2008, see *Chapter Four*). This is the first time, to the knowledge of the author, that individual aerosol filter collected samples have undergone a separate kinetic evaluation of the release of Fe in seawater, as well as being one of a limited number of studies that have used seawater as the leach medium. All previous studies have either adopted one equilibration time (typically between 1 - 2 hours, Hardy and Crecelius 1981; Chester *et al.* 1993, see Table 1.5) or instantaneous desorption (Buck *et al.* 2006; Sedwick *et al.* 2007). Each dissolution study was conducted within strictly controlled experimental conditions, i.e. 25 ± 0.1 °C in the dark at a low stirring rate in 0.5 L of seawater.

Initial experiments included dissolution studies in triplicate of (i) the operational blank filters from each of the three sampling sites and of (ii) one selected sample from each site; the former to define the blank contributions of the filters and the handling process during sampling and the latter to evaluate the repeatability of three sub-samples.

A 2 cm² perspex template (2 x 1 cm) was prepared for cutting small sections of the filter sample and was acid washed for a week in 80 % high purity HCl (SpA, Romil) and was then stored in a 20 % HNO₃ bath (Trace analysis grade, Fisher Scientific). Prior to dissolution studies, the template was rinsed thoroughly with a copious volume of UHP de-ionised water and left to dry in a laminar flow cabinet. For easier handling to lower the risks of contamination, the selected samples were folded in two and then the template was placed on top of the filter. The filters were manipulated on the “un-cut” side of the

filter using acid washed tweezers. A portion of the filter was then cut using ceramic scissors (Aegis Advanced Materials Ltd., Bewdley, UK), and the 4 cm² filter sample was then carefully placed in the incubation vessel containing the seawater.

The 4 cm² filter sections used in dissolution studies were selected to ensure that the predicted release of Fe into the seawater would be in the low nM range, hence ensuring that the lowest practical particle “concentration” was used whilst allowing good analytical detection. The calculation as to the most appropriate size of filter portion to use was based on (i) literature geometric mean Fe concentrations in the Eastern Mediterranean aerosol (Koçak *et al.* 2004), (ii) volume of air typically sampled through a filter (c. 1000 m³), (iii) area of filter, (iv) expected range of solubilities (based on the “exchangeable” fraction presented by Koçak *et al.* 2007) and (v) volume of seawater to be used (0.5 L).

The reproducibility of cutting the filter into 4 cm² portions using an acid washed filter was assessed at constant temperature and humidity (Table 5.13). The precision was < 3 %, indicating accurate cutting of the filters.

Table 5.13. Reproducibility in cutting 4 cm² of filter portions .

Mass (mg)					Mean	s.d.	RSD (%)
42.8	44.4	41.7	41.2	42.2	42.5	1.10	2.58

Selected high-volume aerosol samples for the three sites were chosen for seawater solubility studies based on (i) their crustal elemental (Al, Fe, Mn) concentrations combined with (ii) the interpretation of their associated back-trajectories (section 5.3.5.), enabling identification of Saharan dust events at each of the three sites as well as (iii) the utilisation of the EF_{crust} of the minor elements identifying aerosol populations derived from anthropogenic sources. Two groups were therefore characterised: anthropogenically and crustally influenced aerosols. Whenever possible samples collected during common dust events at the different sites were included in the selection.

5.3.5. Air mass back trajectories

To aid environmental interpretations and to support selection of aerosol samples which were to undergo iron seawater dissolution, back trajectories indicating the pathway that the sampled air mass took prior to reaching the sampling sites were calculated. The determination of the back trajectory at different altitudes for each sample indicate the likely predominating aerosol source; urban or crustal or a mixture between the two (Figure 5.6).

The air mass back trajectories were determined using the HYSPLIT (HYbrid Single-Particle Lagrangian Integrated Trajectory) model from Air Resources Laboratory. This software is a result of collaboration between (NOAA) and Australia's Bureau of Meteorology, HYSPLIT computes simple air parcel trajectories to complex dispersion and deposition simulations. The model can be run interactively on the web through the READY system on the site for meteorology, air concentrations and trajectory analyses. HYSPLIT allows on-line transport and dispersion models to be created but, for the current study was only used for trajectory modelling. The software allows the calculation of single or up to 3 (space or time) simultaneous trajectories, forward and backward, default vertical motion using vertical velocity field and the possibility to change between isentropic and isobaric trajectories for three different heights in meters (AGL or AMSL), trajectories with label intervals between 6 to 24 h, and an option to allow the inclusion of meteorological variables (e.g. temperature, rainfall and solar radiation flux). For the current study, three-day back trajectories arriving at 1,000; 2,000 and 4,000 m levels were calculated for each sample commencing at 10.00 UTC (Figure 5.6). All back trajectories are presented in *Appendix B*.

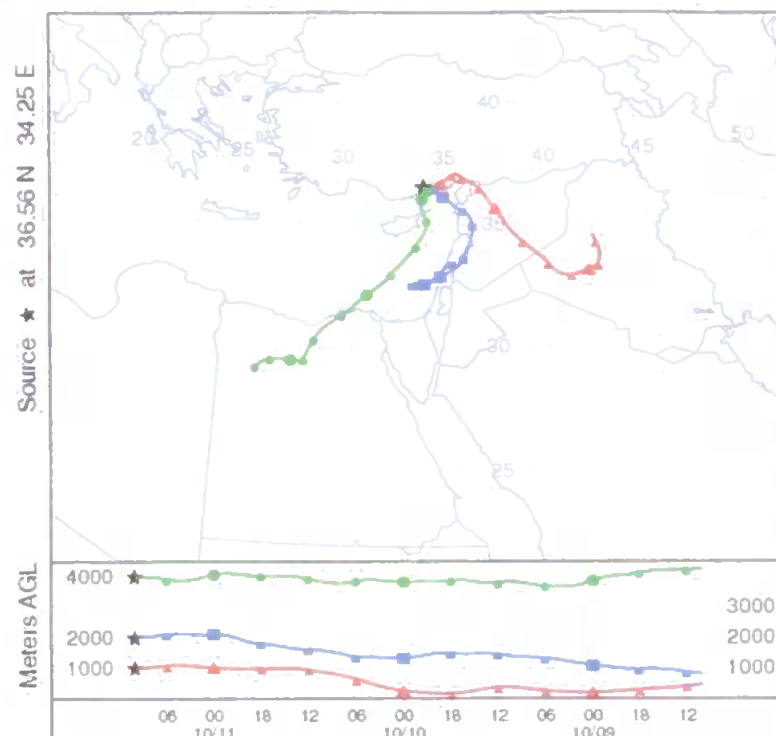


Figure 5.6. Example of calculated 3-day back trajectories arriving at Erdemli on the 11th of October at 1,000; 2,000 and 4,000 m determined using HYSPLIT model.

Back trajectories arriving at Erdemli and Tel-Shikmona have, in the past, been divided into six (Koçak *et al.* 2005) or five (Koçak *et al.* 2004) different sectors. However Koçak *et al.* (2005) had a library of in excess of 400 samples allowing such a detailed categorisation to be made, for the current study a simpler categorisation was adopted which included two sectors (i) Northern air masses and (ii) Southern air masses (Saharan / Arabian, Figure 5.7).



Figure 5.7. Classification of 3-days back trajectories. northern and southern air masses.

5.4. RESULTS AND DISCUSSION

5.4.1 The overall chemical characteristics of the Eastern Mediterranean aerosols

Table 5.14 presents the arithmetic and geometric means and ranges of the overall aerosol elemental (Al, Fe, Mn, Ti, Zn, Ca, Mg, Na, K) concentrations for the Eastern Mediterranean aerosols. The dataset represents 92 samples and 11 operational blank filters collected during October 2007 (and up to the end of December 2007 for Haifa). It is apparent from the arithmetic means and standard deviations and the concentration ranges that there was a high variability in the elemental concentrations. Such a high variability has been observed previously in other aerosol datasets describing European aerosol populations, e.g. Eastern Mediterranean (Kubilay and Saydam 1995; Herut *et al.* 2001; Koçak *et al.* 2004) and Western Mediterranean (Chester *et al.* 1990). Previous studies have shown that a log normal distribution best describes aerosol datasets (e.g. Fones 1996; Koçak 2001) and hence the use of the geometric mean is often adopted in the literature.

The current aerosol datasets were tested for their log normality using the Kolmogorov-Smirnov test. This is a non-parametric t-test for independent samples. However, unlike the parametric t-test for independent samples, the Kolmogorov-Smirnov test is sensitive to differences in the general shapes of the distributions in the two sample populations, and hence was applied to assess the goodness of fit of the data to lognormal distributions. The Kolmogorov-Smirnov test involves the whole distribution of the studied variable and compares the empirical cumulative distribution function to that of the hypothesized distribution. After application of the Kolmogorov-Smirnov test, using the statistical software Minitab 15 Statistical Software English, the distributions of the aerosol elemental concentrations at all three collection sites were found to be lognormal within the 95 % confidence interval. Owing to the log normality of the population distribution the geometric mean would be the more representative mean to describe the aerosol trace metal concentration datasets.

Table 5.14. Geometric and arithmetic mean of aerosol elemental concentrations (ng m⁻³) observed at Haifa, Erdemli and Heraklion during October 2008.

Element	Erdemli			Tel-Shikmona			Heraklion		
	Arithmetic Mean	Range	Geometric Mean	Arithmetic Mean	Range	Geometric Mean	Arithmetic Mean	Range	Geometric Mean
Al	2,150 ± 2,040	256 – 6,910	1380	1,150 ± 1,020	16 – 4,440	740	1,130 ± 2,300	45 – 1,100	423
Fe	1,480 ± 1,420	103 – 4,670	911	898 ± 684	136 – 3,260	683	740 ± 1,260	92 – 6,170	386
Ti	141 ± 136	14 – 448	88	77 ± 65	9.1 – 313	53	64 ± 23	5 – 655	23
Mn	29 ± 25	2.8 – 82	20	17 ± 13	3 – 60	13	14.6 ± 20.5	100 – 196	8.6
Zn	14 ± 4.5	8.2 – 22.1	14	42 ± 30	n.d. – 170	36	19 ± 13	n.d. – 32	13
Ca	5,810 ± 4,350	1,040 – 15,500	4480	4,080 ± 2,910	698 – 14,440	3,280	3,410 ± 4,260	832 – 22,300	2,420
Mg	1,140 ± 919	338 – 3,067	851	1,340 ± 1,040	432 – 5,760	1,090	660 ± 748	197 – 3,960	498
Na	1,310 ± 985	499 – 4,540	1090	3,960 ± 6,540	n.d. – 31,630	2,230	1,070 ± 950	n.d. – 1,940	717
K	703 ± 539	136 – 1,840	533	479 ± 345	69 – 1,710	382	446 ± 603	96 – 3,070	287

For those elements that have a dominant crustal origin (see *section below*) there was a distinct difference in the geometric means between the three sites, the order being Erdemli>Tel-Shikmona>Heraklion. Table 5.15 compares the elemental concentrations from the current study with those reported in the literature. Al, Fe and Mn concentrations in the current study were lower for Tel-Shikmona (but in contrast higher at Erdemli) than those reported by Herut *et al.* (2001) and Koçak *et al.* (2004), the Ti concentration was higher than that reported by Koçak *et al.* (2004) for Erdemli. The latter two sets of values, however, were based on larger datasets spanning several years (Koçak *et al.* 2004) and seasons (Herut *et al.* 2001). For this study a more limited sampling period was used, and as a result the elemental concentrations observed at each of the three sites were more influenced by short-term variations in the number and intensity of dust events in the region which lead to differences with the comparative literature dataset for the same sites. This clearly highlights the importance of the collection of aerosol samples over a prolonged sampling period.

Table 5.15. Comparison of elemental aerosol concentrations (ng m^{-3}) for the current study ($n = 92$) and literature values representative of the Eastern Mediterranean. TS= Tel-Shikmona.

Element	Current study			Koçak <i>et al.</i> (2004)		Herut <i>et al.</i> (2001)	Orif (2008)
	Erdemli	TS	Heraklion	Erdemli	TS	TS	Red Sea
Al	1,380	740	423	567	952	865	2,589
Fe	911	683	386	407	724	787	2,262
Ti	88	53	23	34	-	-	-
Mn	20	13	8.6	7.9	16.7	15.7	49.3
Zn	14	36	13	16	22	-	32
Ca	4,480	3,280	2,420	2,188	-	-	-
Mg	851	1,090	498	490	-	-	-
Na	1,090	2,230	717	2,090	-	-	-
K	533	382	287	380	-	-	-

The anthropogenically derived trace metal, Zn, exhibited higher concentrations at Tel-Shikmona than those detected at Erdemli and Heraklion, and this trend has also been reported in the literature (Koçak *et al.* 2004). Industrial complexes are present to the north

of the Tel-Shikmona sampling site and will introduce local anthropogenic contributions to the atmosphere, whereas the area around Heraklion and the immediate area around the sampling site at Erdemli are less influenced by such activities and as a consequence anthropogenic inputs will have lower impacts.

5.4.2. Aerosol elemental sources: application of the enrichment factor (EF_{crust})

Calculation of the EF_{crust} has been used previously to help define aerosol elemental sources (see section 5.2). The crustal enrichment factor is a useful method for internal and external comparisons of aerosol population chemical characteristics, but enrichment factors should be interpreted cautiously. The EF_{crust} does not take into account regional variations in the mineralogy of the crustal precursor material, chemical fractionation during weathering processes or physical fractionation via dust generation (Guieu *et al.* 2002b). Hence, assessment of the relative contributions of anthropogenic and crustal sources to aerosol populations using the EF_{crust} based on global element/Al ratios is not an exact science. It is for this reason that authors have applied the “< 10” rule to take into account these possible uncertainties (Chester *et al.* 1997; Chester *et al.* 1999; Herut *et al.* 2001). However, in order to more accurately assess the non-crustal elemental contributions, the element/Al ratios in this study for a number of elements were taken from those derived from the analysis of material associated with an intense Saharan dust event (Andreae *et al.* 2002). Appendix B presents element/Al ratios for the average upper crust and various Saharan end members. For Fe, Mn, Ti, Ca, K, Na and K (Andreae *et al.* 2002), Zn (Koçak *et al.* 2004) Saharan end members were used to calculate EF values. However, it would be appropriate to redefine the EF_{crust} term to take into account the use of the “Saharan-end-member” elemental/Al ratios. Instead of using EF_{crust} for these elemental enrichment factors, the term EF_{sd} (Saharan dust enrichment factor) was used (Koçak *et al.* 2004; Koçak 2006).

Considering the aerosol EF_{sd} values at the three sites over the whole sampling period it is apparent that all elements except Na (except for Erdemli) and Zn (and Mg for Haifa) have geometric means < 10 , with Ti and Fe having $EF_{sd} < 2$ (i.e. non enriched elements - predominantly crustal sourced). This is consistent with the observations in the literature for Erdemli and Tel-Shikmona (Koçak 2006). In contrast, Zn is defined as an enriched element (EE's, Chester 2000) at all sites, with geometric means for the EF_{sd} at Tel-Shikmona, Heraklion and Erdemli being 77, 28 and 12 respectively. The higher EF_{sd} observed at Tel-Shikmona was a result of local anthropogenic inputs to the aerosol whilst Na was also found to be enriched (EF_{sd} 51 and 157 for Heraklion and Tel-Shikmona respectively), indicative of a non-crustal source i.e. sea salt production.

Table 5.16. Comparison of the geometric means of the EF_{sd} and ranges (in brackets) for the current study with those in the literature. (TS = Tel-Shikmona).

Element	Heraklion	Tel-Shikmona	Erdemli	Erdemli	TS
	Current Study		Koçak (2006)		
Al	1	1	1	1	1
Fe	1.5 (0.9 - 3.3)	2.0 (0.9 - 23)	1.0 (0.6 - 1.2)	1.1	1.3
Mn	2.7 (1.0 - 11.7)	2.5 (1.1 - 26.3)	1.5 (1.4 - 2.1)	1.5	1.9
Ti	1.0 (0.6 - 2.6)	1.4 (7.8)	1.1 (0.9 - 1.2)	1	-
Zn	28 (1.1 - 86)	77 (4 - 1745)	12 (3.4 - 45)	21.9	22.4
Ca	5.9 (1.4 - 20.4)	5.3 (1.3 - 56)	2.6 (1.8 - 5.6)	3.1	-
Mg	5.9 (1.1 - 31)	11.3 (2 - 134)	3.6 (2.6 - 7.8)	5.1	-
Na	51 (0.8 - 384)	157 (0.8 - 1444)	2.4 (0.3 - 22.6)	12.4	-
K	4.3 (1.4 - 11.6)	5.1 (1.2 - 31)	1.0 (0.7 - 1.7)	2.3	-

For samples collected at Erdemli in October 2007, minor element concentrations were determined and the geometric means of the EF_{sd} are presented (Table 5.17). Copper and lead, along with zinc, were enriched elements ($EF_{sd} > 10$) and hence for these elements their sources are predominantly anthropogenic in origin. However, during large dust events (see section 5.3.4) their individual EF_{sd} were < 10 (see range of values) as a result of the large contribution to the aerosol of Saharan dust. In contrast, however, the highest EF_{sd} occurred during low dust intensities and when mass back trajectories had European origin (see section 5.3.4). Hence, dual behaviour was noted for these elements.

The EF_{sd} , together with the back trajectories, were used to select aerosol samples for Fe seawater dissolution experiments which represented “anthropogenically” influenced aerosol populations.

Table 5.17. Geometric means and range in brackets of EF_{sd} for minor elements from samples collected at Erdemli during October 2007.

Cu	Cr	Zn	Pb	Ni
10	3.4	12	7.6	2.9
(2.1 – 53)	(1.2 – 8.1)	3.4 – 45	1.2– 28	0.8 – 7.8

The EF_{sd} were compared with those from the literature for Erdemli (Herut *et al.* 2001; Koçak 2006, Table 5.18). These represent the EF_{sd} values taken over > 1 year of sampling and are therefore more representative of the chemical character of the marine aerosol at each site in comparison with the current study which covered relatively shorter periods, EF_{sd} values decreased in the order $Pb > Cu \sim Zn$. However, for the current study all EF_{sd} were lower at Erdemli as a result of the greater influence of Saharan dust events over the October sampling period compared with their influence over an annual period. Both Ni and Cr exhibited $EF_{sd} < 10$ indicating that they came from a predominantly crustal source.

Table 5.18. Comparison of the geometric mean of EF_{sd} for the current study with the literature. * adapted from Kubilay and Saydam (1995).

	this study	Koçak (2006)	Herut <i>et al.</i> (2001)*
Cu	10.0	23.9	-
Cr	3.4	-	29
Zn	12.1	21.9	31
Pb	7.6	84.8	176
Ni	2.9	-	-

5.4.3. Inter-elemental relationships

Aerosol elemental concentrations will show a high degree of variability as stated in section 5.3.1. By comparing elemental concentration variability using the correlation coefficient, common process(es) can be identified. Such common processes include: (i) similar sources (ii) similar generation and/or removal mechanism and/or (iii) similar

transport patterns. For the current dataset therefore, the Rank-Spearman correlation was calculated for paired elemental concentrations. The Rank-Spearman correlation is a non-parametric version of the Pearson correlation coefficient. The inter-elemental correlation coefficients (r) between aerosol trace metals are presented in Table 5.19, along with their statistical significance.

Table 5.19. Rank spearman coefficient for the elements determined in the collected aerosol samples (correlations in bold significant at $p < 0.05$) for the three sites.

a) Tel-Shikmona								
	Al	Ca	Fe	K	Mg	Mn	Na	Ti
Ca	0.796							
Fe	0.960	0.893						
K	0.730	0.702	0.770					
Mg	0.586	0.734	0.653	0.890				
Mn	0.942	0.882	0.988	0.773	0.653			
Na	0.263	0.195	0.255	0.640	0.646	0.237		
Ti	0.964	0.892	0.979	0.761	0.674	0.968	0.275	
Zn	0.094	0.451	0.265	0.338	0.350	0.290	0.067	0.245
b) Heraklion								
	Al	Ca	Fe	K	Mg	Mn	Na	Ti
Ca	0.823							
Fe	0.978	0.840						
K	0.872	0.804	0.860					
Mg	0.579	0.436	0.591	0.581				
Mn	0.867	0.805	0.886	0.86	0.665			
Na	-0.164	-0.164	-0.112	0.017	0.546	-0.007		
Ti	0.959	0.772	0.947	0.786	0.597	0.803	-0.120	
Zn	0.629	0.582	0.689	0.728	0.448	0.753	0.181	0.576
c) Erdemli								
	Al	Ca	Fe	K	Mg	Mn	Na	Ti
Ca	0.954							
Fe	0.993	0.952						
K	0.977	0.976	0.977					
Mg	0.939	0.936	0.937	0.943				
Mn	0.983	0.965	0.989	0.979	0.955			
Na	-0.101	-0.002	-0.089	0.017	0.148	-0.055		
Ti	0.997	0.946	0.993	0.971	0.945	0.984	-0.077	
Zn	0.863	0.754	0.851	0.766	0.835	0.835	-0.163	0.880

The common source for Al, Ca, Fe, K, Mg, Mn, Ti and Zn (except for Tel-Shikmona) is emphasised by the excellent statistical significance of the Rank Spearman inter-elemental correlations for all sampling sites. For all elements, correlations were significant at $p < 0.05$ (Table 5.6). No significant statistical correlations were detected for Zn and the other elements for the Tel-Shikmona dataset, confirming its non-crustal source, nor were there significant correlations (95 % confidence limits) between Na and the other elements at the three sites (except with Mg and K at Tel-Shikmona and with Mg at Heraklion) which were to be expected owing to its marine source. However, in contrast, Zn correlated significantly with the crustal elements at Erdemli/Heraklion, highlighting the lower anthropogenic source influence and proportionally higher contribution made by crustal sources to the aerosol for this element, also supported by the lower EF_{sd} calculated than previously stated in the literature (section 5.3.2).

5.4.4. Temporal variation in elemental aerosol concentrations

The temporal variations of the aerosol elemental concentrations are presented in Figures 5.8.a - c for the three sites. As stated in section 5.3.3, it is not surprising that all elements except Na and Zn exhibited significant correlations and hence similar temporal trends at each site. The key features of the temporal variation exhibited by the crustally derived elements at each of the three sites can be summarised as follows:

- (i) Erdemli: two dust events (as defined by $Al > 1000 \text{ ng m}^{-3}$) occurred between 9th - 13th and 19th -24th October 2007.
- (ii) Tel Shikmona: four dust events occurred on the following dates: 9th - 10th, 12th -13th, 17th - 18th and 29th - 31st October 2007.
- (iii) Heraklion: one major dust event took place between 29th - 31st, with a low dust event around the 20th October 2007.

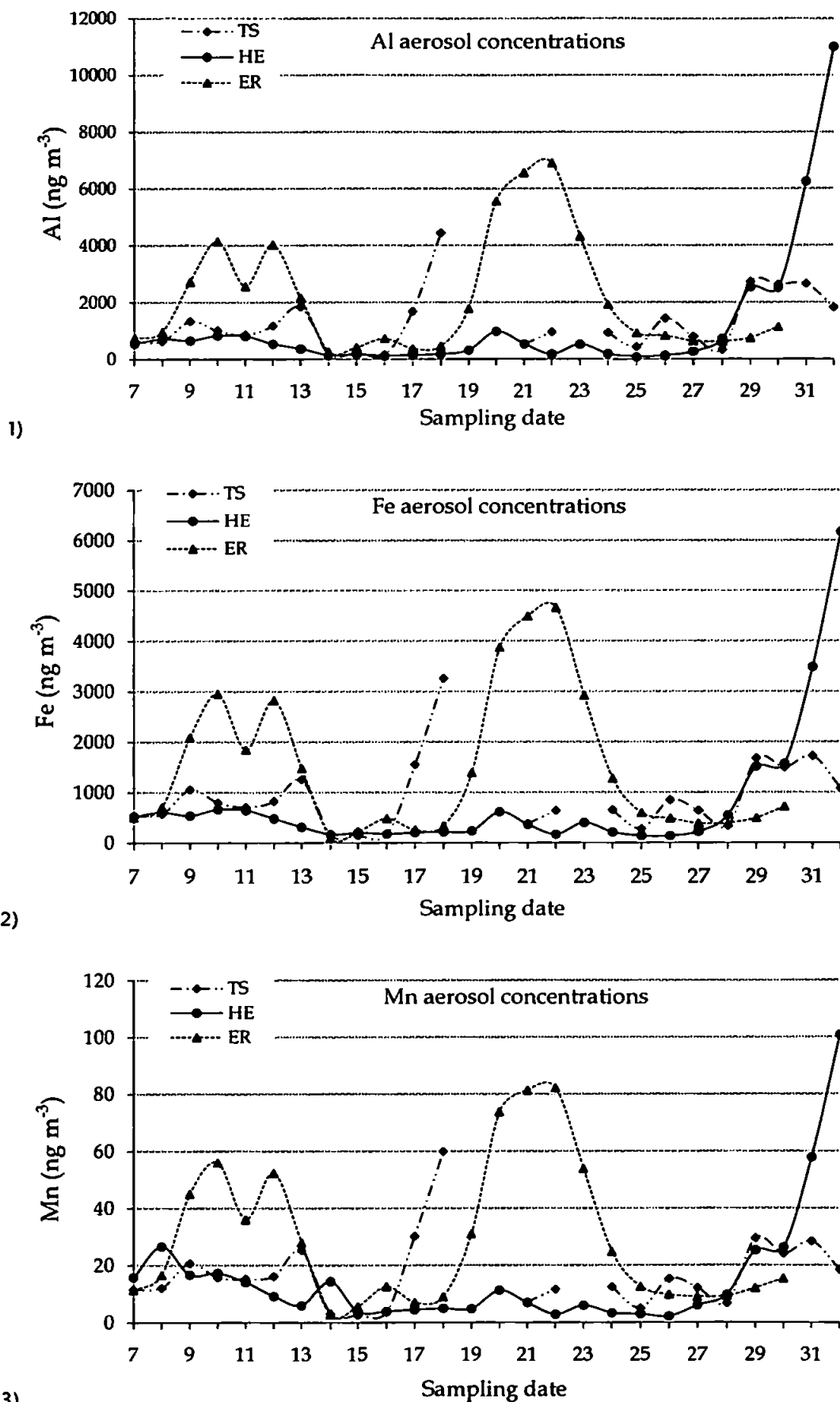


Figure 5.8. a) Temporal variations (October 2007) in 1) Al, 2) Fe and 3) Mn aerosol concentrations (ng m^{-3}) at all sites: Erdemli (ER), Tel Shikmona (TS) and Heraklion (HE).

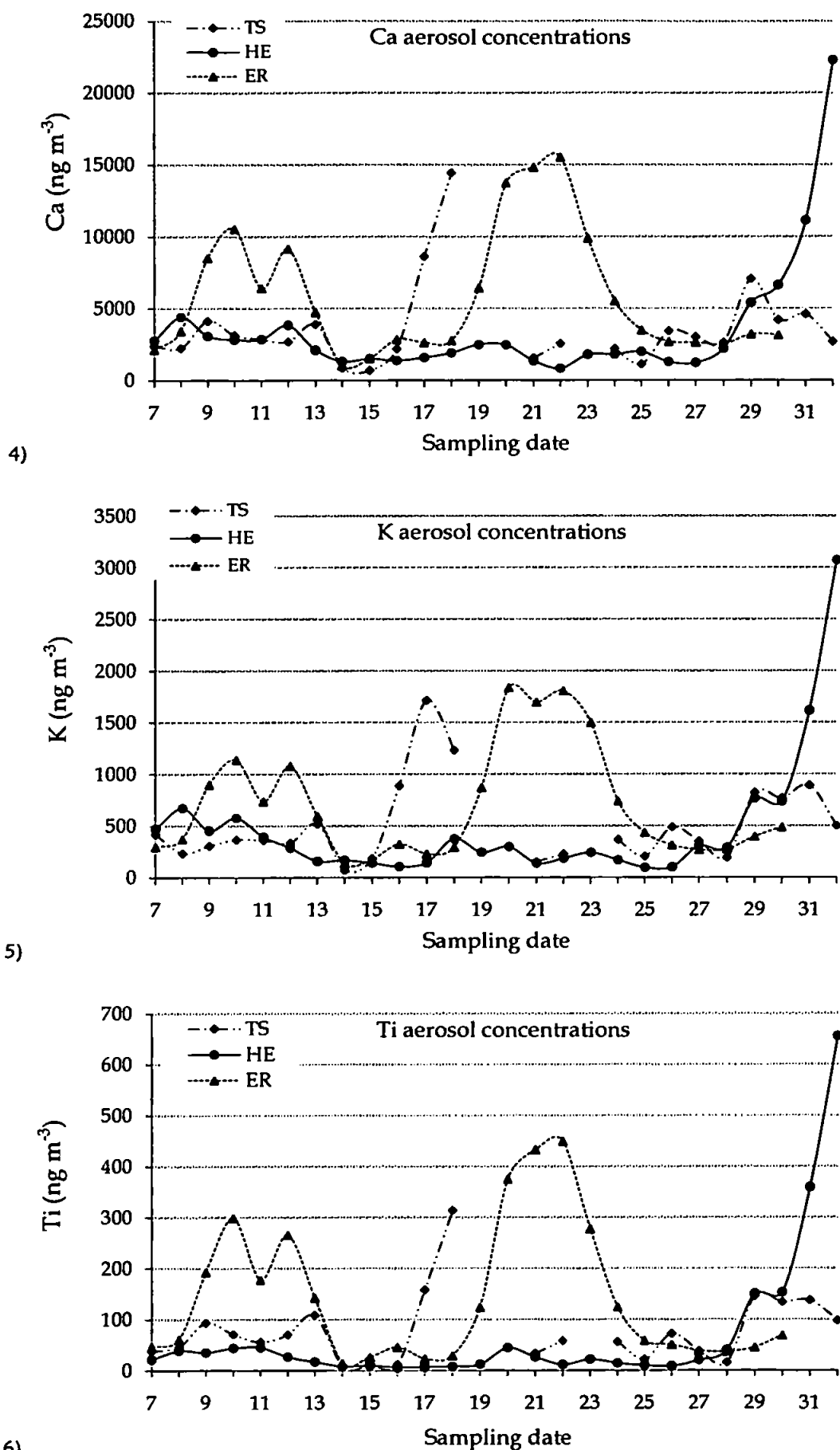


Figure 5.8. b) Temporal variations (October 2007) in 4) Ca, 5) K and 6) Ti aerosol concentrations (ng m^{-3}) at all sites: Erdemli (ER), Tel Shikmona (TS) and Heraklion (HE).

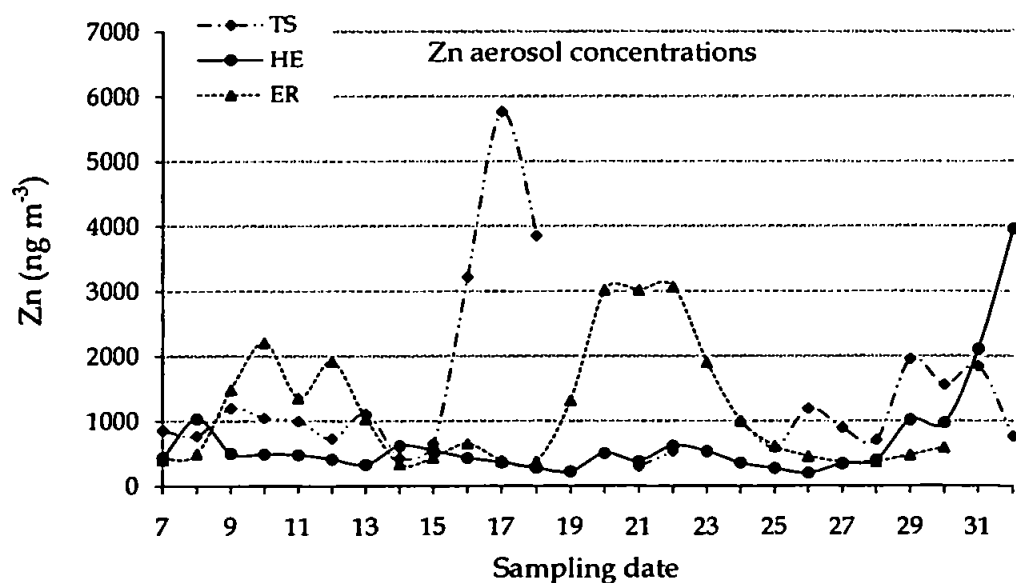
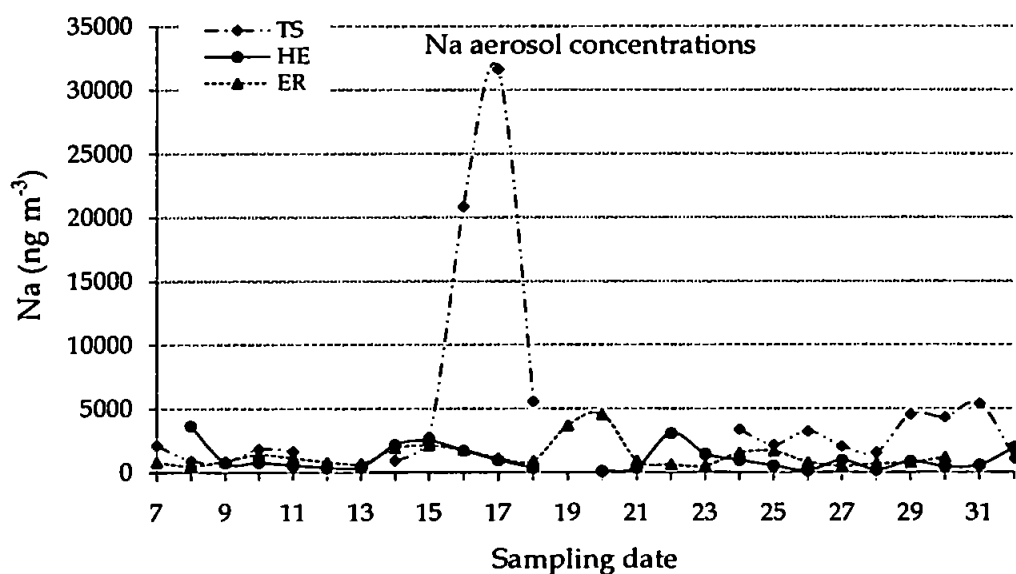
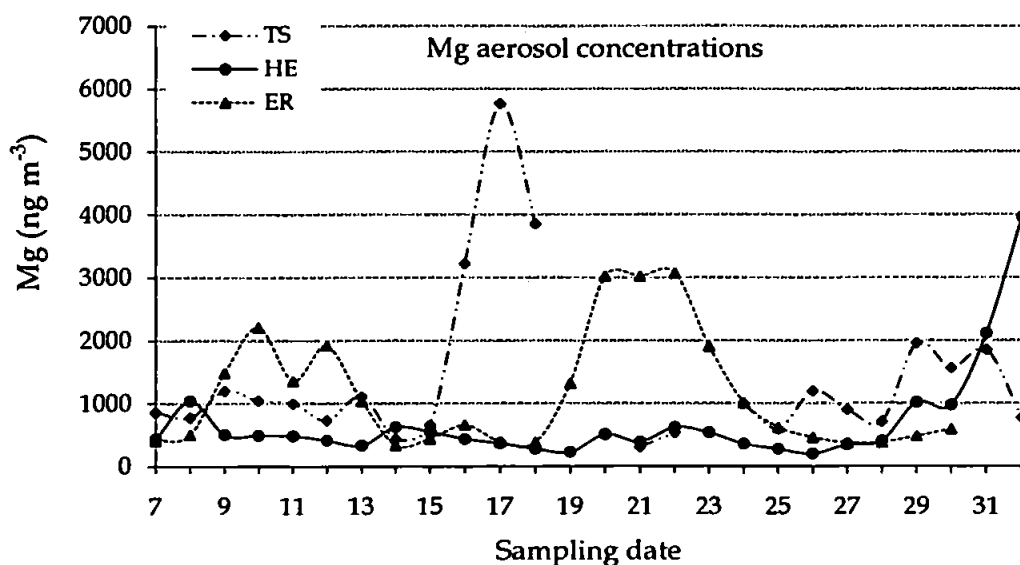
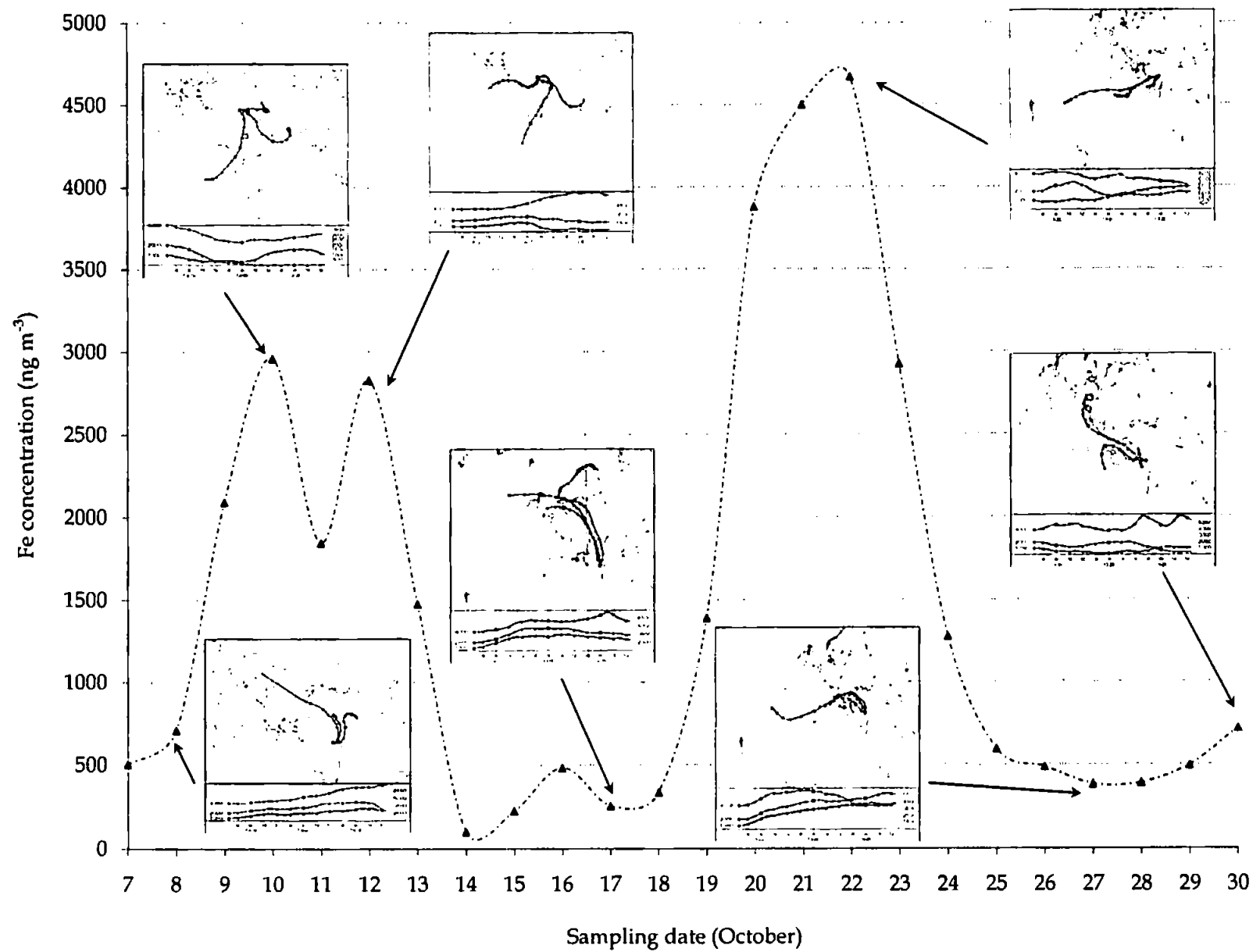


Figure 5.8. c) Temporal variations (October 2007) in 7) Mg, 8) Na and 9) Zn aerosol concentrations (ng m^{-3}) at all sites: Erdemli (ER), Tel Shikmona (TS) and Heraklion (HE).

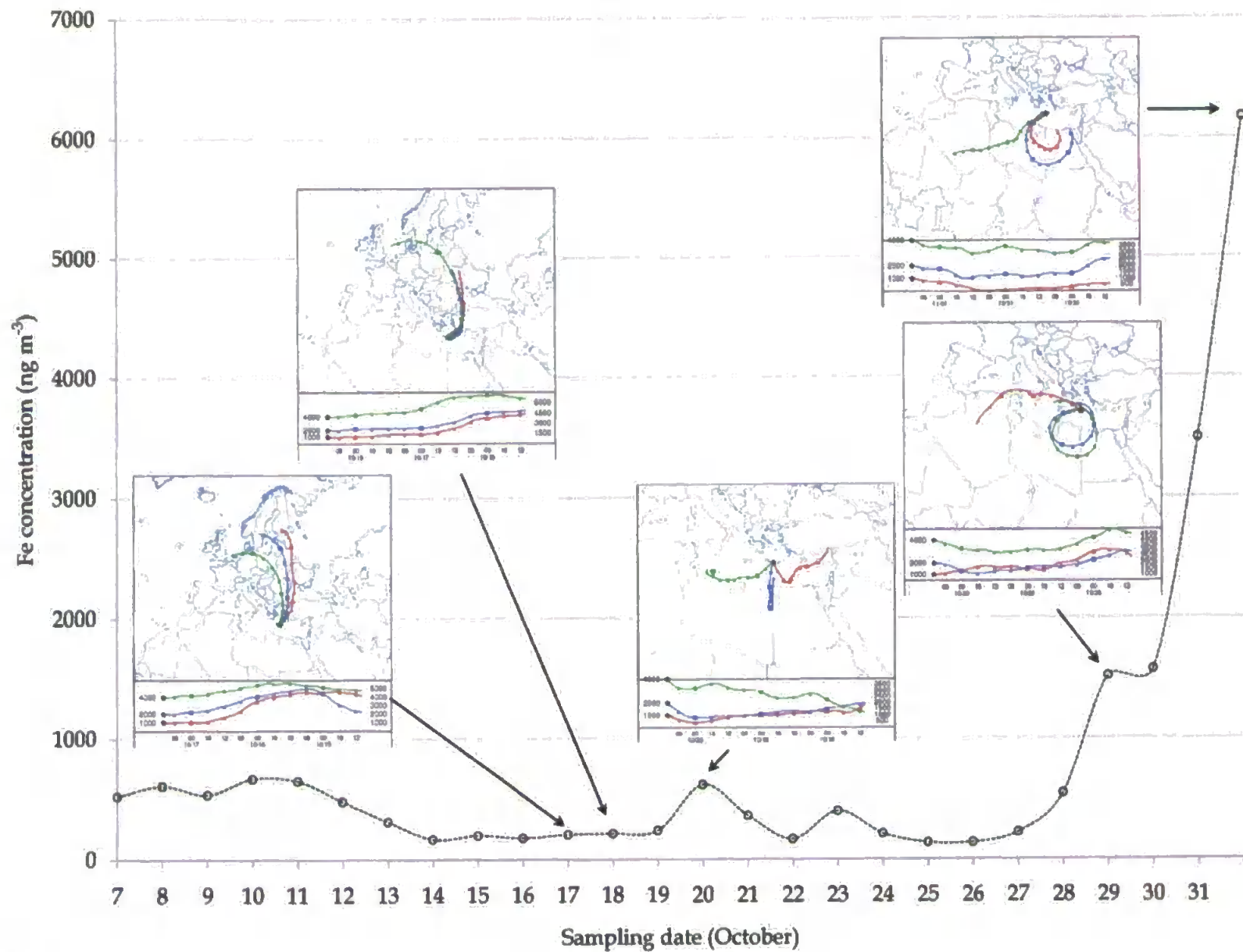
The impact of air mass transport on the chemical character of the collected aerosol population at each site is illustrated by Figures 5.9a - c using Fe aerosol concentrations as a proxy for dust events and air mass back trajectories for each sampling day (3 day, three altitudes: 1000 m, 2000 m and 4000 m). Figure 5.9a shows that at Erdemli the initial dust event over the period 9th - 13th October was generally a result of higher altitude transport of dust from the North Eastern Saharan desert. High altitude transport of Saharan dust to the sampling site at Erdemli has previously been observed by Koçak *et al.* (2004; 2005) and Kubilay and Saydam (1995). The end of this dust event (13th October), with the subsequent decrease in aerosol iron concentrations ($< 1000 \text{ ng m}^{-3}$), was due to a switch in the air mass source, changing to the Eastern Mediterranean and then to Central Europe. It was also apparent that the source of material during the second, and largest, dust event was the West, Central and Eastern Saharan desert. The subsequent decrease in iron concentration (after 24th October) was a result of air masses derived from Eastern Europe.

No dust event was detected at Heraklion during the initial period of sampling (Figure 5.9.b). This is also supported by the air mass back trajectories suggesting sources from Central Europe (7th - 8th October) then mainly from the Eastern Mediterranean (9th - 14th) and then again from Central Europe (15th - 19th). A small, short dust event, originating from the West / Central Saharan desert, was detected (around the 20th), followed by relatively low Fe concentrations until the latter part of the month (29th onwards) when an intense event developed as a result of dust transport from the Eastern Saharan desert.

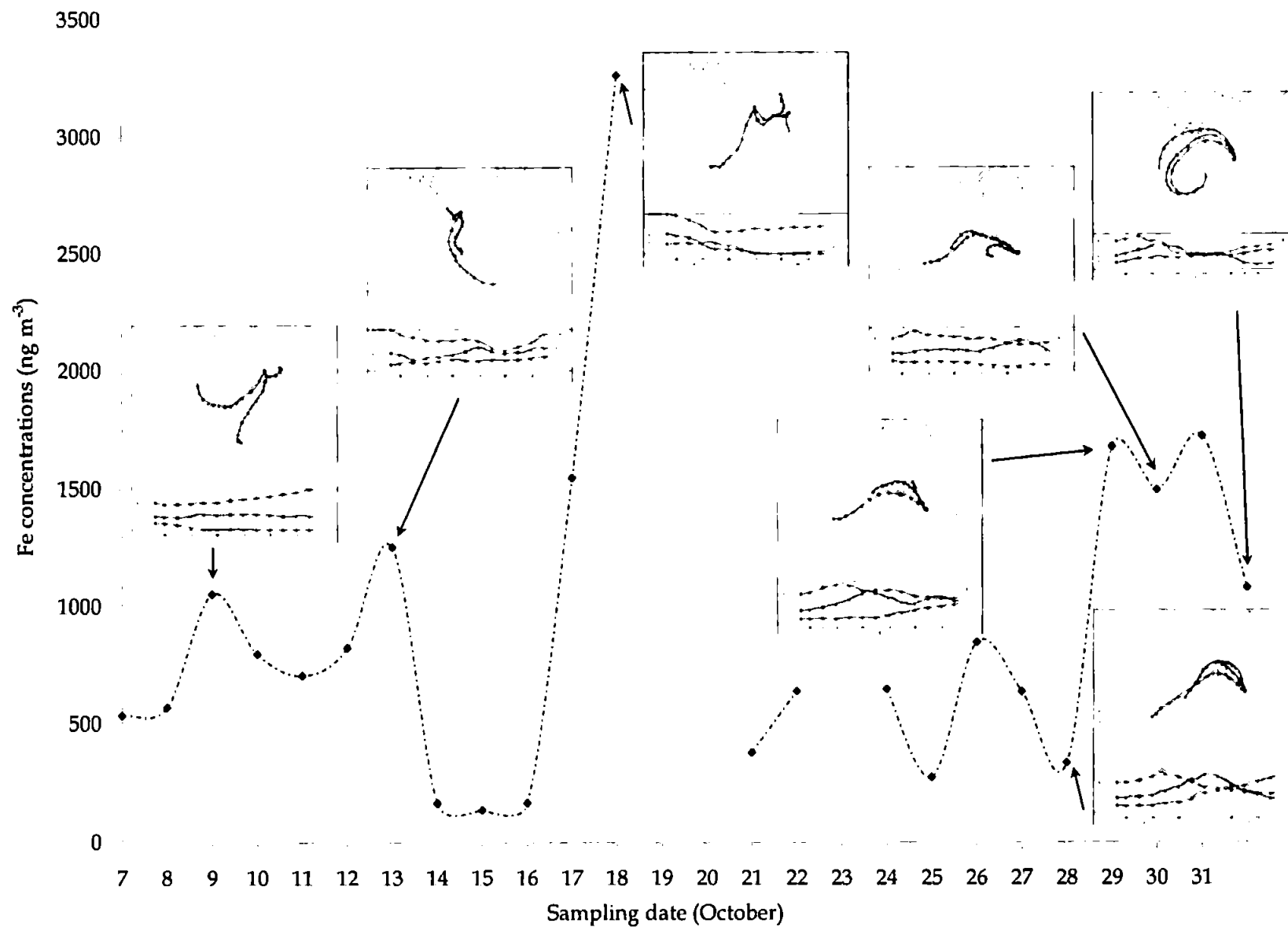
At Tel Shikmona (Figure 5.9.c), the dust events detected during 9th - 10th, 12th -13th and 17 - 18th were a result of dust transport from the eastern Saharan desert (the initial two events coinciding with those observed at Erdemli, Figure 5.9.a). The dust event observed towards the end of the month had sources from the Central Saharan desert, similar to the large dust event occurring at Heraklion during the same period.



a) Erdemli



b) Heraklion



c) Tel-Shikmona

Figure 5.9. Impacts of air mass transport on Fe aerosol concentrations as a proxy for dust events at a) Erdemli, b) Heraklion and c) Tel-Shikmona.

5.4.5. The seawater solubility of iron in the Eastern Mediterranean marine aerosol

Using the back trajectories presented in Figures 5.9.a to 5.9.c (and *Appendix C*), as well as elemental aerosol concentrations, in particular for iron, a selection of crustally derived and anthropogenically influenced (using corresponding EF_{sd} for samples from Erdemli, see *section 5.3.2.*) aerosol samples were identified and selected for iron dissolutions in seawater as described in *section 5.2.4* (Table 5.20).

Table 5.20. Selected aerosol samples for iron dissolution studies.

Anthropogenically influenced aerosols		Saharan dust dominated aerosols	
Location	Date	Location	Date
Erdemli	08-Oct-07	Erdemli	10-Oct-07
Erdemli	17-Oct-07	Erdemli	12-Oct-07
Erdemli	27-Oct-07	Erdemli	22-Oct-07
Heraklion	17-Oct-07	Erdemli	30-Oct-07
Heraklion	18-Oct-07	Heraklion	01-Nov-07
Heraklion	20-Oct-07	Heraklion	30-Oct-07
Tel-Shikmona	28-Oct-07	Tel-Shikmona	01-Nov-07
Tel-Shikmona	29-Oct-07	Tel-Shikmona	18-Oct-07
-	-	Tel-Shikmona	30-Oct-07

Determination of the contribution of the operational blank filter during dissolution studies

As discussed in *section 5.3.4*, portions (4 cm²) of blank filters for each sampling site underwent seawater dissolutions (carried out in triplicate) to assess the degree of contamination derived from both the filter and its manipulation during sampling and storage. The means and standard deviations after an 8 h equilibration time with seawater are presented on Table 5.21.

Table 5.21. Filter blank (n = 3) contributions (nM) to the seawater over an 8 h dissolution study.

Filter blank concentrations (nM)	
Heraklion	0.11 ± 0.23
Tel-Shikmona	0.14 ± 0.10
Erdemli	< 0.02

The filter blank concentrations were determined by subtraction of the mean seawater iron concentration (2.4 nM, collected from the Canary Basin, salinity = 32.1) from

the concentration of iron following an 8 h incubation with the filter present. The data clearly indicate minimal contamination from the added filter portions to the seawater and no adsorption of dissolved iron in seawater onto the filter.

Repeatability of the determination of the solubility of iron from crustally derived aerosol samples

To assess the repeatability of the dissolution studies a crustally derived aerosol sample from each of the three sites was used in triplicates. It was decided to assess the samples collected on 30th October 2007. The solubility of iron in seawater from these crustally derived samples was subsequently observed to be low; < 0.3 %. Figure 5.10 and Table 5.22 highlight the solubility of the three samples from each site with their corresponding 3-day air mass back-trajectories (Figure 5.11). Figure 5.10 also highlights their solubilities for each time interval sub-sampled (2, 4, and 8 h) along with their standard deviations. Three different trends were observed: increase during the 8 h dissolution (Heraklion), no variation (Erdemli) and increase up to 4 h followed by a plateau (Tel-Shikmona), although statistically there were no differences between all of the observed concentrations between the different contact times.

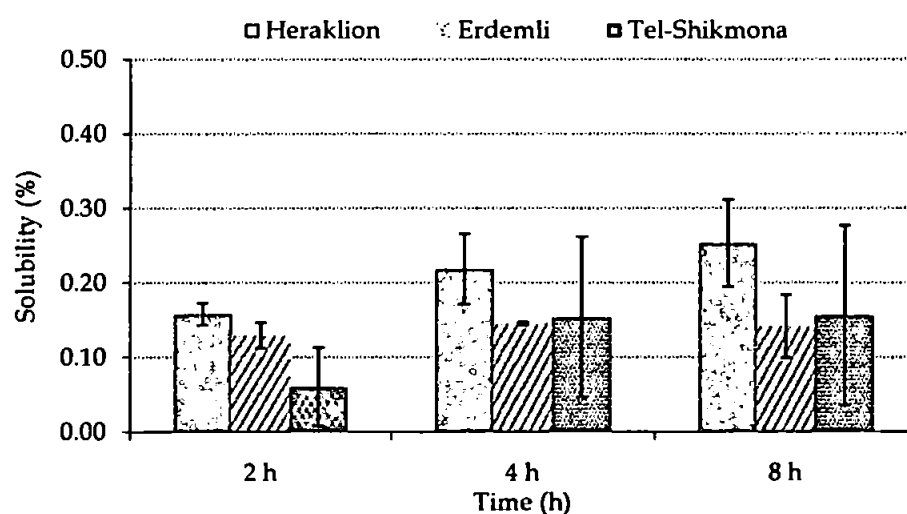


Figure 5.10. Repeatability study ($n = 3$) of a crustally derived aerosol sample from each site. HE = Heraklion, ER = Erdemli, TS = Tel-Shikmona. Error bars = ± 1 s.d.

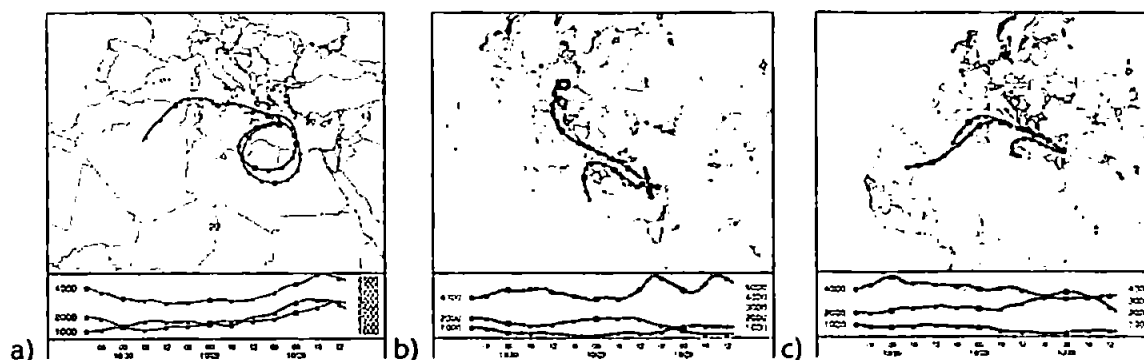


Figure 5.11. Corresponding 3-day air mass back-trajectory arriving at the three sites for the samples collected on the 30th October. a) Heraklion, b) Erdemli and c) Tel-Shikmona.

Table 5.22. Percent solubility (± 1 s.d.) of triplicate dissolutions of sample collected on the 30th October, from each site.

Site	Time of sub-sampling		
	2 h	4 h	8 h
Heraklion	0.16 ± 0.01	0.22 ± 0.05	0.25 ± 0.06
Tel-Shikmona	0.06 ± 0.05	0.15 ± 0.11	0.16 ± 0.12
Erdemli	0.13 ± 0.02	0.15 ± 0.01	0.14 ± 0.04

Good repeatability was observed, in particular, for samples collected from Heraklion and Erdemli (with standard deviation ranging between 0.01 and 0.06 %), whereas greater variability was observed for the sample collected from Tel Shikmona (0.06 - 0.12 %), presumably as a result of the comparatively lower homogeneity of the collected dust on the filter paper. The homogeneity and chemical composition of this aerosol sample might have been impacted by the various dust origin sources, Western, Northern and Eastern Saharan regions (Figure 5.11.c), (Formenti *et al.* 2008) whilst the other two samples had more localised back trajectories (Figure 5.11.a and b.).

Solubility of iron in seawater in the eastern Mediterranean marine aerosol

A summary of the observed iron solubilities in seawater for the selected aerosol populations are presented in Table 5.23 and compared with data from the literature for similar aerosol populations. The overall solubility of iron in seawater from the two populations of the eastern Mediterranean marine aerosol ($n = 23$) was 3.9 ± 7.1 %. However, the solubility of the crustally derived samples and anthropogenic influenced aerosol samples was 0.32 ± 0.40 % and 10.6 ± 8.9 % respectively. This is a crude separation

but has been used by many authors (Chester *et al.* 1996; Guerzoni *et al.* 1999b; Bonnet and Guieu 2004; Mendez *et al.* 2009). The mean of the solubility in seawater for the anthropogenic aerosols was clearly much higher ($\times 33$) than that for the crustal derived aerosols.

Table 5.23. Solubility of iron in seawater from aerosols originated from the Eastern Saharan desert. Med. = Mediterranean Sea.

	this study Levantine Basin	Bonnet and Guieu (2004) Western Med.	Chen <i>et al.</i> (2006) Gulf of Aqaba	Chase <i>et al.</i> (2006)	Milne (2007) Eastern Med.
Crustally derived (n = 15)	$0.32 \pm 0.40 \%$	no change	-	-	0.008 % to 0.03 %
Anthropogenically influenced (n = 8)	$10.6 \pm 8.9 \%$	$\sim 0.8 \%$	-	-	-
Mixed	-	-	0.7 % (0.003 % to 2 %)	2%	-
Contact time	2 - 8 h	24 h	30 min	theoretical	8 days

For this study, dissolutions were carried out on freshly collected aerosol samples in seawater, allowing the determination of the solubility for the two populations. It is apparent that the observed solubilities were higher compared with those presented in the literature. For example Bonnet and Guieu (2004), who used sieved soil as a proxy for Saharan dust, reported a change in concentration of iron released in seawater only after 7 days. Milne (2007), who monitored dissolution in seawater of a series of sieved soils and atmospherically processed, mesh collected Saharan dust, obtained seawater solubilities ranging between 0.008 % to 0.03 % (after an 8 day equilibration time). The sieved soils used in the two studies are likely to be less representative of Saharan dust than the collected filter samples. This is due to (i) a larger particle size spectrum and (ii) lack of any “atmospheric processing” (for sieved soils) i.e. potential surface evaporation and condensation reactions taking place during transport, which might modify the iron solid phase association at the particle surface, leading to an enhanced solubility (Spokes and Jickells 1996). In contrast, however, the current values were slightly higher than, but comparable, with solubilities in seawater observed from aerosols collected from the Gulf of Aqaba (Chase *et al.* 2006; Chen *et al.* 2006), even though their approach was different;

(polycarbonate filters, low volume collection and 30 min contact time with seawater). Chase *et al.* (2006) suggested after aerosol collection around the Gulf that the average solubility was 2 %. This is in agreement with Chen *et al.* (2006) who observed up to 2 % solubility. The Gulf of Aqaba marine aerosol would be expected to have a slightly lower seawater solubility than the Eastern Mediterranean marine aerosol owing to the relatively greater crustal character of the aerosol as well as lower anthropogenic influences.

A large variation in the current dataset was apparent within the two population types which is not unexpected as no one aerosol population is either completely “crustal” (or Saharan) or “anthropogenic” in nature, but is a mixture of varying proportions of these two “end-member” populations. The observed difference between the populations is supported by observations in the literature (Bonnet and Guieu 2004; Baker *et al.* 2006b; Sedwick *et al.* 2007; Mendez *et al.* 2009). The difference in solubility between the two populations is, in part, a result of the differences in the “potential” soluble pool of iron present on the aerosol particles (as the seawater and dissolution experimental conditions were kept constant).

Crustally derived and anthropogenically influenced aerosol populations have contrasting solid state phases associated with iron (Chester *et al.* 1989). Anthropogenically influenced aerosols have a higher iron content present in the “exchangeable” and “oxide / carbonate” phases compared with the crustally derived aerosol particles (Chester *et al.* 1989; Koçak *et al.* 2007). This difference has been illustrated by Baker *et al.* (2006c) who used a sequential leaching scheme to determine the “exchangeable” and total concentration of iron in aerosols collected over the Atlantic Ocean. They observed 1.7 % solubility (1.4 to 4.1 %) for samples originated from the Western Sahara and 7.8 % solubility (4.0 to 19 %) for samples collected from the northern Atlantic Ocean whilst samples originating from Europe had solubilities ranging from 15 to 54 %. This clear trend in increasing solubility with anthropogenically influenced aerosols was investigated by

Koçak *et al.* (2007) who applied the three stage sequential leach scheme from Chester *et al.* (1989), (see section 1.3.1) to aerosols collected over the Levantine Basin in the Eastern Mediterranean. Crustally derived aerosols had lower “exchangeable” (determined using 1 M ammonium acetate) and “oxide/carbonate” (determined using 25 % acetic acid and 1 M hydroxylamine hydrochloride) iron, $0.9 \pm 0.6\%$ and $2.9 \pm 1.6\%$ fractions respectively, compared with anthropogenically influenced aerosols, which were $2.6 \pm 1.1\%$ and $7.2 \pm 3.2\%$ respectively.

Recently Journet *et al.* (2008) showed that the solubility of iron from crustal material is dependent on the dominating mineral type. They mimicked rainwater dissolution of different types of dusts originating from the Western Saharan with contrasting mineral character: iron (hydro-) oxide, clay and feldspar with the iron content being in the order: feldspar < clays < (hydro-) oxides. A decrease in the observed solubility was observed from < 0.010 % for hydro- / iron oxide (e.g. Hematite, Magnetite) to ~ 2 % for clays (e.g. Illite, Montmorillonite) and ~ 4 % for feldspar (with iron present as amorphous free iron impurities, e.g. Oligoclase, Orthoclase). The nature of the dust, therefore, can impact on the maximum release of iron from dusts during dry and wet deposition modes (see Chapter One).

The collected samples within the two defined aerosol populations represent a spectrum of mixing proportions of the contrasting anthropogenic and crustal sources, rather than being pure aerosol populations. Therefore the iron elemental solid state speciation characteristics of aerosol populations, and possibly the iron solubility in seawater, are dependent upon the relative mixing of the two major sources or end-members. Therefore, to investigate the range of aerosol mixtures for samples which underwent dissolutions in seawater, the iron solubility was plotted against their percentage crustal contributions. The percentage of the crustal contribution of iron for each aerosol sample was determined from the following equation:

$$\% \text{ crustal contribution} = \left\{ \left[C_{Al_{aero}} \times \left(\frac{C_{Fe}}{C_{Al}} \right)_{crust} \right] / C_{Fe_{aero}} \right\} \times 100 \quad \text{Equation 5.3}$$

where ($C_{Fe_{aero}}$ and $C_{Al_{aero}}$) are the concentrations of iron and aluminium in the individual aerosol samples, and $(C_{Fe}/C_{Al})_{crust}$ is the ratio of their concentrations in crustal material, taken from Andreae *et al.* (2002), (see section 5.2 and Appendix B).

Figure 5.12 highlights the relationship between the crustal contribution to the iron aerosol concentration and the soluble fraction for each selected sample. The majority of the samples were crustally derived, with a high percentage contribution to the aerosol iron (> 85 %), whilst some samples were anthropogenically influenced, exhibiting a comparatively lower iron aerosol crustal percentage contribution (down to 40%). A limitation, however, of this approach is that one Fe / Al ratio is used in equation 5.3. Hence for some samples ($n = 6$) a crustal contribution of > 100 % was calculated, indicating variability in the aerosol Fe / Al precursor crustal material.

Despite the limited number of samples ($n = 23$), and the assumption made in the percentage crustal contribution calculation, a statistically significant linear ($r = -0.889$; $p < 0.01$) response was detected (Figure 5.12a). This would suggest for the Eastern Mediterranean marine aerosol that the short term solubility in seawater (< 2 h) of the aerosol population is strongly influenced by the relative proportions of mixing between the contrasting end-member aerosol populations (although this relationship decreased in statistical significance for solubility data derived over 4 h and 8 h contact time, see *next section*). Figure 5.12b additionally highlights the solid state speciation of aerosol Fe derived from the studies of Koçak *et al.* (2007) for the same region (samples collected from Erdemli). Their raw data were superimposed over the solubility in seawater data from this study. A surprising fact was that the percentage “exchangeable” fraction (1 M ammonium acetate, pH = 7, leach, see section 1.3.1. for more details) produced consistently lower values than the solubilities in seawater, whereas the stage 2 fraction (oxide / carbonate solid phases) were in the same range as the solubility.

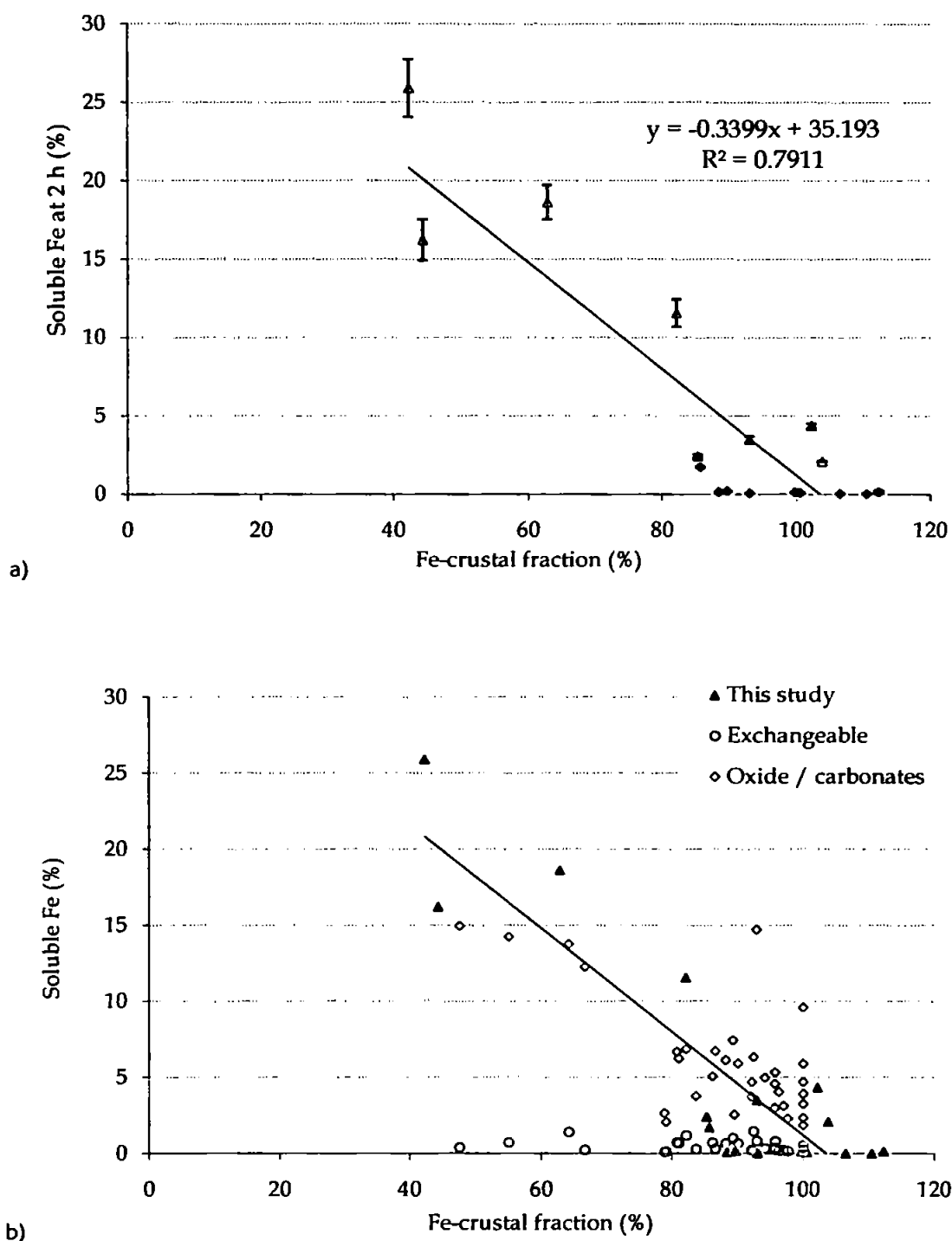


Figure 5.12. Percentage of the iron soluble fraction against the crustal fraction contribution of iron in aerosols. a) Soluble iron fraction versus the iron crustal contribution to the aerosol population after a 2 h contact time. Open triangle = anthropogenically influenced aerosol, diamond = crustally derived aerosol. b) superimposed exchangeable (circle) and oxide / carbonate phases (diamond) for the Eastern Mediterranean marine aerosol, after Koçak *et al.* (2007).

Previous studies, e.g. Chester *et al.* (1993; 1994), have suggested that the “exchangeable” fraction using this approach represents the upper limit of the soluble fraction in seawater for some trace metals. This is not the case for the current study. The

aerosol samples for the current study underwent dissolution studies after being stored frozen. However, Buck *et al.* (2006) suggested that storage of aerosol samples at room temperature will lead to a decrease in the apparent solubility in seawater. The aerosol samples in the study by Koçak *et al.* (2007) were not stored frozen which may explain the comparatively lower exchangeable fraction. It is possible that during storage at room temperature there may have been a phase change of the iron from the “exchangeable” to the less soluble “oxide / carbonate” phase. This is suggested owing to the similar values for the “oxide / carbonate” phase percentages and the solubilities in seawater determined in this work. To test this hypothesis a three stage leach and a seawater dissolution study should be carried out on the same aerosol samples.

Figure 5.13 a-c summarises the temporal variation of the aerosol concentration of iron at the three sampling sites during October 2007 and the corresponding solubility in seawater is quoted for each selected sample along with the sample back trajectory. These data further support the important influence of air mass source, and hence aerosol source, on the solubility in seawater of iron. The highest values were detected at Heraklion on the 17th October, amounting to 25.9 % with corresponding 3-day air mass back trajectories all indicating central European sources (at all altitudes). The lowest solubility was detected in the sample collected for Erdemli on the 22nd October, having a solubility of 0.06%. The sample was collected at the peak of a dust event lasting several days 19th – 24th October, (section 5.3.4), with the iron aerosol concentration being in excess of 4,500 ng m⁻³ and the 3-day air mass back trajectories indicating sources from the Western Central to the Mid Northern Saharan desert. All of the other samples exhibited values between these two extremes and they generally are consistent with the contrasting sources and mixture of sources depicted by each of the accompanying 3-day air mass back trajectories, showing low iron solubility for crustally derived samples and higher solubility for anthropogenically influenced samples.

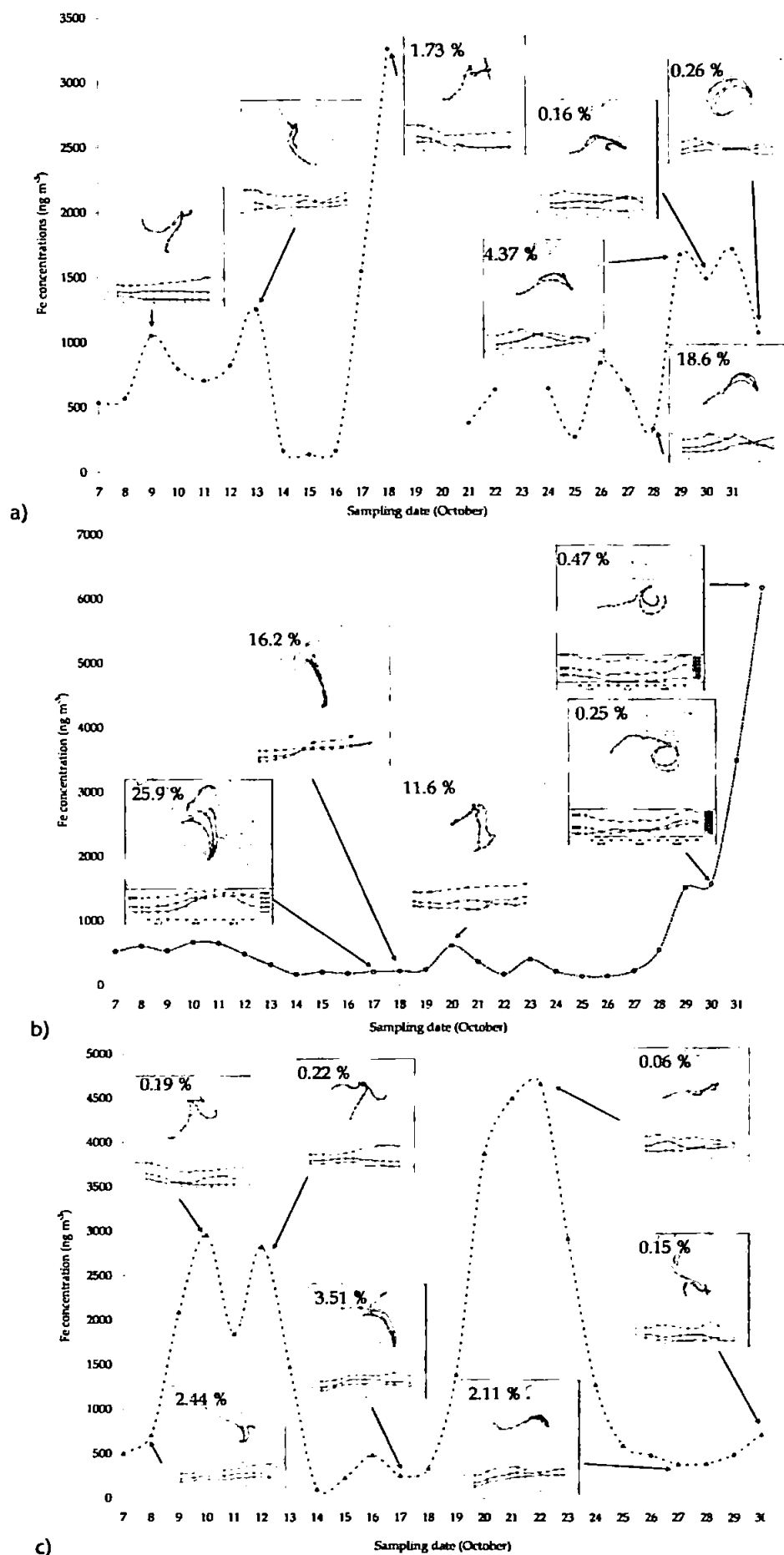


Figure 5.13. Temporal variation of iron concentrations (ng m⁻³) for the three sites along with maximum solubility (taken at variable contact time), a) Tel-Shikmona, b) Heraklion and c) Erdemli.

Kinetic profiles for the dissolution of iron

Crustally derived samples selected to undergo dissolutions, from Heraklion ($n = 2$), Tel-Shikmona ($n = 3$) and Erdemli ($n = 4$), were based on the elemental concentrations and back trajectory analysis (see section 5.3.4). The changes in solubility are presented in Table 5.24 and are plotted in Figure 5.14. The overall maximum solubility was 0.32 ± 0.40 % for the three sites, being reached at different times. Different kinetic trends were observed: (i) the maximum solubility release was reached within 2 h followed by a decrease (Erdemli 10/10, 22/10 and Tel-Shikmona 18/10), (ii) maximum solubility was reached at 4 h and was followed by a decrease (Tel-Shikmona 1/11), (iii) the solubility increased and did not seem to have attained its maximum solubility after 8 h (Heraklion 1/11, Erdemli 12/10), (iv) the solubility exhibited no change with time (Erdemli 30/10, Tel-Shikmona 30/10, Heraklion 30/10, see *earlier section*). These variations illustrate the differences of aerosol sources and so their chemical compositions and atmospheric ageing processes.

Table 5.24. Percentage solubility in crustally derived aerosols from Erdemli (ER, $n = 4$), Heraklion (HE, $n = 2$) and Tel-Shikmona (TS, $n = 3$). Error bars = ± 1 s.d.

Sites	Sampling date	Solubility at collection time (%)		
		2 h	4 h	8 h
Erdemli	10-Oct-07	0.12 ± 0.02	0.01 ± 0.00	0.22 ± 0.02
	12-Oct-07	0.19 ± 0.02	0.02 ± 0.02	adsorption
	22-Oct-07	0.06 ± 0.01	adsorption	adsorption
	30-Oct-07	0.13 ± 0.02	0.15 ± 0.00	0.14 ± 0.04
Heraklion	30-Oct-07	0.16 ± 0.01	0.22 ± 0.05	0.25 ± 0.06
	01-Nov-07	0.15 ± 0.10	0.25 ± 0.04	0.47 ± 0.13
	18-Oct-07	1.73 ± 0.05	0.56 ± 0.04	0.29 ± 0.05
Tel-Shikmona	30-Oct-07	0.06 ± 0.05	0.15 ± 0.11	0.16 ± 0.12
	01-Nov-07	0.03 ± 0.02	0.26 ± 0.03	0.09 ± 0.02

In order to test statistically if sub-samples (i.e. samples collected at 2, 4 and 8 h) for each selected aerosol sample were different, ANOVA tests were carried out using Statgraphics plus 5.1. The three sub-samples for all aerosol samples were significantly different at the 99.0 % confidence level, $P < 0.0036$ (except for the triplicate dissolutions of the crustal sample collected on the 30th October for the three sites, where no statistical difference was detected).

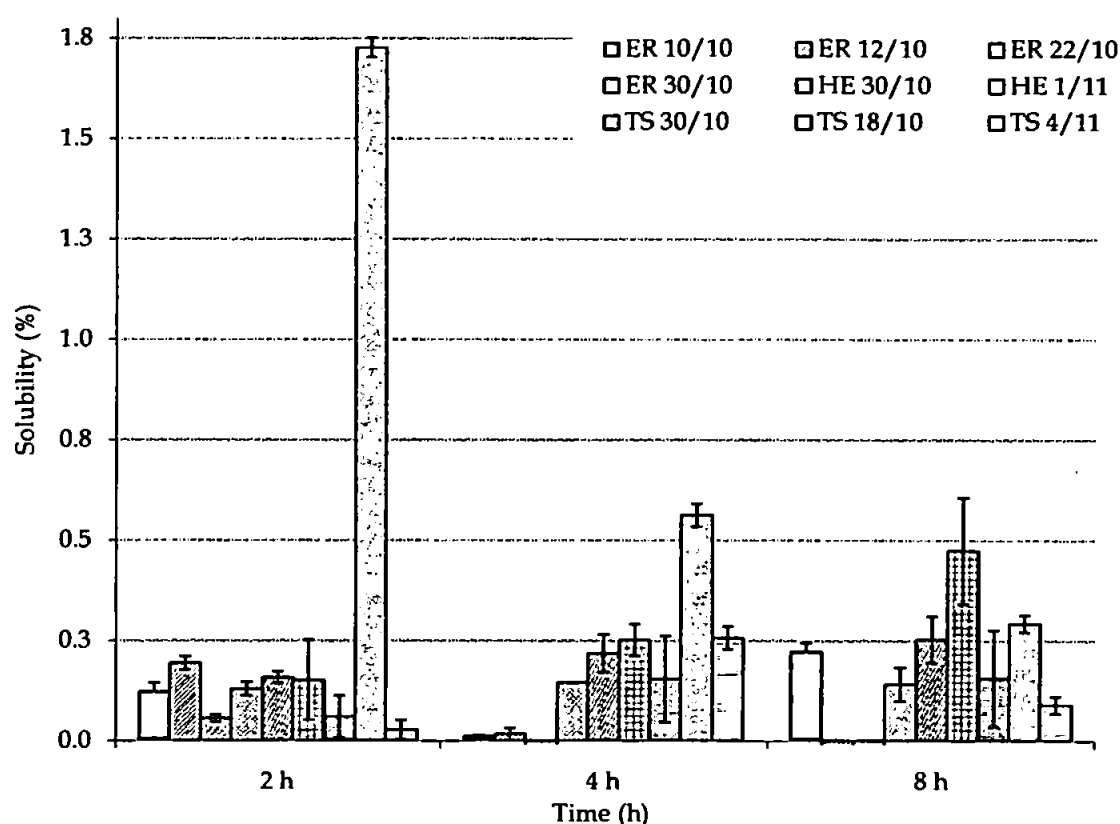


Figure 5.14. Percentage solubility of iron release during dissolutions of crustally derived samples from the three sites ($n = 9$). ER = Erdemli. HE = Heraklion. TS = Tel-Shikmona. Error bars = ± 1 s.d.

Anthropogenically influenced samples which underwent dissolutions were chosen based on the elemental concentrations and back trajectory analysis, and the EF_{sd} analysis for samples from Erdemli (Heraklion and Tel-Shikmona, $n = 3$ and Erdemli, $n = 2$, see section 5.3.4). The solubilities for the selected samples are presented in Table 5.25 and are plotted in Figure 5.15. All samples, in contrast to the crustal dominated samples, exhibited a consistent kinetic trend with the maximum solubility being attained within 2 h of contact with seawater followed by sharp decrease, as previously observed for the anthropogenic end member used in Chapter Four.

ANOVA tests were carried out on each of the three sub-samples for the selected aerosol samples using Statgraphics plus 5.1 as before. The three sub-samples for all aerosol samples were again significantly different at the 99.0 % confidence level.

Table 5.25. Percentage solubility in anthropogenically influenced aerosol samples from Erdemli (ER, $n = 3$), Heraklion (HE, $n = 3$) and Tel-Shikmona (TS, $n = 2$). Error bars = ± 1 s.d.

Sites	Sampling date	Solubility at collection time (%)		
		2 h	4 h	8 h
Erdemli	8-Oct-07	2.44 ± 0.11	0.57 ± 0.06	0.24 ± 0.10
	17-Oct-07	3.51 ± 0.19	1.02 ± 0.14	0.36 ± 0.21
	27-Oct-07	2.11 ± 0.04	1.30 ± 0.15	0.45 ± 0.10
Heraklion	17-Oct-07	25.91 ± 1.85	10.38 ± 0.72	9.90 ± 0.44
	18-Oct-07	16.2 ± 1.32	6.37 ± 0.54	2.47 ± 0.20
	20-Oct-07	11.6 ± 0.88	4.08 ± 0.82	3.63 ± 0.34
Tel-Shikmona	28-Oct-07	18.6 ± 1.10	4.31 ± 0.97	3.56 ± 0.30
	29-Oct-07	4.37 ± 0.15	1.91 ± 0.20	0.28 ± 0.05

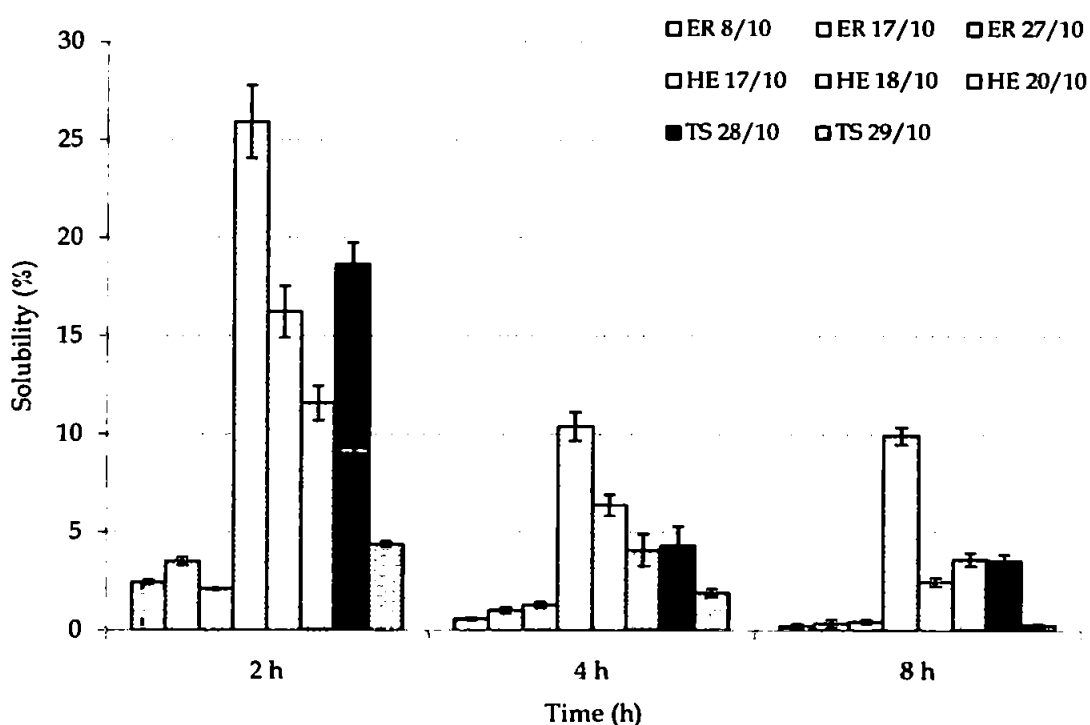


Figure 5.15. Percentage solubility of iron release during dissolutions of anthropogenically influenced samples from the three sites ($n = 8$). ER = Erdemli, HE = Heraklion, TS = Tel-Shikmona. Error bars = ± 1 s.d.

This kinetic approach adopted for the filter samples applied a lower temporal resolution of sub-sampling compared with the studies carried out in *Chapter Four*, and focused more on the short term kinetics of iron release from the aerosols. This is appropriate for the aerosol samples more strongly influenced by anthropogenic sources, because the maximum solubility for all such samples was reached < 2 h. The decrease in solubility after 2 h is likely to be as a result of re-adsorption onto the aerosol particles on the Whatman 41 filter paper (but not on the filter material as no adsorption was apparent

whilst equilibrating the blank filter in seawater) or attainment of the dissolved equilibration speciation in the seawater, i.e. conversion to the iron hydroxide species/organic complexes. The short-term release of iron also confirmed that a short equilibration time as applied in other studies is the best approach for defining the maximum solubility for anthropogenically derived aerosols (Chen *et al.* 2006, 30 min; Buck *et al.* 2006, instantaneous; Chester *et al.* 1993, 1 h). However, it was not always the case that fast release was observed for crustally dominated filter samples and a longer equilibration time might be required. Longer term kinetics of iron release from Saharan dust has been reported in the literature. For example, Bonnet and Guieu (2004) carried out seawater dissolution studies over 24 h and 7 days of contact, whilst Milne (2007) exposed Saharan dust and sieved soils for 24 h and 8 days, with a greater iron release being observed after 8 days. More recently Mendez *et al.* (2009) showed both fast release of iron (within the temporal resolution of their sampling approach) but also an additional second release after > 14 days.

5.4.6. Dry atmospheric fluxes of seawater soluble iron over the Levantine Basin

The importance of atmospheric inputs to the open ocean and coastal marine systems such as the Mediterranean Sea has been highlighted in *sections 1.1.1* and *5.2*. Many studies over the last decade have attempted to define the atmospheric deposition of trace metals (Koçak *et al.* 2005 and references therein). The aim of this section is to highlight how the soluble iron in seawater data generated from *section 5.3.5*. can be used to calculate, as a first approximation, the corresponding dry inputs of soluble iron to the Levantine Basin of the Eastern Mediterranean Sea.

Reliable dry deposition flux estimates require representative metal aerosol concentrations (owing to their variability) over an extended sampling period (over at least an annual sampling period, but preferably over several years) and appropriate elemental settling velocities. For the current calculations, Heraklion was excluded owing to a less

extensively documented database (and hence less representative) of iron aerosol concentrations. Dry deposition fluxes (F) are calculated using:

$$F = C_{\text{aerosol}} \times V_d \quad \text{Equation 5.4}$$

where C_{aerosol} is the geometric mean aerosol concentration of Fe and V_d is the elemental settling velocity for these aerosols. In the past, a range of settling velocities have been applied to dry deposition flux calculations and were determined by mass-size distributions in the aerosol population, usually evaluated from cascade impactor data (Ottley and Harrison 1993; Spokes *et al.* 2001), mathematical modelling (Slinn and Slinn 1980) or deployment of surrogate collectors (Hall *et al.* 1994; Chester *et al.* 1999). All the methods adopted have their limitations. However, Koçak *et al.* (2005) using the approach adopted by Spokes *et al.* (2001), after Ottley and Harrison (1993), assumed, for the Eastern Mediterranean marine aerosol, that the V_d for fine particles ($< 2 \mu\text{m}$) was 0.1 cm s^{-1} and for coarse particles ($2 - 10 \mu\text{m}$) the V_d was 2 cm s^{-1} (depositing to regions less than 1000 km from land, Duce *et al.* 1991). The elemental V_d 's used for the current calculations were based on those quoted by Koçak *et al.* (2005) who separated the two size fractions using a Gent PM_{10} stacked filter unit, giving proportions of iron present for each fraction. Weighted means of V_d for iron were then calculated for samples collected at Erdemli during 2001, originating from the southern ($n = 73$) and northern ($n = 154$) air mass sectors (Figure 5.7) using the V_d used by Duce *et al.* (1991) and the iron fine / coarse particle proportions. The calculated size fraction weighted means V_d 's were $1.76 \pm 0.16 \text{ cm s}^{-1}$ for aerosol derived from the south and $1.69 \pm 0.17 \text{ cm s}^{-1}$ for those from the north.

The sample collection for this study was performed only over a month during the transitional period and the mean concentrations will not represent the annual average aerosol Fe concentrations (see section 5.3.1). Therefore, the geometric means of iron aerosol concentrations representative of the southern and northern air mass sectors at both

Erdemli and Tel-Shikmona were taken from Koçak *et al.* (2005), (being representative of several years of sampling).

The atmospheric dry depositional flux of soluble iron in seawater for each site was calculated using a modified version of equation 5.4 (Koçak *et al.* 2005), equation 5.5. Dry deposition fluxes are obtained by multiplying the concentration of the element focusing on and its velocity (Equation 5.4). Then the proportional air mass influence over annual period based on long term air mass back trajectories at both sampling sites were taking in account along with the solubility of crustally derived and anthropogenically influenced samples (see section 5.3.5) to define the flux of soluble iron depending of the two different origins. The dry atmospheric flux at each site was then calculated using:

$$([Fe]_N \times V_d \times R_N \times S_{anthrop}) + ([Fe]_S \times V_d \times R_S \times S_{crust}) \quad \text{Equation 5.5}$$

where $[Fe]_N$ and $[Fe]_S$ are the geometric means of Fe aerosol concentrations for the northern and southern air mass sectors, V_d is the mean of the elemental settling velocities calculated by Koçak *et al.* (2005). R_N and R_S are the ratio of the temporal influence for the northern and southern airflow sectors (Koçak *et al.* 2005) (again calculated for the daily back trajectories over several years for both sites). $S_{anthrop}$ and S_{crust} are the mean soluble fractions of iron in seawater associated with crustally dominated and anthropogenically influenced aerosol samples collected in October 2007. It is assumed that the flux calculated for Tel-Shikmona represents the flux over the Southern Levantine Basin (SLB) and the flux calculated at Erdemli represents the flux over the Northern Levantine Basin (NLB). Hence the calculated dry seawater soluble iron depositional fluxes are reported for the two Levantine Basins in Table 5.26 along with estimates of exchangeable iron dry fluxes from Koçak *et al.* (2005).

Table 5.26. Comparison of iron dry deposition fluxes expressed as $\text{mg m}^{-2} \text{ y}^{-1}$ in the Levantine Basin. ¹ soluble iron fraction, ² exchangeable iron fraction.

this study ¹		Koçak <i>et al.</i> (2005) ²	
Erdemli	Tel-Shikmona	Erdemli	Tel-Shikmona
7.24 ± 8.20	6.11 ± 7.00	0.54 - 2.25	1.03 - 4.13

Having calculated the depositional fluxes it is then possible to calculate the atmospheric inputs across (Table 5.27) the Southern and Northern Basins as well as the total Levantine Basins assuming the surface areas are 436,000 and 111,000 km² respectively (Ludwing and Maybeck 2003).

Table 5.27. Iron atmospheric dry inputs (t y⁻¹) to the Northern and Southern Levantine Basin. ¹this study. ²Koçak *et al.* (2005). Error bars represent ± 1 s.d (n = 7).

Area	Total Fe dry inputs	This study ¹ Seawater soluble fraction	Koçak <i>et al.</i> (2005) ² Exchangeable fraction	Total Levantine Basin soluble
NLB	25,300	804 \pm 910	60 - 250	3,470 \pm 4,150 ¹
SLB	181,400	2,670 \pm 3,050	450 - 1,800	510 - 2,050 ²

The soluble iron for the two areas of the Basin in this study ranged from 804 \pm 910 t y⁻¹ for NLB to 2,670 \pm 3,050 t y⁻¹ for SLB. Koçak *et al.* (2005) reported ranges of inputs from 60 to 250 t y⁻¹ for the Northern Basin and from 450 to 1,800 t y⁻¹ for the Southern Basin. However, the values quoted by Koçak *et al.* (2005) represent an “exchangeable” fraction, not a soluble fraction in seawater. This was determined by a chemical leach using a 1 M ammonium acetate solution, and so is not directly comparable to a seawater leach (see section 1.3.1). A clear trend was observed; the Northern Basin, with higher solubilities, had lower inputs of soluble iron compared with the Southern Basin (which was more influenced by southern air masses). Around 70 % of the air masses arriving to Erdemli originated from Europe whilst ~ 70 % of the air masses arriving at Tel-Shikmona originated from the surrounding deserts (Koçak *et al.* 2005). However, two factors would have enhanced the comparative importance of soluble iron inputs to seawater in the SLB, (i) comparatively higher loadings of iron in the aerosol (air mass weighted mean for the NBL = 581 ng m⁻³ and for SLB = 909 ng m⁻³), (ii) a larger defined surface area of the SLB compared with the NLB. Table 5.27 also highlights higher estimates of the dry soluble inputs to the Levantine Basin compared with those quoted by Koçak *et al.* (2005). This difference may result from several factors. For example, the samples collected for this study were kept frozen until digestion / dissolution. A previous study (Buck *et al.* 2006)

reported that the iron solubility of filter collected aerosol may decrease with time if stored at room temperature. By freezing the samples, the iron solid state speciation is more likely to be preserved compared with the samples collected by Koçak *et al.* (2005), which were stored at ambient temperature, prior to being treated by 1 M ammonium acetate leach, (being defined as the exchangeable fraction). It is conceivable that if there were changes in a portion of the exchangeable phase during aerosol storage at room temperature, such as conversion into iron oxide phases then, as shown by Buck *et al.* (2006), the solubility of this solid fraction may be lower, which would lead to a potential decrease in the apparent solubility of iron from the aerosol samples. However, there are no other input values available to enable a comparison with the current calculations which emphasises the novelty of the dataset. However, it is accepted that this dataset is limited and hence there is a need to carry out more studies to enhance our knowledge and better refine our input calculations.

5.4.7. Residence time of seawater soluble iron in the Cretan Sea

From the dry deposition fluxes, previously calculated, over the Levantine Basin it was possible to estimate the residence time of dFe in the mixed layer of the Cretan Sea. This was only possible by assuming that the main source of this iron is by atmospheric inputs and that the system is at steady state, with removal largely occurring through biological uptake and vertical particle transport to deeper water (Statham and Hart 2005). Inventories of dFe in mixed layer were calculated from Statham and Hart (2005), based on the dFe flux values of Guieu *et al.* (1997, 90 - 180 mol Fe km⁻² yr⁻¹). Inventories ranged from 117 - 126 mol km⁻² in September 1997 to 180 mol km⁻² in March 1997. Residence time for the two contrasting seasons were calculated by dividing the inventory of dFe in the different mixed layers by the mean atmospheric flux of soluble iron from both Erdemli (130 mol Fe km⁻² yr⁻¹) and Tel-Shikmona (109 mol Fe km⁻² yr⁻¹). The results are presented in Table 5.28. The residence times of dFe ranged from 0.90 - 1.15 y in September to 1.39 - 1.65 y in March.

Table 5.28. Residence time of soluble dFe over the Cretan Sea with respect to atmospheric inputs calculated from this study and from Statham and Hart (2005). Inventories of dFe for the mixed layers at different time of the year were taken from Guieu *et al.* (1997), calculated from Statham and Hart (2005).

	This study		Statham and Hart (2005)	
	September	March	September	March
Inventory of dFe in mixed layer (mol km ⁻²)	117 - 126	180	117 - 126	180
Residence time (yr)	0.90 - 1.15	1.39 - 1.65	0.7 - 1.3	1.0 - 2.0

These residence times were in accordance with estimates from Statham and Hart (2005). However residence times in this study were only based on dry deposition fluxes from the Levantine Basin (*see section 5.4.6*) and would over-estimate residence times over the Cretan Sea whilst calculated with wet deposition fluxes, the residence times would be lowered. Estimation of the inventory of dFe in mixed layer in the Levantine Basin is required to calculate its residence times in the Eastern Mediterranean.

5.5. CONCLUSIONS

Mixed aerosol samples from the Eastern Mediterranean were collected in October 2007 at three sites surrounding the Levantine Basin, Heraklion, Erdemli and Tel-Shikmona. These sites were chosen to investigate the seawater solubility of iron from freshly collected aerosols, along with the spatial and temporal variations in the major elemental concentrations, in order to chemically characterise the marine aerosol during collection. The combination of elemental concentrations with back trajectories is a useful tool to examine the influences of crustal and anthropogenic sources on the marine aerosol. Sample collection during October 2007 (a transitional period, characterised by frequent and intense dust events) enabled:

- (i) Observation of a gradient in crustal elemental aerosol concentrations from Erdemli > Tel-Shikmona > Heraklion which contradicted, in part, the literature due to the decreasing gradient from Erdemli to Tel-Shikmona. Hence the importance of aerosol sampling over long periods (> one year) was highlighted in order to obtain representative aerosol concentrations.

(ii) Identification of dust events occurring over the three sites, including common dust events, and anthropogenically influenced samples from which a sub-set of samples for subsequent iron seawater dissolution studies was selected.

(iii) Determination of the solubility of iron in seawater of two contrasting populations of marine aerosols. The crustally derived aerosol samples were characterised by a variable kinetic profile in the release of iron from the particles with an observed maximum solubility of 0.39 ± 0.52 %. The anthropogenically influenced aerosol samples exhibited consistent kinetic profiles (fast release < 2 h; followed by adsorption) with a maximum detected solubility of 10.6 ± 8.9 %.

(iv) An approximation of the atmospheric dry inputs of soluble iron in seawater to the Levantine Basin for the first time, ranging from 804 ± 910 t y⁻¹ for NLB to $2,670 \pm 3,050$ t y⁻¹ for SLB.

(v) An estimation of the residence time of soluble iron in the Cretan Sea, ranging from 0.90 – 1.15 y in September 1997 to 1.39 – 1.65 y in March 1997.

This work has also highlighted the practicality of processing a relatively small portion (4 cm²) of a high volume collected aerosol sample using Whatman 41 filters for the evaluation of the solubility of aerosol iron in seawater. The method had low blanks (typically < analytical detection limits) and minimal adsorption onto the filter material. Kinetic studies were carried out for the first time, on each selected sample. From the results it is recommended that in the future, different approaches should be adopted regarding the contact time of the aerosol sample with seawater, depending on the predominant source of the aerosol material. Seawater dissolutions involving crustally dominated aerosol populations should be carried out for at least 8 h and preferably longer; whilst dissolution studies involving anthropogenically influenced samples can be carried using an equilibration time ≤ 2 h. A more detailed temporal resolution (see *Chapter Four*) would identify the time needed to obtain the maximum release of iron from these aerosol samples. The repeatability of dissolutions showed that aerosol samples were

relatively homogeneous on the filter paper and that separate portion of the same filter could be used to compare dissolutions in seawater under specific conditions, as dark / light, absence / presence of ligands to investigate the impact of these conditions. Finally, more dissolution studies of mixed aerosol samples, which are representative of the marine aerosol, compared with end-member aerosols, should be carried out for a better understanding of the dissolution processes, post-deposition, occurring in the Eastern Mediterranean.

CONCLUSIONS AND FUTURE WORK

6.1 CONCLUSIONS

Laboratory based studies were carried out using a novel approach to investigate and understand the processes occurring during the dissolution of aerosol iron in seawater. Work carried out to achieve the aims of the study, previously highlighted in *Chapter One*, enabled the following conclusions to be drawn:

- (i) A sensitive FI-CL technique can be used to determine picomolar concentrations of iron in seawater in a laboratory environment.
- (ii) DOC and dFe concentrations can be lowered by utilisation of a UV photo-oxidation system, in particular with columns for the removal of iron.
- (iii) An autosampler can be interfaced with a dissolution system for the contamination free collection of sub-samples from the incubation vessel to investigate the effect of chemical and physical factors on the kinetic dissolution of iron from particles in seawater.
- (iv) The incubation vessel can be adapted for dissolution experiments of high volume collected aerosol filter samples from crustal and anthropogenic sources.

6.1.1. Automation of a FI-CL detection system

To analyse samples collected during dissolution experiments, an ultra-sensitive FI-CL detection system was developed, automated and optimised. The limit of detection of the manual system was 0.2 nM, an order of magnitude higher than the one reported by Bowie *et al.* (1998), with relatively poor precision (from 2.9 to 12 %). Following the automation of the system and its optimisation, e.g. cleaning of the reagents, utilisation of LDPE bottles, increased the sensitivity which reduced the limit of detection to 0.04 ± 0.03 nM ($n = 26$) with an improved precision ranging from 0.18 to 10.8 % ($n = 156$). Good agreement with a certified reference material (NASS-4) and an in-house reference material validated the accuracy of the optimised FI-CL system. Furthermore, useful protocols, maintenance and troubleshooting sections were documented for effective utilisation of the FI-CL technique.

6.1.2. Seawater treatment system

A photo-oxidation system was assembled to produce seawater with low DOC and dFe concentrations and its efficiency was assessed using HTCO, FI-CL and CLE-ASCV. Once optimised, the breakdown of organic compounds was ~ 50 % for two different ocean seawaters (Atlantic Ocean and Canary Basin) and up to 95 % for a 100 μM DOC standard in UHP de-ionised water. The apparent removal of dFe was ~ 90 % for the two seawaters, treated with the UV lamp only. The breakdown of the complexing ligands in the Canary Basin seawater represented 60 % of the total ligand concentration whilst this breakdown was more variable in the Atlantic Ocean. These efficiencies did not achieve the required breakdown for DOC, dFe and complexing ligands. The relatively poor DOC breakdown was probably due to a combination of: nature of seawater, saturation of the Sep-Pak C18 columns, incomplete oxidation by UV irradiation and bacterial leaching from the filter and the resins. The low breakdown of the complexing ligands might be due to the utilisation of FEP tubing instead of quartz coil, lowering the light transmitted through the coil and samples. The removal of dFe from seawater was suspected to be due adsorption of iron onto the walls of the FEP coil tubing or interferences in the signal of the FI-CL manifold by generation of hydrogen peroxide and radicals.

6.1.3. Effect of chemical and physical parameters on dust dissolution kinetics

An automatic sampler composed of a 10-way distribution valve and peristaltic pump was designed and integrated with an aerosol incubation vessel, for the extraction of sub-samples during dissolution experiments of aerosol iron in seawater. Analyses were carried out using flow injection with chemiluminescence detection for the determination of iron in seawater (at pM / nM concentrations). The incubation vessel coupled with the autosampler had a low risk of contamination, no adsorption onto the walls and low contribution of iron from the autosampler lines and filter. Moreover, the autosampler was applied to study the effect of chemical and physical parameters on the extent and kinetics of the dissolution of aerosol iron in seawater under carefully controlled experimental

conditions. Experiments were carried out using the end-member NIST 1648, under dark and light conditions, with and without addition of a model siderophore, Desferrioxamine B (DFOB), at 25 ± 0.2 °C. A consistent kinetic dissolution profile using the NIST 1648 end-member was observed at different dust concentrations. The solubility of iron released from the aerosol particles in seawater increased over the first 120 min followed by a decrease, and a net adsorption of the dFe onto the particles after 720 min. The natural complexing ligand DFOB enhanced the solubility of iron and stabilised dFe in solution. A faster dissolution rate was observed at high dust loading compared with a low dust loading, but no apparent “dust concentration effect” was observed. Under dark conditions, 0.36 ± 0.12 % of iron was released from 0.5 mg L^{-1} NIST 1648 after 90 min followed by re-adsorption. The addition of 20 nM DFOB enhanced the solubility of iron up to 200 min followed by relatively constant solubilities ($0.76 \pm 0.11\%$), and hence stabilisation of iron in solution, illustrating the important impact of complexing ligands. Higher concentrations of DFOB induced a higher release of iron and also maintained dFe in solution. Lower release of iron was observed in dark conditions compared with light conditions, 0.36 ± 0.12 % and 0.50 % respectively. Under light conditions, the “Fe-DFOB” complex underwent adsorption, possibly as a result of photochemically induced structural changes. The effect of these key parameters dissolution of the NIST 1648 end-member provide a template for investigating iron dissolution from mixed aerosol populations.

6.1.4. Iron solubility in seawater from Eastern Mediterranean marine aerosols

Mixed aerosol samples were collected at three sites in the Eastern Mediterranean, and characterised for metals by total digestions. Elemental concentrations and back trajectory analysis identified two contrasting aerosol populations. A gradient in the crustal elemental aerosol concentration was observed from Erdemli > Tel-Shikmona > Heraklion, contradicting previous studies. The importance of sampling over a long period of time (> 1 year) was highlighted. Aerosol samples from two populations, crustally derived and

anthropogenically influenced, were selected to undergo dissolution experiments in seawater. Sub-sampling was adapted from the knowledge gained from the dissolution experiments reported in *Chapter Four* involving the urban end-member (NIST 1648), and was carried over a total equilibration time of 8 h rather than 1 day. The study highlighted the contrasting solubilities of aerosol iron in seawater; with iron present in anthropogenically influenced samples being up to 25 % soluble and in crustally (Saharan) derived samples < 0.5 % soluble. This study also showed the importance of studying in parallel NIST 1648 end-member and freshly collected aerosol samples (inevitably having a mixed source character). The release of dFe from the crustally derived aerosol samples was characterised by a variable kinetic profile whilst the anthropogenically influenced aerosol samples exhibited consistent kinetic profiles (fast release < 2 h; followed by adsorption onto the aerosol particle). The observed maximum solubility was 0.39 ± 0.52 % and 10.6 ± 8.9 % for the crustally derived and anthropogenically influenced sample populations respectively. From this information it was possible to estimate the atmospheric dry inputs of soluble iron in seawater to the Levantine Basin which ranged from 804 ± 910 t y⁻¹ for the Northern Basin to $2,670 \pm 3,050$ t y⁻¹ for the Southern Basin and also the residence time of dissolved iron in the Cretan Sea, ranging from 0.90 – 1.15 y in September 1997 to 1.39 – 1.65 y in March 1997. This work has also shown the practicality of using a relatively small portion of a Whatman 41 filter for the evaluation of the solubility of iron in seawater from high volume collected aerosol population.

6.1.5. Summary of factors impacting upon the aerosol seawater solubility of Fe

A summary of the factors impacting upon the solubility of aerosol iron pre- and post-deposition to the sea surface is presented on Figure 6.1. This diagram has been modified from Baker and Croot (2008) to take into account the work carried out during this study (signified with an “*”; sections 6.1.4 and 6.1.5). Figure 6.1 also states whether there are positive / negative impacts and identifies in the community knowledge.

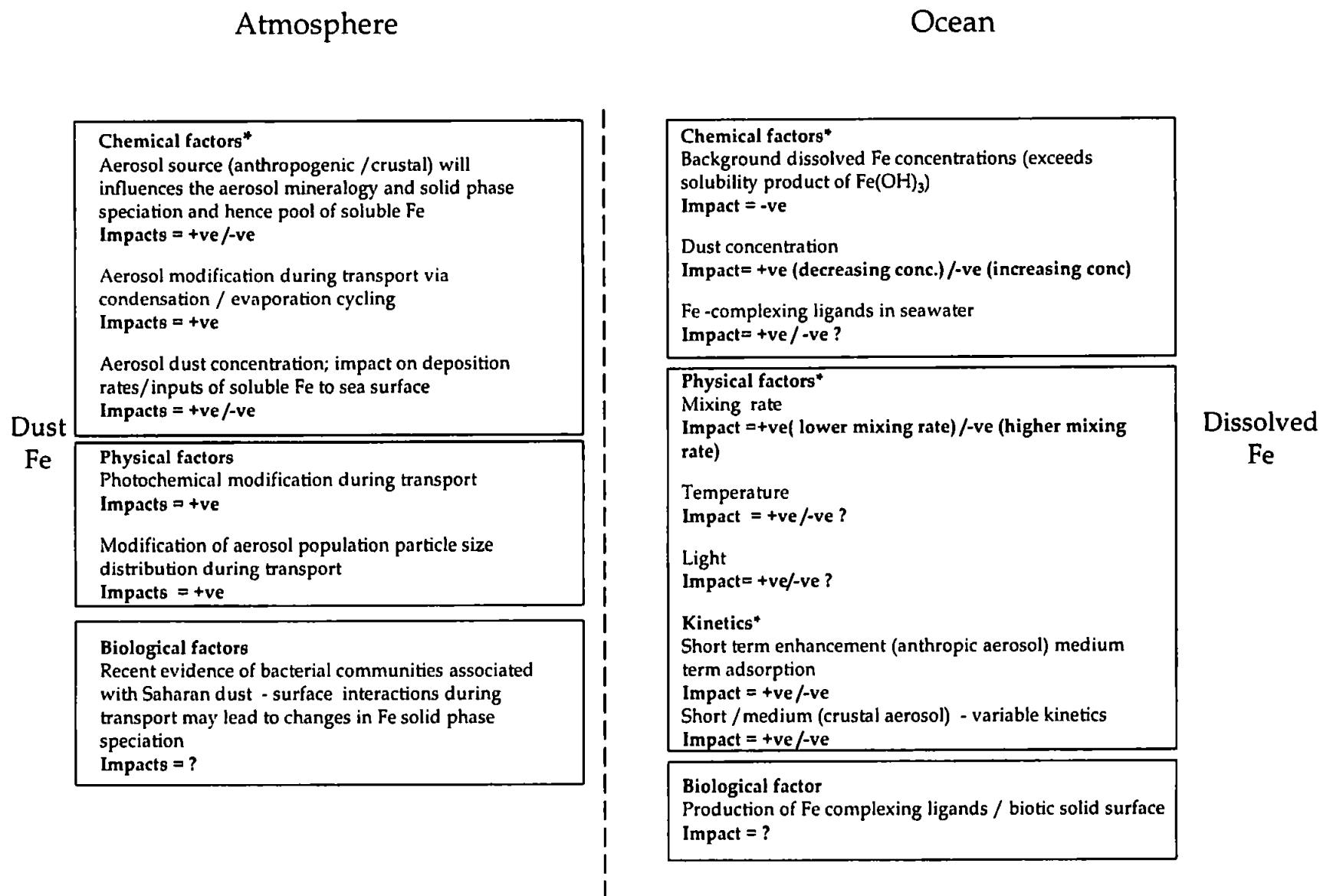


Figure 6.1. Diagram summarising the effects of chemical, physical and biological parameters on the dissolution of aerosol iron in seawater. *: factors investigated in this study.

6.2. FUTURE WORK

During the analytical development, problems associated with the detection of iron using FI-CL were due to clogged frits and degradation of the preconcentration column. Further research should be carried out to use thinner and more flexible material, to enhance the life time of the 8-HQ columns that need, currently, repacking every 6 months.

Further improvements to the seawater treatment system for future investigations, should include the placement of the system under a laminar flow cabinet (except the aluminium housing and UV lamp), extension of the length of the FEP coil and regeneration of the resins after processing every 10 L of treated seawater. Once developed, DOC and dFe concentrations and ligand complexing capacities should be defined, at each stage of the treatment, using the photo-oxidation system.

Further dissolution studies, to investigate both short and long term kinetics (1 day to > 7 days) are recommended at two temperatures 5 °C and 25 °C. Complimentary dissolution experiments should be carried out in dark and light conditions to investigate the effect of light on the dissolution process. The main focus of these studies should be the impact on iron solubility in seawater of biological factors, such as the presence of bacteria or phytoplankton, with an emphasis on the production of natural organic complexing ligands. Moreover, cultures of phytoplankton species characteristic of specific oceanic regions would greatly improve our knowledge on their regional impacts. Complementary analysis with SEM and fluorescence for the phytoplankton and bacterial populations, along with speciation analysis using electro-spray mass-spectrometry would characterise the siderophores and complexing ligands released from these populations. A better understanding of these organic complexing ligands and siderophores are needed as few have been identified (e.g. Mawji *et al.* 2008).

As shown in *Chapter Five*, separate portions of the same high volume collected aerosol filter samples could be used to investigate how the solubility of iron in seawater changes with experimental conditions, including dark / light; absence / presence of model organic ligands, changes in stirring rate, contrasting temperature. It is clear from the kinetic studies of the filter samples collected from the Eastern Mediterranean that the contact time of the samples with the seawater should be chosen with care. It is recommended that dissolution studies involving anthropogenically influenced samples should be carried out over the initial 2 h, with a fine (15 min) temporal resolution, to more accurately constrain the maximum release of iron, giving more details on the short term kinetics of dissolution. It is also recommended that the size of the filter portion for anthropogenically influenced aerosol samples is reduced to 2 or 3 cm² (in 500 mL of seawater). In contrast, for dissolutions involving crustally derived samples, kinetic studies should be carried out over at least 1 day, applying the same temporal resolution as previously used in those studies reported in *Chapter Four*. The size of the filter portion used should be increased to 6 or 8 cm², giving an observed release of iron in the same range for anthropogenically influenced aerosol samples.

REFERENCES

REFERENCES

- ACHTERBERG E.P. and VAN DEN BERG C.M.G. (1994). In-line ultraviolet-digestion of natural water samples for trace metal determination using an automated voltammetric system. *Analytica Chimica Acta* **291**, 213-232.
- ACHTERBERG E.P. and VAN DEN BERG C.M.G. (1997). Chemical speciation of chromium and nickel in the western Mediterranean. *Deep Sea Research Part II: Topical Studies in Oceanography* **44**, 693-720.
- ACHTERBERG E.P., BRAUNGARDT C.B., SANDFORD R.C. and WORSFOLD P.J. (2001a). UV digestion of seawater samples prior to the determination of copper using flow injection with chemiluminescence detection. *Analytica Chimica Acta* **440**, 27-36.
- ACHTERBERG E.P., HOLLAND T.W., BOWIE A.R., MANTOURA R.F.C. and WORSFOLD P.J. (2001b). Determination of iron in seawater. *Analytica Chimica Acta* **442**, 1-14.
- AGUILAR-ISLAS A., WU J., REMBER R., JOHANSEN A.M. and SHANK L.M. (2009). Dissolution of aerosol-derived iron in seawater: Leach solution chemistry, aerosol type, and colloidal iron fraction. *Marine Chemistry In press*.
- ALPERT P., ENEMA U. and SHAY-EL Y. (1990). Inter-monthly variability of cyclone tracks in the Mediterranean. *Journal of Climate* **3**, 1,474-1,478.
- ANDREAE T.W., ANDREAE M.O., ICHOKU C., MAENHAUT W., CAFMEYER J., KARNIELI A. and ORLOVSKY L. (2002). Light scattering by dust and anthropogenic aerosol at a remote site in the Negev desert, Israel. *Journal of Geophysical Research* **107**, 1-18.
- ARIMOTO R., DUCE R.A., RAY B.J. and UNNI C.K. (1985). Atmospheric trace elements at Enewetak Atoll: 2. Transport to the ocean by wet and dry deposition. *Journal of Geophysical Research* **90**, 2,391-2,408.
- ARIMOTO R., DUCE R.A., RAY B.J., HEWITT A.D. and WILLIAMS J. (1987). Trace elements in the atmosphere of American Samoa: Concentrations and depositions to the tropical south Pacific. *Journal of Geophysical Research* **92**, 8,465-8,479.
- ARIMOTO R., RAY B.J., DUCE R.A., HEWITT A.D., BOLDI R. and HUDSON A. (1990). Concentrations, sources, and fluxes of trace elements in the remote marine atmosphere of New Zealand. *Journal of Geophysical Research* **95**, 22,389-22,405.
- ARTAXO P., GERAB F., YAMASOE M.A. and MARTINS J.V. (1994). Fine mode aerosol composition at three long-term atmospheric monitoring sites in the Amazon Basin. *Journal of Geophysical Research* **99**, 22,857-22,868.
- AZOV Y. (1991). Eastern Mediterranean—a marine desert? *Marine Pollution Bulletin* **23**, 225-232.
- BAKER A.R., KELLY S.D., BISWAS K.F., WITT M. and JICKELLS T.D. (2003). Atmospheric deposition of nutrients to the Atlantic Ocean. *Geophysical Research Letters* **30**, 1-4.
- BAKER A.R., FRENCH M. and LINGE K.L. (2006a). Trends in aerosol nutrient solubility along a west-east transect of the Saharan dust plume. *Geophysical Research Letters* **33**, 1-4.
- BAKER A.R., JICKELLS T.D., BISWAS K.F., WESTON K. and FRENCH M. (2006b). Nutrients in atmospheric aerosol particles along the Atlantic Meridional Transect. *Deep Sea Research II* **53**, 1,706-1,719.

- BAKER A.R., JICKELLS T.D., WITT M. and LINGE K.L. (2006c). Trends in the solubility of iron, aluminium, manganese and phosphorus in aerosol collected over the Atlantic Ocean. *Marine Chemistry* **98**, 43-58.
- BARBEAU K., RUE E.L., BRULAND K.W. and BUTLER A. (2001). Photochemical cycling of iron in the surface ocean mediated by microbial iron (III)-binding ligands. *Nature* **413**, 409-413.
- BARBEAU K., RUE E.L., TRICK C.G., BRULAND K.W. and BUTLER A. (2003). Photochemical reactivity of siderophores produced by marine heterotrophic bacteria and cyanobacteria, based on characteristic Fe(III) binding groups. *Limnology and Oceanography* **48**, 1,069-1,078.
- BETHOUX J.P. (1980). Mean water fluxes across sections in the Mediterranean Sea, evaluated on the basis of water and salt budgets and of observed salinities. *Oceanologica Acta* **1**, 79-88.
- BISCOMBE A. (2004). Factors influencing the seawater solubility of aerosol associated trace metals, School of Earth, Ocean and Environmental Sciences, University of Plymouth, Plymouth, pp. 251.
- BISCOMBE A., NIMMO M., GLEDHILL M. and ACHTERBERG E. (2004). An automated monitor to determine trace metal particle/dissolved interactions in natural waters. *Analytica Chimica Acta* **521**, 69-76.
- BONELLI P., BRAGA MARCAZZAN G.M. and CERADA E. (1996). Elemental composition and air trajectories of African dust transported in northern Italy. In *The impact of desert dust across the Mediterranean* (ed. Guerzoni S. and Chester R.), Kluwer Academic Publishers. pp. 275-283.
- BONNET S. and GUIEU C. (2004). Dissolution of atmospheric iron in seawater. *Geophysical Research Letters* **31**, 1-4.
- BONNET S., GUIEU C., CHIAVERINI J., RAS J. and STOCK A. (2005). Effect of atmospheric nutrients on the autotrophic communities in a low nutrient, low chlorophyll system. *Limnology and Oceanography* **50**, 1,810-1,819.
- BORBÉLY-KISS I., KOLTAY E., SZABÓ G.Y., BOZÓ L. and TAR K. (1999). Composition and sources of urban and rural atmospheric aerosol in eastern Hungary. *Journal of Aerosol Science* **30**, 369-391.
- BORER P.M., SULZBERGER B., REICHARD P. and KRAEMER S.M. (2005). Effect of siderophores on the light-induced dissolution of colloidal iron(II) (hydr)oxides. *Marine Chemistry* **93**, 179-193.
- BOWIE A. (1999). Flow injection with chemiluminescence detection for the determination of iron in surface Atlantic waters, School of Earth, Ocean and Environmental Sciences, University of Plymouth, Plymouth, pp. 301.
- BOWIE A.R., ACHTERBERG E.P., MANTOURA R.F.C. and WORSFOLD P.J. (1998). Determination of sub-nanomolar levels of iron in seawater using flow injection with chemiluminescence detection. *Analytica Chimica Acta* **361**, 189-200.
- BOWIE A.R., WHITWORTH D.J., ACHTERBERG E.P., MANTOURA R.F.C. and WORSFOLD P.J. (2002a). Biogeochemistry of Fe and other trace elements (Al, Co, Ni) in the upper Atlantic Ocean. *Deep-Sea research Part I*. **49**, 605-636.

- BOWIE A.R., ACHTERBERG E.P., SEDWICK P.N., USSHER S. and WORSFOLD P.J. (2002b). Real-time monitoring of picomolar concentrations of iron(II) in marine waters using automated Flow Injection-Chemiluminescence instrumentation. *Environmental Science and Technology* **36**, 4,600-4,607.
- BOYD P.W., WONG C.S., MERRILL J., SNOW J., HARRISON P.J. and GOWER J. (1998). Atmospheric iron supply and enhanced vertical carbon flux in the NE subarctic Pacific: Is there a connection? *Global Biogeochemical Cycles* **12**, 429-441.
- BOYD P.W., LAROCHE J., GALL M., FREW R. and MCKAY M.L. (1999). Role of iron, light, and silicate in controlling algal biomass in subantarctic waters SE of New Zealand. *Journal of Geophysical Research* **104**, 13,395-13,408.
- BOYD P.W., WATSON A.J., LAW C.S., ABRAHAM E.R., TRULL T., MURDOCH R., BAKKER D.C.E., BOWIE A.R., BUESSELER K.O., CHANG H., CHARETTE M., CROOT P., DOWNING K., FREW R., GALL M., HADFIELD M., HALL J., HARVEY M., JAMESON G., LA ROCHE J., LIDICOAT M., LING R., MALDONADO M.T., MCKAY R.M., NODDER S., PICKMERE S., PRIDMORE R., RINTOUL S., SAFI K., SUTTON P., STRZEPEK R., TANNEBERGER K., TURNER S., WAITE A. and ZELDIS J. (2000). A mesoscale phytoplankton bloom in the polar Southern Ocean stimulated by iron fertilization. *Nature* **407**, 695-702.
- BOYD P.W. and ABRAHAM E.R. (2001). Iron-mediated changes in phytoplankton photosynthetic competence during SOIRE. *Deep Sea Research II* **48**, 2,529-2,550.
- BOYD P.W. and DONEY S.C. (2003). The impact of climate change and feedback processes on the ocean carbon cycle. In *Ocean Biogeochemistry: The role of the ocean carbon cycle in Global change* (ed. M.J.R. Fasham), Springer-Verlag, Berlin Heidelberg New York. pp. 157-193.
- BOYE M., NISHIOKA J., CROOT P.L., LAAN P., TIMMERMANS K.R. and DE BAAR H.J.W. (2005). Major deviations of iron complexing during 22 days of a mesoscale iron enrichment in the open Southern Ocean. *Marine Chemistry* **96**, 257-271.
- BRULAND K.W. and RUE E.L. (2001). Chapter 6: Iron: Analytical methods for the determination of concentrations and speciation. In *The biogeochemistry of iron in seawater* (ed. Hunter K.A. and Turner D.R.), Wiley J. and Sons, Ltd, Baltimore. pp. 255-289.
- BRULAND K.W., RUE E.L., SMITH G.J. and DiTULLIO G.R. (2005). Iron, macronutrients and diatom blooms in the Peru upwelling regime: brown and blue waters of Peru. *Marine Chemistry* **93**, 81-103.
- BUCCIARELLI E., BLAIN S. and TRÉGUER P. (2001). Iron and manganese in the wake of the Kerguelen Islands (Southern Ocean). *Marine Chemistry* **73**, 21-36.
- BUCK C.S., LANDING W.M., RESING J.A. and LEBON G.T. (2006). Aerosol iron and aluminium solubility in the northwest Pacific Ocean: Results from the 2002 IOC cruise. *Geochemistry Geophysics Geosystems* **7**, 1-21.
- BUCK C.S., LANDING W.M., RESING J.A. and MEASURES C.I. (2009). The solubility and deposition of aerosol Fe and other trace elements in the North Atlantic Ocean: Observations from the A16N CLIVAR/CO2 repeat hydrography section. *Marine Chemistry* In Press.
- BUCK K.N., LOHAN M.C., BERGER C.J.M. and BRULAND K.W. (2007). Dissolved iron speciation in two distinct river plumes and an estuary: Implications for riverine iron supply. *Limnology and Oceanography* **52**, 843-855.

- CANNIZZARO V., BOWIE A.R., SAX A., ACHTERBERG E.P. and WORSFOLD P.J. (2000). Determination of cobalt and iron in estuarine and coastal waters using flow injection with chemiluminescence detection. *The Analyst* **125**, 51-57.
- CARBO P., KROM M.D., HOMOKY W.B., BENNING L.G. and HERUT B. (2005). Impact of atmospheric deposition on N and P geochemistry in the southeastern Levantine basin. *Deep Sea Research II* **52**, 3,041-3,053.
- CAUWET G. (1994). HTCO method for dissolved organic carbon analysis in seawater: influence of catalyst in blank estimation. *Marine Chemistry* **47**, 55-64.
- CHAPIN T.P., JOHNSON K.S. and COALE K.H. (1991). Rapid determination of manganese in sea water by flow-injection analysis with chemiluminescence detection. *Analytica Chimica Acta* **249**, 469-478.
- CHARLSON R.J., LOVELOCK J.E., ANDREAE M.O. and WARREN S.G. (1987). Oceanic phytoplankton, atmospheric sulphur, cloud albedo and climate. *Nature* **326**, 655-661.
- CHASE Z., JOHNSON K.S., ELROD V.A., PLANT J.N., FITZWATER S.E., PICKELL L. and SAKAMOTO C.M. (2005). Manganese and iron distributions off central California influenced by upwelling and shelf width. *Marine Chemistry* **95**, 235-254.
- CHASE Z., PAYTAN A., JOHNSON K.S., STREET J. and CHEN Y. (2006). Input and cycling of iron in the Gulf of Aqaba, Red Sea. *Global Biogeochemical Cycles* **20**, 1-11.
- CHEN Y. and SIEFERT R.L. (2004). Seasonal and spatial distributions and dry deposition fluxes of atmospheric total and labile iron over the tropical and subtropical North Atlantic Ocean. *Journal of Geophysical Research* **109**, 1-14.
- CHEN Y., STREET J. and PAYTAN A. (2006). Comparison between pure-water- and seawater-soluble nutrient concentrations of aerosols from the Gulf of Aqaba *Marine Chemistry* **101**, 141-152.
- CHESTER R., ELDERFIELD H. and GRIFFIN J.J. (1971). Dust transported in the northeast and southeast trade winds of the Atlantic Ocean. *Nature* **233**, 474-476.
- CHESTER R., SAYDAM A.C. and SHARPLES E.J. (1981). An approach to the assessment of local trace metal pollution in the Mediterranean marine atmosphere. *Marine Pollution Bulletin* **12**, 426-431.
- CHESTER R., LIN F.J. and MURPHY K.J.T. (1989). A three stage sequential leaching scheme for the characterisation of the sources and environmental mobility of trace metals in the marine aerosol. *Environmental Technology Letters* **10**, 887-900.
- CHESTER R., NIMMO M., MURPHY K.J.T. and NICHOLAS E. (1990). Atmospheric trace metals transported to the Western Mediterranean: Data from a station on Cap Ferrat. In *Water Pollution Research Pollution* (ed. J.-M. Martin and H. Barth), Commission of the European Communities, The Netherlands. pp. 597-612.
- CHESTER R., NIMMO M., ALARCON M. and CORCORAN P. (1991). The chemical character of the North Western Mediterranean aerosol. In *Water Pollution Research Reports*, vol. 28 (ed. J.-M. Martin and H. Barth), Commission of the European Communities, The Netherlands. pp. 495-504.
- CHESTER R., MURPHY K.J.T., LIN F.J., BERRY A.S., BRADSHAW G.A. and CORCORAN P.A. (1993). Factors controlling the solubilities of trace metals from non-remote aerosols deposited to the sea surface by the "dry" deposition mode. *Marine Chemistry* **42**, 107-126.

CHESTER R., BRADSHAW G.F. and CORCORAN P.A. (1994). Trace metal chemistry of the North Sea particulate aerosol; concentrations, sources and sea water fates. *Atmospheric Environment* **28**, 2,873-2,883.

CHESTER R., NIMMO M. and KEYSE S. (1996). The influence of Saharan and Middle Eastern desert-derived dust on the trace metal composition of Mediterranean aerosols and rainwaters: an overview. In *The impact of desert dust across the Mediterranean*, vol. 11 (ed. Guernozi S. and Chester R.), Kluwer Academic Publishers, Dordrecht/ Boston/ London. pp. 253-273.

CHESTER R., NIMMO M. and CORCORAN P.A. (1997). Rain water-aerosol trace metal relationships at Cap Ferrat: A coastal site in the Western Mediterranean. *Marine Chemistry* **58**, 293-312.

CHESTER R., NIMMO M. and PRESTON M.R. (1999). The trace metal chemistry of atmospheric dry deposition samples collected at Cap Ferrat: a coastal site in the Western Mediterranean. *Marine Chemistry* **68**, 15-30.

CHESTER R. (2000). *Marine geochemistry*, vol. Second edition (ed. Blackwell Science), Oxford. pp. 506.

CHESTER R., M. N., FONES G.R., KEYSE S. and ZHANG J. (2000). Trace metal chemistry of particulate aerosols from the UK mainland coastal rim of the NE Irish Sea. *Atmospheric Environment* **34**, 949-958.

COALE K.H., JOHNSON K.S., STOUT P.M. and SAKAMOTO C.M. (1992). Determination of copper in sea water using a flow-injection method with chemiluminescence detection. *Analytica Chimica Acta* **266**, 345-351.

COALE K.H., JOHNSON K.S., FITZWATER S.E., GORDON R.M., TANNER S., CHAVEZ F.P., FERIOLO L., SAKAMOTO C., ROGERS P., MILLERO F.J., STEINBERG P., NIGHTINGALE P., COOPER D., COCHLAN W.P., LANDRY M.R., CONSTANTINOU J., ROLLWAGEN G., TRASVINA A. and KUDELA R. (1996). A massive phytoplankton bloom induced by an ecosystem-scale iron fertilization experiment in the equatorial Pacific Ocean. *Nature* **383**, 495-501.

COALE K.H., FITZWATER S.E., GORDON R.M., TANNER S.A. and JOHNSON K.S. (1999). Iron limitation of phytoplankton growth affects nutrient drawdown ratios in the Southern Ocean (abstract). *EOS, Transactions, American Geophysical Union* **80**, 67.

COLIN J.L., JAFFREZO J.L. and GROS J.M. (1990). Solubility of major species in precipitation: factors of variation. *Atmospheric Environment* **24A**, 537-544.

COWEN J.P. and SILVER M. (1984). The association of iron and manganese with bacteria on macroparticulate material. *Science* **224**, 1,340-1,342.

COWEN J.P. and BRULAND K.W. (1985). Metal deposits associated with bacteria: implication for Fe and Mn marine biogeochemistry. *Deep-Sea Research* **32**, 253-272.

CRECELIUS E.A. (1980). The solubility of coal fly ash and marine aerosols in seawater. *Marine Chemistry* **8**, 245-250.

CROOT P.L. and JOHANSSON M. (2000). Determination of iron speciation by cathodic stripping voltammetry in seawater using the competing ligand 2-(2-Thiazolylazo)-*p*-cresol (TAC). *Electroanalysis* **12**, 565-576.

CROOT P.L., LAAN P., NISHIOKA J., STRASS V., CISEWSKI B., BOYE M., TIMMERMANS K.R., BELLERBY R.G., GOLDSOON L., NIGHTINGALE P. and DE BAAR H.J.W. (2005). Spatial and

- temporal distribution of Fe(II) and H₂O₂ during EisenEx, an open ocean mesoscale iron enrichment. *Marine Chemistry* **95**, 65-88.
- CRUMBLISS A.L. (1991). CRC Handbook of microbial iron chelates (ed. G. Winkelmann), CRC Press, Boca Raton, Florida. pp. 177.
- D'ALMEIDA G.A. and SCHUTZ L. (1983). Number, mass and volume distributions of mineral aerosol and soils of the Sahara. *Journal of Climatology and Applied Meteorology* **22**, 233-243.
- DAVIDSON C.I., BERGIN M.H. and KUHNS H.D. (1996). The deposition of particles and gases to ice sheets. In *Chemical exchange between the atmosphere and polar snow*, vol. 43, Springer-Verlag, New York. pp. 275-306.
- DE BAAR H.J.W. and DE JONG J.T.M. (2001). Chapter 5. Distributions, sources and sinks of iron in seawater. In *The biogeochemistry of iron in seawater* (ed. Turner D.R. and Hunter K.A.), Wiley J. and Sons, Ltd, Baltimore. pp. 123-253.
- DE JONG J.T.M., BOYE M., SCHOEMANN V.F., NOLTING R.F. and DE BAAR H.J.W. (2000). Shipboard techniques based on flow injection analysis for measuring dissolved Fe, Mn and Al in seawater. *Journal of Environmental Monitoring* **2**, 496-502.
- DEDIK A.N., HOFFMANN P. and ENSLING J. (1992). Chemical characterization of iron in atmospheric aerosols. *Atmospheric Environment* **26A**, 2,545-2,548.
- DELANY A.C., CLAIRE DELANY A., PARKIN D.W., GRIFFIN J.J., GOLDBERG E.D. and REIMANN B.E.F. (1967). Airborne dust collected at Barbados. *Geochimica et Cosmochimica Acta* **31**, 885-909.
- DONAT J.R., STATHAM P.J. and BRULAND K.W. (1986). An evaluation of a C18 solid phase extraction technique for isolating metal-organic complexes from central North Pacific Ocean waters. *Marine Chemistry* **18**, 85-99.
- DONAT J.R. and BRULAND K.W. (1988). Direct determination of dissolved cobalt and nickel in seawater by differential pulse cathodic stripping voltammetry preceded by adsorptive collection of cyclohexane-1,2-dione dioxime complexes. *Analytical Chemistry* **60**, 240-244.
- DONAT J.R. and BRULAND K.W. (1994). Chapter 11: Trace Elements in the Oceans. In *Trace Elements in Natural Waters* (ed. Steinnes and Salbu), CRC Press. pp. 247-281.
- DUCE R.A., ARIMOTO R., RAY B.J., UNNI C.K. and HARDER P.J. (1983). Atmospheric trace elements at Enewetak Atoll: 1, Concentrations, sources, and temporal variability. *Journal of Geophysical Research* **88**, 5,321-5,342.
- DUCE R.A. (1986). The impact of atmospheric nitrogen, phosphorus, and iron species on marine biological productivity. In *The role of air-sea exchange in geochemical cycling* (ed. P. Buat-Ménard), Reidel, Dordrecht. pp. 479-529.
- DUCE R.A., LISS P.S., MERRILL J.T., ATLAS E.L., BUAT-MENARD P., HICKS B.B., MILLER J.M., PROSPERO J.M., ARIMOTO R., CHURCH T.M., ELLIS W., GALLOWAY J.N., HANSEN L., JICKELLS T.D., KNAP A.H., REINHARDT K.H., SCHNEIDER B., SOUDINE A., TOKOS J.J., TSUNOGAI S., WOLLAST R. and ZHOU M. (1991). The atmospheric input of trace species to the ocean. *Global Biogeochemical Cycles* **5**, 193-259.
- DUCE R.A. and TINDALE N.W. (1991). Chemistry and biology of iron and other trace metals. *Limnology and Oceanography* **36**, 1715-1726.

- DUCE R.A. (1995). Sources, distributions, and fluxes of mineral aerosols and their relationship to climate. In *Aerosol forcing of climate* (ed. R.J. Charlson and J. Heintzenberg), John Wiley and Sons, Chichester. pp. 43-72.
- DUGDALE R.C. and WILKERSON F.P. (1988). Nutrient sources and primary production in the Eastern Mediterranean. *Oceanologia Acta Spec*, 179-184.
- ELBAZ-POULICHET F., CAUWET G., MING GUAN D., FAGUET D., BARLOW R. and MANTOURA R.F.C. (1994). C18 Sep-Pak extractable trace metals in waters from the Gulf of Lions. *Marine Chemistry* 46, 67-75.
- ELDERFIELD H. and SCHULTZ A. (1996). Mid-ocean ridge hydrothermal fluxes and the chemical composition of the ocean. *Annual Review of Earth and Planetary Sciences* 24, 191-224.
- ELROD V.A., JOHNSON K.S. and COALE K.H. (1991). Determination of subnanomolar levels of iron(II) and total dissolved iron in seawater by flow injection and analysis with chemiluminescence detection. *Analytical Chemistry* 63, 893-898.
- ENGELSTAEDTER S., TEGEN I. and WASHINGTON R. (2006). North African dust emissions and transport. *Earth-Science Reviews* 79, 73-100.
- FALKOWSKI P.G., BARBER R.T. and SMETACEK V. (1998). Biogeochemical controls and feedbacks on ocean primary production. *Science* 281, 200-206.
- FANG Z. (1995). Chapter 8: On-line preconcentration for flame and hydride generation atomic absorption spectrometry. In *Flow injection atomic absorption spectrometry* (ed. J. Wiley and Sons Ltd), Wiley, Chichester. pp. 143-174.
- FAUST B.C. and ZEEP R.G. (1993). Photochemistry of aqueous iron(III)-polycarboxylate complexes: roles in the chemistry of atmospheric and surface waters. *Environmental Science and Technology* 27, 2517-2522.
- FERNÁNDEZ Y., MARAÑÓN E., CASTRILLÓN L. and VÁZQUEZ I. (2005). Removal of Cd and Zn from inorganic industrial waste leachate by ion exchange. *Journal of Hazardous Materials* B16, 169-175.
- FISCHER A.F., KROON J.J., VERBURG T.G., TEUNISSEN T. and WOLTERBEEK H.T. (2007). On the relevance of iron adsorption to container materials in small-volume experiments on iron marine chemistry: ⁵⁵Fe-aided assessment of capacity, affinity and kinetics. *Marine Chemistry* 107, 533-546.
- FITZWATER S.E., JOHNSON K.S., ELROD V.A., RYAN J.P., COLETTI L.J., TANNER S.J., GORDON R.M. and CHAVEZ F.P. (2003). Iron, nutrient and phytoplankton biomass relationships in upwelled waters of the California coastal system. *Continental Shelf Research* 23, 1523-1544.
- FONES G.R. (1996). Atmospheric deposition of trace metals to urban and coastal environments, Department of Chemistry, University of Central Lancashire, Preston, pp. 365.
- FORMENTI P., RAJOT J.L., DESBOEUF K., CAQUINEAU S., CHEVALLIER S., NAVA S., GAUDICHET A., JOURNET E., TRIQUET S., ALFARO S., CHIARI M., HAYWOOD J., COE H. and HIGHWOOD E. (2008). Regional variability of the composition of mineral dust from western Africa: Results from the AMMA SOP0/DABEX and DODO field campaigns. *Journal of Geophysical Research* 113, 1-12.

- FRY B., PELTZER E.T., HOPKINSON JR. C.S., NOLIN A. and REDMOND L. (1996). Analysis of marine DOC using a dry combustion method. *Marine Chemistry* **54**, 191-201.
- FUKAMI K., SIMIDU U. and TAGA N. (1983). Change in a bacterial population during the process of degradation of a phytoplankton bloom in a brackish lake. *Marine Biology* **76**, 253-255.
- GANOR E., LEVIN Z. and VAN GRIEKEN R. (1998). Composition of individual aerosol particles above the Israelian Mediterranean coast during the summer time. *Atmospheric Environment* **32**, 1,631-1,642.
- GANOR E. and FONER H.A. (2001). Mineral dust concentrations, deposition fluxes and deposition velocities in dust episodes over Israel. *Journal of Geophysical Research* **106**, 18,431-18,437.
- GAO Y., KAUFMAN Y.J., TANRÉ D., KOLBER D. and FALKOWSKI P.G. (2001). Seasonal distributions of aeolian iron fluxes to the global ocean. *Geophysical Research Letters* **28**, 29-32.
- GERMAN C.R., HOLLIDAY B.P. and ELDERFIELD H. (1991). Hydrothermal scavenging at the Mid-Atlantic Ridge: modification of trace metal dissolved element dissolved fluxes. *Earth and Planetary Science Letters* **107**, 101-114.
- GINOUX P., CHIN M., TEGEN I., PROSPERO J.M., HOLBEN B., DUBOVIK O. and LIN S.-J. (2001). Sources and distributions of dust aerosols simulated with the GOCART model. *Journal of Geophysical Research* **106**, 20,255-20,273.
- GLEDHILL M. and VAN DEN BERG C.M.G. (1994). Determination of complexation of iron (III) with natural organic complexing ligands in seawater using cathodic stripping voltammetry. *Marine Chemistry* **47**, 41-54.
- GLEDHILL M., VAN DER BERG C.M.G., NOLTING R.F. and TIMMERMANS K.R. (1998). Variability in the speciation of iron in the North Sea. *Marine Chemistry* **59**, 283-300.
- GOMES L., BERGAMETTI G., COUDE-GAUSSSEN G. and ROGNON P. (1990). Submicron desert dusts: A sandblasting process. *Journal of Geophysical Research* **95**, 13,927-13,935.
- GOUDIE A.S. and MIDDLETON N.J. (1992). The changing frequency of dust storms through time. *Climatic Change* **20**, 197-225.
- GOUDIE A.S. (2009). Dust storms: Recent developments. *Journal of Environmental Management* **90**, 89-94.
- GRAEDEL T.E., WESCHLER C.J. and MANDICH M.L. (1985). Influence of transition metal complexes on atmospheric droplet acidity. *Nature* **317**, 240-242.
- GRAN H.H. (1931). II- On the conditions for the production of plankton in the sea. *Rapport et Procès-Verbaux du Conseil Permanent International pour l'Exploration de la Mer* **75**, 37-46.
- GROSSART H.-P., KIØRBOE T., TANG K. and PLOUG H. (2003). Bacterial colonization of particles: growth and interactions. *Applied and Environmental Microbiology* **69**, 3,500-3,509.
- GUERNOZI S., MOLINAROLI E., ROSSINI P., RAMPAZZO G., QUARANTOTTO G., DE FALCO G. and CRISTINI S. (1999a). Role of desert aerosol in metal fluxes in the Mediterranean area. *Chemosphere* **39**, 229-246.

- GUERZONI S., CHESTER R., DULAC F., HERUT B., LOÏE-PILOT M.-D., MEASURES C.I., MIGON C., MOLINAROLI E., MOULIN C., ROSSINI P., SAYDAM C., SOUDINE A. and ZIVERI P. (1999b). The role of atmospheric deposition in the biogeochemistry of the Mediterranean Sea. *Progress in Oceanography* **44**, 147-190.
- GUIEU C., DUCE R. and ARIMOTO R. (1994). Dissolved input of manganese to the ocean: Aerosol source. *Journal of Geophysical Research* **99**, 18,789-18,800.
- GUIEU C., CHESTER R., NIMMO M., MARTIN J.-M., GUERZONI S., NICOLAS E., MATEU J. and KEYSE S. (1997). Atmospheric input of dissolved and particulate metals to the northwestern Mediterranean. *Deep-Sea Research Part II* **44**, 655-674.
- GUIEU C., BOZEC Y., RIDAME C., SARTHOU G. and LEBLOND N. (2002a). Impact of high Saharan dust inputs on dissolved iron concentrations in the Mediterranean Sea. *Geophysical Research Letters* **29**, 17.1-17.4.
- GUIEU C., LOYE-PILOT M.-D., RIDAME C. and THOMAS C. (2002b). Chemical characterization of the Saharan dust end-member: some biogeochemical implications for the Western Mediterranean Sea. *Journal of Geophysical Research* **107**, ACH 5 1-11.
- HALL D.J., UPTON S.L. and MARSLAND G.W. (1994). Designs for a deposition gauge and a flux gauge for monitoring ambient dust. *Atmospheric Environment* **28**, 2,963-2,979.
- HAND J.L., MAHOWALD N.M., CHEN Y., SIEFERT R.L., LUO C., SUBRAMANIAM A. and FUNG I. (2004). Estimates of atmospheric-processed soluble iron from observations and a global mineral aerosol model: Biogeochemical implications. *Journal of Geophysical Research* **109**, 1-21.
- HARDY J.T. and CRECELIUS E.A. (1981). Is atmospheric particulate matter inhibiting marine primary productivity. *Environmental Science and Technology* **15**, 1,103-1,106.
- HARVEY H.W. (1939). Substances controlling the growth of a diatom. *Journal of the Marine Biological Association of the United Kingdom* **23**, 499-520.
- HAYGOOD M.G. and HOLT P.D. (1993). Aerobactin production by a planktonic marine *Vibrio* sp. *Limnology and Oceanography* **38**, 1,091-1,097.
- HERRING J.G. and MOREL F.M.M. (1993). *Principles and applications of aquatic chemistry*, New York, pp. 588.
- HERUT B., KROM M.D., PAN G. and MORTIMER R. (1999). Atmospheric input of nitrogen and phosphorus to the Southeast Mediterranean: Sources, fluxes, and possible impact. *Limnology and Oceanography* **44**, 1,683-1,692.
- HERUT B., NIMMO M., MEDWAY A., CHESTER R. and KROM M.D. (2001). Dry atmospheric inputs of trace metals at the Mediterranean coast of Israel (SE Mediterranean): sources and fluxes. *Atmospheric Environment* **35**, 803-813.
- HERUT B., COLLIER R. and KROM M.D. (2002). The role of dust in supplying nitrogen and phosphorus to the Southeast Mediterranean. *Limnology and Oceanography* **47**, 870-878.
- HERUT B., ZOHARY T., KROM M.D., MANTOURA R.F.C., PITTA P., PSARRA S., RASSOULZADEGAN F., TANAKA T. and THINGSTAD T.F. (2005). Response of East Mediterranean surface water to Saharan dust: On-board microcosm experiment and field observations. *Deep Sea Research II* **52**, 30,24-3,040.

- HIEMSTRA T. and VAN RIEMSDIJK W.H. (2006). Biogeochemical speciation of Fe in ocean water. *Marine Chemistry* **102**, 181-197.
- HODGE V., JOHNSON S.R. and GOLDBERG E.D. (1978). Influence of atmospherically transported aerosols on surface ocean water composition. *Geochemical Journal* **12**, 7-20.
- HONG H. and KESTER D.R. (1986). Redox state of iron in the offshore waters of Peru. *Limnology and Oceanography* **31**, 512-524.
- HSU S.-C., WONG G.T.F., GONG G.-C., SHIAH F.-K., HUANG Y.-T., KAO S.-J., TSAI F., CANDICE LUNG S.-C., LIN F.-J., LIN I.I., HUNG C.-C. and TSENG C.-M. (2009). Sources, solubility, and dry deposition of aerosol trace elements over the East China Sea. *Marine Chemistry* In Press.
- HUDSON R.J.M. and MOREL F.M.M. (1990). Iron transport in marine phytoplankton: kinetics of cellular and medium coordination reactions. *Limnology and Oceanography* **35**, 1,002-1,020.
- HUNTER K.A. and BOYD P.W. (2007). Iron-binding ligands and their role in the ocean biogeochemistry of iron. *Environmental Chemistry* **4**, 221-232.
- HUSAR R.B., PROSPERO J.M. and STOWE L.L. (1997). Characterization of tropospheric aerosols over the oceans with the NOAA advanced very high resolution radiometer optical thickness operational product. *Journal of Geophysical Research* **102**, 16,889-16,909.
- HUTCHINS D.A., DiTULLIO G.R. and BRULAND K.W. (1993). Iron and regenerated production: evidence for biological iron recycling. *Limnology and Oceanography* **38**, 1,242-1,255.
- HUTCHINS D.A. and BRULAND W.A. (1994). Grazer-mediated regeneration and assimilation of Fe, Zn and Mn from planktonic prey. *Marine Ecology Progress Series* **110**, 259-269.
- ING G.K.T. (1969). A dust storm over central China, april 1969. *Weather* **27**, 136-145.
- ITTEKOT V. (1993). Organic mineral interactions in the sea: implications for atmospheric CO₂ removal. *Global and Planetary Change* **8**, 17-25.
- JICKELLS T.D., DORLING S., DEUSER W.G., CHURCH T.M., ARIMOTO R. and PROSPERO J.M. (1998). Air-borne dust fluxes to a deep water sediment trap in the Sargasso Sea. *Global Biogeochemical Cycles* **12**, 311-321.
- JICKELLS T.D. and SPOKES L.J. (2001). Chapter 4. Atmospheric iron inputs to the Oceans. In *The Biogeochemistry of iron in seawater*. (ed. Turner D.R. and Hunter K.A.), Wiley J. and Sons, Ltd, Baltimore. pp. 85-121.
- JICKELLS T.D., AN Z.S., ANDERSEN K.K., BAKER A.R., BERGAMETTI G., BROOKS N., CAO J.J., BOYD P.W., DUCE R.A., HUNTER K.A., KAWAHATA H., KUBILAY N., LAROCHE J., LISS P.S., MAHOWALD N., PROSPERO J.M., RIDGWELL A.J., TEGEN I. and TORRES R. (2005). Global iron connections between desert dust, ocean biogeochemistry, and climate. *Science* **308**, 67-71.
- JOHNSON K.S., COALE K.H., ELROD V.A. and TINDALE N.W. (1994). Iron photochemistry in seawater from the Equatorial Pacific. *Marine Chemistry* **46**, 319-334.

- JOHNSON K.S., GORDON R.M. and COALE K.H. (1997). Marine Chemistry Discussion Paper: What controls dissolved iron concentrations in the world ocean? *Marine Chemistry* 57, 137-161.
- JOHNSON K.S., CHAVEZ F.P. and FRIEDERICH G.E. (1999). Continental shelf sediment as a primary source of iron for coastal phytoplankton. *Nature* 398, 697-700.
- JOURNET E., DESBOEUF K.V., CAQUINEAU S. and COLIN J.L. (2008). Mineralogy as a critical factor of dust iron solubility. *Geophysical Research Letters* 35, 1-5.
- KANE M.M., RENDELL A.R. and JICKELLS T.D. (1994). Atmospheric scavenging processes over the North Sea. *Atmospheric Environment* 28, 2,523-2,530.
- KIM G. and CHURCH T.M. (2001). Seasonal biogeochemical fluxes of ^{234}Th and ^{210}Po in the upper Sargasso Sea: Influence from atmospheric iron deposition. *Global Biogeochemical Cycles* 15, 651-661.
- KOÇAK M. (2001). Investigation of the chemical composition of the lower tropospheric aerosols in the eastern Mediterranean region: implications regarding sources and long range transport., Institute of Marine Sciences, Middle East Technical University, Erdemli, Turkey, pp. 150.
- KOÇAK M. (2006). Comprehensive chemical characterization of aerosols in the Eastern Mediterranean: sources and long range transport, Department of Chemical Oceanography, Institute of Marine Sciences of Middle East Technical University, Erdemli, pp. 335.
- KOÇAK M., NIMMO M., KUBILAY N. and HERUT B. (2004). Spatio-temporal aerosol trace metal concentrations and sources in the Levantine Basin of the Eastern Mediterranean. *Atmospheric Environment* 38, 2,133-2,144.
- KOÇAK M., KUBILAY N., HERUT B. and NIMMO M. (2005). Dry atmospheric fluxes of trace metals (Al, Fe, Mn, Pb, Cd, Zn, Cu) over the Levantine Basin: A refined assessment. *Atmospheric Environment* 39, 7,330-7,341.
- KOÇAK M., KUBILAY N., HERUT B. and NIMMO M. (2007). Trace metal solid state speciation in aerosols of the Northern Levantine Basin, East Mediterranean. *Journal of Atmospheric Chemistry* 56, 239-257.
- KONHAUSER K.O., AMSKOLD L., LALONDE S.V., POSTH N.R., KAPPLER A. and ANBAR A. (2007). Decoupling photochemical Fe(II) oxidation from shallow-water BIF deposition. *Earth and Planetary Science Letters* 258, 87-100.
- KRAEMER S.M. (2004). Iron oxide dissolution and solubility in the presence of siderophores. *Aquatic Science* 66, 3-18.
- KRESS N. and HERUT B. (1998). Hypertrophication in the Oligotrophic Eastern Mediterranean: a Study in Haifa Bay (Israel). *Estuarine, Coastal and Shelf Science* 46, 645-656.
- KRESS N. and HERUT B. (2001). Spatial and seasonal evolution of dissolved oxygen and nutrients in the Southern Levantine Basin (Eastern Mediterranean Sea): chemical characterization of the water masses and inferences on the N:P ratios. *Deep Sea Research Part I: Oceanographic Research Papers* 48, 2,347-2,372.

- KROM M.D., KRESS N., BRENNER S. and GORDON L.I. (1991). Phosphorus limitation of primary productivity in the eastern Mediterranean Sea. *Limnology and Oceanography* **36**, 424-432.
- KUBILAY N. and SAYDAM A.C. (1995). Trace elements in atmospheric particulates over the Eastern Mediterranean; concentrations, sources, and temporal variability. *Atmospheric Environment* **29**, 2,289-2,300.
- KUBILAY N., YEMENICIOGLU S. and SAYDAM A.C. (1995). Airborne material collections and their chemical composition over the Black Sea. *Marine Pollution Bulletin* **30**, 475-483.
- KUBILAY N., NICKOVIC S., MOULIN C. and DULAC F. (2000). An illustration of the transport and deposition of mineral dust onto the eastern Mediterranean. *Atmospheric Environment* **34**, 1,293-1,303.
- KUBILAY N., KOÇAK M., ÇOKACAR T., OGUZ T., KOUVARAKIS G. and MIHALOPOULOS N. (2002). Influence of Black Sea and local biogenic activity on the seasonal variation of aerosol sulfur species in the eastern Mediterranean atmosphere. *Global Biogeochemical Cycles* **16**, 1-27.
- KUBILAY N., OGUZ T., KOÇAK M. and TORRES O. (2005). Ground-based assessment of Total Ozone Mapping Spectrometer (TOMS) data for dust transport over the northeastern Mediterranean. *Global Biogeochemical Cycles* **19**, 1-9.
- KUMA K., NISHIOKA J. and MATSUNAGA K. (1996). Controls on iron(III) hydroxide solubility in seawater: the influence of pH and natural organic chelators. *Limnology and Oceanography* **41**, 396-407.
- LAES A. (2004). Biogéochimie du fer le long de la marge continentale du Golfe de Gascogne: Distributions, sources et transport, Institut Universitaire Européen de la Mer, Université de Bretagne Occidentale, Brest, pp. 155.
- LANDING W.M., HARALDSSON C. and PAXEUS N. (1986). Vinyl polymer agglomerate based transition metal cation chelating ion-exchange resin containing the 8-hydroxyquinoline functional group. *Analytical Chemistry* **58**, 3,031-3,035.
- LANDING W.M. and BRULAND K.W. (1987). The contrasting biogeochemistry of iron and manganese in the Pacific Ocean. *Geochimica and Cosmochimica Acta* **51**, 29-43.
- LINSINGER T. (2005). Application note 1: Comparison of a measurement result with the certified value. *European Commission - Joint Research Centre Institute for Reference Materials and Measurements (IRMM) Geel, Belgium*, http://www.bam.de/pdf/service/referenzmaterialien/erm_application_note_1_en.pdf.
- LOÏE-PILOT M.D., MARTIN J.M. and MORELLI J. (1986). Influence of Saharan dust on the rain acidity and atmospheric input to the Mediterranean. *Nature* **321**, 427-428.
- LOHAN M.C. and BRULAND K.W. (2008). Elevated Fe(II) and dissolved Fe in hypoxic shelf waters off Oregon and Washington: an enhanced source of iron to coastal upwelling regimes. *Environmental Science and Technology* **42**, 6,462-6,468.
- LOWENTHAL D.H. and RAHN K.A. (1987). The use of Whatman 41 filter papers for high volume aerosol sampling. *Atmospheric Environment* (1967) **21**, 2,732-2,734.
- LUDWING W. and MAYBECK M. (2003). Riverine transport of water, sediments and pollutants to the Mediterranean sea. In *MAP Technical Report Series* (ed. United Nations Environment Programme Mediterranean Action plan and (UNEP/MAP)), pp. 111.

- LUO C., MAHOWALD N.M. and DEL CORRAL J. (2003). Sensitivity study of meteorological parameters on mineral aerosol mobilization, transport, and distribution. *Journal of Geophysical Research* **108**, AAC 5.1 - AAC 5.21.
- MACKEY D.J. (1983). The strong complexing capacity of seawater- an investigation of south-eastern Australian coastal waters. *Marine Chemistry* **14**, 73-87.
- MAHOWALD N., RASCH P.J., EATON B.E., WHITTLESTONE S. and PRINN R.G. (1997). Transport of ²²²Rn to the remote troposphere using the Model of Atmospheric Transport and Chemistry and assimilated winds from ECMWF and the National Center for Environmental Prediction/NCAR. *Journal of Geophysical Research* **102**, 28,139-28,151.
- MAHOWALD N.M., ZENDER C.S., LUO C., SAVOIE D., TORRES O. and DEL CORRAL J. (2002). Understanding the 30-year Barbados desert dust record. *Journal of Geophysical Research* **107**, AAC7.1- AAC7.7.
- MAHOWALD N.M. and LUO C. (2003). A less dusty future? *Geophysical Research Letters* **30**, CLM6.1-CLM6.4.
- MAHOWALD N.M., BAKER A.R., BERGAMETTI G., BROOKS N., DUCE R.A., JICKELLS T.D., KUBILAY N., PROSPERO J.M. and TEGEN I. (2005). Atmospheric global dust cycle and iron inputs to the ocean. *Global Biogeochemical Cycles* **19**, 1-15.
- MALDONADO M.T. and PRICE N.M. (1999). Utilization of iron bound to strong organic ligands by plankton communities in the subarctic Pacific Ocean. *Deep-Sea Research II* **46**, 2,447-2,473.
- MALDONADO M.T. and PRICE N.M. (2000). Nitrate regulation of Fe reduction and transport by Fe-limited *Thalassiosira oceanica*. *Limnology and Oceanography* **45**, 814-826.
- MARING H.B. and DUCE R.A. (1987). The impact of atmospheric aerosols on trace metal chemistry in open ocean surface seawater. 1- Aluminium. *Earth and Planetary Science Letters* **84**, 381-392.
- MARING H.B. and DUCE R.A. (1989). The impact of atmospheric aerosols on trace metal chemistry in open ocean surface seawater. 2- Copper. *Journal of Geophysical Research* **94**, 1039-1045.
- MARING H.B. and DUCE R.A. (1990). The impact of atmospheric aerosols on trace metal chemistry in open ocean surface seawater. 3. Lead. *Journal of Geophysical Research* **95**, 5,341-5,347.
- MARTIN J.H. (1990). Glacial-interglacial CO₂ change: the iron hypothesis. *Paleoceanography* **5**, 1-13.
- MARTIN J.H. and FITZWATER S.E. (1988). Iron deficiency limits phytoplankton growth in the north-east subarctic Pacific. *Nature* **321**, 341-343.
- MARTIN J.H. and GORDON R.M. (1988). Northeast Pacific iron distributions in relation to phytoplankton productivity. *Deep-Sea Research* **35**, 177-196.
- MARTIN J.H., GORDON R.M., FITZWATER S.E. and BROENKOW W.W. (1989). VERTEX: phytoplankton/iron studies in the Gulf of Alaska. *Deep-Sea Research* **36**, 649-680.
- MARTIN J.H., GORDON R.M. and FITZWATER S.E. (1990). Iron in Antarctic waters. *Nature* **345**, 156-158.

- MARTIN J.H., FITZWATER S.E., MICHAEL GORDON R., HUNTER C.N. and TANNER S.J. (1993). Iron, primary production and carbon-nitrogen flux studies during the JGOFS North Atlantic bloom experiment. *Deep Sea Research Part II: Topical Studies in Oceanography* **40**, 115-134.
- MARTIN J.H., COALE K.H., JONHSON K.S., FITZWATER S.E., GORDON R.M., TANNER S.J., HUNTER C.N., ELROD V.A., NOWICKI J.L., COLEY T.L., BARBER R.T., LINDSEY S., WATSON A.J., VAN SCOY K., LAW C.S., LIDDICOAT M.I., LING R., STANTON T., STOCKEL J., COLLINS C., ANDERSON A., BIDIGARE R., ONDRUSEK M., LATASA M., MILLERO F.J., LEE K., YAO W., ZHANG J.Z., FRIEDERICH G., SAKAMOTO C., CHAVEZ F., BUCK K., KOLBER Z., GREENE R., FALKOWSKI P., CHISHOLM S.W., HOGE F., SWIFT R., YUNGEL J., TURNER S., NIGHTINGALE P., HATTON A., LISS P. and TINDALE N.W. (1994). Testing the hypothesis in ecosystems of the equatorial Pacific Ocean. *Nature* **371**, 123-129.
- MARTIN J.M. and MAYBECK M. (1979). Elemental mass balance of material carried by major world rivers. *Marine Chemistry* **7**, 173-206.
- MARTINEZ J.S., HAYGOOD M.G. and BUTLER A. (2001). Identification of a natural desferrioxamine siderophore produced by a marine bacterium. *Limnology and Oceanography* **46**, 420-424.
- MAWJI E., GLEDHILL M., MILTON J.A., TARRAN G.A., USSHER S.J., THOMPSON A., WOLFF G.A., WORSFOLD P.J. and ACHTERBERG E.P. (2008). Hydroxamate siderophores: occurrence and importance in the Atlantic Ocean. *Environmental Science and Technology*, **42**, 8,675-8,680.
- MCCARTHY M., HEDGES J. and BENNER R. (1996). Major biochemical composition of dissolved high molecular weight organic matter in seawater. *Marine Chemistry* **55**, 281-297.
- MEASURES C.I., YUAN J. and RESING J.A. (1995). Determination of iron in seawater by flow injection analysis using in-line preconcentration and spectrophotometric detection. *Marine Chemistry* **50**, 3-12.
- MENDEZ J., GUIEU C. and ADKINS J. (2009). Atmospheric input of manganese and iron to the ocean: Seawater dissolution experiments with Saharan and North American dusts. *Marine Chemistry* In press.
- MENZEL D.W. and RYTHER J.H. (1961). Nutrients limiting the production of phytoplankton in the Sargasso sea, with special reference to iron. *Deep Sea Research* (1953) **7**, 276-281.
- MILLER W.L., KING D.W., LIN J. and KESTER D.R. (1995). Photochemical redox cycling of iron in coastal seawater. *Marine Chemistry* **50**, 63-77.
- MILLERO F.J. and SOTOLONGO S. (1989). The oxidation of Fe(II) with H₂O₂ in seawater. *Geochimica and Cosmochimica Acta* **53**, 1,867-1,873.
- MILLS G.L., HANSON A.K., QUINN J.G., LAMMELA W.R. and CHASTEEN N.D. (1982). Chemical studies of copper-organic complexes isolated from estuarine waters using C₁₈ reverse-phase liquid chromatography. *Marine Chemistry* **11**, 355-377.
- MILLS M.M., RIDAME C., DAVEY M., LAROCHE J. and GEIDER R.J. (2004). Iron and phosphorus co-limit nitrogen fixation in the eastern tropical North Atlantic. *Nature* **429**, 292-294.

- MILNE A. (2007). Marine biogeochemistry studies of iron and hydrogen peroxide using flow injection-chemiluminescence, School of Earth, Ocean and Environmental Sciences, University of Plymouth, Plymouth, pp. 214.
- MOFFETT J.W. (2001). Chapter 8. Transformations among different forms of iron in the ocean. In *The biogeochemistry of iron in seawater* (ed. Turner D.R. and Hunter K.A.), Wiley J. and Sons, Ltd, Baltimore. pp. 343-372.
- MOORE R.M., MILLEY J.E. and CHATT A. (1984). The potential for biological mobilization of trace metals from aeolian dust in the ocean and its importance in the case of iron. *Oceanology Acta* 7, 221-228.
- MOREL F.M.M. and HUDSON R.J.M. (1985). The geobiological cycle of trace elements in aquatic systems: Redfield revisited. In *Chemical processes in Lakes* (ed. S. W.), Wiley, New York. pp. 251-281.
- MOREL F.M.M. and HERING J.G. (1993). Reactions on solid surfaces. In *Principles and applications of aquatic chemistry* (ed. Wiley), New York. pp. 509-570.
- MOREL F.M.M. and PRICE N.M. (2003). The biogeochemical cycles of trace metals in the oceans. *Science* 300, 944-947.
- MOULIN C., LANMBERT C.E., DULAC F. and DAYAN U. (1997). Control of atmospheric export of dust from North Africa by the North Atlantic Oscillation. *Nature* 387, 691-694.
- MOULIN C., LAMBERT C.E., DAYAN U., MASSON V., RAMONET M., BOUSQUET P., LEGRAND M., BALKANSKI Y.J., GUELLE W., MARTICORENA B., BERGAMETTI G. and DULAC F. (1998). Satellite climatology of African dust transport in the Mediterranean atmosphere. *Journal of Geophysical Research* 103, 13,137-13,144.
- MURPHY K.J.T. (1985). The trace metal chemistry of the Atlantic aerosol, University of Liverpool Liverpool, pp. 265.
- MUSANI L., VALENTA P., NÜRNBERG H.W., KONRAD Z. and BRANICA M. (1980). On the chelation of toxic trace metals by humic acid of marine origin. *Estuarine and Coastal Marine Science* 11, 639-649.
- NICKSON R.A., HILL S.J. and WORSFOLD P.J. (1995). Analytical perspective. Solid phase techniques for the preconcentration of trace metals from natural waters. *Analytical Proceedings* 32, 387-395.
- NIMMO M. and FONES G. (1994). Application of adsorptive cathodic stripping voltammetry for the determination of Cu, Cd, Ni and Co in atmospheric samples. *Analytica Chimica Acta* 291, 321-328.
- NISHIOKA J., TAKEDA S., WONG C.S. and JOHNSON W.K. (2001). Size-fractionated iron concentrations in the northeast Pacific Ocean: Distribution of soluble and small colloidal iron. *Marine Chemistry* 74, 157-179.
- NISHIOKA J., TAKEDA S., DE BAAR H.J.W., CROOT P.L., BOYE M., LAAN P. and TIMMERMANS K.R. (2005). Changes in the concentration of iron in different size fractions during an iron enrichment experiment in the open Southern Ocean. *Marine Chemistry* 95, 51-63.
- NOLTING R.F., DE BAAR H.J.W., VAN BENNEKOM A.J. and MASSON A. (1991). Cadmium, copper and iron in the Scotia Sea, Weddell Sea and Weddell/Scotia Confluence (Antarctica). *Marine Chemistry* 35, 219-243.

- NOLTING R.F., GERRINGA L.J.A., SWAGERMAN M.J.W., TIMMERMANS K.R. and DE BAAR H.J.W. (1998). Fe (III) speciation in the high nutrient, low chlorophyll Pacific region of the Southern Ocean. *Marine Chemistry* **62**, 335-352.
- O'SULLIVAN D.W., HANSON A.K., MILLER W.L. and KESTER D.R. (1991). Measurement of Fe(II) in surface water of the equatorial Pacific. *Limnology and Oceanography* **36**, 1,727-1,741.
- O'SULLIVAN D.W., HANSON JR. A.K. and KESTER D.R. (1995). Stopped flow luminol chemiluminescence determination of Fe(II) and reducible iron in seawater at sub-nanomolar levels. *Marine Chemistry* **49**, 65-77.
- OBATA H., KARATANI H. and NAKAYAMA E. (1993). Automated determination of iron in seawater by chelating resin concentration and chemiluminescence detection. *Analytical Chemistry* **65**, 1,524-1,528.
- OBATA H., KARATANI H., MATSUI M. and NAKAYAMA E. (1997). Fundamental studies for chemical speciation of iron in seawater with an improved analytical method. *Marine Chemistry* **56**, 97-106.
- ORIF M. (2008). The impacts of atmospheric derived metals on coastal marine systems, School of Earth, Ocean and Environmental Sciences, University of Plymouth, Plymouth, pp. 241.
- OTT S.T., OTT A., MARTIN D.W. and YOUNG J.A. (1991). Analysis of a Trans-Atlantic Saharan dust outbreak based on satellite and GATE data. *Monthly Weather Review* **119**, 1,832-1,850.
- OTTELEY C.J. and HARRISON R.M. (1993). Atmospheric dry deposition flux of metallic species to the North Sea. *Atmospheric Environment. Part A. General Topics* **27**, 685-695.
- PALENIK B., BRAHAMSHA B., LARIMER F.W., LAND M., HAUSER L., CHAIN P., LAMERDIN J., REGALA W., ALLEN E., MCCARREN J., PAULSEN I., DUFRESNE A., PARTENSKY F., WEBB E.A. and WATERBURY J. (2003). The genome of a motile marine Synechococcus. *Nature* **424**, 1,037-1,042.
- PELTZER E.T., FRY B., DOERING P.H., MCKENNA J.H., NORRMAN B. and ZWEIFEL U.L. (1996). A comparison of methods for the measurement of dissolved organic carbon in natural waters. *Marine Chemistry* **54**, 85-96.
- PITTY A. (1968). Particle size of the Saharan dust which fell in Britain in July 1968. *Nature* **220**, 364-365.
- PORCAL P., HEJZLAR J. and KOPÁČEK J. (2004). Seasonal and photochemical changes of DOM in an acidified forest lake and its tributaries. *Aquatic Science* **66**, 211-222.
- POWELL R.T., KING D.W. and LANDING W.M. (1995). Iron distributions in the surface waters of the south Atlantic. *Marine Chemistry* **50**, 13-20.
- POWELL R.T. and DONAT J.R. (2001). Organic complexation and speciation of iron in the south and Equatorial Atlantic. *Deep-Sea research Part II*. **48**, 2,877-2,893.
- PROSPERO J., GINOUX P., TORRES O. and NICHOLSON S.E. (2002). Environmental characterization of global sources of atmospheric soil dust derived from the NIMBUS-7 TOMS absorbing aerosol product. *Reviews of Geophysics* **40**, 2.1-2.31.

- PROSPERO J.M., BONATTI E., SCHUBERT C. and CARLSON T.N. (1970). Dust in the Caribbean atmosphere traced to an African dust storm. *Earth and Planetary Science Letters* 9, 287-293.
- PROSPERO J.M., NEES R.T. and UEMATSU M. (1987). Deposition rate of particulate and dissolved aluminium derived from Saharan dust in precipitation at Miami, Florida. *Journal of Geophysical Research* 92, 14,723-14,731.
- PROSPERO J.M., UEMATSU M. and SAVOIE D.L. (1989). Mineral aerosol transport to the Pacific Ocean. In *Chemical Oceanography*, vol. 10 (ed. J.P. Riley, R. Chester and R.A. Duce), Academic Press, London. pp. 187-218.
- PROSPERO J.M. (1996). Saharan dust transport over the North Atlantic Ocean and Mediterranean: an overview. In *The impact of desert dust across the Mediterranean*, vol. Environmental Science and Technology Library: 11 (ed. Guerzoni S. and Chester R.), Kluwer Academic Publishers, Dordrecht, Boston, London. pp. 133-153.
- PROSPERO J.M. (1999). Long range transport of mineral dust in the global atmosphere ;Impacts of African dust on the environment of the south eastern United States. *Proceedings of the National Academy of Sciences of the United States of America* 96, 3,396-3,403.
- PYE K. (1987). *Aeolian dust and dust deposits*. Academic Press, New York, pp. p 334.
- QUÉGUINER B., TRÉGUER P., PEEKEN I. and SCHAREK R. (1997). Biogeochemical dynamics and the silicon cycle in the Atlantic sector of the Southern Ocean during austral spring 1992. *Deep Sea Research Part II: Topical Studies in Oceanography* 44, 69-89.
- RAHN K.A., BORYS R.D., SHAW G.E., SCHUTZ L. and JAENICKE R. (1979). Long-range impact of desert aerosol on atmospheric chemistry: two examples. In *Saharan Dust* (ed. Morales C.), Wiley. pp. 243-266.
- RASCH P., MAHOWALD N. and EATON B. (1997). Representations of transport, convection, and the hydrologic cycle in chemical transport models: Implications for the modeling of short-lived and soluble species. *Journal of Geophysical Research* 102, 28,127-28,138.
- REDFIELD A.C., KETCHUM B.H. and RICHARDS F.A. (1963). The influence of organisms on the composition of sea-water. In *The Sea*, vol. 2 (ed. Hill M.N.), Wiley J. and Sons, New York. pp. 26-77.
- REIFF J., FORBES G.S., SPIEKMA F.T.M. and REYNDERS J.J. (1986). African Dust Reaching Northwestern Europe: A Case Study to Verify Trajectory Calculations. *Journal of Applied Meteorology* 25, 1,543-1,567.
- RESING J.A. and MOTTI M.J. (1992). Determination of manganese in seawater using flow injection analysis with on-line preconcentration and spectrophotometric detection. *Analytical Chemistry* 64, 2,682-2,687.
- RIDAME C. and GUIEU C. (2002). Saharan input of phosphate to the oligotrophic water of the open western Mediterranean Sea. *Limnology and Oceanography* 47, 856-869.
- RIJKENBERG M.J.A., GERRINGA L.J.A., VELZEBOER I., TIMMERMANS K.R., BUMA A.G.J. and DE BAAR H.J.W. (2006). Iron-binding ligands in Dutch estuaries are not affected by UV induced photochemical degradation. *Marine Chemistry* 100, 11-23.
- RIJKENBERG M.J.A., POWELL C.F., DALL'OSTO M., NIELSDOTTIR M.C., PATEY M.D., HILL P.G., BAKER A.R., JICKELLS T.D., HARRISON R.M. and ACHTERBERG E.P. (2008). Changes in

- iron speciation following a Saharan dust event in the tropical North Atlantic Ocean. *Marine Chemistry* **110**, 56-67.
- RILEY J.P. and TAYLOR D. (1968). Chelating resins for the concentration of trace elements from sea water and their analytical use in conjunction with atomic absorption spectrophotometry. *Analytica Chimica Acta* **40**, 479-485.
- ROOF A.A.M. (1982). Aquatic photochemistry. In *The Handbook of Environmental Chemistry, Reaction and Processes*, vol. 2 Part B (ed. Springer-Verlag), Berlin, Germany. pp. 43-72.
- ROSE A.L. and WAITE T.D. (2001). Chemiluminescence of luminol in the presence of iron(II) and oxygen: oxidation mechanism and implications for its analytical use. *Analytical Chemistry* **73**, 5,920-5,929.
- RUE E.L. and BRULAND K.W. (1995). Complexation of iron (III) by natural organic ligands in the Central North Pacific as determined by a new competitive ligand equilibration/adsorptive cathodic stripping voltammetric method. *Marine Chemistry* **50**, 117-138.
- RUE E.L. and BRULAND K.W. (1997). The role of organic complexation on ambient iron chemistry in the equatorial Pacific Ocean and the response of a mesoscale iron addition experiment. *Limnology and Oceanography* **42**, 901-910.
- SAKAMOTO-ARNOLD C.M. and JOHNSON K.S. (1987). Determination of picomolar levels of cobalt in seawater by flow injection analysis with chemiluminescence detection. *Analytical Chemistry* **59**, 1,789-1,794.
- SANDFORD R.C. (2001). Chapter Six: Development of a UV photo-oxidation stage for the determination of total Cu(II) in seawater by FI-CL, School of Earth, Ocean and Environmental Sciences, University of Plymouth, Plymouth, pp. 217-251.
- SARTHOU G. and JEANDEL C. (2001). Seasonal variations of iron concentrations in the Ligurian Sea and iron budget in the Western Mediterranean Sea. *Marine Chemistry* **74**, 115-129.
- SARTHOU G., BAKER A.R., BLAIN S., ACHTERBERG E.P., BOYE M., BOWIE A.R., CROOT P., LAAN P., DE BAAR H.J.W., JICKELLS T.D. and WORSFOLD P.J. (2003). Atmospheric iron deposition and sea-surface dissolved iron concentrations in the eastern Atlantic Ocean. *Deep-Sea research Part I*. **50**, 1,339-1,352.
- SARTHOU G.R., JEANDEL C., BRISSET L., AMOUROUX D., BESSON T. and DONARD O.F.X. (1997). Fe and H₂O₂ distributions in the upper water column in the Indian sector of the Southern Ocean. *Earth and Planetary Science Letters* **147**, 83-92.
- SCHAREK R., LATASA M., KARL D.M. and BIDIGARE R.R. (1999a). Temporal variations in diatom abundance and downward vertical flux in the oligotrophic North Pacific gyre. *Deep Sea Research Part I: Oceanographic Research Papers* **46**, 1,051-1,075.
- SCHAREK R., TUPAS L.M. and KARL D.M. (1999b). Diatom fluxes to the deep sea in the oligotrophic North Pacific gyre at Station ALOHA. *Marine Ecology Progress Series* **182**, 55-67.
- SCHULZ K.G., ZONDERVAN I., GERRINGA L.J.A., TIMMERMANS K.R., VELDHUIS M.J.W. and RIEBESELL U. (2004). Effect of trace metal availability on coccolithophorid calcification. *Nature* **430**, 673-676.

SCHUTZ L.W., PROSPERO J.M., BUAT-MENARD J.M., CARVALHO R.A.C., CRUZADO A., HARRISS P., HEIDAM N.Z. and JAENICKE R. (1990). The long range transport of mineral aerosols: Group report. In *The long range atmospheric transport of natural and contaminant substances* (ed. A.H. Knap), Kluwer, Dordrecht. pp. 197-229.

SEDWICK P.N. and DiTULLIO G.R. (1997). Regulation of algal blooms in Antarctic Shelf Waters by the release of iron from melting sea ice. *Geophysical Research Letters* **24**, 2,515-2,518.

SEDWICK P.N., CHURCH T.M., BOWIE A.R., MARSAY C.M., USSHER S.J., ACHILLES K.M., LETHABY P.J., JOHNSON R.J., SARIN M.M. and MCGILLICUDDY D.J. (2005). Iron in the Sargasso Sea (Bermuda Atlantic Time-series Study region) during summer: Eolian imprint, spatiotemporal variability, and ecological implications. *Global Biogeochemical Cycles* **19**, 1-11.

SEDWICK P.N., SHOLKOVITZ E.R. and CHURCH T.M. (2007). Impact of anthropogenic combustion emissions on the fractional solubility of aerosol iron: Evidence from the Sargasso Sea. *Geochemistry Geophysics Geosystems* **8**, 1-21.

SÉGURET M.J.M., USSHER S.J., WORSFOLD P.J., NIMMO M. and WOOD J.W. (2008). Automatic sampler coupled with flow injection-chemiluminescence detection to monitor particle/natural water interactions. *Instrumentation Science and Technology* **36**, 18-31.

SEITZ W.R. and HERCULES D.M. (1972). Determination of trace amounts of iron(II) using chemiluminescence analysis. *Analytical Chemistry* **44**, 2,143-2,149.

SILLÉN L.G. and MARTELL A.E. (1964). *Stability constants of metal ion complexes*. Special Publication 17, Chemical Society, London, pp. 754.

SLINN S.A. and SLINN W.G.N. (1980). Predictions for particle deposition on natural waters. *Atmospheric Environment* (1967) **14**, 1,013-1,016.

SPASOJEVIĆ I., ARMSTRONG S.K., BRICKMAN T.J. and CRUMBLISS A.L. (1999). Electrochemical behavior of the Fe(III) complexes of the cyclic hydroxamate siderophores alcaligin and desferrioxamine E. *Inorganic Chemistry* **38**, 449-454.

SPOKES L.J., JICKELLS T.D. and LIM B. (1994). Solubilisation of aerosols trace metals by cloud processing: A laboratory study. *Geochimica et Cosmochimica Acta* **58**, 3,281-3,287.

SPOKES L.J. and JICKELLS T.D. (1996). Factors controlling the solubility of aerosol trace metals in the atmosphere and on mixing into seawater. *Aquatic Geochemistry* **1**, 355-374.

SPOKES L.J., JICKELLS T.D. and JARVIS K. (2001). Atmospheric inputs of trace metals to the northeast Atlantic Ocean: the importance of southeasterly flow. *Marine Chemistry* **76**, 319-330.

SPYRES G., NIMMO M., WORSFOLD P., ACHTERBERG E.P. and MILLER A.E.J. (2000). Determination of dissolved organic carbon in seawater using high temperature catalytic oxidation techniques. *Trends in analytical chemistry* **19**, 498-506.

STAFFORD R.G. and ETTINGER H.J. (1972). Filter efficiency as a function of particle size and velocity. *Atmospheric Environment* **6**, 353-362.

STATHAM P.J. and CHESTER R. (1988). Dissolution of manganese from marine atmospheric particulates into seawater and rainwater. *Geochimica et Cosmochimica Acta* **52**, 2,433-2,437.

- STATHAM P.J. and HART V. (2005). Dissolved iron in the Cretan Sea (eastern Mediterranean). *Limnology and Oceanography* 50, 1,142-1,148.
- STEVENSON C.M. (1969). The dustfall and severe storms of 1 July 1968. *Weather* 24, 126-132.
- SUGIMURA Y. and SUZUKI Y. (1988). A high-temperature catalytic oxidation method for the determination of non-volatile dissolved organic carbon in seawater by direct injection of a liquid sample. *Marine Chemistry* 24, 105-131.
- SUNDA W.G. and HUNTSMAN S.A. (1997). Interrelated influence of iron, light, and cell size on growth of marine phytoplankton. *Nature* 390, 389-392.
- SUNDA W.G. (2001). Chapter 3. Bioavailability and bioaccumulation of iron in the Sea. In *The biogeochemistry of iron in seawater* (ed. Turner D.R. and Hunter K.A.), Wiley J. and Sons, Ltd, Baltimore. pp. 41-84.
- SWAP R., GARSTANG M., GRECO S., TALBOT R. and KÄLLBERG P. (1992). Saharan dust in the Amazon Basin. *Tellus B* 44, 133-149.
- SWAP R., ULANSKI S., COBBETT M. and GARSTANG M. (1996). Temporal and spatial characteristics of Saharan dust outbreaks. *Journal of Geophysical Research* 101, 4,205-4,220.
- TEGEN I., WERNER M., HARRISON S.P. and KOHFELD K.E. (2004). Relative importance of climate and land use in determining present and future global soil dust emission. *Geophysical Research Letters* 31, 1-4.
- THEIS T.L. and SINGER P.C. (1974). Complexation of iron(II) by organic matter and its effect on iron(II) oxygenation. *Environmental Science and Technology* 8, 569-573.
- THEODOSI C., MARKAKI Z. and MIHALOPOULOS N. (2008). Iron speciation, solubility and temporal variability in wet and dry deposition in the Eastern Mediterranean. *Marine Chemistry*, In press.
- TORTELL P.D., MALDONADO M.T. and PRICE N.M. (1996). The role of heterotrophic bacteria in iron-limited ocean ecosystems. *Nature* 383, 330-332.
- TORTELL P.D., MALDONADO M.T., GRANGER J. and PRICE N.M. (1999). Marine bacteria and biogeochemical cycling of iron in the oceans. *FEMS Microbiology Ecology* 29, 1-11.
- TORTELL P.D., PAYNE C.D., LI Y., TRIMBORN S., ROST B., SMITH W.O., RIESSELMAN C., DUNBAR R.B., SEDWICK P.N. and DiTULLIO G.R. (2008). CO₂ sensitivity of Southern Ocean phytoplankton. *Geophysical Research Letters* 35, 1-5.
- TURLEY C.M. (1999). The changing Mediterranean Sea - a sensitive ecosystem? *Progress in Oceanography* 44, 387-400.
- TURLEY C.M., BIANCHI M., CHRISTAKI U., CONAN P., J.R.W. H., PSARRA S., RUDDY G., STUTT E.D., TSELEPIDES A. and VAN WAMBEKE F. (2000). Relationship between primary producers and bacteria in an oligotrophic sea—the Mediterranean and biogeochemical implications. *Marine Ecology Progress Series* 193, 11-18.
- TURNER A. and OLSEN Y.S. (2000). Chemical versus enzymatic digestion of contaminated estuarine sediment: relative importance of iron and manganese oxides in controlling trace metal Bioavailability. *Estuarine, Coastal and Shelf Science* 51, 717-728.

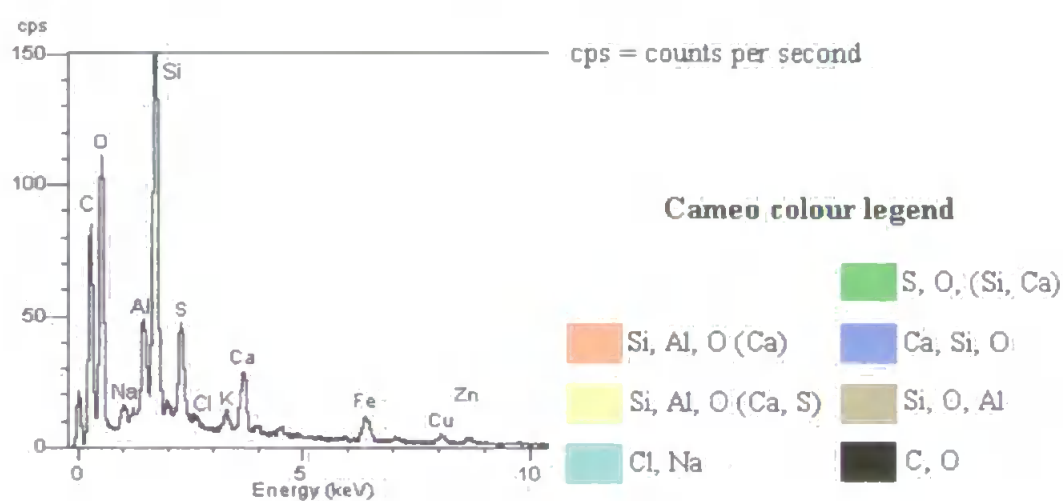
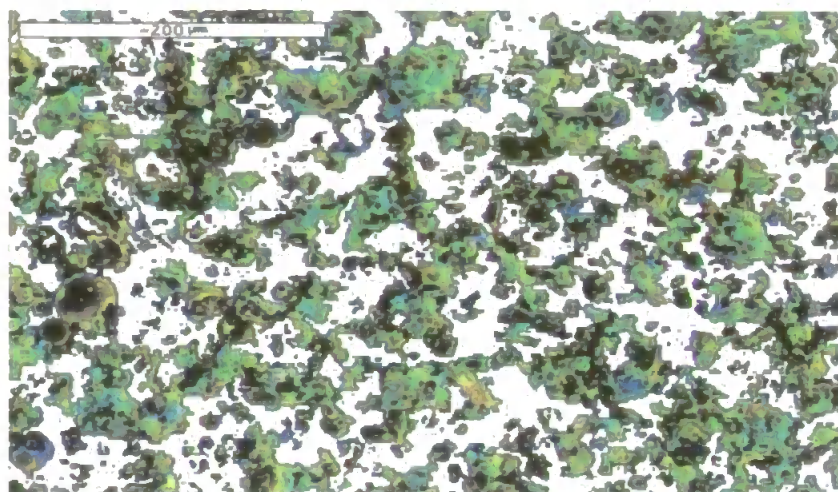
- TURNER A. (2006). Enzymatic mobilisation of trace metals from estuarine sediment. *Marine Chemistry* **98**, 140-147.
- TURNER S.M., NIGHTINGALE P.D., SPOKES L.J., LIDDICOAT M.I. and LISS P.S. (1996). Increased dimethyl sulfide concentrations in seawater from in situ iron enrichment. *Nature* **383**, 513-517.
- UEMATSU M., DUCE R.A. and PROSPERO J.M. (1985). Deposition of atmospheric mineral particles in the North Pacific Ocean. *Journal of Atmospheric Chemistry* **3**, 123-138.
- USSHER S.J. (2005). Determination of dissolved iron speciation in the North East Atlantic Ocean by flow injection chemiluminescence, School of Earth, Ocean and Environmental Sciences, University of Plymouth, Plymouth, pp. 203.
- USSHER S.J., YAQOOB M., ACHTERBERG E.P., NABI A. and WORSFOLD P.J. (2005). Effect of model ligands on iron redox speciation in natural waters using flow injection with luminol chemiluminescence detection. *Analytical Chemistry* **77**, 1,971-1,978.
- VAN DEN BERG C.M.G. (1995). Evidence for organic complexation of iron in seawater. *Marine Chemistry* **50**, 139-157.
- VERA E., DORNIER M., RUALES J., VAILLANT F. and REYNES M. (2003). Comparison between different ion exchange resins for the deacidification of passion fruit juice. *Journal of Food Engineering* **57**, 199-207.
- VINK S. and MEASURES C.I. (2001). The role of dust deposition in determining surface water distributions of Al and Fe in the South West Atlantic. *Deep-Sea research Part II*. **48**, 2,787-2,809.
- VÖELKER B.M. and SEDLAK D.L. (1995). Iron reduction by photoproducted superoxide in seawater. *Marine Chemistry* **50**, 93-102.
- VON DAMM K.L., EDMOND J.M., GRANT B., MEASURES C.I., WALDEN B. and WEISS R.F. (1985a). Chemistry of submarine hydrothermal solutions at 21 °N, East Pacific Rise. *Geochimica et Cosmochimica Acta* **49**, 2,197-2,220.
- VON DAMM K.L., EDMOND J.M., MEASURES C.I. and GRANT B. (1985b). Chemistry of submarine hydrothermal solutions at Guaymas Basin, Gulf of California. *Geochimica et Cosmochimica Acta* **49**, 2,221-2,237.
- VON DAMM K.L. and BISCHOFF J.L. (1987). Chemistry of hydrothermal solutions from the southern Juan de Fuca Ridge. *Journal of Geophysical Research* **92**, 11,334-11,346.
- WAGENER T., PULIDO-VILLEDA E. and GUIEU C. (2008). Dust iron dissolution in seawater: Results from a one-year time-series in the Mediterranean Sea. *Geophysical Research Letters* **35**, 1-6.
- WAITE D.T. and MOREL F.M.M. (1984). Photoreductive dissolution of colloidal iron oxides in natural waters. *Environmental Science and Technology* **18**, 860-868.
- WAITE D.T., SZYMCAK R., ESPEY Q.I. and FURNAS M.J. (1995). Diel variations in iron speciation in Northern Australian shelf waters. *Marine Chemistry* **50**, 79-91.
- WAITE T.D. (2001). Chapter Seven: Thermodynamics of the iron system in seawater. In *The biogeochemistry of iron in seawater* (ed. Turner D.R. and Hunter K.A.), Wiley J. and Sons, Ltd, Baltimore. pp. 291-342.

- WATSON A.J. (2001). Chapter Two. Iron limitation in the oceans. In *The biogeochemistry of iron in seawater* (ed. Turner D.R. and Hunter K.A.), Wiley J. and Sons, Ltd, Baltimore. pp. 9-39.
- WEDEPOHL K.H. (1995). The composition of the continental crust. *Geochimica et Cosmochimica Acta* **59**, 1,217-1,232.
- WEFER G., FISCHER G., FUTTERER D. and GERSONDE R. (1988). Seasonal particle flux in the Bransfield Strait, Antarctica. *Deep-Sea Research* **35**, 891-898.
- WELLS M., MAYER L.M., DONARD O.F.X., DE SOUZA SIERRA M.M. and ACKELSON S.G. (1991). The photolysis of colloidal iron in the oceans. *Nature* **353**, 248-250.
- WELLS M., PRICE N.M. and BRULAND K.W. (1995). Iron chemistry in seawater and its relationship to phytoplankton: a workshop report. *Marine Chemistry* **48**, 157-182.
- WELLS M. (1999). Manipulating iron availability in nearshore waters. *Limnology and Oceanography* **44**, 1,002-1,008.
- WELLS M.L. and GOLDBERG E.D. (1992). Marine sub-micron particles. *Marine Chemistry* **40**, 5-18.
- WELLS M.L. and GOLDBERG E.D. (1994). The distribution of colloids in the North Atlantic and Southern Oceans. *Limnology and Oceanography* **39**, 286-302.
- WEST C.E. (2007). The photodegradation of diazepam and its human metabolites in water, School of Earth, Ocean and Environmental Sciences, University of Plymouth, Plymouth, pp. 377.
- WIEPRECHT W., ACKER K., MÜLLER K., SPINDLER G., BRÜGGEMANN E., MAENHAUT W., CHI X., HITZENBERGER R., BAUER H. and TEN BRINK H. (2004). INTERCOMP2000: ionic constitution and comparison of filter and impactor. *Atmospheric Environment* **38**, 6,477-6,486.
- WINGENTER O., HAASE K.B., STRUTTON P., FRIEDERICH G., MEINARDI S., BLAKE D.R. and ROWLAND F.S. (2004). Changing concentrations of CO, CH₄, C₅H₈, CH₃Br, CH₃I, and dimethyl sulfide during the Southern Ocean Iron Enrichment Experiments. *Proceedings of the National Academy of Sciences* **101**, 8,537-8,541.
- WINKELMANN G. (1991). Specificity of iron transport in bacteria and fungi. In *CRC Handbook of microbial iron chelates* (ed. G. Winkelmann), CRC Press, Florida. pp. 366.
- WITTER A.E., HUTCHINS D.A., BUTLER A. and LUTHER III G.W. (2000). Determination of conditional stability constants and kinetic constants for strong model Fe-binding ligands in seawater. *Marine Chemistry* **69**, 1-17.
- WOLFF E.W., HALL J.S., MULVANEY R., PASTEUR E.C., WAGENBACH D. and LEGRAND M. (1998). Relationship between chemistry of air, fresh snow and firn cores for aerosol species in coastal Antarctica. *Journal of Geophysical Research* **103**, 11,057-11,070.
- WU J. and LUTHER III G.W. (1994). Size-fractionated iron concentrations in the water column of the Northwest Atlantic Ocean. *Limnology and Oceanography* **39**, 1,119-1,129.
- WU J. and LUTHER III G.W. (1995). Complexation of Fe (III) by natural organic ligands in the Northwest Atlantic Ocean by a competitive ligands equilibration method and a kinetic approach. *Marine Chemistry* **50**, 159-177.

- WU J., BOYLE E., SUNDA W. and WEN L.-S. (2001). Soluble and colloidal iron in the oligotrophic North Atlantic and North Pacific. *Science* **293**, 847-849.
- WU J., REMBER R. and CAHILL C. (2007). Dissolution of aerosol iron in the surface waters of the North Pacific and North Atlantic oceans as determined by a semicontinuous flow-through reactor method. *Global Biogeochemical Cycles* **21**, 1-10.
- YAAQUB R.R., DAVIES T.D., JICKELLS T.D. and MILLER J.M. (1991). Trace elements in daily collected aerosols at a site in southeast England. *Atmospheric Environment. Part A. General Topics* **25**, 985-996.
- YAGER J.E. and YUE C.D. (1988). Evaluation of the xenon arc lamp as a light source for aquatic photodegradation studies: Comparison with natural sunlight. *Environmental Toxicology and Chemistry* **7**, 1,003-1,011.
- YOUNG R.W., CARDER K.L., BETZER P.R., COSTELLO D.K., DUCE R.A., DiTULLIO G.R., TINDALE N.W., LAWS E.A., UEMATSU M., MERRILL J.T. and FEELEY R.A. (1991). Atmospheric iron inputs and primary productivity: Phytoplankton responses in the North Pacific. *Global Biogeochemical Cycles* **5**, 119-134.
- ZENDER C.S., BIAN H. and NEWMAN D. (2003). Mineral dust entrainment and deposition (DEAD) model: Description and 1990s dust climatology. *Journal of Geophysical Research* **108**, AAC 8.1- 8.19.
- ZHAO X., ZHAO G., WANG J. and YUN G. (2005). Selective extraction of trace mercury and cadmium from drinking water sources. *Water Environment Research* **77**, 212-218.
- ZHU X.R., PROSPERO J.M. and MILLERO F.J. (1997). Diel variability of soluble Fe (II) and soluble total Fe in North African dust in the trade winds at Barbados. *Journal of Geophysical Research* **102**, 21,297-21,305.
- ZHUANG G., DUCE R.A. and KESTER D.R. (1990). The dissolution of atmospheric iron in surface seawater of the open ocean. *Journal of Geophysical Research* **95**, 16,207-16,216.
- ZHUANG G., YI Z., DUCE R.A. and BROWN P.R. (1992a). Link between iron and sulphur cycles suggested by detection of Fe(II) in remote marine aerosols. *Nature* **355**, 537-539.
- ZHUANG G., YI Z., DUCE R.A. and BROWN P.R. (1992b). Chemistry of iron in marine aerosols. *Global Biogeochemical Cycles* **6**, 161-173.

APPENDICES

Appendix A. EDAX spectrum and Cameo image of the NIST 1648 end-member



Appendix B

Tables B.1-B.5 below summarise the instrumental settings and standard solution ranges applied for the analyses of total digest solutions from Tel-Shikmona, Heraklion and Erdemli.

Method Parameters

B.1. Emission lines adopted for the major elements, for the samples collected in Heraklion and Tel-Shikmona.

Element	Emission line
Al	396.152
Fe	238.204
Ca	422.673
Na	588.995
K	766.491
Mg	280.27
Mn	257.61
Ti	334.941
Zn	213.857

B.2. Emission lines adopted for the major elements, for the samples collected in Erdemli.

Element	Emission line
Al	396.152
Fe	238.204
Ca	422.673
Na	589.592
K	766.491
Mg	285.213
Mn	257.61
Ti	336.122
Zn	213.857

B.3. Working conditions (All emission lines share the setting below).

Power (kW)	Plasma flow (L/min)	Auxillary flow (L/min)	Nebuliser flow (L/min)	Replicate time(s)	Stab time (s)	Height (mm)
1.4	15	1.5	0.68	2	10	8

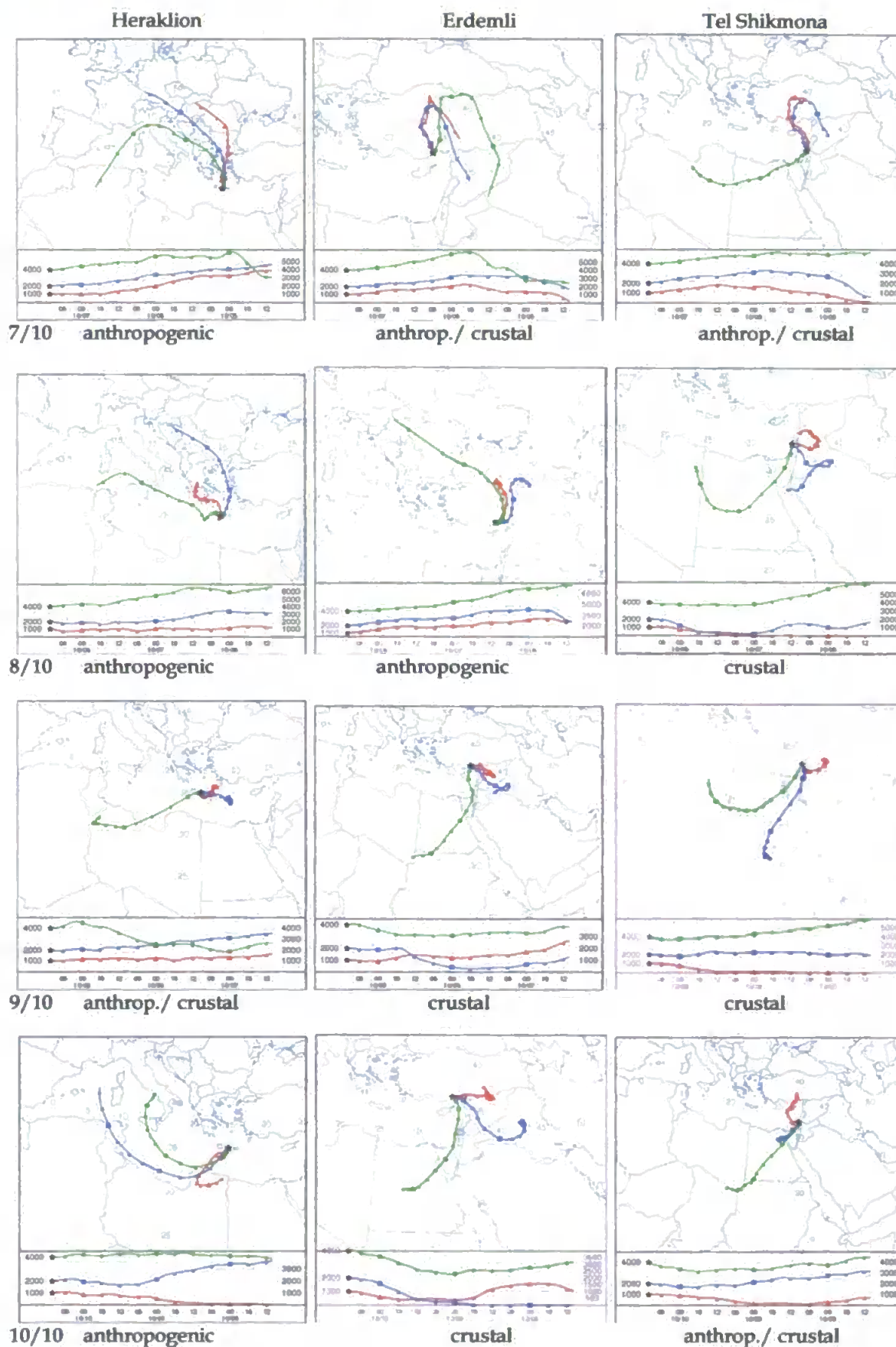
B.4. Sample introduction.

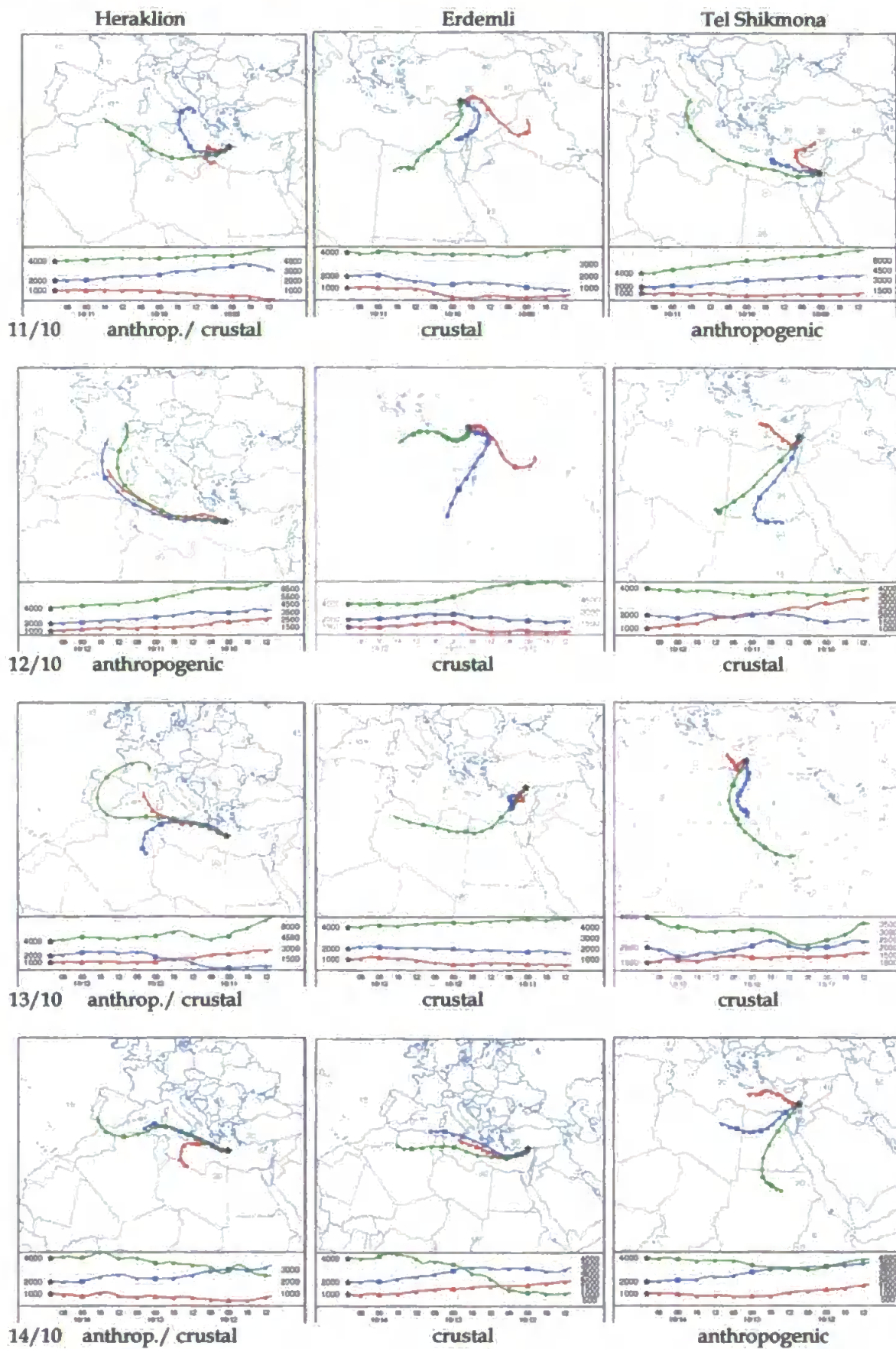
Sample uptake (s)	Rinse time (s)	Pump rate (rpm)	Fast pump
20	10	7	On

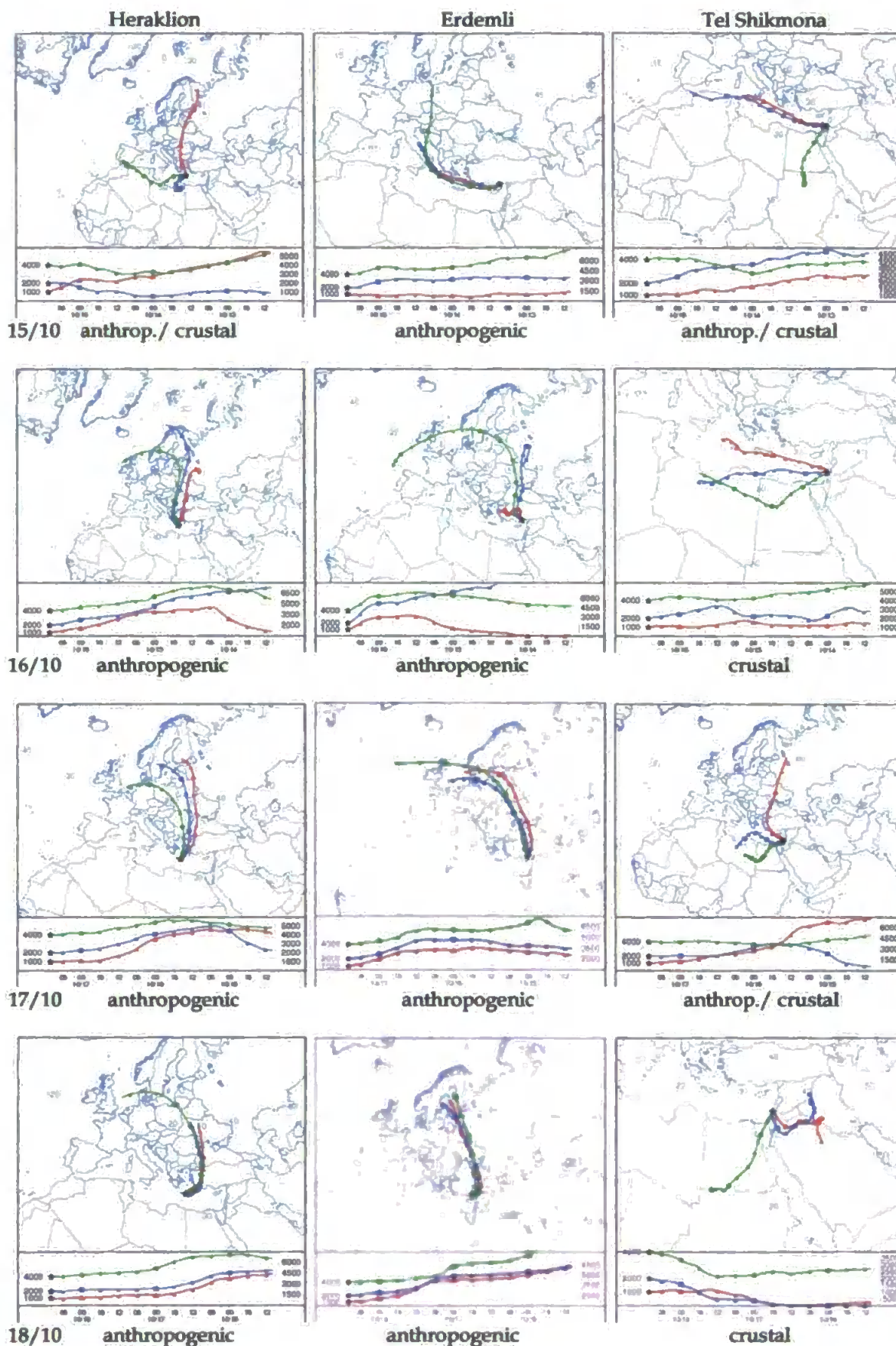
B.5.

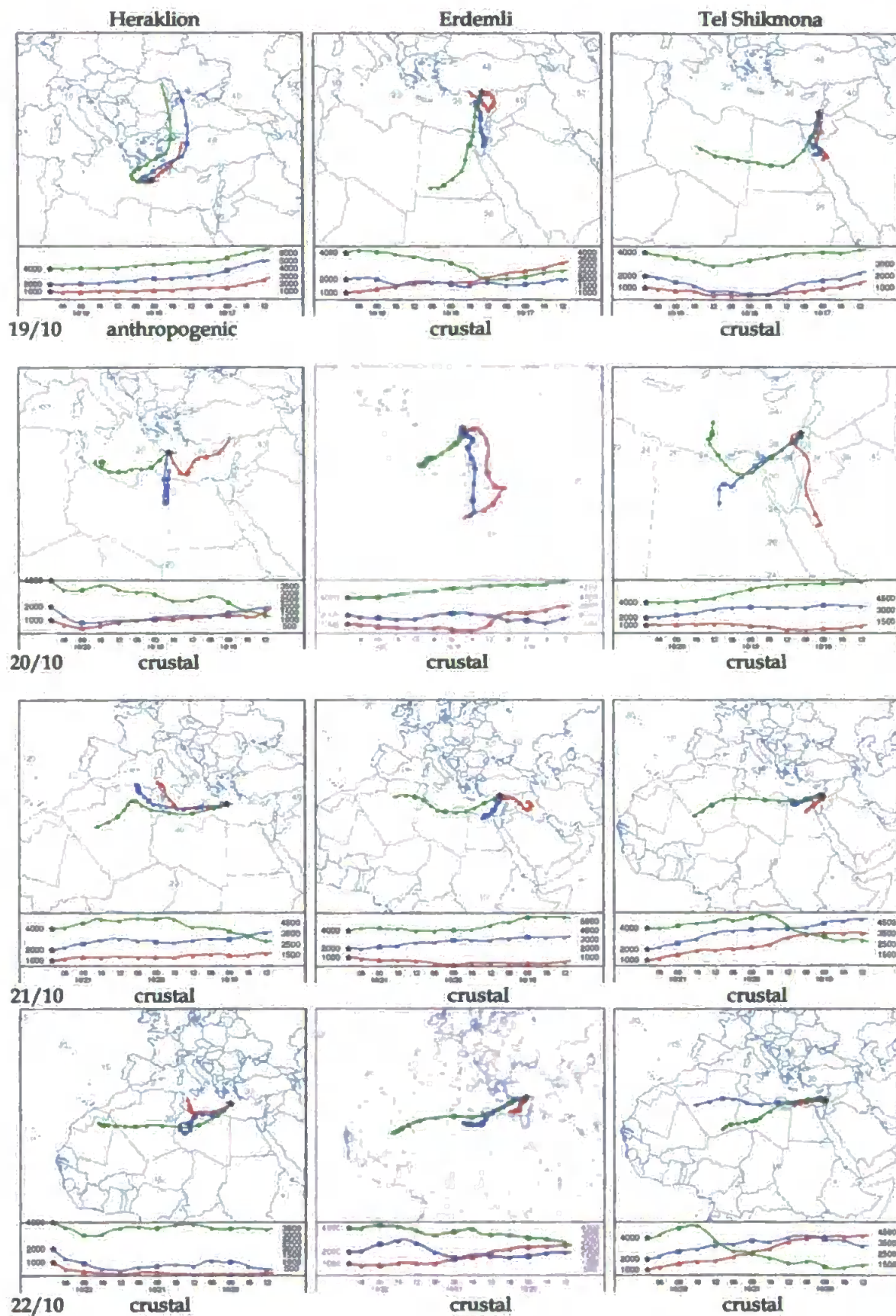
Element	Upper Crust	Saharan End Member		
	Wedepohl (1995)	Kocak <i>et al.</i> (2004)	Andreae <i>et al.</i> (2002)	Guieu <i>et al.</i> (2002b)
Fe	4.0×10^{-1}	-	6.3×10^{-1}	6.3×10^{-1}
Ca	3.8×10^{-1}	-	12.5×10^{-1}	-
Na	3.3×10^{-1}	-	1.1×10^{-1}	-
Mg	1.7×10^{-1}	-	3.0×10^{-1}	-
K	3.7×10^{-1}	-	1.9×10^{-1}	-
Ti	4.0×10^{-2}	-	5.7×10^{-2}	-
Mn	6.8×10^{-3}	-	9.3×10^{-3}	-
Cr	4.5×10^{-4}	1.1×10^{-3}	-	-
Zn	6.7×10^{-4}	1.2×10^{-3}	2.1×10^{-3}	-
Ni	2.4×10^{-4}	-	6.7×10^{-4}	-
Cu	1.9×10^{-4}	5.5×10^{-4}	3.4×10^{-4}	-
Co	1.5×10^{-4}	-	-	-
Pb	2.2×10^{-4}	4.7×10^{-4}	14.5×10^{-4}	3.4×10^{-4}
Sb	4.0×10^{-6}	-	-	-
Cd	1.4×10^{-6}	6.4×10^{-6}	-	-

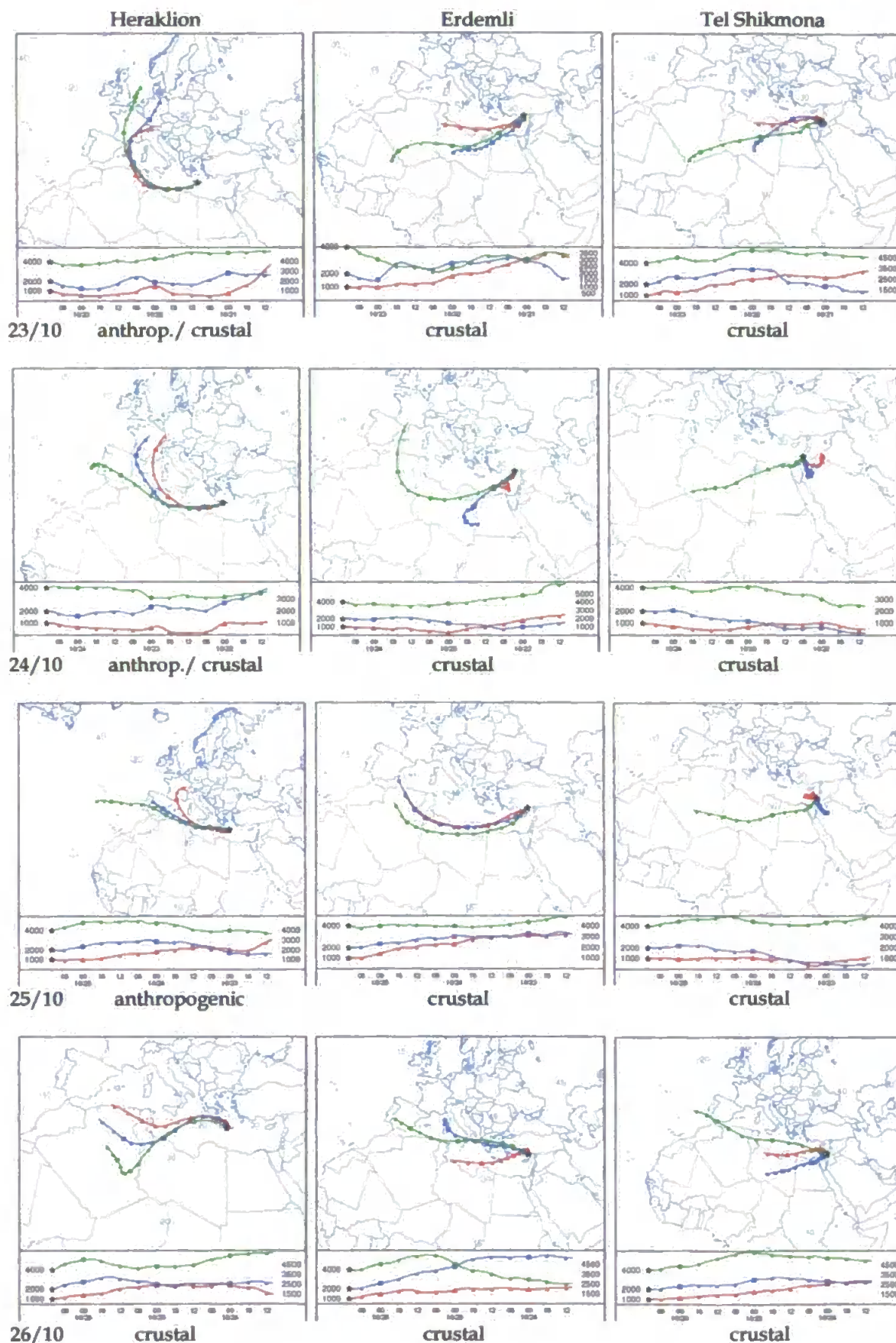
Appendix C. Back trajectories for the three sites during October 2007, indicating the dominating origin of the aerosols.

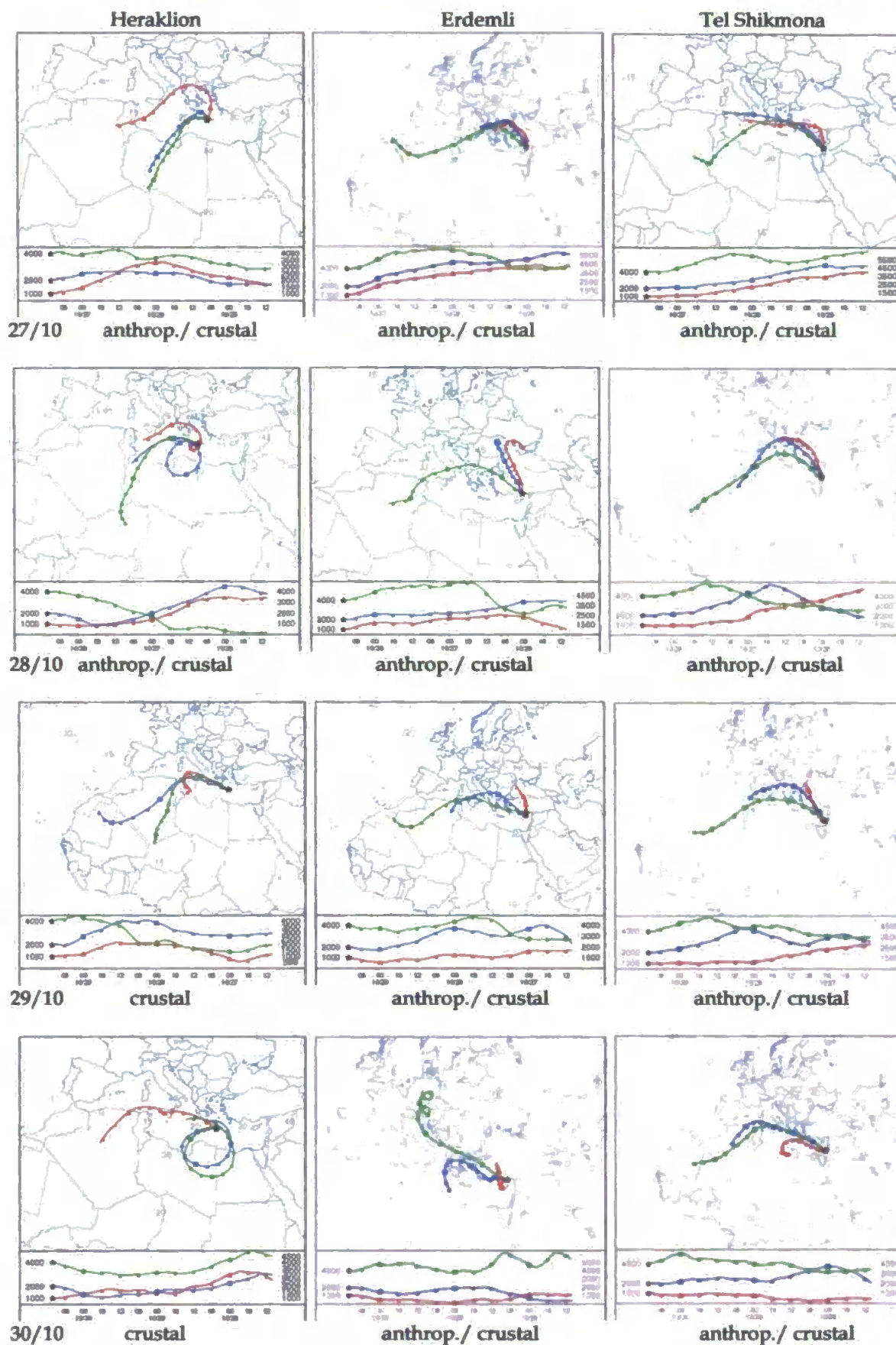


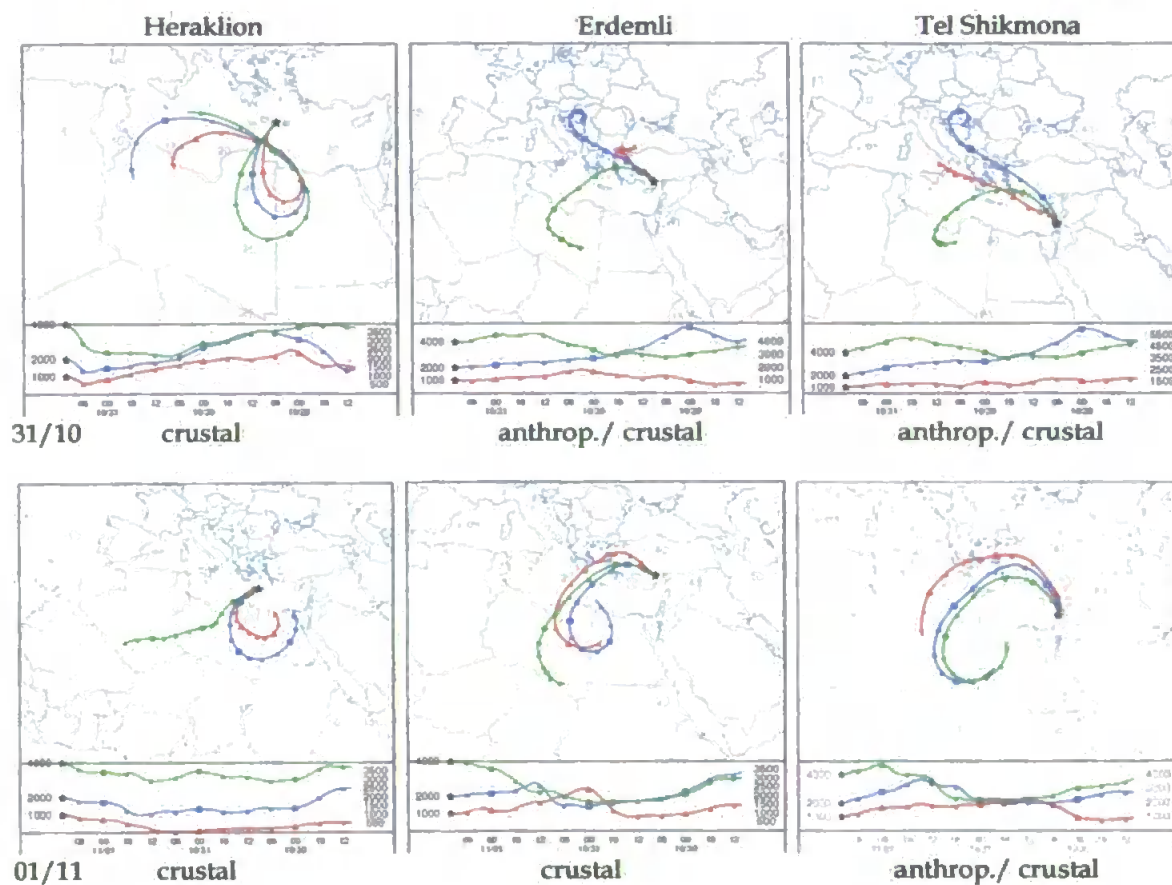












PUBLICATION

Automatic Sampler Coupled with Flow Injection-Chemiluminescence Detection to Monitor Particle/Natural Water Interactions

Marie J. M. Séguret,¹ Simon J. Ussher,¹ Paul J. Worsfold,¹
Malcolm Nimmo,¹ and John W. Wood²

¹School of Earth, Ocean and Environmental Sciences, University of
Plymouth, Plymouth, UK

²Ruthern Instrument, Penmenoth, Ruthern Bridge, Bodmin, UK

Abstract: An automatic sampler for natural waters under LabVIEW control is described. The sampler was integrated with an incubation system and coupled with a flow injection-chemiluminescence detection system to study the dissolution of aerosol iron in seawater at environmentally relevant concentrations. Automated sampling of seawater was achieved using a peristaltic pump and a 10-way distribution valve. The software allows full control of the sampler for both short (hours) and long term (days) dissolution kinetics. The environmental application of the sampler highlighted its reliability (short and extended temporal resolution), flexibility, ease of use and collection of contamination free samples.

Keywords: Automatic sampler, Iron, Aerosols, Flow injection-chemiluminescence detection, Kinetics, Seawater

INTRODUCTION

It has been recognised that the deposition of dust and its partial dissolution in the euphotic zone of the ocean is an important stage in the geochemical cycle of many elements: iron^[1] and aluminium,^[2] zinc and copper,^[3] lead,^[4]

Correspondence: Marie J. M. Séguret, School of Earth, Ocean and Environmental Sciences, University of Plymouth, Plymouth PL4 8AA, UK. E-mail: marie.seguret@plymouth.ac.uk

manganese,^[5] and macro-nutrients: nitrogen,^[6,7] phosphorus and silicon.^[7] More recently, the atmosphere has been identified as the main external source of iron to open ocean surface seawater, by aeolian dust transport.^[8,9] Because iron is an essential nanonutrient for marine organisms,^[10] and plays an important role in their metabolism,^[3,11] influencing the rates of primary production, exchange of CO₂,^[12] and release of dimethyl sulphides^[13] across the atmosphere-ocean boundary and, hence, impacting on climate change,^[14] this study focuses on its dissolution from dusts into seawater.

In surface seawater, dissolved iron concentrations vary due to (i) large spatial and temporal differences in the rate of dust inputs and subsequent particulate removal from the water column^[10] and (ii) the variable seawater solubility of aerosol associated iron.^[15,16] Therefore, owing to the importance of atmospheric inputs, this flux needs to be defined, in particular the extent to which iron undergoes dissolution in seawater post atmospheric deposition, as this controls the quantity of iron available for primary production. A high degree of variation in the percentage of aerosol associated iron which is soluble in seawater is reported, ranging from 0.05% to 54%.^[5,17] Generally, however the seawater solubility of iron is low, ranging from 0.45 to 2.2% in urban aerosol material and from 0.05 to 1.6% in Saharan dust.^[17]

The conventional method for monitoring trace metal desorption kinetics is by batch experiments,^[18,19] where sub-samples of seawater are withdrawn from the reaction vessel at certain times.^[17,20] This step is followed by batch filtration, terminating the reaction between the particles and seawater, and subsequent analysis of the element(s) of interest. This type of approach limits the temporal resolution of sample collection at the start of a dissolution study which may mask any potential fast release of the elements, but also increases the sample handling, which enhances the risk of contamination. When low particle concentrations are required to mimic the dissolution of aerosol elements in the open ocean, very low dissolved iron concentrations would be expected (pM-nM). Therefore, minimising the risk of sample contamination is essential. Hence, an automatic sampler has been developed and integrated with an aerosol incubation vessel to monitor the dissolution of iron from aerosol material at low concentrations in seawater.

Bonnet and Guieu^[17] presented data on the long term (7 days) release of iron from the urban aerosol material, NIST 1648 (solubility 0.45–2.2%) while Buck et al.^[21] reported a high instantaneous solubility, from 0.26 to 26.3% from aerosols collected in the western North Pacific Ocean. Consequently, a sampler that can collect discrete samples, over short periods of time, during the first few hours of a study to define the short term kinetics and also over an extended period (i.e., several days) to monitor medium term kinetic processes is required. As picomolar iron concentrations need to be measured in such studies a very sensitive detection system with a low detection limit and associated low analytical blanks is required. Hence, for this study, the sampler-incubation vessel has been coupled to an FI-CL

(flow injection-chemiluminescence) detection system similar to that developed by Bowie et al.^[22,23]

The extent and kinetics of the seawater solubility of aerosol iron are influenced by a complex array of chemical and physical processes. These include (i) chemical influences, i.e., end-member aerosols sources (urban/crustal); concentration and composition of organic Fe complexing ligands, (ii) physical influences, i.e., dark/light conditions, seawater aerosol concentrations, temperature. Therefore using this instrumentation, dust was introduced at seawater concentrations ranging from 0.25 to 2 mg L⁻¹ into the aerosol incubation vessel, the lower dust concentration being representative of a medium to strong Saharan dust event over a 10 m mixed surface layer,^[17] whilst varying the physical (light intensity; temperature) and chemical parameters (dissolved organic ligands; type of aerosol material). This is a challenging procedure, requiring high accuracy and precision, high temporal resolution and a low detection limit. During dissolution studies seawater samples were extracted from the incubation vessel using a peristaltic pump, in-line filtration system and 10-way distribution valve. Samples were taken over a 5-day period and total iron (II + III) was determined in each sample after acidification and sulphite reduction by FI-CL. Instrument control, sample collection and data processing were facilitated by a graphical programming environment (LabVIEW) which is discussed in detail below.

EXPERIMENTAL

Sampler Associated with an Incubation Vessel

Figure 1 highlights the set up of the automatic sampler integrated with an aerosol incubation vessel. The pump was a peristaltic pump (MS/CA4-E/8-

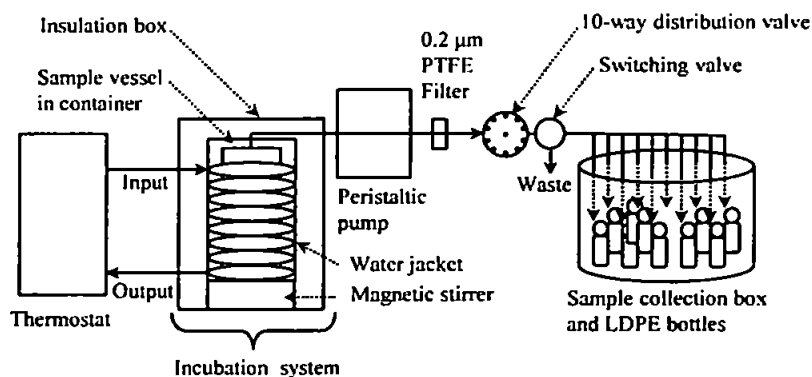


Figure 1. Components of the sampler-incubation vessel for the sampling of dissolved iron released in seawater during model dissolution studies.

100C, Ismatec) placed in a IP62 pump housing (Ruthern Instruments, UK), powered by an AC/DC switch mode power supply (Type 9921, Mascot, Norway) and operated at 5 V dc (TTL). Extracted seawater samples were filtered using an acid washed PTFE acrodisc syringe membrane filter (0.2 μm pore size, Pall Corporation, UK). The 10-way distribution valve was a multi-position microelectric valve (EMHMA-CE, Valco instruments Co. Inc., USA) automated by a multi-position actuator control module (P/N EMHCA-CE, Valco Instruments Co. Inc., USA) and assembled in an IP62 valve housing (Ruthern Instruments, UK). The actuator of the 10-way distribution valve was powered by a power adapter (FSA46A240-B2, Fortron Source, UK). The switching valve was a PTFE 3-way, 2 position solenoid valve (EW-01367-72, Cole-Parmer, UK) and operated at 12 V dc (solenoid). 30 mL LDPE bottles (Low Density PolyEthylene, Nalgene, Fisher Scientific, UK) were placed in sealed plastic bags and positioned inside a hermetically sealed box. The system was positioned in a Class-100 laminar flow hood whilst the interface and computer were positioned outside. The temperature of the incubation vessel was controlled using a heater/chiller system (Endocal RTE-100; Neslab Instruments Inc., USA) via a water jacket which consisted of a plastic rubber tube which was coiled (1 m long and 2 cm i.d.) around the incubation vessel (a 2 L Teflon FEP (Fluorinated Ethylene-Propylene) bottle; Nalgene, Fisher Scientific, UK). The incubation vessel and water jacket were placed in a plastic container, filled with water and fully enclosed to mimic dark conditions (eliminating any photochemical reactions) and finally insulated by a polystyrene box. Seawater was mixed by a magnetic stirrer rotating at its lowest practical setting (Stuart, Barloworld Scientific, UK). During dissolution studies, temperatures in this study were set at 5°C or 25/30°C, to represent marine systems at high and low equatorial latitudes.

Flow lines, fittings, PTFE filter and connectors were cleaned with 1 M super pure HCl (Romil, UK) and UHP (Ultra High Purity) water (18.2 M Ω cm⁻¹, Elgastat Maxima) prior to use. Manifold tubing was 0.75 mm i.d. PTFE (Fisher Scientific, UK) and peristaltic pump tubing was flow-rated PVC (Elkay, UK).

During a dissolution study the following controls were collected: 2 UHP blanks, 2 filter blanks, 3 sub-samples of the seawater in the incubation vessel before addition of the aerosol material (i.e., T_{seawater}) and a UHP water blank from a LDPE bottle, followed by the collection of 10 samples (at time T_0 , T_{15} , T_{30} , T_{60} , T_{2h} , T_{4h} , T_{8h} , T_{12h} , T_{24h} , and T_{48h}). Each sample was automatically collected over a period of 150 s (Table 1), between T_0 to $T_{48\text{hours}}$ and the last sample at $T_{120\text{hours}}$ was collected via a different programme.

Interface

Process control was achieved using a control and data acquisition instrument (Ruthern Instruments, UK). This instrument is based on a NI USB-6008,

Table 1. Timing sequence and operation state for each component per position of the 10-way distribution valve (cycle)

Elapsed time (s)	Pump	Switching valve	10-way selection valve position ^a	Operation
0	On	On	1	Sample goes to waste
20	On	On	1	Start collection of sample
150	Off	Off	1	End collection of sample

^a10-way selection valve position switches from position 1 to 10 depending of the time of collection.

multifunction data acquisition device (National Instruments Corp., UK) with 12 digital input/output TTL lines, 12-bit analogue input resolution of up to 10 k samples s⁻¹. NI-DAQmx Base is a software multiplatform driver with a subset of the NI-DAQmx programming interface (National Instruments Corp., UK). Virtual instrument (VI) software (Ruthern Instruments, UK) was written in LabVIEW version 7.1 (National Instruments Corp., UK). The control instrument had five modules, one for the USB system controller, one for the solenoid and relay controlling switching valves, one for the PMT integrator and amplifier, one for the TTL output controlling the pumps and one for the sample pump of the FI-CL system (Minipuls 3, Gilson, France) (Figure 2). The LabVIEW VI front panel contained ready-to-use switches, buttons, controls and graphical displays of timing cycle and global timing and positions of the 10-way distribution valve and each element was connected to the block diagram (Figure 3) which included timing of operations.

FI-CL Manifold

Figure 4 shows the applied automated FI-CL manifold similar to the one previously described by Bowie et al.^[23] allowing the determination of dissolved iron in seawater at pM concentrations. Pumps were 4-channel peristaltic pumps (Minipuls 3, Gilson, France). The injection valve was an electronic rotary injection valve (NDV0008, Valco instruments Co. Inc., USA) automated by a micro-electric actuator (EHCACE, Valco Instruments Co. Inc., USA) powered by a power supply (DPS55, Astec, UK). The switching valve was a PTFE 3-way, 2 position solenoid valve (EW-01367-72, Cole-Parmer, UK). Pumps were operated at 5 V dc (TTL) and the switching valve at 12 V dc. The detection system consisted of an end-window photo-multiplier tube (Thorn EMI, 9798 QA) contained in a μ -metal shield for magnetic insulation (MS52D), a built-in current-to-voltage amplifier (C634), an ambient temperature shielded housing (Electron Tubes, B2F/RFI) and a 1.1 kV power supply (Thorn EMI, PM28B). The amplifier was supplied with 15 V from an independent power supply (BBH Power Products).

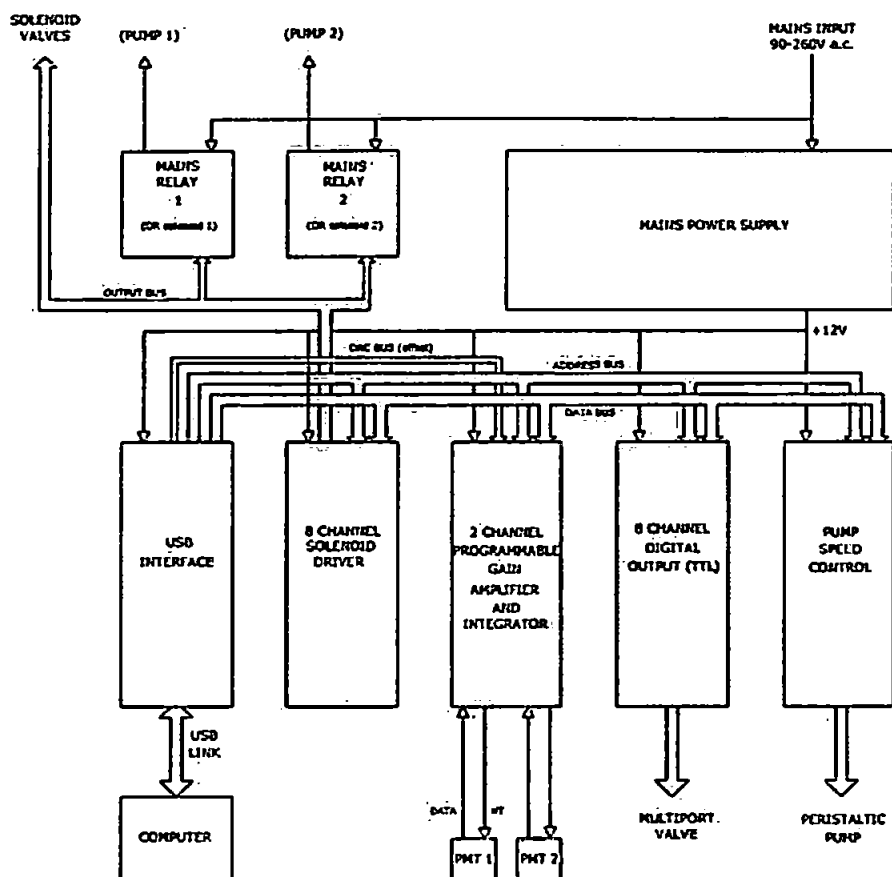


Figure 2. Block diagram of the interface, incorporating the 5 units: USB system controller, solenoid and relay controlling switching valves, PMT integrator (2 channels), TTL output and pump.

Flow lines, fittings and connectors were cleaned following the same procedures as for the sampler (described above). Manifold tubings and peristaltic pump tubings were the same as those used in the sampler (Fisher Scientific, UK and Elkay, UK). Pre-concentration of the samples, elimination of the seawater matrix and cleaning of the buffer and UHP water were performed in-line using 8-hydroquinoline (8-HQ) covalently attached to a vinyl co-polymer resin packed into 50 μL micro-columns.^[23] Samples for total iron (II + III) were acidified (stored for 3 weeks) to pH ~ 1.7 with super pure HCl and reduced (overnight) using 100 μM sulphite reducing reagent prior to analysis.

The analytical cycle consisted of 4 replicates measurements including sample-UHP loads (43 s each) and elutions (35 s each) with 0.05 M HCl, followed by a UHP rinse (75–100 s). The time taken for one analytical cycle amounted to around 10 min.

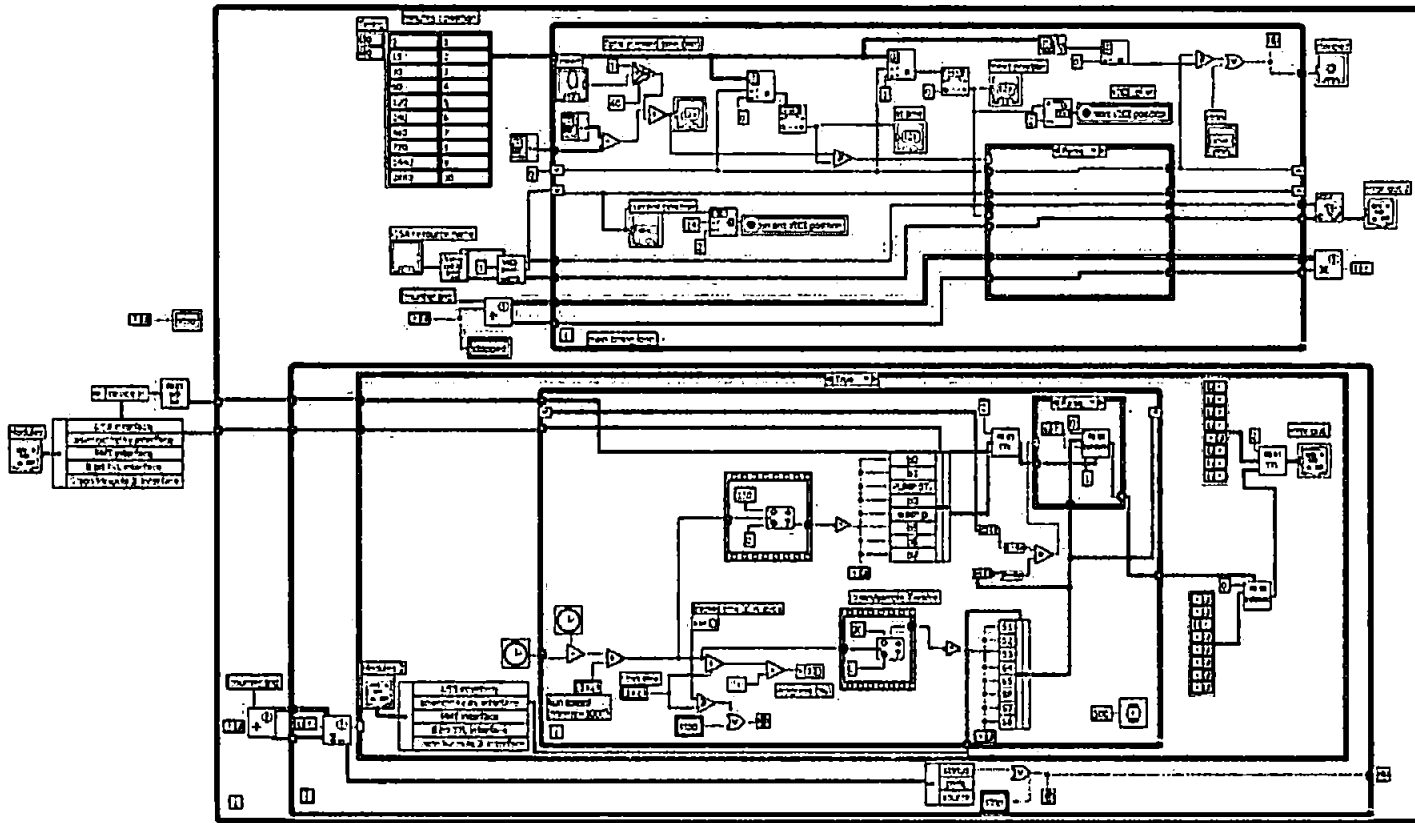


Figure 3. Wiring diagram showing the graphical code for instrument control, driving the functions of the interface.

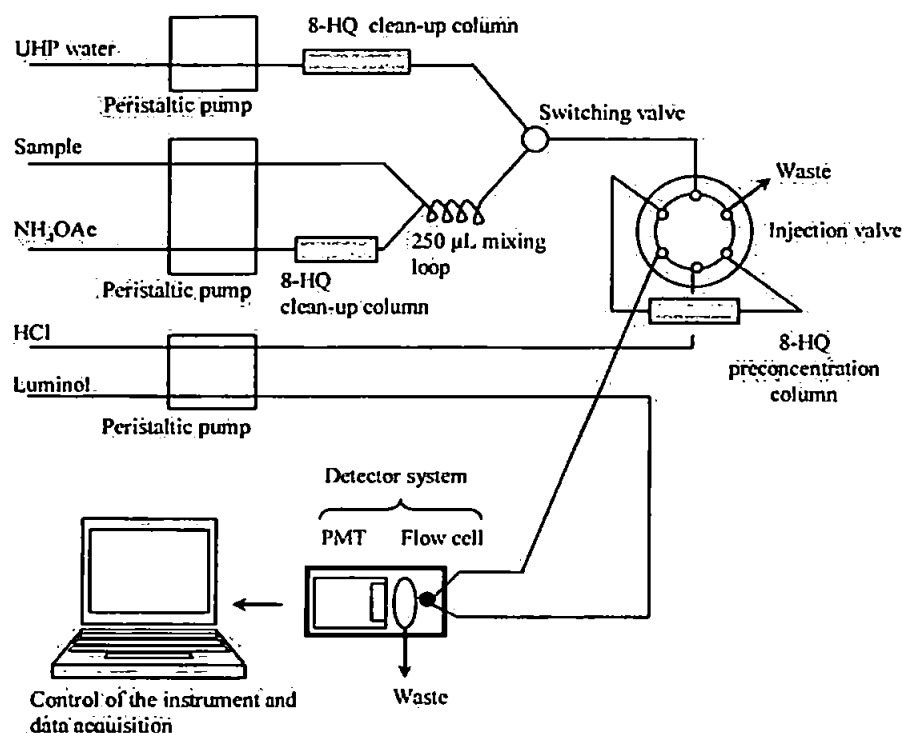


Figure 4. FI-CL manifold used for the determination of total dissolved iron(II + III) during aerosol dissolution studies in seawater.

Reagents and Standards

Chemicals were obtained from Fisher Scientific (UK), unless otherwise stated; reagents and standards were prepared in UHP water. Plasticware for the manifold system was cleaned by soaking in baths: in hot 5% (v/v) micro detergent (Decon) for 24 h, in 50% (v/v) hydrochloric acid (6 M, AnalaR) for one week and in 20% (v/v) nitric acid (2 M, AnalaR) for one week. Between each bath, labware was rinsed thoroughly with UHP water and then stored in re-sealable plastic bags. The 2 L incubation vessel and magnetic stirrer were cleaned in separate acid baths. To avoid any risks of contamination, handling of standards and reagents was carried out under a class-100 laminar flow hood.

A stock of diammonium ferrous sulphate hexahydrate ($\text{Fe}(\text{NH}_4)_2(\text{SO}_4)_2 \cdot 6\text{H}_2\text{O}$) was used to prepare daily iron(II) standards in 0.1 M super pure hydrochloric acid (Romil, UK). A 10 μM luminol (5-amino-2,3-dihydro-1,4-phthalazinedione, Fluka) stock was prepared by dilution of a 0.01 M stock in 0.1 M of sodium carbonate, adjusted to pH 12.2 with 2 M sodium hydroxide. This reagent was passed through a column containing Chelex-100 (Sigma-Aldrich, UK) chelating resin, in order to reduce the baseline noise generated by impurities in the luminol reagent. Ammonium

acetate buffer (0.4 M) was prepared from a stock solution (2 M) and adjusted to pH 5.5 with acetic acid and cleaned in-line using an 8-HQ microcolumn. The sulphite reducing reagent, 100 μ M for iron(III), was prepared by dissolving sodium sulphite (extra pure, Merck) in 0.4 M ammonium acetate buffer (pH 5.5) and cleaned by passing through an 8-HQ column. The eluant was 0.05 M super pure hydrochloric acid (SpA, Romil, UK) and the acid to clean the system between each injection was 1 M of the same reagent. Low iron and low DOC (dissolved organic carbon) seawater was obtained by passing open ocean seawater (Canary Basin, Cruise P332 in 2006) through an on-line UV photo-oxidation system.^[24]

An urban particulate reference material, NIST 1648, was chosen to represent an anthropogenic dominated aerosol population (National Institute of Standards and Technology, USA) and was used as received.

RESULTS AND DISCUSSION

Detector Performance

The PMT interface contained a 16-position switched gain amplifier (Figure 2), providing gain settings of 1 to 8000, selectable by the control VI software and

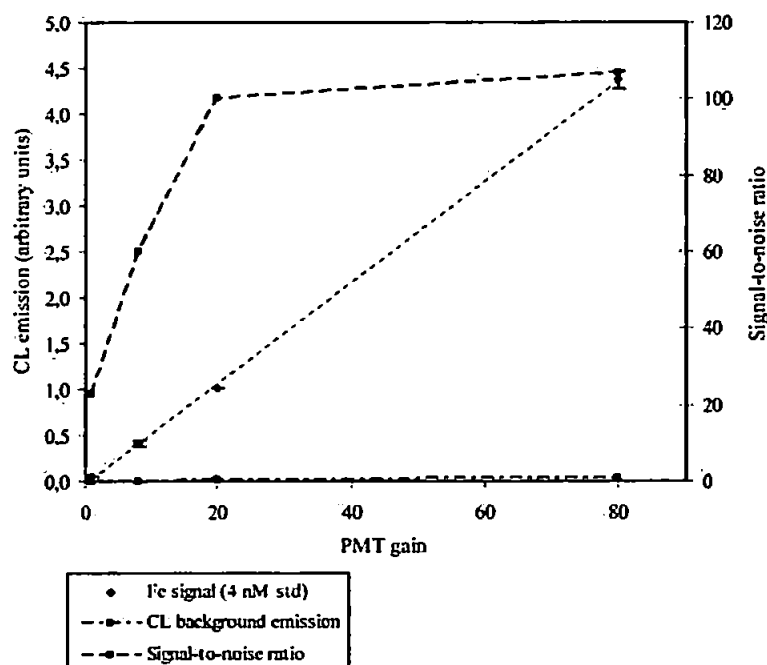


Figure 5. Effects of changing the PMT detector gain on the CL background emission, analyte signal and signal-to-noise ratio. (Errors bars indicate ± 1 sd).

allowing the adjustment of the sensitivity of the detector to suit the variability of concentrations of iron in seawater. The effect of changing the gain on the CL background emission, signal-to-noise ratio and Fe signal for a 4.0 nM iron(II) standard is presented in Figure 5. While the CL background emission showed little change with gain settings, the CL emission for the standard increased linearly with PMT gain. The signal-to-noise ratio increased linearly up to 100 and then reached a plateau, owing to an increased detector noise at the X 80 gain setting. Consequently, a low gain setting was the most suitable (X 8) for initial dust dissolution studies when comparatively higher dissolved iron concentrations (up to 16 nM) were expected, whilst for experiments using low dust concentrations, picomolar concentrations of dissolved iron were expected, therefore a higher gain setting (X 20) was used.

Analytical Figures of Merit

Figure 6 shows a typical flow injection trace for the blank and standard addition of 2–16 nM iron(II) spikes of a seawater sample used for the dissolution studies. The standard addition plot exhibited good linearity ($R^2 = 0.997$) over this range. The typical range of relative standard deviation was between 1 and 10% ($n = 4$). The typical range of iron(II) blanks was between 49 and 140 pM, resulting in a limit of detection varying between 47 and 316 pM (defined as $3 \times$ standard deviation of the blank divided by the slope). The major contributions to the blank signal were from iron impurities in the ammonium acetate buffer whereas blanks associated with UHP water, eluting acid and sulphite used for sample pre-treatment were all below the limit of detection. Therefore an 8-HQ column was included in-line (Figure 4)

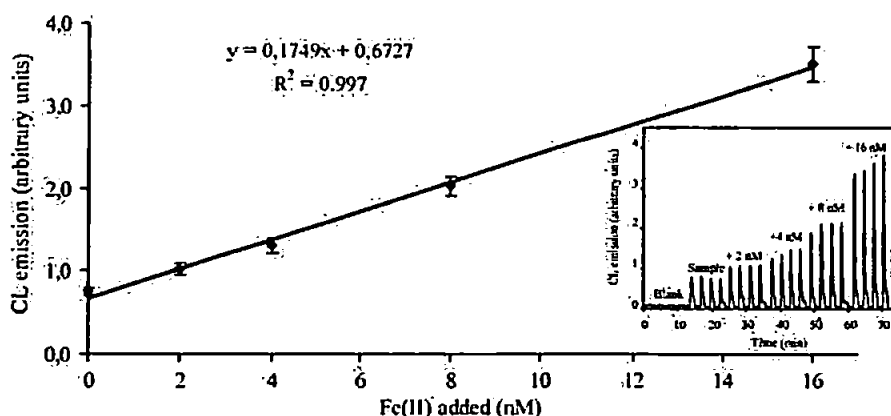


Figure 6. Calibration peaks and corresponding standard additions plot for iron over the range of 2–16 nM. (Error bars indicate ± 1 sd).

to minimise the buffer blank signal. Furthermore blank contributions from the sampler (reaction vessel, line and filters) were also below the limit of detection. This demonstrates that the sampler allows the collection of contamination free samples. The accuracy was determined using an internal reference material (Canary Basin surface water IFA2). The measured concentration was 0.85 ± 0.01 nM which compared favorably with the "certified" value of 0.85 ± 0.02 nM.

Aerosol Dissolution Experiment

Figure 7 presents a typical temporal change in dissolved iron concentration following the addition of 1.97 mg L^{-1} of NIST 1648 dust to seawater (30°C , dark conditions, low DOC concentration $81.35 \mu\text{M} \pm 0.96$), as monitored by the sampler and detection system. This illustrates the fast release of dissolved iron, up to a concentration of 6.2 nM, representing a solubility of 0.45% (solubility = (amount of Fe released into seawater/total Fe in added aerosol) $\times 100$) from the aerosol material into the seawater, occurring within the first two hours. Subsequent to this, dissolved Fe concentrations decreased, down to 1.95 nM (0.14% of solubility) after two days, possibly due to re-adsorption onto aerosol particles and/or colloidal formation as a result of speciation changes of the dissolved Fe. Equilibrium

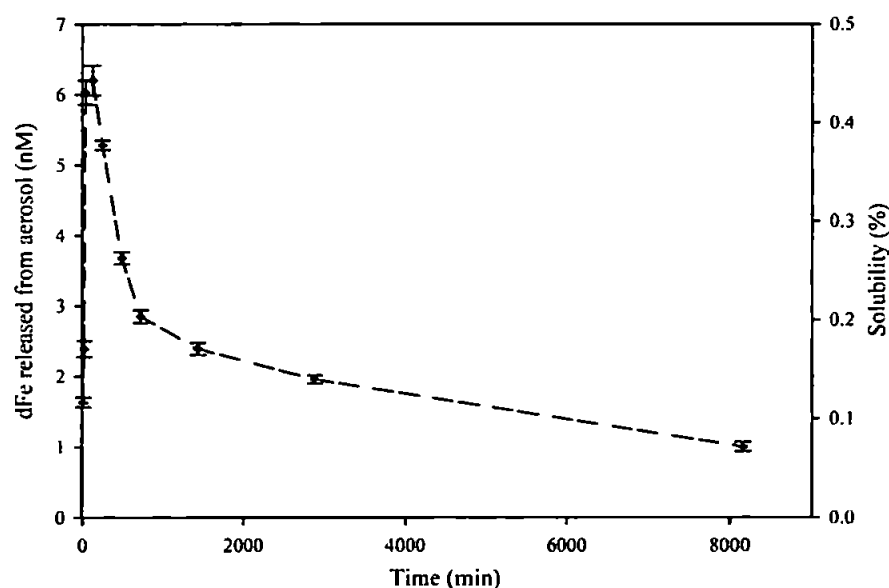


Figure 7. Temporal profile of dissolved iron (dFe) released (nM) after the addition of 1.97 mg L^{-1} of NIST 1648 to seawater and the percentage of soluble iron (%), under dark conditions, low DOC ($81.35 \mu\text{M} \pm 0.96$), 30°C . (Errors bars indicate ± 1 sd).

was reached at day 5 with the dissolved Fe concentration being 1.00 nM (0.07% solubility).

This dissolution profile demonstrates the reliability of the integrated system over a period of 5 days for monitoring the kinetics of Fe dissolution with no downtime. Indeed, the user-friendly software allows flexibility in controlling the time of sample collection.

CONCLUSIONS

The described automatic sampler controls a 10-way distribution valve for the extraction of the seawater sub-samples and uses flow injection with chemiluminescence detection for the determination of iron in seawater (at picomolar concentrations). This is an inexpensive and robust system suitable for the laboratory as well as for shipboard deployment, within a clean environment that minimises the risk of contamination. The automatic sampler allows the monitoring of the fast release of iron from aerosol material into seawater, particularly within the first two hours. The interface allows easy and full control of the sampling strategy: collection time (i.e., T_0 , T_5 , T_{10}), number of samples (from 1 to 10 without additional rinse of the lines), and also the duration of sampling (i.e., 30 s, 200 s, 1,000 s) ensuring high precision of sampling. In addition, although this study focuses on the dissolution of iron from aerosols into seawater, the user friendly software and reliable interface makes the sampler adaptable and suitable for studying other important environmental dissolved/particle interactions, for example dissolution of aerosol trace metals other than iron (e.g., aluminium, manganese) and nutrients (e.g., nitrate, phosphate) into natural waters.

ACKNOWLEDGMENT

M. J. M. Séguret would like to thank the University of Plymouth for the award of a scholarship.

REFERENCES

1. Moore, R.M.; Milley, J.E.; Chatt, A. The potential for biological mobilization of trace metals from aeolian dust in the ocean and its importance in the case of iron. *Oceanol. Acta* **1984**, *7*, 221–228.
2. Vink, S.; Measures, C.I. The role of dust deposition in determining surface water distributions of Al and Fe in the South West Atlantic. *Deep-Sea Res. Part II* **2001**, *48*, 2787–2809.
3. Sunda, W.G.; Huntman, S.A. Iron uptake and growth limitation in oceanic and coastal phytoplankton. *Mar. Chem.* **1995**, *50*, 189–206.

4. Maring, H.B.; Duce, R.A. The impact of atmospheric aerosols on trace metal chemistry in open ocean surface seawater. 3. Lead. *J. Geophys. Res.* **1990**, *9* (C4), 5341–5347.
5. Baker, A.R.; Jickells, T.D.; Witt, M.; Linge, K.L. Trends in the solubility of iron, aluminium, manganese and phosphorus in aerosol collected over the Atlantic Ocean. *Mar. Chem.* **2006**, *98*, 43–58.
6. Prospero, J.M.; Barrett, K.; Church, T.; Dentener, F.; Duce, R.A.; Galloway, J.N.; Levy, H., II; Moody, J.; Quinn, P. Atmospheric deposition of nutrients to the North Atlantic Basin. *Biogeochemistry* **1996**, *35*, 27–73.
7. Baker, A.R.; French, M.; Linge, K.L. Trends in aerosol nutrient solubility along a west-east transect of the Saharan dust plume. *Geophys. Res. Lett.* **2006**, *33* (L07805), doi:10.1029/2005GL024764.
8. Duce, R.A.; Tindale, N.W. Chemistry and biology of iron and other trace metals. *Limnol. Oceanogr.* **1991**, *36* (8), 1715–1726.
9. Duce, R.A.; Liss, P.S.; Merrill, J.T.; Atlas, E.L.; Buat-Menard, P.; Hicks, B.B.; Miller, J.M.; Prospero, J.M.; Arimoto, R.; Church, T.M.; Ellis, W.; Galloway, J.N.; Hansen, L.; Jickells, T.D.; Knap, A.H.; Reinhardt, K.H.; Schneider, B.; Soudine, A.; Tokos, J.J.; Tsunogai, S.; Wollast, R.; Zhou, M. The atmospheric input of trace species to the ocean. *Global Biogeochem. Cycles* **1991**, *5*, 193–259.
10. Wells, M.; Price, N.M.; Bruland, K.W. Iron chemistry in seawater and its relationship to phytoplankton: a workshop report. *Mar. Chem.* **1995**, *48*, 157–182.
11. Sunda, W.G.; Huntman, S.A. Interrelated influence of iron, light, and cell size on growth of marine phytoplankton. *Nature* **1997**, *390*, 389–392.
12. Watson, A.J.; Bakker, D.C.E.; Ridgwell, A.J.; Boyd, P.W.; Law, C.S. Effect of iron supply on Southern Ocean CO₂ uptake and implications for glacial atmospheric CO₂. *Nature* **2000**, *407*, 730–733.
13. Turner, S.M.; Nightingale, P.D.; Spokes, L.J.; Liddicoat, M.I.; Liss, P.S. Increased dimethyl sulfide concentrations in seawater from in situ iron enrichment. *Nature* **1996**, *383*, 513–517.
14. Martin, J.H. Glacial-interglacial CO₂ change: the iron hypothesis. *Paleoceanography* **1990**, *5*, 1–13.
15. Chester, R.; Murphy, K.J.T.; Lin, F.J.; Berry, A.S.; Bradshaw, G.A.; Corcoran, P.A. Factors controlling the solubilities of trace metals from non-remote aerosols deposited to the sea surface by the “dry” deposition mode. *Mar. Chem.* **1993**, *42*, 107–126.
16. Hand, J.L.; Mahowald, N.M.; Chen, Y.; Siefert, R.L.; Luo, C.; Subramaniam, A.; Fung, I. Estimates of atmospheric-processed soluble iron from observations and a global mineral aerosol model: biogeochemical implications. *J. Geophys. Res.* **2004**, *109* (D17205), 1–21.
17. Bonnet, S.; Guieu, C. Dissolution of atmospheric iron in seawater. *Geophys. Res. Lett.* **2004**, *31* (L03303), doi:10.1029/2003GL018423.
18. Guieu, C.; Duce, R.; Arimoto, R. Dissolved input of manganese to the ocean: Aerosol source. *J. Geophys. Res.* **1994**, *99* (D9), 18789–18800.
19. Nimmo, M.; Fones, G.R.; Chester, R. Atmospheric deposition: a potential source of trace-metal organic complexing ligands to the marine environment. *Croat. Chem. Acta.* **1998**, *71*, 323–341.
20. Guernozi, S.; Molinaroli, E.; Rossini, P.; Rampazzo, G.; Quarantotto, G.; de Falco, G.; Cristini, S. Role of desert aerosol in metal fluxes in the Mediterranean area. *Chemosphere* **1999**, *39* (2), 229–246.

21. Buck, C.S.; Landing, W.M.; Resing, J.A.; Lebon, G.T. Aerosol iron and aluminium solubility in the northwest Pacific Ocean: results from the 2002 IOC cruise. *Geochem. Geophys. Geosyst.* **2006**, *7* (4), doi:10.1029/2005GC000977.
22. Bowie, A.R.; Achterberg, E.P.; Mantoura, R.F.C.; Worsfold, P.J. Determination of sub-nanomolar levels of iron in seawater using flow injection with chemiluminescence detection. *Anal. Chim. Acta* **1998**, *361*, 189–200.
23. Bowie, A.R.; Achterberg, E.P.; Ussher, S.; Worsfold, P.J. Design of an automated flow injection-chemiluminescence instrument incorporating a miniature photomultiplier tube for monitoring picomolar concentrations of iron in seawater. *J. Autom. Meth. Manag. Chem.* **2005**, *2*, 37–43.
24. Donat, J.R.; Bruland, K.W. Direct determination of dissolved cobalt and nickel in seawater by differential pulse cathodic stripping voltammetry preceded by adsorptive collection of cyclohexane-1,2-dione dioxime complexes. *Anal. Chem.* **1988**, *60* (3), 240–244.

Received July 28, 2007

Accepted September 12, 2007

Manuscript 1658